Theory of Ozone Isotopic Effects and Various Electron Transfer Reactions

Thesis by

Yi Qin Gao

In Partial Fulfillment of the Requirements

for the Degree of

Doctor of Philosophy

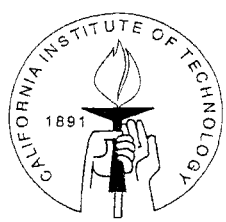

California Institute of Technology

Pasadena, California

2001

(Submitted April 26, 2001)

© 2001
Yi Qin Gao
All Rights Reserved

Acknowledgments

The five years I have spent at Caltech were certainly fruitful and enjoyable. Caltech not only opened my door to scientific research, but also broadened my knowledge in many other areas. I feel very thankful to the institute and the people working here.

Having Professor Rudy Marcus as my research advisor has been the most fortunate and wonderful part of my graduate study. He has always been available for guidance and consultations. In science, I have learned and am learning from him more than from anybody else. Given any chance for my future career as a scientist, I will carry with me his advice on being a theoretician, always working on something that is measurable.

Professor Aron Kuppermann, Professor Fred Anson and Professor Okumura are not only members of my Ph.D. committee, but also mentors who have generously provided their insightful thoughts and encouragement on many occasions. Professor Sunny Chan has offered me so much guidance that once he called me "a half student" of his.

Everyone in Marcus group is a close friend of mine. I have learned so much from these friends. Dr. Yuri Georgievskii not only taught me physics and mathematics but also fixed my car numerous times. Dr. Chao-Ping Hsu helped me to overcome many difficulties during my first several years here. With Dr. Thomas Renger, I have shared so much fun in playing Ping-Pong, in hiking and in discussing scientific problems. Dr. Bryan Hathorn gave me any help he could when I was working on the ozone problem, Miss Shachi Gosavi is always ready whenever I had a problem with the computer, and the discussion with Dr. Pavel Frantsuzov is certainly one of the most exciting things. I should also thank Mrs. Ruth de Silveira for much help in everyday life and in preparing several manuscripts.

Although my parents did not get much education because of the wars in China, they have been trying their best to pass the family tradition to my generation: read

as many good books as we can. I always remember that there is a whole supportive family wishing me happy and successful. Special thanks belong to my wife, Hui Fu, and my daughter, Can Gao. They are always beside me, encouraging me to explore whatever brings joy and satisfaction. Without their love, nothing would have been possible.

Abstract

Three separate topics, each stimulated by experiments, are treated theoretically in this dessertation: isotopic effects of ozone, electron transfer at interfaces, and intramolecular directional electron transfer in a supramolecular system.

The strange mass-independent isotope effect for the enrichment of ozone, which has been a puzzle in the literature for some 20 years, and the equally puzzling unconventional strong mass-dependent effect of individual reaction rate constants are studied as different aspects of a symmetry-driven behavior. A statistical (RRKM-based) theory with a hindered-rotor transition state is used. The individual rate constant ratios of recombination reactions at low pressures are calculated using the theory involving (1) small deviation from the statistical density of states for symmetric isotopomers, and (2) weak collisions for deactivation of the vibrationally excited ozone molecules. The weak collision and partitioning among exit channels play major roles in producing the large unconventional isotope effect in "unscrambled" systems. The enrichment studies reflect instead the non-statistical effect in "scrambled" systems. The theoretical results of low-pressure ozone enrichments and individual rate constant ratios obtained from these calculations are consistent with the corresponding experimental results. The isotopic exchange rate constant for the reaction $^{16}O + {}^{18}O^{18}O \rightarrow {}^{16}O^{18}O + {}^{18}O$ provides information on the nature of a variationally determined hindered-rotor transition state using experimental data at 130 K and 300 K. Pressure effects on the recombination rate constant, on the individual rate constant ratios and on the enrichments are also investigated. The theoretical results are consistent with the experimental data. The temperature dependence of the enrichment and rate constant ratios is also discussed, and experimental tests are suggested. The desirability of a more accurate potential energy surface for ozone in the transition state region is also noted.

Electron transfer reactions at semiconductor/liquid interfaces are studied using

a tight-binding model for the semiconductors. The slab method and a z-transform method are employed in obtaining the tight-binding electronic structures of semiconductors having surfaces. The maximum electron transfer rate constants at Si/viologen$^{2-/+}$ and InP/$Me_2Fc^{+/0}$ interfaces are computed using the tight-binding type calculations for the solid and the extended-Hückel for the coupling to the redox agent at the interface. These electron transfer reactions are also studied using a free electron model for the semiconductor and the redox molecule, where Bardeen's method is adapted to calculate the coupling matrix element between the molecular and semiconductor electronic states. The calculated results for maximum rate constant of the electron transfer from the semiconductor bulk states are compared with the experimentally measured values of Lewis and coworkers, and are in reasonable agreement, without adjusting parameters. In the case of InP/liquid interface, the unusual current *vs* applied potential behavior is additionally interpreted, in part, by the presence of surface states.

Photoinduced electron transfer reactions in small supramolecular systems, such as 4-aminonaphthalimide compounds, are interesting in that there are, in principle, two alternative pathways (directions) for the electron transfer. The electron transfer, however, is unidirectional, as deduced from pH-dependent fluorescence quenching studies on different compounds. The role of electronic coupling matrix element and the charges in protonation are considered to explain the directionality of the electron transfer and other various results. A related mechanism is proposed to interpret the fluorescence behavior of similar molecules as fluorescent sensors of metal ions.

Table Of Contents

Introduction

The research presented in this thesis focuses on the theoretical treatment of two types of chemical reactions: the recombination reaction of ozone and electron transfer reactions at semiconductor/liquid and metal/liquid interfaces and within a supramolecule. In this Introduction, I summarize the various chapters. The strange isotopic effects of the formation of ozone have been a puzzle in the geophysics and geochemistry literature for some 20 years and we hope to provide here a systematic explanation of the many and varied experimental observations. The research on the semiconductor/liquid interfacial electron transfer, as well as that on the directional electron transfer reaction in 4-aminonaphthalimide was also stimulated by experiments, the semiconductor experiments being those of Nate Lewis and coworkers at this institute.

Various ozone isotopic effects are considered in Chapters 1 and 2. Both the strange "mass-independent" isotope effect in ozone formation in "scrambled" system and the equally puzzling large unconventional mass-dependent effect in "unscrambled" systems are treated. The field itself, it has been suggested in the literature, provides added insight into diverse phenomena, such as stratospheric/tropospheric mixing, oxidative processes in the stratosphere and mesosphere, and the nature of ancient atmospheres. (References for the remarks in this introduction are given in the appropriate chapters.)

A small non-statistical factor introduced by Hathorn and Marcus is employed in applying the RRKM theory to the present treatment. However, the present study extends this previous work in our group in two major aspects, which now permit the treatment of a large body of data at various temperatures and pressures, instead of only at low temperatures (130 K) and low pressures (Most of the experimental data are at the room temperature.): (1) a hindered rotor transition state determined variationally is used instead of assuming a "loose" transition state, and (2) a weak collisional energy transfer and a master equation formalism is used for the recombination reaction of ozone, instead of the strong collision assumption used earlier. The

importance of weak collisions in the activation-deactivation processes has long been recognized, especially for understanding detailed experimental results on pressure effects in unimolecular reactions. Pressure and temperature effects on the recombination reaction rate constants, on the enrichment, and on the rate constant ratios are all treated in Chapters 3 and 4 of this thesis. These various experiments are listed in Table 1 of Chapter 1.

The information on the transition state is obtained from the temperature dependence of exchange reactions rate constant. Although the exchange reactions are studied at low pressures, the information they provide is, under a certain condition noted in Chapter 2, closely related to that which is normally provided by the high pressure rate constant. The assumption of a loose transition state, i.e., free rotation of the reacting diatomic molecule in the transition state, leads to a positive or only extremely small negative temperature dependence. Accordingly, to conform with the experimental data, which show a large negative temperature dependence, a hindered rotation of the diatomic species is incorporated in the present treatment of the transition state. The latter is located variationally and is then applied to study all the other effects considered in this thesis.

In Chapter 3, a treatment of the effect of pressure on bimolecular recombination and unimolecular dissociation is discussed. The analysis of recombination and dissociation is made by showing how the nonequilibrium energy (E) and angular momentum (J)-dependent steady-state population distribution functions for these reactions are related to each other and to the equilibrium population distribution function at that E and J. As a special case a strong collision model for the collisional angular momentum transfer and a step ladder model for the energy transfer, also used in Chapter 1 and 2, are used here. An analytical result is obtained for states below the dissociation threshold.

Electron transfer reactions at interfaces are treated in Chapters 4, 5 and 6. Electron transfer reactions at semiconductor electrode/liquid interfaces have been of interest in many experimental and theoretical studies. The understanding of the dynamics of these reactions has the potential of being helpful in constructing efficient and

stable photoelectrochemical cells and other applications, and in understanding the basic chemical reactions. Due to the instability and the non-ideal behavior of most semiconductor electrodes in contact with liquids, only recently have reliable kinetic measurements been performed at semiconductor/electrolyte interfaces. In Chapter 4 an estimate is made for the electronic coupling strength between the semiconductor bulk states and the molecular electron acceptor, using a tight-binding treatment of the solid and an extended Hückel treatment of the molecule. The semiconductor electronic wave functions are obtained using a "slab" method and a method developed some years ago in our group, the z transform method. The maximum electron transfer rate constant at Si/viologen$^{2+/+}$ and InP/$Me_2Fc^{+/0}$ interfaces are then calculated and compared with experiments.

Mainly motivated by the non-ideal behavior of the current/applied potential behavior at the InP/$Me_2Fc^{+/0}$ interface, the role of surface states in interfacial electron transfer reactions was also investigated. In treating the electron transfer at InP/$Me_2Fc^{+/0}$ interfaces, the possibility of surface states was subsequently included in Chapter 4, as one interpretation of the non-ideal current *vs* applied potential behavior in the experiments.

For a simpler description of the electron transfer reactions between the semiconductor bulk states and the molecular acceptors, a free electron model is developed in Chapter 5. In this model, the electrons in the semiconductor are treated as free electrons in a semi-infinite potential well with a constant potential inside the well and a known effective mass. The electronic wave function of the molecule is obtained by solving a Schrödinger equation whose potential is constant inside a spherical potential well and is zero outside. The electronic coupling matrix element is then obtained by adapting Bardeen's method, and from it an approximate expression for the maximum electron transfer rate constant.

In Chapter 7, the z-transform method is adapted to treat composite materials, e.g., solid/solid interfaces and "molecular wire"/solid interfaces. It proves to be useful for the study of both bulk and interfacial states for these materials. The existing conditions for interfacial states are obtained and discussed using this method. There

are many applications which could be made using this technique, evaluating and comparing with other methods which have been used in these systems, but the present study for this thesis was limited to being an exploratory one and to showing the feasibility of applying this approach to these series of problems of both scientific and technological interest.

In Chapter 8, photoinduced intramolecular electron transfer reactions in a supramolecular system (4-aminonaphthalimide) are treated. Of particular interest is the directionality of the electron transfer observed in the experiments. This selection of the electron transfer pathway was explained in the literature by assuming that a local internal electric field created on a molecular scale by excitation serves to direct the electron transfer. In the present study, the structure of the model system and the pH-dependent quenching of the fluorescence are considered, and an alternative explanation is proposed based on the calculation of the coupling matrix elements for the electron transfer reactions through the two different pathways. This mechanism also provides an explanation for the shift of spectra measured at different pH, and is also proposed to interpret the fluorescence behavior of similar molecules as fluorescent sensors of metal ions. Experimental tests are proposed.

In summary, the present doctoral dissertation treats theoretically problems in a variety of fields, which have in common that all were stimulated by striking, and in some cases puzzling, results in the literature. In the case of ozone problem, the results have previously defied explanation and it is hoped that the theory developed in this dissertation will provide a stimulation for understanding more deeply at the chemical physics level the wide variety of analogous recombination reactions in the upper atmosphere using isotopic tools. Many examples of unconventional isotopic effects have been reported in the geochemistry/geophysics/physical chemistry literature, but until now there has been no underlying theory which had the possibility of explaining them.

Chapter 1

Strange and unconventional isotopic
effects in ozone formation
(Submitted to Science)

Strange and Unconventional Isotope Effects in Ozone Formation

Yi Qin Gao and R. A. Marcus

Noyes Laboratory of Chemical Physics, Mail Code 127-72
California Institute of Technology
Pasadena, California 91125

Abstract

The puzzling mass-independent isotopic enrichment in ozone formation contrasts markedly with the more recently observed large unconventional mass-dependent ratios of the individual ozone formation rate constants in certain systems. An RRKM-based theory is used to treat both effects. This theory contains deviations from the statistical density of states, greater for the vibrationally hot symmetric than for the asymmetric ozone isotopomers, weak collisions for the deactivation of the vibrationally hot molecules, and variationally determined hindered rotor transition states. The resulting restrictions of symmetry on how energy is shared among the rotational/vibrational states of the ozone isotopomer, together with an analysis of the competition between the transition states of its two exit channels, permit the calculation of isotope effects consistent with a wide array of experimental results. Different types of experiments emphasize these different theoretical effects.

Introduction

A puzzling "mass-independent" isotope effect, reported in 1973 for $^{16}O/^{17}O/^{18}O$ ratios in meteorites initially was attributed to nucleosynthetic processes (*1*). The validity of that description is still uncertain. In 1981 the enrichment of ^{18}O in ozone in the upper atmosphere was observed (*2-6*), and in 1983 the mass-independent effect was found for ozone formation in the laboratory (*7-15*) and then in the upper atmosphere (*16-18*). Laboratory studies of the formation of ozone from the recombination of oxygen atoms and oxygen molecules have shown that there is an approximately equal enrichment of ^{17}O and ^{18}O over ^{16}O , instead of the enrichment ratio being the standard literature mass-dependent value (*19,20*) close to 1/2 found in other reactions [(cf., also (*21-24*)]. A "mass-independent" effect is also seen in heavily enriched mixtures (*25-29*). More recently, and paradoxically, large unconventional mass-dependent isotopic effects were observed under special experimental conditions ("unscrambled" conditions, i.e., little complication from isotopic exchange) (*30-33*). The theoretical treatment given in the present article is designed to treat mass-independent and mass-dependent processes, as well as others (*5,12-15,34-41*), and to show that there are two distinctly different effects in the theory, one dominant in the scrambled and the other dominant in the unscrambled experiments.

It was once thought that the explanation of the mass-independent effect might have a simple symmetry origin: In the formation of ozone with trace ^{17}O and ^{18}O, these isotopes have in common that they alone can form an asymmetric isotopomer, e.g., $^{17}O + {}^{16}O\ {}^{16}O \rightarrow {}^{17}O\ {}^{16}O\ {}^{16}O$. Statistically, $^{16}O\ {}^{16}O\ {}^{16}O$ possesses, because of the symmetry of the symmetric ozone, one half the number of quantum states that $^{17}O\ {}^{16}O\ {}^{16}O$ and $^{18}O\ {}^{16}O\ {}^{16}O$

do. However, it was subsequently recognized that this simple statistical factor of 1/2 is automatically incorporated into the definition of the enrichment [(cf also (*24*)], and so a different explanation was needed – even if it might involve symmetry in a subtler role (*42,43*).

Here we present a theory which draws upon the statistical (RRKM, Rice, Ramsperger, Kassel, Marcus) theory of unimolecular dissociation/bimolecular recombination reactions (*44,45*) in its variational form (*46-49*). It initially involves the formation of vibrationally excited ozone isotopomers from the recombination of O and O_2.

RRKM theory

In RRKM theory (*50*) for a bimolecular recombination X + YZ → XYZ^* (the asterisk denoting a vibrationally excited molecule) the vibrational-rotational energy of XYZ^* is assumed to be statistically distributed among its vibrational-rotational modes, consistent with the given total energy E of those modes (that is, a microcanonical distribution) and total angular momentum J. The molecule can redissociate, $XYZ^* \rightarrow$ XY + Z or X + YZ, or lose or gain in its excess energy by collisions, the losing being the more prominent, and eventually form a stabilized XYZ molecule. In the present instance of ozone formation, X, Y and Z may be the same isotope or any combination of different isotopes ^{16}O, ^{17}O, ^{18}O.

Because of the statistical assumption and the use of transition state theory (*50*), the unimolecular dissociation rate constant k_{EJ} for a vibrationally excited molecule of vibrational-rotational energy E and total angular momentum J is (*44-48*)

$$k_{EJ} = N^{\dagger}_{EJ} / h\rho_{EJ} \qquad (1)$$

where $N^{\ddagger}_{EJ}$ is the number of quantum states accessible to the "transition state" for the dissociation for the given E and J, and ρ_{EJ} is the density (number per unit energy) of quantum states of the vibrationally excited molecule. The bimolecular rate constant to form this hot molecule is given by a related expression, e.g., (*42, 43, 49*), because of "microscopic reversibility."

Nonstatistical aspects

As a modification of RRKM theory it is argued that the effective ρ_{EJ} in Eq. 1 might be less than the statistical value, and more so for the *symmetric* isotopomers XYX* than for XYZ*. This ρ_{EJ} should be only the density of the quantum states of the triatomic molecule that are sufficiently dynamically coupled to the two "exit channels" that they can lead to the dissociation of the molecule in the typical lifetime of the latter: After the formation of the vibrationally excited molecule the subsequent redistribution of the energy among its vibrational-rotational modes at the given E and J proceeds at some finite rate and may be incomplete during the typical lifetime of the molecule (the non-RRKM effect). The ρ_{EJ} in Eq. 1 should then refer only to the quantum states which have been equilibrated intramolecularly.

Examples are known from various experiments, e.g., (*51-53*), which illustrate the time needed for this internal equilibration of isolated molecules. Since there are fewer dynamical coupling terms (e.g., anharmonic vibration-vibration and Coriolis vibration-rotation) in the symmetric XYX than in the asymmetric XYZ, some terms being forbidden by the symmetry, it was suggested (*42,54*) that this nonstatistical (non-RRKM) effect for ρ_{EJ} is expected to be greater for XYX than for XYZ. This idea remains to be

tested by direct real-time experiments proposed later, or by very detailed accurate quantum dynamical calculations yet to be made.

The situation just described is depicted schematically in the cartoon in Fig. 1: during the typical lifetime of the dissociating ozone the shaded regions indicate the ozone quantum states sufficiently strongly coupled dynamically to the two exit channels so as to contribute to ρ_{EJ} during that lifetime. The shaded region for the asymmetric molecule is drawn as a greater fraction of the total region than is that for the symmetric molecule for the dynamics-based reason given above. The ratio of the fraction of shaded to total region for the asymmetric molecule to the same fraction for the symmetric molecule is denoted by η, a symbol introduced previously for this purpose (*42,54*).

New features in present treatment

In the recent article (*43*) which applied these ideas in (*42*) the simplest possible transition state for the reaction $X + YZ \rightarrow XYZ^*$ was assumed for convenience, namely, a transition state $XYZ^\dagger$, frequently called "loose," in which the YZ rotates freely. The transition state for a barrierless recombination reaction is typically loose when the energy of the recombining particles is low enough, e.g., (*43,55-58*). However, more generally, it is expected that the rotation of YZ is somewhat hindered in the transition state $XYZ^\dagger$, particularly with increasing total vibrational-rotational energy E of the ozone (*43, 55-58*). If, as at low energies, the $O_2 \ldots O$ distance in the $O_3^\dagger$ transition state is large, the O_2 indeed can rotate more or less freely. Although this simple assumption of free rotation of the O_2 in $O_3^\dagger$ was very useful in (*43*), we avoided it here in order to generalize this

previous work and so include in the treatment a much wider range of experimental temperatures and pressures. The two approaches are compared in (*49*).

A second major difference between the treatment in the present article and that in (*42, 43*) is the elimination of a "strong collision" assumption: it was assumed in (*43*) that every collision of the XYZ^* with a molecule M in the surrounding gas deactivates (and so stabilizes) an XYZ^*. In the case of "weak" collisions, on the other hand, the average energy lost by XYZ^* in "downward" collisions $\langle \Delta E \rangle$ and the energy gained in "upward" collisions can be relatively small. Some limited information on collisional energy transfer with vibrationally hot molecules such as XYZ^* is available in the literature from experiments and from classical trajectory calculations (*59-62*). A "master equation" (*47-49*) is now used to treat these weak collisions. The limitation imposed by weak collisions is profound: only XYZ^*'s with low energies (excess above threshold) can be deactivated at low pressures, collisions being few then, thereby affecting various properties, as listed later in Table 1.

To determine the nature of the transition state (e.g., loose, "tight," hindered) variational RRKM theory can be used, but some potential energy surface for the ozone formation is needed. At present, the *ab initio* surface in the literature (*63*) is inadequate. For example, there should be no energy barrier in the entrance channel from X + YZ (*64*). The use of an empirically modified surface (*65*) which eliminates this barrier led to results which disagreed (*49*) with the known isotopic exchange rate data. In the interim we have adopted (*49*) an approximate model which is consistent with those data. The potential energy surface and the calculation of the number of states $N_{E,J}$ along the reaction coordinate in a given exit channel serves to determine variationally (*50*) the transition

state (TS) for that channel, whose N_{EJ} is then denoted by $N_{EJ}^{\dagger}$, and appears in Eq. 1. The choice of transition state affects mostly the pressure effects and the temperature effects at higher pressures, and the isotopic exchange reactions, but it also has some influence on the other quantities listed later in Table 1.

Application to ozone formation

We consider a reaction scheme involving recombination, deactivation, activation and redissociation, given by $X + YZ \rightarrow XYZ^*$, $XYZ^* \rightarrow X + YZ$, $XYZ^* \rightarrow XY + Z$, and, further, a series of collisional activation/deactivation steps which can lead eventually to a full deactivation, $XYZ^* + M \rightarrow XYZ + M$. The second and third steps represent the two dissociative exit channels from XYZ^*, a and b, and are equivalent when Z = X. As a convention in these studies a was chosen (*42*) to be the exit channel with the lower zero-point energy of the diatomic molecule. The bimolecular rate constant of the above reaction, $X + YZ \rightarrow XYZ$, is denoted below by k_{bi}^{a} or k_{bi}^{b}, according as YZ or XY has the lower zero-point energy.

An expression can be obtained for the net bimolecular reaction rate constant k_{bi} for the recombination: To implement the collisional deactivation/activation scheme we employed (*49*) for simplicity a "stepladder" model (*48*), in which the XYZ^* gains or loses its energy in collisions in discrete amounts ("steps"), ΔE. In the interests of brevity, we use as an illustration here an expression for k_{bi} which is a special case of our more general results: We consider the special case where there is only one step of the ladder that is reactive but where there are any number of steps below the dissociation threshold of XYZ^* (*66*). We then have (*66*)

$$k_{bi}^{a} = \sum_{J} \int_{\Delta E} \frac{k_a k_{diff}}{k_a + k_b + k_{diff}} g_{eq} dE \qquad (2)$$

where $k_{a,b} \equiv k_{a,b}(EJ)$ is the dissociation rate constant given by Eq. 1. The k_{diff} denotes the rate constant for the stepwise collisional deactivation of XYZ^* (a stepwise "diffusion" process in energy space), and g_{eq} is the equilibrium distribution function of the (EJ) states of XYZ^*. The integration over E is over an interval equal to the step size ΔE, and the summation (or integration) is over all J. At low pressures, the k_{diff} in the denominator can be neglected, and in that case the factor $k_a/(k_a + k_b)$ in the integrand plays a prominent role for the individual rate constants. It equals $N_{EJ}^{a\dagger}/(N_{EJ}^{a\dagger} + N_{EJ}^{b\dagger})$ and was termed the partitioning factor Y_a in (*42, 43*), because it "partitions" the dissociation rate of XYZ^* into the two dissociation channels. The "strong collision" model used in (*42, 43*) can be retrieved from Eq. 2 by letting ΔE become very large. In that case it can also be shown that k_{diff} equals ω, the collision frequency appearing in (*42, 43*).

Enrichments

The enrichment δ of ^{17}O and that of ^{18}O over ^{16}O in the formation of ozone, denoting the ^{17}O or ^{18}O by Q , is defined by (*67,68*)

$$\delta^{Q} = \frac{Q/O \text{ in ozone}}{Q/O \text{ in oxygen}} - 1 \qquad (3)$$

Expressions for each δ^Q were given in (*42*) in terms of the individual rate constants and certain equilibrium constants.

When the study is made, instead, of systems heavily enriched in ^{17}O and/or ^{18}O, the definition used for the enrichment for an ozone molecule of mass M relative to $^{48}O_3$ is E^M (*25, 42*):

$$E^{M} = \left[\left(\frac{^{M}O_3}{^{48}O_3} \right)_{meas} \Big/ \left(\frac{^{M}O_3}{^{48}O_3} \right)_{calc} \right] - 1 \qquad (4)$$

The denominator in Eq. 4 is calculated statistically from the isotopic composition of the O_2 (*42*). The E^M can be shown to reduce to the δ^Q upon reducing the mole fractions of ^{17}O and ^{18}O to trace amounts (*49*).

Individual rate constants and ratios

The ratios of rate constants calculated for the specific isotopomeric recombination reactions, X + YZ → XYZ, are used to compare with the experimental data on them and also to calculate the enrichments δ^Q and E^M (*69*) and compare with the data on the latter. The expression (*42, 43*) for the exchange rate constants X + YY → XY + Y at low pressures, where the measurements of the isotopic exchange rates are made, was also readily obtained (*42, 43*): In the solution of the master equation in the low-pressure limit we note that the large majority of XYZ*'s will redissociate. When dissociation occurs via the other exit channel, an isotopic exchange has occurred. A simple expression for the isotopic exchange rate constant was then obtained. It is independent of the details of the collision process (*42*).

The individual recombination rate constants at low pressures were obtained using a more elaborate version of Eq. 2, one which involves the detailed solution of the master equation for the collisional deactivation/activation and reaction steps, for many "steps" in the stepladder (*49*). A ΔE ~210 cm^{-1} was used for the deactivating collisions (*49*). The two quantities, ΔE and η (= 1.18), were chosen to fit the two experimentally measured rate constant ratios at 300 K, $^{16}O + {}^{18}O^{18}O/{}^{16}O + {}^{16}O^{16}O$ and $^{18}O + {}^{16}O^{16}O/{}^{18}O + {}^{18}O^{18}O$ (*70*).

We note in passing that in Eq. 2 k_{diff} and the ρ_{EJ} in the k's occur as a product, since the k_{EJ} (here k_a and k_b) in Eq. 1 is proportional to $1/\rho_{EJ}$ and the g_{eq} is proportional to ρ_{EJ}. Thereby, all results for the present data would be unchanged if the η-effect were ascribed instead to a k_{diff}, as examined in (*49*).

Results

The various experimental results (Table 1, Figs. 2-4) are compared with the calculations. The results in Figs. 2 and 3 for the "unscrambled systems" show a strong and unconventional mass-dependence. Their correlation with ratios of masses given in Fig. 3 of (*43*) contrasts with the usual isotopic mass-dependence described for other reactions in a pioneering article (*71*). The results in Fig. 4 for E^M and those for δ^Q for trace systems show the "mass-independence": Although the enrichments of all isotopometers XYY + YXY in Fig. 4 are not exactly equal, i.e., strictly mass-independent, they are seen to vary far less widely than the ratios of k_{bi}'s do in Figs. 2 and 3. We have also indicated in Table 1 the relative importance of the various properties Y, η, ΔE, and TS (transition state) in each type of measurement.

Discussion

We first note that in the formation of ozone, the insertion reaction of O into O_2 is assumed to be negligible, in agreement with current data (*32*). Before proceeding to discuss the present results, we first comment on the heart of the explanation (*42,43*) for the paradox described earlier: Under *unscrambled* conditions the vibrationally hot molecule XYZ^* is formed only from one entrance channel, the channel depending on the

initial choice of reactants. Small differences in zero-point energies of these two entrance or exit channels lead to major effects on k_{bi}^{a} and k_{bi}^{b}: The unexpected effect of small differences in zero-point energies on the individual rate constants and rate constant ratios occurs by affecting the partitioning factors Y_a and Y_b. At the lowest energies $Y_a = 1$ and $Y_b = 0$, while once the zero-point energy of b has been exceeded, the number of states $N_{EJ}^{b\dagger}$ grows approximately as the square of its excess energy above this zero-point energy (*49*), but meanwhile $N_{EJ}^{a\dagger}$ has been growing roughly as the square of its excess over its zero-point energy. The result is a large difference (*49*) in Y_a and Y_b for most of the energy region of interest at low pressures (energies less than the step size), and so a k_{bi}^{a} can be quite large. For k_{bi}^{b}, in contrast, there is no low energy region where $Y_b = 1$. Instead, Y_b typically begins at $Y_b \cong 0$. In (*43*) it was shown that the individual recombination rate constants k_{bi} correlated well with a property which depended only on certain differences in masses, namely zero-point energies, moments of inertia, or reduced masses, all three of which were shown to be simply related to each other. (Cf Fig. 3 in (*43*) and the remarks in its Legend and in Sec. VI there.) Indeed, in the theory all three properties contribute to Y_a and Y_b (*43*).

Under isotopically "scrambled" conditions, i.e., conditions where extensive isotopic exchange affects the observations, both entrance channels leading to XYZ^{*} are accessed and it was shown mathematically that the partitioning factors Y_a and Y_b have disappeared (*42*). The essence of the underlying physical basis is surprisingly simple: entrance via the a channel yields a Y_a factor at low pressures, while entrance via the b channel yields Y_b. The sum $Y_a + Y_b$ is unity and so, for the enrichments, the partitioning

factors and their dramatic nonconventional isotope effect have vanished, because of this access to XYZ^* from both entrance channels. The nonstatistical effect mentioned earlier is the only influence now left and yields the "mass-independent" effect (*42, 43*), which is exhibited in Fig. 4 and in Table 1. The disappearance of the partitioning factors in the enrichment experiments yields the dramatic effect in Fig. 4, seen in the marked contrast between the $\eta = 1$ and the $\eta = 1.18$ results.

As the above discussions of the theory illustrate there are two types of isotope effects in the theory for the phenomena: There is the partitioning effect between the two competing transition states, which affects strongly the ratios of rate constants measured in "unscrambled" experiments, as in Figs. 2 and 3. There is also the non-RRKM effect in the ozone molecule itself, namely a deviation from the statistical (RRKM, microcanonical) density of states $\rho_{E,J}$ of the ozone isotopomer itself, and which differs for vibrationally excited symmetric (XYX) as compared with asymmetric (XYZ) ozone molecules. It is the principal factor affecting the enrichments. Thus, the two types of isotope effects, which are seen to have distinctly different theoretical origins, are also revealed separately by the two types of experiments, scrambled and unscrambled.

The comparison of many experiments and theory is summarized in Table 1. We first note that in the large body of experimental data listed there, some data are sensitive to the weak collision aspect, ΔE, but relatively insensitive to the nature of the transition state, while others are sensitive to the partitioning factors Y. Still others are sensitive to the nature of the potential energy surface and the transition state, and are denoted in Table 1 by TS. We have indicated in this Table which measurements are sensitive most to each of the quantities, ΔE, Y, η, and TS. For example, all of the data in Figs. 2-4, the low

pressure k_{bi} for $^{16}O + {}^{32}O_2 \rightarrow {}^{48}O_3$ and its temperature exponent n, are dependent on ΔE, the mean downward energy transferred from the XYZ^* per collision, but are *relatively* insensitive to TS, in particular to the short-range effects of the potential energy surface (*49*). The temperature effect on the individual rate constants is influenced by ΔE: the smaller the ΔE, the larger the negative exponent n in Table 1, since a smaller ΔE implies that a smaller proportion of the reacting molecules at the higher temperatures can contribute to the recombination rate at low pressures.

We have not shown the pressure effects on the enrichments and individual rate constant ratios but note that we have found the calculated results to be in reasonable agreement with the experiments (*49, 72*). The temperature effect on enrichment (*15*) remains to be explored theoretically, but one factor may be a decrease in η with decreasing temperature, because of a longer lifetime of O_3^* at low temperatures and so more time for redistribution. Dynamical information on η and ΔE which can be inferred from temperature effects, within the assumptions of the present theory, are described in the concluding remarks. Given an experimentally measured enrichment δ^o for Q = 17, 18 at other temperatures, predictions can be made of the various k_{bi}^a and k_{bi}^b's at those temperatures (*49*) and an example is given in (*49*).

The present results provide a rationale for an *ad hoc* assumption used in (*43*), though not here. In (*43*) a "loose transition state," which is appropriate for low energies, was used, together with strong collisions, to treat the experimental data in Figs. 2-4. The *ad hoc* assumption was that the ratios of these rate constants would approximate the ratios at room temperature, even though the latter have a hindered transition state. The

existence of the present $\bullet E$ tends to limit the actual low pressure studies to low energies. Thus, ozone molecules formed with an energy excess over the threshold greater than ΔE are not deactivated in a single collision regime, which is the regime occurring at low pressures, so providing a rationale for the use in (*43*) of low energy k_{bi}'s.

The key isotope effects in the present paper, η and Y, are in a sense symmetry-driven: the deviation of the Y's from 1/2 occurs for the asymmetric isotopomers, and the Y's are responsible for the large differences in individual rate constants and their ratios. The origin of η is also a consequence of symmetry.

The future

The question arises as to where the theory may go from here. There are individual features of the theory which can be tested using delicate molecular beam/laser excitation experiments (*49*), e.g., "pump-dump" or direct high overtone absorption to well-defined energies E: The weak dynamical couplings could lead to a real-time biexponential or multiexponetial dissociative decay, instead of the single exponential decay expected from the usual RRKM (microcanonical) behavior. The dissociative decay at long times would arise from the ozone quantum states weakly coupled to the two exit channels. An example of a biexponential decay exhibited in classical trajectory studies of a vibrationally excited triatomic molecule is seen in (*73*).

Further experiments on temperature effects are highly desirable and could provide further evaluation of concepts related to the lifetime of O_3^* and its effect on η and ΔE. For example, it was noted earlier that η and ΔE were calculated using two pieces of data: k_{bi} for $^{16}O + {}^{18}O{}^{18}O \rightarrow {}^{52}O_3$ and for $^{18}O + {}^{16}O{}^{16}O \rightarrow {}^{50}O_3$. A similar use of data at other temperatures, when they become available, would provide information on these two

quantities at the new temperatures (*74*). Alternatively, if ΔE were assumed to be approximately temperature-independent, then the enrichment at some temperature would suffice to determine η at that temperature, from which all other relevant quantities in Table 1 could be calculated and compared with future data (*74,75*). However, when possible, the first choice would be the use of the above two rate constant ratios.

Isotopic effects are widely studied for other reactions in the upper atmosphere, though not yet in the detail accorded to the ozone formation. For gas phase reactions where symmetric intermediates can occur the η would again enter, while for intermediates which are structurally asymmetric, the isotopic effect on η would disappear but some of the isotopic effect on Y can survive, leading to unconventional isotope effects. Thoroughly detailed studies of the type available for ozone would be highly desirable for these other reactions, and assist in the detailed understanding of them. Unconventional isotope effects have been invoked in discussions of stratospheric/atmospheric mixing, oxidative processes in the upper atmosphere, and ancient atmospheres (*76-79*).

In conclusion we note that the present theory is consistent with the experiments we have treated thus far, and can be used to make predictions. If the concepts are correct, it also provides detailed information on several dynamical effects.

References and Notes

1. R. N. Clayton, L. Grossman, T. K. Mayeda, *Science*, **182**, 485 (1973).
2. K. Mauersberger, *Geophys. Res. Lett.* **8**, 935 (1981).
3. M. M. Abbas, J. Guo, B. Carli, F. Mencaraglia, M. Carlotti, I. G. Nolt, *J. Geophys. Res.* **92**, 13231 (1987).
4. B. Carli, J. H. Park, *J. Geophys. Res.* **93**, 3851 (1988).
5. F. W. Irion, M. R. Gunson, C. P. Rinsland, Y. L. Yung, M. C. Abrams, A. Y. Chang, A. Goldman, *Geophys. Res. Lett.* **23**, 2377 (1996).
6. D. Krankowsky, P. Lammerzahl, K. Mauersberger, *Geophys. Res. Lett.* **27**, 2593 (2000).
7. J. E. Heidenreich III, M. H. Thiemens, *J. Chem. Phys.* **78**, 892 (1983).
8. M. H. Thiemens, J. E. Heidenreich III, *Science* **219**, 1073 (1983).
9. J. Yang, S. Epstein, *Geochim. Cosmochim. Acta* **51**, 2011 (1987).
10. M. H. Thiemens, T. Jackson, *Geophys. Res. Lett.* **14**, 624 (1987).
11. J. E. Heidenreich III, M. H. Thiemens, *J. Chem. Phys.* **84**, 2129 (1986).
12. M. H. Thiemens, T. Jackson, *Geophys. Res. Lett*, **15**, 639 (1988).
13. S. K. Bains-Sahota, M. H. Thiemens, *J. Phys. Chem.* **91**, 4370 (1987).
14. M. H. Thiemens, T. Jackson, *Geophys. Res. Lett.* **17**, 717 (1990).
15. J. Morton, J. Barnes, B. Schueler, K. Mauersberger, *J. Geophys. Res.* **95**, 901 (1990).
16. K. Mauersberger, *Geophys. Res. Lett.* **14**, 80 (1987).
17. B. Schueler, J. Morton, K. Mauersberger, *Geophys. Res. Lett.* **17**, 1295 (1990).
18. D. Krankowsky, F. Bartecki, G. G. Klees, K. Mauersberger, K. Schellenbach, *Geophys. Res. Lett.* **22**, 1713 (1995).

19. An excellent review of the conventional (mass-dependent) effect in chemistry, as well as of the history of the mass-independent effect and of previous attempts to explain it is given in (*20*). It also includes an up-dated review of a correlation-symmetry view of the mass-independent effect in (*21*). An early review and theoretical examination of the mass-independent effect is given in (*23*).

20. R. E. Weston, Jr. *Chem. Rev.* **99**, 2115 (1999).

21. G. I. Gellene, *Science* **274**, 1344 (1996) and references cited therein.

22. J. A. Kaye, D. F. Strobel, *J. Geophys. Res.* **88**, 8447 (1983).

23. J. A. Kaye, *J. Geophys. Res.* **91**, 7865 (1986).

24. S. M. Anderson, J. A. Kaye, *Geophys. Res. Lett.* **24**, 91 (1987).

25. J. Morton, B. Schueler, K. Mauersberger, *Chem. Phys. Lett.* **154**, 143 (1989).

26. K. Mauersberger, J. Morton, B. Schueler, J. Stehr, S. M. Anderson, *Geophys. Res. Lett.* **20**, 1031 (1993).

27. D. Krankowsky, K. Mauersberger, *Science* **274**, 1324 (1996).

28. K. Mauersberger, B. Erbacher, D. Krankowsky, J. Günther, R. Nickel, *Science* **283**, 370 (1999).

29. S. Wolf, B. Biter, D. Krankowsky, K. Mauersberger, *J. Chem. Phys.*, **113**, 2684 (2000).

30. S.M. Anderson, D. Hülsebusch, K. Mauersberger, *J. Chem. Phys.* **107**, 5385 (1998).

31. J. Günther, B. Erbacher, D. Krankowsky, K. Mauersberger, *Chem. Phys. Lett.* **306**, 209 (1999).

32. C. Janssen, J. Günther, D. Krankowsky, K. Mauersberger, *J. Chem. Phys.* **111**, 7179 (1999).

33. J. Günther, D. Krankowsky, K. Mauersberger, *Chem. Phys. Lett.* **324**, 31 (2000).

34. J. C. Johnston, M. H. Thiemens, *J. Geophys. Res.* **102**, 25395 (1997).

35. J. Sehested, O. J. Nielsen, H. Egsgaard, N. W. Larsen, T. Pedersen, L. K. Christensen, M. Wiegell, *J. Geophys. Res.* **100**, 20979 (1995).

36. L. K. Christensen, N. W. Larsen, F. M. Nicolaisen, T. Pedersen, G. O. Sorensen, H. Egsgaard, *J. Mol. Spectrosc.* **175**, 220 (1996).

37. A. Meier, J. Notholt, *Geophys. Res. Lett.* **23**, 551 (1996).

38. M. R. Wiegell, N. W. Larsen, T. Pedersen, H. Egsgaard, *Int. J. Chem. Kinet.* **29**, 745 (1997).

39. J. Sehested, O. J. Nielsen, H. Egsgaard, N. W. Larsen, T. S. Andersen, T. Pedersen, *J. Geophys. Res.* **103**, 3545 (1998).

40. S. M. Anderson, F. S. Klein, F. Kaufman, *J. Chem. Phys.* **83**, 1648 (1985).

41. H. Hippler, R. Rahn, J. Troe, *J. Chem. Phys.* **93**, 6560 (1990).

42. B. C. Hathorn, R. A. Marcus, *J. Chem. Phys.* **111**, 4087 (1999).

43. B. C. Hathorn, R. A. Marcus, *J. Chem. Phys.* **113**, 9497 (2000).

44. R. A. Marcus, *J. Chem. Phys.* **20**, 359 (1952).

45. R. A. Marcus, *J. Chem. Phys.* **43**, 2658 (1965), *J. Chem. Phys.* **52**, 1018 (1970).

46. D. M. Wardlaw, R. A. Marcus, *Adv. Chem. Phys.* **70**, 231 (1988).

47. R. G. Gilbert, S. C. Smith, *Theory of Unimolecular and Recombination Reactions* (Blackwell Scientific Publications, Boston, 1990).

48. K. A. Holbrook, M. J. Pilling, S. H. Robertson, *Unimolecular Reactions* John Wiley & Sons, New York, (1996), 2nd ed.

49. Y. Q. Gao, R. A. Marcus, *J. Chem. Phys.* submitted for publication.

50. Transition state theory, a theory in the chemical literature for some sixty-five years, is still the standard theory of choice for treating chemical reaction rates at a given temperature. Its counterpart for molecules of a given energy E is RRKM theory (microcanonical transition state theory), which was developed some fifteen years later (*44*). In its usual formulation either theory assumes a quasi-equilibrium between the reactant or reactants and the "transition state," a critical set of configurations from which, once reached, there is no return to the original reactant or reactants but rather the system proceeds to form the product or products. Because of the quasi-equilibrium aspect, concepts such as "free energy of activation" and "statistical mechanical partition function" appear in the canonical (i.e., temperature-based) transition state theory and concepts such as number of quantum states $N^{\ddagger}_{EJ}$ in the transition state and density of states ρ_{EJ} of the unimolecularly dissociating or isomerizing molecule appear in its microcanonical counterpart, RRKM theory (Eq. 1). The transition state for the forward reaction is the same as that of the reverse reaction and it occurs at the maximum of a free energy barrier in canonical transition state theory, or at the minimum of an entropy barrier (minimum N_{EJ}) at the given energy E and J in RRKM theory. This maximum or minimum property confers on it the title "variational transition state theory" or "variational RRKM theory."

51. I. Oref, B. S. Rabinovitch, *Accts. Chem. Res.* **12**, 166 (1979), and references cited therein.

52. R. Weinkauf, P. Archer, G. Wesley, J. Grotemeyer, E. W. Schlag, *J. Chem. Phys.* **98**, 8381 (1994). See also (*80*).

53. S. K. Kim, J. Guo, J. S. Baskin, A. H. Zewail, *J. Phys. Chem.* **100**, 9202 (1996).

54. The shaded region for XYZ in the present Fig. 1 was assumed to be absent in (*42*). This assumption affects only absolute rates, but has no effect on the ratios of the rate constants, and so no effect on the present Figs. 2-4.

55. W. L. Hase, *J. Chem. Phys.* **64**, 2442 (1976).

56. M. Quack, J. Troe, *Ber. Bunsenges. Phys. Chem.* **81**, 329 (1977).

57. G. P. Smith, D. M. Golden, *Int. J. Chem. Kinet.* **10**, 489 (1978).

58. S. J. Klippenstein, R. A. Marcus, *J. Chem. Phys.* **91**, 2280 (1989).

59. E.g., G. Lendvay, G. C. Schatz in *Advan. Chem. Kinet. Dyn.* **2B**, 481 (1995), and references cited therein.

60. J. R. Barker, B. M. Toselli, *Int. Revs. Phys. Chem.* **12**, 305 (1993), and references cited therein.

61. R. G. Gilbert, *Aust. J. Chem.* **48**, 1787 (1995) (review).

62. A. J. Stace, J. N. Murrell, *J. Chem. Phys.* **68**, 3028 (1978).

63. C. Leforestier, F. LeQuéré, K. Yamishita, K. Morokuma, *J. Chem. Phys.* **101,** 3806 (1994).

64. The need for a barrierless potential energy surface is reflected in the negative temperature coefficient of the various recombination and isotopic exchange reactions, e.g., in (*45*) and in (*38*), and also in Table 1, and in the absolute values of the rate constants given there. Apart from an electronic degeneracy factor, they are near gas-kinetic. The expression in (*63*) gives, instead, an energy barrier.

65. A. Gross, G. D. Billing, *Chem. Phys.* **217**, 1 (1999).

66. R. A. Marcus, Y. Q. Gao, *J. Chem. Phys.* **114**, 0000 (2001) (June 8 issue).

67. H. Craig, *Geochim. Cosmochim. Acta.* **12**, 133 (1957).

68. Y. Matsuhisa, J. R. Goldsmith, R. N. Clayton, *Geochim. Cosmochim. Acta.* **42**, 173 (1978).

69. The E^M was expressed in (*42*) in terms of the individually calculated recombination rate constants. To obtain an expression for these enrichments E^M and δ^Q and still allow for the numerous isotopomers of each species, it was noted that certain ratios of statistical mechanical partition functions (not the partitioning factors *Y*!) were equal to unity, within several thousandths (*42*). This approximation provided a considerable simplification of a large number of reaction equations involving the many permutations of X, Y and Z and led to simple final expressions in (*42*) involving individual rate constants k_{bi} and certain equilibrium constants.

70. For the present calculations of the rate constants and of the enrichments E^M for the many isotopomers, only 26 of the 54 isotopomeric vibration frequencies were known, and the missing ones were needed in the calculations for densities of states ρ_{EJ}. A second-order perturbation formulation gave the unknown frequencies to an accuracy of about 1 cm^{-1}, quite sufficient for the present purpose (*81*). The long-range part of the interaction potential $-C_6/r^6$ was used in the calculation of the potential energy surface, in addition to the short-range potential terms, C_6 being obtained from collision cross-sections for $O + O_2$ (*82*). The anharmonicity effect on the density of states ρ_{EJ} was obtained from vibrational spectra of ozone molecules (*83*), by fitting those data to a theoretical expression containing the various anharmonicity constants (*49*). The various enrichments and rate constants were calculated using the relevant equations given in (*42, 43*) but now using the presently calculated values of the various k_{bi}'s and of the various equilibrium constants appearing in those expressions.

71. J. Bigeleisen, M. G. Mayer, *J. Chem. Phys.* **15**, 261 (1947).

72. One effect on which we have not commented thus far is the role of collisions in stimulating vibrational energy redistribution within a molecule, a known process: In principle, some "active states" formed in the recombination, and so contributing to ρ_{EJ}, could be converted to the less active states by collision and so have their dissociative lifetime prolonged prior to the next collision. Unless the collision cross-section for energy redistribution were extremely large, the calculated low pressure results in Table 1 and Figs. 2-4 would be unaffected by these collisions at low pressures.

73. R. A. Marcus, W. L. Hase, R. N. Swamy, *J. Phys. Chem.* **88**, 6717 (1984).

74. Within certain limits, the inference of ΔE from the data can only be very approximate: The calculated k_{bi} ratio for $^{16}O + {}^{18}O{}^{18}O \rightarrow {}^{52}O_3/{}^{16}O + {}^{16}O{}^{16}O$ was changed from 1.53 to 1.50 when ΔE was changed from 210 cm^{-1} to 250 cm^{-1}. In contrast, an unrealistic ΔE = 23 cm^{-1} changes this k_{bi}^{a} ratio to about 2.36 (namely, 2η) and the related k_{bi}^{b} to 0. The dependence of Fig. 4 on η is seen by comparing the results there for η = 1.0 with those for η = 1.18. Analogous plots for several values of η are given in (*43*).

75. An example is given in (*53*) for 130 K.

76. J. Farquhar, H. M. Bao, M. H. Thiemens, *Science* **289**, 756 (2000).

77. H. Bao, M. H. Thiemens, J. Farquhar, D. A. Campbell, C. C.-W. Lee, K. Heine, D. B. Loope, *Nature* **406**, 176 (2000).

78. M. H. Thiemens, *Science* **283**, 341 (1999).

79. M. H. Thiemens, T. Jackson, E. C. Zipf, P. W. Erdman, C. van Egmond, *Science* **270,** 969 (1995).

80. R. Knochenmuss, *J. Phys. Chem.* **99**, 3381 (1995).

81. B. C. Hathorn, R. A. Marcus, *J. Phys. Chem. A*, **105**, 0000 (2001), June 14 issue

82. B. Brunetti, G. Liuti, E. Luzzatti, F. Pirani, F. Vecchiocattivi, *J. Chem. Phys.* **74**, 6734 (1981), Table I.

83. V. G. Tyuterev, S. Tashkun, P. Jensen, A. Barbe, T. Cours, *J. Mol. Spectrosc.* **198**, 57 (1999).

84. It is a pleasure to acknowledge the support of this research by the National Science Foundation, and the helpful discussions with Dr. Bryan Hathorn in its early stages. The authors are very pleased to acknowledge helpful comments by Professors Konrad Mauersberger, Stuart Anderson, and Mark Thiemens, by Dr. Ralph Weston, by Dr. Jesse Smith, and by the reviewers.

Table 1. Comparison of experiment and theory. All quantities in units of cm^3 molecule$^{-1}s^{-1}$ are to be multiplied by 10^{-12}. In the last column, the quantities in parentheses are less important. The quantities are defined in the text.

Experiments	Calculated Results	Sensitivity
Ratios of rate constants, Figs. 2 and 3 (*28, 30-33*)	Figs. 2 and 3	ΔE, Y, η
Enrichments ^{17}O (11.3%), ^{18}O (13.0%) at 300 K (*7-15*)	12.0 and 12.2%, respectively	η , (ΔE)
Heavily enriched systems, Fig. 4 (*25-29*)	Fig. 4	η , (ΔE)
Low pressure $^{16}O + {}^{32}O_2 + M \rightarrow {}^{48}O_3 + M$, $k_{bi} = 5 \times 10^{-34}$ cm^6 molecule$^{-2}s^{-1}$ (*41*)	9×10^{-34} cm^6 molecule $^{-2}s^{-1}$	ΔE
$k_{bi} \alpha T^{-n}$, $n = 2.6$ (130-300 K) (*41*)	$n = 2.2$	ΔE
k_{ex} $^{16}O + {}^{18}O\,{}^{18}O \rightarrow {}^{16}O{}^{18}O + {}^{18}O$, 2.9 ± 0.8 cm^3 molecule$^{-1}s^{-1}$ (300 K), 5.6 cm^3 molecule$^{-1}s^{-1}$ (130 K), $k_{ex} \alpha T^{-m}$, $m = 0.88 \pm 0.26$ (*38*)	Fitted to data: 2.7 cm^3 molecule$^{-1}s^{-1}$ (300 K), 4.3 cm^3 molecule$^{-1}s^{-1}$ (130 K), $m = 0.53$	TS
High pressure k_{bi} $^{16}O + {}^{32}O_2 \rightarrow {}^{48}O_2$, 18 cm^3 molecule$^{-1}s^{-1}$ (130 K), >4 cm^3 molecule$^{-1}s^{-1}$ (300 K) (limiting value not reached) (*41*)	10.4 cm^3 molecule$^{-1}s^{-1}$ (130 K), 6.5 cm^3 molecule$^{-1}s^{-1}$ (300 K)	TS, ΔE (at high T)
Pressure effects on enrichments (*14,15*)	Broad agreement (*53*)	η , (ΔE)
Pressure effects on rate constant ratios (*33*)	Broad agreement (*53*)	ΔE, Y, η
Temperature effect on rate constant ratios	Approximate prediction from temperature effect on enrichments δ^Q	ΔE, Y, η
Temperature effect on enrichment (*15*)		

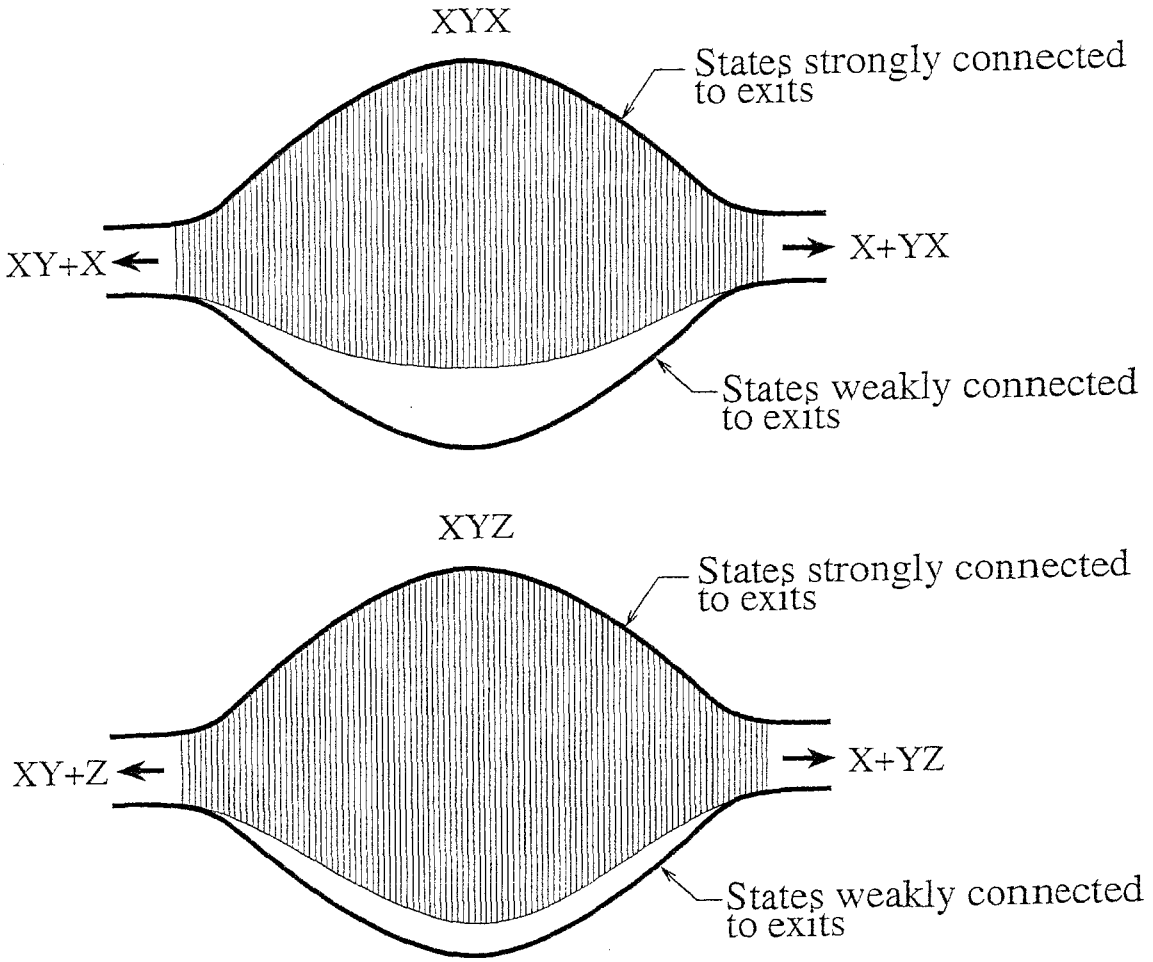

FIG. 1. Schematic picture for XYX and for XYZ of differences in ratios of rotational-vibrational states of ozone strongly coupled (shaded region) to the two dissociation exit channels of ozone and those that weakly coupled (unshaded region) to the exit channels. This difference in ratios has an origin in symmetry, as noted in the text and discussed in (*42*). In one limit the unshaded region is absent for XYZ.

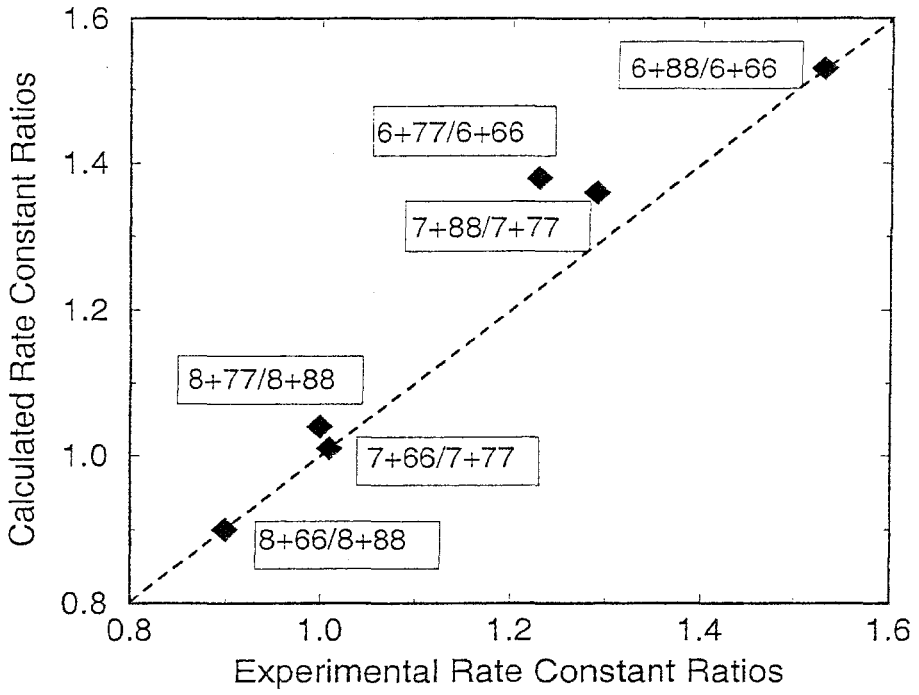

FIG. 2. Comparison of calculated and experimental(*28*) relative atom + diatomic rate constant ratios, k_{X+YY}/k_{X+XX}, at 300 K with $\eta = 1.18$. A typical symbol in a box, such as 8+77/8+88, refers to the ratio of rate constants for $^{18}O + {}^{17}O^{17}O \rightarrow {}^{18}O^{17}O^{17}O$ to $^{18}O + {}^{18}O^{18}O \rightarrow {}^{18}O^{18}O^{18}O$. The (uncertain) concentration ^{18}O cancels when the ratios of such rate constants are obtained from mass spectrometric measurements.

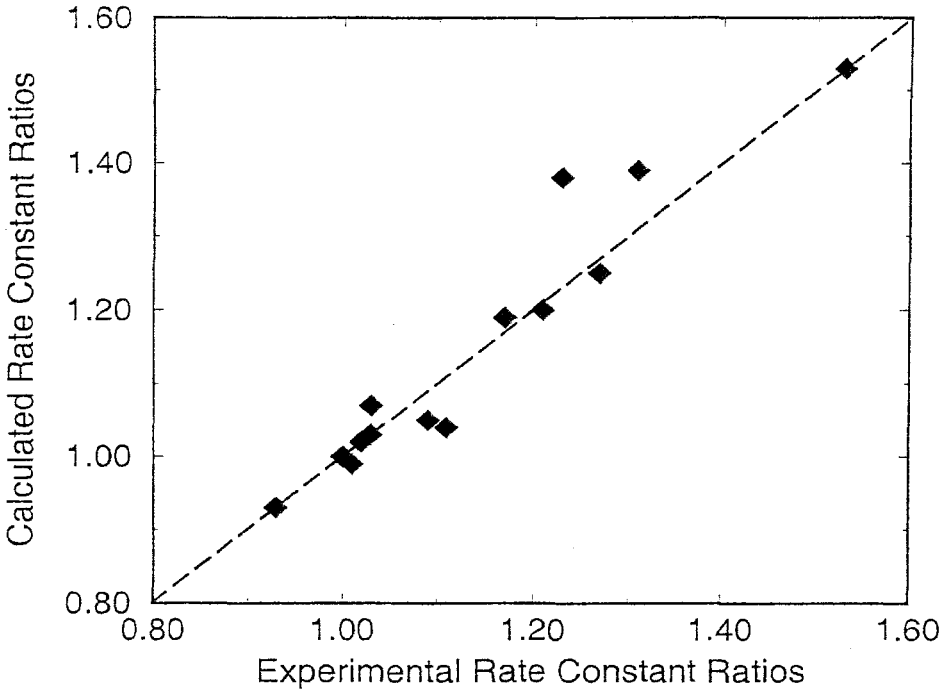

FIG. 3. Comparison of calculated and experimental(*28*) relative atom + diatomic rate constant ratios, k_{X+YZ}/k_{6+66}, at 300 K with $\eta = 1.18$. Some of the experimental rate constants are "derived quantities"(*28*). The $6+66$ denotes the recombination reaction $^{16}O + {}^{16}O^{16}O \rightarrow {}^{16}O^{16}O^{16}O$.

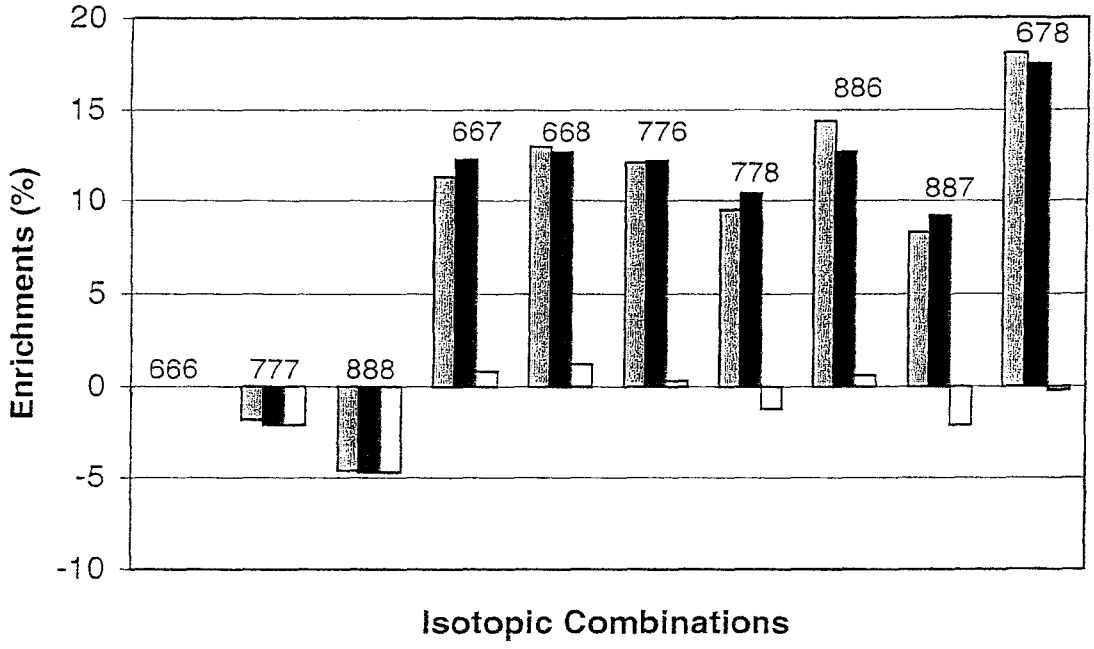

FIG. 4. Experimental(*28*) (gray bars) and calculated isotopic enrichments for scrambled systems heavily enriched in heavy isotopes at 300 K, with $\eta = 1.18$ (dark bars) and $\eta = 1.0$ (light bars) respectively. A typical symbol, such as 668, denotes an ozone with the isotopic composition $^{16}O^{16}O^{18}O$ and consists of the asymmetric ($^{16}O^{16}O^{18}O$) and symmetric ($^{16}O^{18}O^{16}O$) isotopomers.

Chapter 2

On the theory of the strange and unconventional isotopic effects in ozone formation
(Submitted to J. Chem. Phys.)

On the theory of the strange and unconventional Isotopic Effects in Ozone Formation

Yi Qin Gao and R.A. Marcus

Noyes Laboratory, 127-72
California Institute of Technology
Pasadena, CA 91125

Abstract

The strange mass-independent isotope effect for the enrichment of ozone and the contrastingly unconventional strong mass-dependent effect of individual reaction rate constants are studied here as different aspects of a symmetry-driven behavior. A statistical (RRKM) based theory with a hindered-rotor transition state is used. The individual rate constant ratios of recombination reactions at low pressures are calculated using the theory involving (1) small deviation from the statistical density of states for symmetric isotopomers, and (2) weak collisions for deactivation of the vibrationally excited ozone molecules. The weak collision and partitioning among exit channels play major roles in producing the large unconventional isotope effect in "unscrambled" systems. The enrichment studies reflect instead the non-statistical effect in "scrambled" systems. The theoretical results of low-pressure ozone enrichments and individual rate constant ratios obtained from these calculations are consistent with the corresponding experimental results. The isotopic exchange rate constant for the reaction $^{16}O + {}^{18}O^{18}O \rightarrow {}^{16}O^{18}O + {}^{18}O$ provides information on the nature of a variationally determined hindered-rotor transition state using experimental data at 130 K and 300 K. Pressure effects on the recombination rate constant, on the individual rate constant ratios and on the enrichments are also investigated. The theoretical results are consistent with the experimental data. The temperature dependence of the enrichment and rate constant ratios is also discussed. Experimental tests are

suggested. The desirability of a more accurate potential energy surface for ozone in the transition state region is also noted.

It is shown that the two type of experiments (scrambled and unscrambled) reveal markedly different aspects of the ozone problem. In unscrambled systems the partitioning effect is dominant, and it is shown how small differences in zero-point energies of the two exit channels of dissociation of an asymmetric ozone isotopomer lead to large differences in numbers of states in the two transition states and, thereby, to large differences in the individual recombination rate constants. For experiments on scrambled systems it was shown [*J. Chem. Phys.* **112**, *9497 (2000)*] that the partitioning factors disappear exactly and what is left is the nonstatistical effect. It is pointed out how both aspects can be regarded as "symmetry driven" isotopic effects.

I. INTRODUCTION

There is a wide variety of observations involved in the study of the isotopic effect in the recombination of oxygen atoms and oxygen molecules. We have summarized these results elsewhere.[1] The various experiments involve a "mass-independent" isotope effect in ozone formation in scrambled systems[2–24] and contrastingly different experimental results[25–29] in unscrambled systems, which show dramatic unconventional mass-dependent effects. In addition, there is the temperature effect on the low-pressure recombination reaction,[30] the isotopic exchange reaction,[31] and the isotopic enrichment,[12] and the pressure effect on the recombination rate constant,[30] the isotopic enrichment[9,12,13,28] and the individual rate constant ratios.[28] It has been proposed that the field itself provides added insight into diverse phenomena, such as stratospheric/tropospheric mixing, oxidative processes in the stratosphere and mesosphere, and other aspects.[32–35]

As noted in earlier papers from our group,[36,37] the difference in physical terms in the theory of the two types of experiments, scrambled and unscrambled, is that in the unscrambled experiments only one of the entrance channels from $O + O_2$ to form a vibrationally excited ozone isotopomer, such as XYY*, is accessed, e.g., $X + YY \rightarrow XYY^*$. In scrambled experiments XYY* is formed also *via* the additional channel, $Y + XY \rightarrow XYY^*$, since the isotopic exchange reaction $X + YY \rightleftharpoons XY + Y$ is extensive under scrambled conditions. A different and mass-specific percentage of the transition state phase space of the two exit channels, described by a "partitioning factor," is occupied when the access to it arises only from one channel. This difference in conditions led in the kinetic scheme to a marked difference in the theoretical expressions[36] for the two types of experiments.

The present study extends the previous work in our group in this field in two major aspects, which permits the treatment of a large body of data at various temperatures and pressures, instead of just[37] at low temperatures: (1) a hindered rotor transition state determined variationally is used instead of a "loose" transition state, and (2) a weak collisional energy transfer and a master equation formalism is used for the

recombination reaction of ozone, instead of the strong collision model used earlier.[37] The importance of weak collisions in the activation-deactivation processes has long been recognized,[38–43] especially for understanding the detailed experimental results on pressure effects.[44–49]

As before variational RRKM theory[50,51] is used as the zeroth-order theory, with a small perturbation correction for the effective density of states of symmetric isotopomeric ozone molecules, XXX and XYX, as compared with the asymmetric ones YXX or YXZ. (This correction is apart from symmetry numbers, which are also included.) The "non-RRKM" correction is small (the density of states for the symmetric ozone isotopomers are reduced by a factor η, chosen later to be 1.18) relative to what such a correction could be, but is large in its consequence for the phenomena discussed in the present paper.[36] More generally, as noted elsewhere,[1] the asymmetric ozone may also show deviation from the statistical behavior, but the deviation is greater for the symmetric ozones. In the latter certain anharmonic vibrational coupling and Coriolis rotational-vibrational coupling terms are absent, because of the symmetry, so leading to an extra nonstatistical effect for the symmetric isotopomers. It is the coupling terms which are responsible for the intramolecular statistical behavior.

By introducing the weak collision model for the deactivation of the excited ozone molecule by collisions with bath gas molecules (in this study, N_2), rate equations for the population density as a function of the energy E and of the total angular momentum J are obtained for ozone recombination reactions. For the collisional angular momentum transfer of ozone a strong collision model is used, which leads to a one-dimensional model for the energetic ozone in the energy space. A similar reduction of the dimension of the master equations for a unimolecular dissociation reaction had been used by Smith and Gilbert.[52]

An important quantity in the weak collisions is the average energy of downward transfer ΔE, $\langle \Delta E \rangle$, for the deactivating collisions. Studies have revealed that typically the results for the energy transfer depend mainly on this $\langle \Delta E \rangle$, and are relatively insensitive to the functional form of the energy transfer.[44,45] In the present study, for

simplicity, a stepladder model is used. In the latter the energy transferred between the excited ozone molecule and a bath gas molecule occurs in discrete steps, ΔE. Thus, at low pressures where only one collision is important during the lifetime of a vibrationally excited ozone molecule only low energy states of the energetic ozone molecules, those with energy less than ΔE above the threshold, can lead to stabilized (deactivated) ozones.

The isotopic exchange reaction of ozone is also considered in the present study. Normally, information about the transition state for a recombination reaction, such as $^{16}O + {}^{32}O_2 \rightarrow {}^{48}O_3$, would be inferred from the magnitude and temperature dependence of the high pressure rate constant. However, for ozone formation the behavior of the rate constant k_{bi} versus third-body pressure becomes surprisingly complex at high pressures, except at the lowest temperature studied, 130 K: A plot of $\log(k_{bi})$ versus $\log(pressure)$ swoops upward at high pressures, before tending to approach a high-pressure limit. Until the complexity of the high pressure behavior is understood (and several possibilities have been suggested[30]), information about the transition state must be sought from other sources. One such set of data, which would be collision-free, would be the dissociation behavior of ozone, studied as a function of energy in suitable "pump-dump" time-resolved molecular beam experiments. However, these experiments have yet to be done.

An actually available source of data are the isotopic exchange reactions,[31,53,54] which are studied at low pressures. Under a certain condition noted later they provide information closely related to that which normally would be provided by the high pressure rate constant. In particular, under a certain assumption noted below, an expression for the isotopic exchange rate constant is given by Eq. (8) below [Eq. (1.12) of Ref. 36]. It is seen there to be independent of the density of the quantum states of the energetic ozone molecule and of the deactivational effect of third-bodies, factors that are prominent in the expression for the low pressure limit of k_{bi}. It is also free of the complicating effects of pressure at high pressures.

The principal assumption made in this interpretation of the isotopic exchange rate constant is that once an energetic ozone molecule is formed in the recombination it

loses its memory of its initial conditions, apart from the presence of certain constants of the motion. This common statistical assumption is by no means proven for the present system but is useful as a zeroth-order starting point. Indeed, we mentioned a postulated small deviation from statistical theory for symmetric isotopomers, but even this correction need not influence the partitioning of the states between the two exit channels and hence the exchange reaction.

In utilizing the isotopic exchange rate constant data of the reaction

$$^{16}O + ^{18}O_2 \rightarrow ^{16}O^{18}O + ^{18}O \qquad (1)$$

we consider both the absolute value of the rate constant and its negative temperature coefficient. This negative dependence[31] is particularly important, since the assumption of a loose transition state, i.e., free rotation of the reacting diatomic molecule in the transition state, leads to a positive or only an extremely small negative temperature dependence. Accordingly, to conform with the experimental data[31] we have found that it is necessary to have a hindered rotation of the diatomic species in the transition state.

A third topic in the present article is on various pressure effects on ozone formation reactions. There exist mainly three types of experiments on the pressure effects: that on the recombination reaction $^{16}O + ^{32}O_2 \rightarrow ^{48}O_3$ at different temperatures,[30] that on the isotopic enrichment,[9,12,13,28] and that on the individual recombination rate constant ratios for forming ozone isotopomers.[28] In the present study, these pressure effects are treated using the weak collision approximation and a hindered-rotor transition state. A method of solving the rate equations at any given pressure is developed for the recombination reactions using a strong collision model for the rotational angular momentum transfer. Without further approximation, the master equation with E and J as coordinates is reduced to a one-dimensional problem with E as the coordinate and then solved numerically.

A fourth topic discussed in the present article is the temperature effect on the isotopic enrichment[12] and on the individual recombination rate constant ratios.

The manner in which the present paper is distinguished from previous papers[36,37]

from our group is three-fold: (1) a weak collision model is introduced, implemented in the present paper using a stepladder model for a series of deactivating and activating collisions, (2) a hindered-rotor variational transition state is used and compared with the free rotor results, and (3) a greater variety of experimental effects can now be treated, such as pressure and temperature effects, because of (1) and (2). In an earlier paper[37] the room temperature data on ratios of reaction rates were indeed treated with very encouraging results. Nevertheless, because the limitation of the transition state used and of the strong collision model, it was necessary to introduce an *ad hoc* assumption in that treatment: low pressure ratios were calculated at low temperatures (130 K, where the transition state is more or less loose) and it was assumed that the same ratio would apply to the room temperature data. This assumption in Ref. 37 is eliminated in the present paper.

The paper is organized as follows: the theory involving a hindered-rotor transition state theory and a master equation approach is described in Sec. II. Expressions are obtained for rate constants of isotopic exchange reaction, the individual recombination reactions including an effective rate constant k_{bi}^{eff}[36] contributing to studies made with isotopically scrambled conditions (extensive isotopic exchange) and so contributing to the theoretical expression for the enrichment δ or E described in Ref. 36. A numerical procedure of treating the pressure effects for recombination reactions is also described there. The expressions are used in Sec. III to calculate the rate constants and for the enrichment, and to obtain various pressure and temperature effects. The results are discussed in Sec. IV. A simple explanation of the large effect of small differences in zero-point energies of the competing exit channels of a dissociating molecule is given in Sec. IV D and Fig. 13 there. Temperature effects on isotopic enrichments and on rate constant ratios are discussed in Sec. IV E.

We use extensively a relation obtained in the first paper of this series,[36] relating the enrichments to the individual rate constants. Those equations are independent of the approximations made in calculating the rate constants, e.g., hindered vs free rotor and weak vs strong collisions.

II. THEORY

A. General Remarks

The kinetic process of an ozone formation reaction involving many collisions, leading ultimately to a master equation, can be written as

$$\mathrm{X} + \mathrm{YZ} \rightarrow \mathrm{XYZ}(E,J) \qquad k_r^a(E,J), \tag{2}$$

$$\mathrm{XYZ}(E,J) + \mathrm{M} \rightarrow \mathrm{XYZ}(E',J') + \mathrm{M} \qquad \omega(E,J \rightarrow E',J'), \tag{3}$$

$$\mathrm{XYZ}(E',J') \rightarrow \mathrm{X} + \mathrm{YZ} \qquad k_a(E',J'), \tag{4}$$

$$\mathrm{XYZ}(E',J') \rightarrow \mathrm{XY} + \mathrm{Z} \qquad k_b(E',J'), \tag{5}$$

and, in a series of steps to form a stable ozone molecule of energy E^l, E^l being an energy sufficiently below the dissociation threshold that the molecule XYZ has a negligible chance of reacquiring enough energy by collisions to dissociate

$$\mathrm{XYZ}(E,J) + \mathrm{M} \rightarrow \mathrm{XYZ}(E^l,J') + \mathrm{M} \qquad \omega(E,J \rightarrow E^l,J'). \tag{6}$$

Here, X, Y and Z denote oxygen atoms, which may or may not be different isotopes. The energy and the total angular momentum are conserved in individual recombination and dissociation reactions. The $k_r^a(E,J)$ and $k_a(E,J)$ ($k_b(E,J)$) are the E and J-dependent rate constants of recombination and dissociation reactions, respectively, and $\omega(E,J \rightarrow E',J')$ is the rate of forming XYZ at (E',J') from (E,J) by a collision with a third body. For dissociation there exist the two distinguishable exit channels, a and b, when X$\neq$Z. For a symmetric molecule, where X=Z, the designation (a,b) is omitted. By convention,[36,37] the channel with the lower zero-point energy of the diatomic species is denoted by a. Thus when YZ has a higher zero-point energy than XY, the rate constant for Eq. (2) would be written as k_r^b instead of k_r^a.

The rate equation for the population distribution function $g(E,J) = c(E,J)/[\mathrm{X}][\mathrm{YZ}]$, $c(E,J)$ being the population of ozone molecules in the various quantum states (E,J), can be written as[55]

$$\frac{dg(E,J)}{dt} = k_r^a(E,J) - [k_d^a(E,J) + k_d^b(E,J) + \omega]g(E,J)$$

$$+\sum_{J'}\int_{E'}\omega(E',J'\rightarrow E,J)g(E',J')dE', \tag{7}$$

where ω is the integral of $\omega(E,J\rightarrow E',J')$ over E' and J'.

B. The Isotopic Exchange Reaction and the Hindered-rotor Transition State Theory

The hindered-rotor transition state theory described in this section is used to obtain an expression for the isotopic exchange reaction rate constant for ozone. The expression for the rate constant k_{ex}^{a} of the isotopic exchange reaction, e.g., Eq. (1), is given by[37]

$$k_{ex}^{a}=\frac{1}{hQ_a}\sum_{J}\int_{E}\frac{N_a^{\dagger}(E,J)N_b^{\dagger}(E,J)}{N_a^{\dagger}(E,J)+N_b^{\dagger}(E,J)}e^{-E/k_BT}dE, \tag{8}$$

where Q_a is the partition function of the reacting pair in the center of mass system of coordinates for channel a, $N_a^{\dagger}(E,J)$ is the number of states of the transition state for exit channel a of ozone dissociation at the given E and J, and $N_b^{\dagger}(E,J)$ is that for the second channel of the energetic ozone molecule. Each of the two exit channels has a transition state (TS) and each TS is determined variationally for each E and J as a function of a selected reaction coordinate for that channel. If a component K of the total angular momentum J, namely the one involving the rotation of the energetic molecule about the axis with the smallest moment of inertia, were also assumed to be an invariant, each $N^{\dagger}(E,J)$ would be replaced by $N^{\dagger}(E,J,K)$ and the summation in Eq. (8) would be over J and K. One common assumption in the unimolecular dissociation/bimolecular recombination literature is to treat K as "active," i.e., not as a constant, and for simplicity we adopt this approximation here.

For the orbital-hindered rotational part of the Hamiltonian, we use body-fixed axes with the line of centers **R** of the atom and the diatomic molecule serving as the body-fixed z-axis. The Hamiltonian H, apart from the kinetic energy for the radial (R) motion, can be written as

$$H=\frac{\mathrm{j}^2}{2I}+\frac{\mathrm{l}^2}{2\mu R^2}+V(r,R,\theta) \tag{9}$$

where $\mathbf{j}^2$ is the square of the angular momentum operator for the diatomic molecule, I the moment of inertia of the latter, $\mathbf{l}^2$ the square of the orbital angular momentum operator, R the distance between the atom and the center of mass of the diatomic fragment, r the instantaneous bond length of that fragment, and θ the angle between $\mathbf{R}$ and $\mathbf{r}$, the vector along the axis of the diatomic molecule. Following a common procedure[56–59] we transform from a space-fixed $|jlm_jm_l\rangle$ representation to another space-fixed $|jlJM_j\rangle$ one, and then from the latter to a body-fixed representation $|jJM_j\Omega\rangle$, where Ω is the component of $\mathbf{J}$ along the body-fixed z-axis. Since $\mathbf{l}$ is perpendicular to the body-fixed z-axis, it follows that Ω is also the component of $\mathbf{j}$ along this z-axis. One finds that $\mathbf{j}^2$ is diagonal in this representation, as is $\mathbf{J}^2$, but not $\mathbf{l}^2$. When $\mathbf{l}^2$ is expressed in terms of $\mathbf{J}$ and $\mathbf{j}$, we have

$$\mathbf{l}^2 = (\mathbf{J}-\mathbf{j})\cdot(\mathbf{J}-\mathbf{j}) = \mathbf{J}^2 - 2\mathbf{j}\cdot\mathbf{J} + \mathbf{j}^2. \tag{10}$$

In body-fixed components $\mathbf{j}\cdot\mathbf{J}$ is $j_zJ_z + j_xJ_x + j_yJ_y$, i.e., $j_zJ_z + j_+J_- + j_-J_+$, where the $J_\pm = J_x \pm iJ_y$, and similarly for $j_\pm$, are the usual raising and lowering operators. In the matrix $\langle j'\Omega'|H|j\Omega\rangle$ in the body-fixed $|j\Omega\rangle$ representation (JM_J is suppressed for notational brevity), we have the well-known result, in units of $\hbar = 1$, for the elements diagonal in Ω ($\Omega' = \Omega$),[56–59]

$$H_{j\Omega,j'\Omega} = \langle j\Omega|H|j'\Omega\rangle = \left[\frac{j(j+1)}{2I} + \frac{J(J+1)+j(j+1)-2\Omega^2}{2\mu R^2}\right]\delta_{jj'} + V_{j\Omega,j'\Omega}. \tag{11}$$

For the elements off-diagonal in Ω ($\Omega' \neq \Omega$), we have

$$H_{j\Omega,j'\Omega'} = \langle j\Omega|H|j'\Omega'\rangle = -\frac{1}{2\mu R^2}[J(J+1)-\Omega\Omega']^{1/2}[j(j+1)-\Omega\Omega']^{1/2}\delta_{jj'}\delta_{\Omega'\Omega\pm1}. \tag{12}$$

The potential energy matrix element in the body-fixed frame $V_{j\Omega,j'\Omega}$ is given by

$$V_{j\Omega,j'\Omega} = \int\int Y^*_{j\Omega}V(r,R,\theta)Y_{j'\Omega}d(\cos\theta)d\phi, \tag{13}$$

where the Y's are spherical harmonics. Integration is immediately made over ϕ. For any given Ω the conditions on the matrix elements are that

$$j \geq |\Omega|, \quad J \geq |\Omega|. \tag{14}$$

In performing the θ-integration in Eq. (13), one half of the $\cos\theta$ domain is assigned to the entrance channel to XYZ, XY + Z $\rightarrow$ XYZ, and the other half to the second entrance channel, X + YZ $\rightarrow$ YXZ.

In the present calculation of the energy levels of the transition state, we shall neglect the elements off-diagonal in Ω ($\Omega' \neq \Omega$), and so diagonalize the matrix by setting $|H_{j\Omega,j'\Omega} - E\delta_{jj'}| = 0$. The neglect of off-diagonal elements ($\Omega' \neq \Omega$) when considering the radial motion of the two reactants has been variously termed in the collision dynamics literature as the "j_z-conserving," "coupled state," or "centrifugal decoupling" approximation.[59] It is well known that typically a zeroth-order body-fixed description is better at short separation distances R than the space-fixed, and vice versa at large R.[57] At very large initial R, Ω is the projection of $\mathbf{j}$ and of $\mathbf{J}$ along the initial wave vector $\mathbf{k}$, the line of the centers. The evolution of Ω as R decreases is of interest in a full collision dynamics calculation, but in the present case of a statistical calculation we are principally interested in the accessibility of the quantum states rather than in the detailed coupling between states of different Ω's.

As a kinetic scheme we consider initially a system forming an energetic ozone molecule with given total angular momentum J and an energy in the range (E, $E + dE$) in the center of mass system of coordinates. The mechanism of the isotopic exchange reaction X+YY$\rightarrow$ XY+Y is given by Eqs. (2), (4) and (5), with the Z being replaced by Y. The expressions for the k's are readily obtained: The probability of finding the (X, YY) pair with the specified J and in a phase space volume element $dqdp$ for motion along the reaction coordinate q is $(2J + 1)\exp(-E/k_BT)dqdp/hQ_a$, where Q_a is the partition function for the reacting pair in this center of mass system of coordinates. To obtain the incident probability flux we divide by dq and multiply by $\dot{q}$, the velocity along the reaction coordinate. The contribution to the rate constant from this J and energy range, (E, $E + dE$), after summing over all accessible states n, is

$$dk_r^a(E, J) = \sum_n (2J + 1)e^{-E/k_BT}h(E - E_n^{J,a})dE/hQ_a \qquad (15)$$

where $h(E - E_n^{J,a})$ is the unit step function, $E_n^{J,a}$ the energy barrier along q associated

with the state Jn for channel a, and where we have used the relation $\dot{q}dp = (p/\mu)dp = d(p^2/2\mu) = dE$, μ being the reduced mass of motion along q. It is noted here that only one half of θ space at the transition state is assigned to the channel leading to the expected product XYZ.

Each state nJ has its own "transition state," corresponding to the maximum of its energy along the reaction coordinate. We assume a local adiabaticity near each maximum, rather than assuming a global one for all values of the reaction coordinate q (taken here to be R), i.e., rather than assuming that Ω is constant through the motion along R. The sum over n in Eq. (15) is over Ω and over the quantum number j for the hindered rotation, since the oxygen molecule remains in its lowest vibrational quantum state in the transition state region in the present system, reflecting the wide spacing of its vibrational energy levels. Before collision the four appropriate quantum numbers were j, l, and their projections on space-fixed axes, but now they are replaced by $JM_J\Omega$ and the quantum number for hindered rotation. The M_J gives rise to the $2J+1$ factor in Eq. (15).[60]

For the $k_d^a(E,J)$ in Eq. (4), the rate constant for dissociation of the vibrationally excited XYY back into the incident channel, the RRKM expression in the present notation is

$$k_d^a(E,J) = \sum_{j,\Omega}(2J+1)h(E - E_{j\Omega}^{J,a})/h\rho(E,J) \tag{16}$$

where $\rho(E,J)dE$ is the number of quantum states of the XYY with the given J and in $(E, E+dE)$. The summation in Eq. (16) and later is over j and Ω, with the restriction $|\Omega| \leq j$. The dE in the numerator arose, as before, from $(dqdp/h)\dot{q}/dq = dE/h$, and the $\rho(E,J)dE$ includes a $2J+1$ factor. If it were assumed that the body-fixed projection Ω were constant during the lifetime of the vibrationally excited XYY ("adiabatic rotation") it would have been added to the EJ in $\rho(E,J)dE$.

For the $k_d^b(E,J)$ in Eq. (5) for dissociation to XY+Y, we have similarly

$$k_d^b(E,J) = \sum_{j,\Omega}(2J+1)h(E - E_{j\Omega}^{J,b})/h\rho(E,J) \tag{17}$$

where the sum is over the states (j,Ω) of the exit channel b.

When a vibrationally excited XYY is formed from X+YY in the energy range dE and with the given J, the probability that it forms the exchange products XY+Y is $k_d^b(E,J)/[k_d^b(E,J)+k_d^a(E,J)]$ at low pressures (i.e., where collisional deactivation or activation is negligible relative to dissociation). Thereby k_{ex}^a, the isotopic exchange rate constant at low ω, becomes

$$k_{ex}^a = \int_E \sum_J \frac{(2J+1)\sum_{j,\Omega} h(E-E_{j\Omega}^{J,a})\sum_{j,\Omega} h(E-E_{j\Omega}^{J,b})e^{-E/k_BT}dE}{[\sum_{j,\Omega} h(E-E_{j\Omega}^{J,a})+\sum_{j,\Omega} h(E-E_{j\Omega}^{J,b})]hQ_a}, \tag{18}$$

which is the same as Eq. (8) in the present notation for the $N^\dagger$'s. When the incident channel is b rather than a, the a's and b's are interchanged.

C. Stepladder model for the collisional energy transfer

In the following, we consider a collisional energy transfer model which is applied in the following sections both to obtain an expression for the low-pressure recombination rate constant and to study the pressure effect on the ozone formation reaction. For simplicity, a stepladder model for the collisional energy transfer is used in the present study. A schematic depiction of this collisional energy transfer model is given in Fig. 1. In this model, only a certain amount of energy ΔE is transferred from an ozone molecule to a bath molecule in a collision. In Fig. 1, there exists a ladder of N steps for the energy levels,[62] E_1, $E_2 = E_1 + \Delta E$, $\cdots$, $E_N = E_1 + (N-1)\Delta E$, where N is some cut-off beyond which the contribution to the formation rate constant is negligible. States with energies less than E_1 are sufficiently below the dissociation threshold that their probability of reacquiring energy to dissociate is negligible, and are treated together as a sink. The energy E_1 is later varied to ensure that the calculated rate constant converge to a finite value. It has been shown that the flux below the threshold can be treated analytically,[61] and the arguments are summarized in the present Appendix B. In such a model, there exist many (an infinite number) sets of ladders, each differing in their starting energy. In the following, we first obtain the solution for a single ladder, i.e., a single set of ladder steps which has a fixed E_1. The total rate constant is then obtained by summing the rate constants over all the

ladders, i.e., integrating over E_1 in an interval (step size) ΔE.

Using the stepladder model, when $E' > E$ the collision becomes a deactivation and the $\omega(E', J' \rightarrow E, J)$ can be written as

$$\omega(E', J' \rightarrow E, J) = \omega_d t(J' \rightarrow J)\delta(E' - E - \Delta E), \tag{19}$$

where ω_d is the deactivation collision frequency and is assumed to be independent of E in the region of interest (close to the dissociation threshold).

The $t(J' \rightarrow J)$ in Eq. (19) is the transition probability from a total angular momentum J' to J. Under an assumption of a strong collision for rotational angular momentum transfer, $t(J' \rightarrow J) = P(J)$, where $P(J)$ is the thermal distribution of the rotational states of XYZ with a total angular momentum J at a given temperature.[52] The frequency ω_a for activation collisions is related to ω_d by microscopic reversibility:

$$\omega_a \rho(E - \Delta E) = \omega_d \rho(E) e^{-\Delta E/k_B T}, \tag{20}$$

where $\rho(E-\Delta E) = \sum_J \rho(E-\Delta E, J)$ and $\rho(E) = \sum_J \rho(E, J)$ (Appendix A). Further, for a range of energies near the dissociation threshold, $\rho(E)$ can be approximated as a constant, and so a relation $\omega_a = \omega_d e^{-\Delta E/k_B T}$ will be used for ω_a and ω_d. It should be noted that under these assumptions the total collision frequency ω in Eq. (7) is now $\omega_a + \omega_d = \omega$.

Using the stepladder and strong rotational collision model described above, the rate equation for the population density of XYZ at (E_n, J), $g(E_n, J)$, can be written as

$$\frac{dg(E_n, J)}{dt} = k_r^a(E_n, J) - [k_d^a(E_n, J) + k_d^b(E_n, J) + \omega]g(E_n, J) + P(J)\omega_d \sum_{J'} g(E_{n+1}, J') + P(J)\omega_a \sum_{J'} g(E_{n-1}, J'), \tag{21}$$

where E_n is an energy in the nth ladder in the stepladder model, and $E_{n+1} - E_n = E_n - E_{n-1} = \Delta E$.

D. Recombination Reactions at Low Pressures

In the present study, as also in Ref. 52 for the dissociation case, the two-dimensional master Eq. (7) is reduced to a one-dimension problem using the strong

collision approximation for rotational angular momentum transfer. The derivation given below is for recombination reactions at the low pressure limit. A derivation which applies at all pressures is given in the following section. We first note that for energies above the threshold, there exist, in principle, in steps Eqs. (2), (4) and (5), two types of quantum states due to the conservation of the total angular momentum. The effective dissociation barrier heights differ for different J's because of their different centrifugal barrier. At each energy above the dissociation threshold, ozone states with small centrifugal barriers are able to dissociate via one or both of the exit channels (open channels), but the states with higher barriers have a zero $k_d(E,J)$ (closed channels), and can only be either further deactivated or activated by collisions in later steps.

Thus, in the following treatment, states with a given energy $E_n > D_0$, where D_0 is the dissociation energy at $J = 0$ of the ozone isotopomer via the exit channel having the smaller zero-point energy, are divided into open and closed states by their total angular momentum. An open state has an angular momentum J such that $k_d^a(E_n,J) + k_d^b(E_n,J) > 0$, while $k_d^a(E_n,J') + k_d^b(E_n,J') = 0$ for a closed state with an angular momentum J'. Clearly, if $E_n < D_0$ there exist only closed states.

The rate equations for the population density g of the closed states contain only collision terms, and thus can be written as

$$\frac{dg(E_n,J)}{dt} = -\omega g(E_n,J) + P(J)\omega_d g_{n+1} + P(J)\omega_a g_{n-1}, \tag{22}$$

where $g_{n+1} = \sum_{J'} g(E_{n+1},J')$, $g_{n-1} = \sum_{J'} g(E_{n-1},J')$, and ω_a and ω_d are treated as independent of n in the region of n of interest. (A more general model which allows for the dependence of ω_a on n is given in Ref. 61.) A rate equation for the sum of the population densities over all closed states at energy E_n is obtained by summing both sides of Eq. (22) over states with $k_d^a(E_n,J') + k_d^b(E_n,J') = 0$ at this energy

$$\frac{dg_n^c}{dt} = -\omega g_n^c + P_n^c\omega_d(g_{n+1}^c + g_{n+1}^o) + P_n^c\omega_a(g_{n-1}^c + g_{n-1}^o), \tag{23}$$

where g_n^c is the sum of population densities over J of closed states with an energy E_n, P_n^c is the sum of $P(J)$ over the closed states at that energy, P_n^o is the corresponding

quantity for the open states, and $g_{n+1} = g^c_{n+1} + g^o_{n+1}$ is the total population density of states with an energy E_{n+1}. We note here that P^c_n is a function of energy, since whether a state with a total angular momentum J is closed or not is dependent on its energy.

Since for any ladder m, where $E_m < D_0$, there exist only closed states, the population density of states with such an energy E_m can be simply written as g_m. The rate equation for g_m contains only collisional terms, thus can be written as

$$\frac{dg_m}{dt} = -\omega g_m + \omega_d g_{m+1} + \omega_a g_{m-1} \qquad 1 < m \leq M, \tag{24}$$

while for $m = 1$,

$$\frac{dg_1}{dt} = -\omega g_1 + \omega_d g_2. \tag{25}$$

For the population density g_0 of states with energy less than E_1, we have

$$\frac{dg_0}{dt} = \omega_d g_1, \tag{26}$$

because these states are treated together as a sink. The rate constant for the formation of a stable ozone molecule via this set of ladders is then given by $\omega_d g_1$.

To obtain the rate equations for the open states, we focus on the recombination reactions at the low pressure limit in the following. In this limit, the collision terms in Eq. (21) are small compared to the terms containing k's, and can be neglected. Under steady-state conditions, the population density of an open state can be obtained by neglecting the ω terms in Eq. (21). We have then in the steady-state at low pressures

$$g(E_n, J) = \frac{k^a_r(E_n, J)}{k^a_d(E_n, J) + k^b_d(E_n, J)}. \tag{27}$$

The rate equations for the population density g^o_n over open states can be written at low pressures, from Eqs. (21) and (27), as

$$\frac{dg^o_n}{dt} = k^a_r(E_n) - k_d(E_n) g^o_n, \tag{28}$$

where g^o_n is the sum of the population densities of the open states, $\sum_{J,open} g(E_n, J)$, $dg^o_n/dt = 0$ in the steady-state,

$$k_r^a(E_n) = \sum_J k_r^a(E_n, J), \tag{29}$$

and the $k_d(E_n)$ is an averaged dissociation rate constant,

$$k_d(E_n) = \frac{\sum_J k_r^a(E_n, J)}{\sum_J [k_r^a(E_n, J)/(k_d^a(E_n, J) + k_d^b(E_n, J))]}. \tag{30}$$

In all cases the summation is over the J of states having a total energy E_n.

Combining the rate equations for the closed states (Eqs. (23)−(25)) and open states (Eq. (27)), and using the steady-state assumption, we have a set of linear equations. In the case of N steps in any ladder, M of which are below the dissociation energy, we have $2N - M$ variables, written as $g_1, \cdots, g_M, g_{M+1}^o, g_{M+1}^c, \cdots, g_N^o, g_N^c$, and $2N - M$ linear equations. From this set of equations, one then obtains the expression for the population density g_1 of molecules with an energy E_1, and thus for the rate constant $\omega_d g_1$ of the reaction via this set of energy ladders. The final expression for the low pressure recombination rate constant for channel a is then obtained by an integration over all sets of ladders,

$$k_{bi}^{0,a} = \frac{\omega_d - \omega_a}{Q_a} \left(\int_0^{\Delta E} \sum_J \rho(E, J) Y_a(E, J) e^{-E/k_B T} \frac{\omega}{\omega_d + \omega_a P^o(E)} dE + \right.$$
$$\left. \int_{\Delta E}^{2\Delta E} \sum_J \rho(E, J) Y_a(E, J) e^{-E/k_B T} \frac{\omega_d P^c(E - \Delta E)}{\omega_d + \omega_a P^o(E - \Delta E)} dE + \cdots \right), \tag{31}$$

where $\rho(E, J)$ is the density of states of the isotopomer, $Y_a(E, J) = N_a^\dagger(E, J)/(N_a^\dagger(E, J) + N_b^\dagger(E, J))$ is the partitioning factor, and $P^o(E - \Delta E)$ is defined as $1 - P^c(E - \Delta E)$. Here, $N_a^\dagger(E, J)$ and $N_b^\dagger(E, J)$ are the number of quantum states in the transition state at the E and J. In Eq. (31) and in later equations D_0, the dissociation energy of the channel with a smaller zero-point energy, is defined as the zero of energy. The states with energies higher than $2\Delta E$ have negligible contributions to Eq. (31) at low pressures (cf Appendix B) and could be neglected. A derivation of Eq. (31) is given in Appendix B.

E. Effective rate constants and enrichments in scrambled systems

The method for the calculation of enrichments for a scrambled system was described in detail in Ref. 36 and 37 and is only sketched here. For a scrambled system

at low pressures the isotopic exchange reactions,

$$\mathrm{X} + \mathrm{YZ} \rightleftharpoons \mathrm{Z} + \mathrm{XY} \tag{32}$$

where $\mathrm{Z} \neq \mathrm{X}$, are extensive, and a local isotopic equilibrium between atomic and diatomic species is readily established. Reaction (32) occurs *via* a highly energetic intermediate, XYZ*, which can either dissociate to form products of (32) or the reactants, or more rarely be deactivated by collision to form XYZ, as discussed in the previous section.

The rate of recombination to form a stabilized XYZ under these conditions of rapid isotopic exchange is

$$\frac{d\mathrm{XYZ}}{dt} = k_{bi}^{0,a}\mathrm{X}\cdot\mathrm{YZ} + k_{bi}^{0,b}\mathrm{Z}\cdot\mathrm{XY} = k_{bi}^{eff,a}\mathrm{X}\cdot\mathrm{YZ} \tag{33}$$

where

$$k_{bi}^{eff,a} = k_{bi}^{0,a} + k_{bi}^{0,b}K_{ex} = k_{bi}^{0,a} + k_{bi}^{0,b}\frac{Q_b}{Q_a}. \tag{34}$$

Here, K_{ex} is the equilibrium constant for reaction (32) and the Q's are conventional partition functions containing the zero-point energies. The combination of rate constants in (35) appears below, and in Refs. 36 and 37, as $k_{6,q6}^{as}+k_{q,66}^{as}K_{ex}$ in an expression for the isotopic enrichment δ, the superscript as denoting the formation of an asymmetric isotopomer. Equations (31) and (33) lead to

$$k_{bi}^{eff,a} = \frac{\omega_d - \omega_a}{Q_a}\left(\int_0^{\Delta E}\sum_J \rho(E,J)e^{-E/k_BT}\frac{\omega}{\omega_d + \omega_a P^o(E)}dE + \int_{\Delta E}^{2\Delta E}\sum_J \rho(E,J)e^{-E/k_BT}\frac{\omega_d P^c(E-\Delta E)}{\omega_d + \omega_a P^o(E-\Delta E)}dE\right) \tag{35}$$

For the $k_{bi}^{eff,b}$, we have a similar expression, but with Q_a replaced by Q_b. We note from this result that, as in the strong collision model, the partitioning factor $N_a^\dagger/(N_c^\dagger+N_b^\dagger)$ and $N_b^\dagger/(N_a^\dagger + N_b^\dagger)$ have disappeared, an exact result.

The enrichments can then be calculated with the rate constants obtained using the method described in Refs. 36 and 37 and the equilibrium constant for the corresponding isotopic exchange reaction. When two of the three isotopes are present in

trace amounts, the enrichment is calculated with equations in Ref. 37: Eqs. (4.18a) and (4.18b) for E_{ijj}, and (4.26) for E_{ijk} for unequal i, j, and k . In Eqs. (4.18a) and (4.18b) there, $k^{as}_{\mathrm{X,YZ}}$ is the rate constant for the channel X+YZ→XYZ only, while in Eq. (4.26) each k^{as} denotes the total formation rate constant for the sum of the two isotopomeric ozone molecules. The enrichment E_{ijj} is readily shown[63] to be the same as ${}^{i}\delta$ when $j = 16$ and when i (=17 or 18) is only present in trace amounts. The derivation of Eqs. (4.18) and (4.26) in Ref. 36 involved treating a large number of permutations of isotopes in the ozone and in the oxygen molecule and atom, and was considerably facilitated by an approximation (good to a few parts per thousand) relating the various isotopic oxygen atom concentrations to the various isotopic oxygen molecule concentrations.

F. Pressure Dependence of Rate Constants and Enrichments

We next describe the solution of rate Eqs. (21) at arbitrary pressures, using the stepladder energy transfer model described in Sec. II C. As in the preceding section, the angular momentum transfer is treated using the strong collision approximation, and the rate equations in coordinates E and J are first reduced to a problem of one coordinate E, and then solved numerically for the ozone formation rate constant.

We first note that under the steady-state approximation, the left-hand side of Eq. (21) is zero, and we have for the population density $g(E_n, J)$,

$$g(E_n, J) = \frac{k_r^a(E_n, J) + P(J)\omega_d \sum_{J'} g(E_{n+1}, J') + P(J)\omega_a \sum_{J'} g(E_{n-1}, J')}{k_d^a(E_n, J) + k_d^b(E_n, J) + \omega}, \qquad (36)$$

where the $\sum_{J'} g(E_{n+1}, J')$ is, as before, denoted by g_{n+1}, the population density of ozone states with an energy E_n. Similarly, $\sum_{J'} g(E_{n-1}, J') = g_{n-1}$, the population density of states with an energy E_{n-1}. Summing both sides of Eq. (36) over the angular momentum J, we have then

$$g_n = U_n + V_n g_{n+1} + W_n g_{n-1} \qquad (37)$$

where

$$U_n = \sum_J \frac{k_r^a(E_n, J)}{k_d^a(E_n, J) + k_d^b(E_n, J) + \omega}, \tag{38}$$

$$V_n = \sum_J \frac{P(J)\omega_a}{k_d^a(E_n, J) + k_d^b(E_n, J) + \omega}, \tag{39}$$

$$W_n = \sum_J \frac{P(J)\omega_d}{k_d^a(E_n, J) + k_d^b(E_n, J) + \omega}, \tag{40}$$

and we note that

$$k_r^a(E_n, J)/k_d^a(E_n, J) = \rho(E_n, J)e^{-E_n/k_BT}/Q_a, \tag{41}$$

where Q_a is the partition function of the X+YZ reactants in the a channel, including the electronic contribution, in the center of mass system of coordinates.

For an N-ladder system described earlier (Fig. 1), the ozone formation reaction rate constant is again given by $\omega_d g_1$, where g_1 is the steady-state population density of the state in the ladder with the lowest energy, since states with energy less than E_1 belong to the sink. For the solution of g_1, a method similar to that given in Appendix B is used. The solution for g_1 can be written as the ratio between the determinants of the matrices **B** and **A**, where the elements of **A** are $A(i,i) = 1$ $(i = 1, 2, \cdots, N)$, $A(i, i-1) = V_i$ $(i = 2, 3 \cdots, N)$, $A(i+1, i) = W_i$ $(i = 1, 2, \cdots, N-1)$, and all other elements vanish. (Thus, **A** is a tridiagonal band matrix.) The elements of **B** are the same as those of **A**, except for those in the first column, which are $B(i, 1) = U_i$. The elements of both **A** and **B** are functions of energy.

The rate constant can then be obtained as an integral over all energies in the range of 0 to ΔE:

$$k_{bi} = \int_0^{\Delta E} \omega_d |\mathbf{B}|/|\mathbf{A}| dE. \tag{42}$$

It should be noted here that the **B** and **A** in Eq. (42), which are defined above, differ from the **B** and **A** defined in Appendix B. Equation (42) contains in $|\mathbf{B}|/|\mathbf{A}|$ a sum of terms, the first from E_{M+1}, the next from E_{M+2}, etc.

At low pressures, U_n, V_n and W_n become

$$U_n = \sum_J \frac{k_r^a(E_n, J)}{k_d^a(E_n, J) + k_d^b(E_n, J)} = \sum_J Y_a(E_n, J)\rho(E_n, J)e^{-E_n/k_BT}/Q_a, \tag{43}$$

$$V_n = \sum_{J,closed} P(J)\omega_a/\omega = P_n^c\omega_a/\omega, \tag{44}$$

$$W_n = \sum_{J,closed} P(J)\omega_d/\omega = P_n^c\omega_d/\omega, \tag{45}$$

where $Y_a(E_n, J)$ is the partitioning factor, and P_n^c is again the sum of $P(J)$ over closed states with the energy E_n . It is readily shown that the rate constant obtained using the U_n, V_n and W_n given by Eqs. (43)−(45) is the same as that obtained in Eq. (31) in the previous section.

On the other hand, at the high pressure limit, U_n, V_n and W_n can be written as

$$U_n = \sum_J k_r^a(E_n, J)/\omega, \tag{46}$$

$$V_n = \omega_a/\omega, \tag{47}$$

$$W_n = \omega_d/\omega, \tag{48}$$

and it then readily follows that the high pressure recombination rate constant is given by

$$k_{bi}^{\infty} = \frac{1}{Q_a h}\sum_J \int_E N_a^{\dagger}(E, J)e^{-E/k_BT}dE, \tag{49}$$

as expected.

III. RESULTS

A. Isotopic Exchange reaction rate constant

To implement Eq. (18) a potential energy surface is needed, particularly in the region of configuration space appropriate to the hindered rotational transition state. The longer O-O bond length in this region is estimated in the calculations given below to be in the neighborhood of 2.6 Å. *Ab initio* calculations of the potential energy surface for ozone have not focused on this transition state region, and instead have been optimized mainly for configurations near the equilibrium configuration or near the equilateral triangle one, where a conical intersection occurs.[64] We have found that the calculated potential energy surface gave a poor result[66] for the temperature

coefficient of the isotopic exchange rate constant, even when an empirically modified version[65] was used. (The modification eliminated, in effect, a potential energy barrier which is known from the observed negative temperature coefficient of the recombination and isotopic exchange rate constant, not to occur.) Instead, a model potential energy surface is used to fit the isotopic exchange reaction rate constant at both room and low (130 K) temperatures. The fitted potential energy surface is then also used for the ozone formation reactions later. When more data or an improved calculation of the potential energy surface become available, this approximation can be removed.

A model potential[67] $V(R, r, \theta) = V_{bf}(R) + V_{bend}(R; \theta)$ is used in the following for the ozone formation and isotopic exchange reaction, where $V_{bf}(R)$ is a bond-fission potential and $V_{bend}(R, \theta)$ is a bending potential, and where the dependence of $V(R, r, \theta)$ on the bond length r of the fragment oxygen molecule is neglected. Here, R is the center to center distance between the oxygen atom and the fragment oxygen molecule, θ is the angle between the line along the axis of the diatomic molecule and the line connecting the two centers of mass, and the $V_{bf}(R)$ is chosen to be $-C_6/R^6$ for large R. The $C_6 = 27.6$ eV Å^6 was obtained from the collision cross-section for $O + O_2$.[68] For small R's, $V_{bf}(R)$ is chosen to be a Morse potential function,[69] $V_{bf}(R) = D(1-\exp(-\beta(R-R_e))^2$,[67] where D, the dissociation energy, is 9107 cm^{-1},[53] β is 2.88 Å^{-1},[70] and R_e, the equilibrium value of R, is 1.667 Å,[53] and the two V_{bf}'s are matched at $R = 2.6$ Å. The bending potential is chosen to be of the form[71]

$$V_{bend}(R; \theta) = V_R \cos^4 \theta, \qquad V_R = V_0 \exp(-\alpha(R - R_0)), \tag{50}$$

where the parameters are chosen to be roughly consistent with the experimental values of the isotopic exchange reaction rate constant at 300 K and its temperature dependence. When R_0 is taken as 2.6 Å, V_0 has a value of 0.35 eV, and α is 5.5 Å^{-1}.

The hindered-rotational potential given in Eq. (50) is then applied to Eq. (11) to obtain elements of the Hamiltonian matrix, and the energies of the hindered rotational states are obtained as the eigenvalues of the Hamiltonian matrix. The energy of the state denoted by $|Jj\Omega\rangle$ can then be written as

$$E(R; J, j, \Omega) = \frac{J(J+1) - 2\Omega^2}{2\mu R^2} + \epsilon(R; j, \Omega), \tag{51}$$

where $\epsilon(R; j, \Omega)$ is an eigenvalue of a two-dimensional hindered rotor state with quantum numbers j and Ω, and is obtained numerically in this study. The $\epsilon(R; j, \Omega)$ is dependent on the potential $V_{bend}(R, \theta)$ and thus is dependent on R. The eigenvalues $\epsilon(R; j, \Omega)$'s are plotted in Fig. 2 in units of $1/2I + 1/2\mu R^2$. Also plotted in that figure are the barrier height V_R and the energies for a free rotor (both in units of $1/2I + 1/2\mu R^2$). It is seen from that Figure that the states with energies well below the barrier resemble those of a harmonic oscillator and the energies of states above the barrier quickly converge to those of a free rotor plus a potential energy averaged over the angle θ. For the $V_R \cos^4\theta$ potential used here, the potential averaged over $\cos\theta$ is $(3/8)V_R$.

As discussed earlier, the $E(R; J, j, \Omega) + V_{bf}(R)$ for each of the two channels is obtained as a function of the reaction coordinate R and is shown in Fig. 3. The $E(R; J, j, \Omega) + V_{bf}(R)$ is plotted there as a function of R for a hindered rotational potential (50) and, for comparison, for a free rotor for the same set of quantum numbers J, j and Ω. It is seen from this Figure that the transition state for each state moves to a smaller value of R because of the hindrance, as expected from other studies.[80–92] For the state (0,0,0), the difference between the energies for systems with and without the rotational hindrance is due to the zero-point energy of the hindered rotor state. The energy barrier $E^J_{j\Omega}$ of a state with quantum numbers J, j and Ω is then obtained as the maximum of $E(R; J, j, \Omega)$ along the reaction coordinate. It is then applied in Eq. (18) for the calculation of the isotopic exchange rate constant. Here, the $N^\dagger_a(E, J)$ is given by

$$N^\dagger_a(E, J) = \frac{1}{2}\sum_J (2J+1)\sum_j \sum_\Omega h(E - E^J_{j\Omega}), \tag{52}$$

where $-J \le \Omega \le J$ and $-j \le \Omega \le j$. The factor 1/2 in Eq. (52) assigns one half of the θ space of the configuration at the transition state to the reaction leading to the XYZ molecule for the reaction X+YZ→ XYZ. The reaction coordinate for this reaction is chosen to be the distance between X and the center of mass of YZ, and the r for the fragment YZ is chosen to be two times the distance between Y and the center of mass of YZ. To illustrate the effect of the hindered rotational barrier, the

plot for the term $N_a^\dagger N_b^\dagger/(N_a^\dagger + N_b^\dagger)$ as a function of energy is very similar to the plot of $N^\dagger$ in Fig. 4.

The rate constant for the isotopic exchange reaction is then obtained using Eq. (18). The calculated results are shown for reactions at both 130 K and 300 K in Table 1. For comparison, the experimental results and the results calculated using the loose transition state are also shown. The partition functions for the collision pair, Q_a, including the electronic partition function, are calculated using Eqs. (4.8)-(4.12) of Ref. 37.

B. Low pressure recombination rate constant for $^{16}O + ^{16}O\ ^{16}O \rightarrow ^{48}O_3$

As seen from Eq. (31), the density of states of ozone is needed for the calculation of the low-pressure recombination rate constant. The density of states for ozone is obtained from a convolution[44,45,49,72] of the rotational and vibrational density of states, as described in Ref. 37. In particular, the vibration frequencies of the various isotopomers were obtained using a second-order perturbation formulation, which gives the unknown frequencies to an accuracy of about 1 cm^{-1}.[73] To include anharmonicity in the calculation of density of states $\rho(E, J)$, vibration frequencies of the ozone molecule $^{48}O_3$ given in Ref. 74 up to 6000 cm^{-1} are fitted using anharmonicity constants, where the energy of a state with vibrational quanta (v_1, v_2, v_3) is given by[75]

$$E(v_1, v_2, v_3) = \sum_{i=1}^{3} hc\omega_i(v_i + \frac{1}{2}) + \sum_{i=1}^{3} hcx_{ii}(v_i + \frac{1}{2})^2 + \sum_{i=1}^{3}\sum_{j>i} hcx_{ij}(v_i + \frac{1}{2})(v_j + \frac{1}{2}). \tag{53}$$

The fit[76] to the vibrational frequencies is given in Fig. 5. The total number of states in the range of 0 to 2000 cm^{-1} above the dissociation threshold, which is more than the maximum range of energy needed for the present study of ozone formation reaction, is calculated with and without inclusion of the anharmonicity. An averaged factor of 1.5 is obtained as the ratio between the total number of states that includes the anharmonicity effect and the one that does not. This factor is taken to be the same for all ozone isotopomers. The effect of anharmonicity on the densities of states for

each isotopomer is then taken into account, in an approximate way, by multiplying this factor with the harmonic density of states of that isotopomer.

Other critical quantities involved in the implementation of the formulas for the rate constants are the sums of states, which are obtained for both the hindered-rotor and the free rotor transition states, the partition function for the collision pair, which is again given by Eqs. (4.8)-(4.12) in Ref. 37, and the collision frequencies. For the collisional frequencies in Eq. (21), we have used a Lennard-Jones collision frequency with a unit collision efficiency, which is also given in Ref. 37 by Eq. (4.14).

The rate constant for the recombination reaction $^{16}O + {}^{32}O_2 \rightarrow {}^{48}O_3$ is calculated using the hindered-rotor and, for comparison, the free rotor transition states, together with the weak collision assumption and the stepladder energy transfer model. Calculated values of k_{bi}^0 for $^{16}O + {}^{32}O_2 \rightarrow {}^{48}O_3$ are given in Table I, and compared there with experimental values and with results calculated using strong collision model. In the calculations using the weak collision assumption, a value of 210 cm^{-1} is used for both 130 K and 300K, for the energy transfered per collision ΔE, which is about 1 $k_B T$ for $T = 300$ K. Other values of ΔE were also used in the stepladder energy transfer model for comparison, and the results for ΔE =180 and 250 cm^{-1} are listed in Footnote *c* to Table I. The results obtained using the free rotor ("loose") transition state for this $^{16}O + {}^{32}O_2 \rightarrow {}^{48}O_3$ reaction are the same as those obtained using the hindered-rotor transition state theory with the same value of ΔE, namely 5.8×10^{-12} cm^{-3} s^{-1} at 130 K and 0.9 $\times 10^{-12}$ cm^{-3} s^{-1} 300 K.

C. Individual rate constant ratios

The individual low-pressure rate constants at 300 K for both channels of the formation of XYZ molecules are calculated using Eq. (31). In these calculations, a small non-RRKM effect η (= 1.18) is assumed for the formation of symmetric ozone molecules. The rate constants for the formation of symmetric molecules are obtained by dividing the values obtained using Eq. (31) by η. The values of η and of ΔE are chosen to fit two experimental rate constant ratios, $^{16}O + {}^{18}O^{18}O/{}^{16}O + {}^{16}O^{16}O$ and

$^{18}O + ^{16}O^{16}O/^{18}O + ^{18}O^{18}O$. The hindered-rotor transition state theory, $\eta = 1.18$ and a ΔE of 210 cm^{-1} are used to obtain the results shown in Tables II, III and IV as well as in Figs. 6 and 7. When a free rotor transition state is used with an $\eta = 1.18$, and a $\Delta E = 260$ cm^{-1}, results within ± 0.02 of those in Tables II and III for all reactions are obtained at these low pressures.

To test the sensitivity of the rate constant ratio results to the choice of ΔE, two different values, 180 cm^{-1} and 250 cm^{-1}, are also used in applying the hindered rotor transition state theory and the weak collision approximation. The calculated rate constant ratio for $^{16}O + ^{36}O_2 \rightarrow ^{16}O^{18}O^{18}O$ varies from 1.55 to 1.53 to 1.50 when ΔE varies from 180 to 210 to 250 cm^{-1}.

D. Isotopic Enrichments

Calculated results for isotopic enrichments at low pressures for "scrambled" systems with large concentrations of heavy isotopes are presented in Table V and Fig. 8. They are obtained from individual isotopomeric rate constants and Eqs. (4.18a), (4.18b) and (4.26) of Ref. 36 for the enrichments. Results obtained using the stepladder energy transfer model are shown for $\Delta E = 210$ cm^{-1}, with no effort being made to obtain a better fit. The individual rate constants used for the enrichment calculations are listed in Tables III and IV, which already include the factor $\eta = 1.18$ in the rate constants for the formation of symmetric molecules.

E. Pressure effect on the recombination rate constant for $^{16}O + ^{32}O_2 \rightarrow ^{48}O_3$, the enrichment $^{18}\delta$ and individual rate constant ratios

The rate constants for the reaction $^{16}O + ^{32}O_2 \rightarrow ^{48}O_3$ at 130 K and 300 K were both calculated as a function of the pressure using the methods described in Sec. II D. The pressure dependence of this ozone formation rate constant at both temperatures is shown in Fig. 9 together with the experimental results. Recombination rate constants for reactions $^{16}O + ^{16}O^{18}O \rightarrow ^{16}O^{16}O^{18}O$, $^{16}O + ^{16}O^{18}O \rightarrow ^{16}O^{18}O^{16}O$ and $^{18}O + ^{16}O^{16}O \rightarrow ^{16}O^{16}O^{18}O$ are also obtained as a function of the pressure. The

enrichment of the isotopic combination $^{16}O + ^{16}O^{16}O^{18}O$, calculated by Eq. (4.18a) of Ref. 36, is then obtained as a function of pressure. The comparison between the experimental and calculated pressure effect on the enrichment is given in Fig. 10, and the pressure dependence of the rate constants for reactions $^{16}O + ^{18}O^{18}O \rightarrow ^{16}O^{18}O^{18}O$ and $^{18}O + ^{18}O^{18}O \rightarrow ^{18}O^{18}O^{18}O$ was also obtained as a function of pressure. The pressure dependence of the individual rate constant ratios, $k_{6,88}/k_{6,66}$ and $k_{8,66}/k_{8,88}$, is plotted in Fig. 11 and compared there with the experimental results. In all these calculations using the hindered-rotor transition state, the $\Delta E = 210$ cm^{-1}, and $\eta = 1.18$ are used.

F. Temperature effect on isotopic enrichments and on individual rate constant ratios

To investigate the temperature effect on η in the absence of individual rate constant ratio data, calculations were performed in the present study by assuming ΔE to be approximately independent of temperature in the temperature range of interest, 140 to 300 K. An $\eta = 1.13$ was then obtained by fitting the experimental data of enrichment of $^{16}O^{16}O^{18}O$ at 140 K. This η and a ΔE of 210 cm^{-1} are then used to predict the rate constant ratios for reactions involving ^{16}O and/or ^{18}O. In addition, enrichments of $^{16}O^{18}O^{18}O$ and $^{18}O^{18}O^{18}O$ are calculated using these rate constant ratios and the appropriate partition functions at 140 K. The predicted results are shown in Table VI, including the results for 300 K.

IV. DISCUSSION

A. The symmetry-related non-RRKM effect

The recombination reaction rate constants for ozone formation at low pressures, the rate constants for the isotopic exchange reactions, and the various temperature and pressure effects are considered in this study. In particular we have focused on an explanation both of the experimentally observed "mass-independent" effect for

scrambled systems[2-24] and the dramatic and unconventional "mass-dependent" effect for unscrambled systems[25-29] in the ozone formation reactions and their pressure dependence. In each case we have seen that reasonable agreement is obtained between the present theoretical results and the experimental values. In the treatment of these various phenomena, we have employed what can be characterized as "symmetry driven" isotopic effects: Lack of symmetry gives rise to the difference between the partitioning factors Y_a and Y_b from 1/2 and, as discussed in Sec. C, this effect is responsible for the large unconventional mass-dependent effects in the individual rate constant ratios in unscrambled systems.

Again, we have introduced a factor $\eta = 1.18$, for the so called non-RRKM effect,[36,37] which is used to reduce the effective density of states for the symmetric species, with a basis discussed in Refs. 36 and 37, and so it too has a symmetry-based origin. (Fewer anharmonic and Coriolis matrix coupling elements, which promote statistical behavior, are present in the symmetric species.) We also note that, in principle, there could be a different origin of this η factor: Since some collisional frequency, such as ω, and ρ occur as a product in the expressions for the rate constants, one may not be able to distinguish between this effect on ρ and an effect on ω on the basis of kinetic data alone: In principle, the lower density of states of symmetric molecules could make the collisional energy transfer less efficient for these molecules and thus make ω smaller.

B. Weak Collision Aspect and Temperature Effect

The weak collision assumption used in the present study provides an explanation for the significant negative temperature dependence of the recombination rate constant at low pressures: As seen in Table I, the experimental rate constant at 130 K is about 8 times faster than that at 300 K, while when a strong collision assumption is used, the present expression reduces to those in Refs. 36 and 37,

$$k_{bi}^{0,a} = \omega \sum_J \int_0^\infty \left[N_a^\dagger/(N_a^\dagger + N_b^\dagger)\right] \rho e^{-E/k_B T} dE/Q_a. \tag{54}$$

The use of Eq. (54) would only give a ratio of the rate constants at these two temperatures to be less than 2. Instead, when the weak collision model is used (Eq. (31)) a factor 6 is obtained, which is in significantly better agreement with the experimental results. This large negative temperature coefficient arises in part, in the present treatment, because of the smaller contribution from the more energetic ozone states populated at the higher temperatures than those from the less energetic ones, reflecting the small amount of energy transferred per collision. The higher the temperature, the less occupied the energetic states that have energy low enough to be deactivated, and thus the smaller the rate constant. The results in Table I using Eqs. (31) are obtained by assuming the same averaged energy transferred per collision ΔE and the same η for both temperatures.[93]

We note that when the weak collision assumption is used the choice of transition state has almost no effect on the low-pressure recombination rate constant and on its temperature dependence (cf Table I). One reason why the free rotor transition state (phase space) theory yields results very close to the more realistic theory at both 130 K and 300 K is that the former is already a good approximation for activationless recombination reactions at low energy, and in the weak collision model, only states within a small range of ΔE above the barrier height contribute to the formation of stable ozone molecules at low pressures. For states with low energies, the transition states tend to be "loose" (free rotor).

The individual rate constants at low pressures are approximately determined by the integration of $(\omega_d - \omega_a) \sum_J \rho e^{-E/k_B T} N_a^\dagger / (N_a^\dagger + N_b^\dagger)$ over energy, which is dependent on the choice of the transition state via the ratio $N_a^\dagger/(N_a^\dagger + N_b^\dagger)$. In the case of a symmetric molecule, the ratio is reduced to a heaviside step function $h(N_a)$, and proves to be quite insensitive to the choice of the transition state. This behavior is easily understood using Fig. 12, where the free and hindered-rotor transition state theories are compared for the effective density of states $\sum_J \rho(E,J) h(N_a^\dagger)$, for the formation of $^{16}O^{16}O^{16}O$. It is seen there that there is very little difference in the effective density of states, especially at energies lower than 300 cm^{-1}, which contribute more significantly to the formation of ozone due to the weak collision effect. As a

result, at low pressures the recombination rate constant for a symmetric molecule is almost independent of the nature of the transition state for the present system and conditions. We turn next to the effect for an asymmetric reaction.

For an asymmetric molecule, the ratio $N_a^\dagger/(N_a^\dagger + N_b^\dagger)$ depends sensitively on the functional form of $N^\dagger$'s. As a result, the ratios of rate constants for the two different entrance channels show a greater dependence on the nature of transition state. To fit the low pressure experimental results of the rate constant ratios using the free rotor transition state, it is recalled, a value of 260 cm^{-1} is needed for ΔE, while when the hindered-rotor transition state is used, a $\Delta E = 210$ cm^{-1} yields good agreement with the experimental values. The reason for the best fit ΔE being smaller for the hindered-rotor transition state is readily seen: Both $N_a^\dagger$ and $N_b^\dagger$ for the hindered rotor transition state (TS) increase more slowly with energy than they do for the free rotor TS, due to the hindrance of the rotation permitting fewer states. Correspondingly, the difference between $N_a^\dagger$ and $N_b^\dagger$ decreases more rapidly as a function of energy in the hindered-rotor model,[79] and so a smaller ΔE suffices. A comparison for the values of $N_a^\dagger$ calculated using the free and hindered-rotor transition states is very similar to that depicted in Fig. 4. The J-averaged quantity $\sum_J \rho e^{-E/k_BT} N_a^\dagger / \sum_J \rho e^{-E/k_BT}(N_a^\dagger + N_b^\dagger)$ is shown in Fig. 13 as a function of energy.

As discussed earlier, in the present model the negative temperature dependence of the recombination rate constant at low pressures for $^{16}O+^{32}O \rightarrow ^{48}O_3$ is mainly due to the small value ($\sim$ 210 cm^{-1}) of ΔE in the deactivation of hot ozone molecules. One would expect the negative temperature coefficient to be less when this collisional deactivation of ozone is not rate-determining. This condition is achieved in isotopic exchange experiments and in recombination reactions at high pressures.

The experimental ratio of the isotopic exchange rate constants at 130 K and 300 K for $^{16}O+^{18}O^{18}O \rightarrow ^{16}O^{18}O+^{18}O$ is about 1.9, which is substantially smaller than the experimental factor of 8 for the low pressure recombination reaction. When the reaction rates are written as proportional to the T^{-m}, where T is the temperature, the coefficient m obtained using the present calculations is 0.53 for the isotopic exchange reaction, and 2.2 for the low pressure recombination reaction, as compared with the

experimental values of 0.88 ± 0.26 and 2.6. The negative temperature dependence obtained in the present theory for the isotopic exchange reaction arises from the increasingly hindered rotation, due to the well-known tightening effect of the transition state, with increasing temperature.[80–92] The effective number of states for exchange $\sum_J N_a^\dagger N_b^\dagger/(N_a^\dagger + N_b^\dagger)$ as a function of energy is similar to the $N_a^\dagger$ plotted in Fig. 4. The smaller number of states for the hindered-rotor transition state, compared to those obtained using a free rotor transition state, is evident, and with the movement of the transition state inward with increasing temperature, the free rotor at low T becomes hindered at high T, and there is a corresponding decrease of the number of states. Thereby, a negative temperature dependence occurs for the isotopic exchange reaction, and similarly for the high pressure recombination rate constant.

The pressure dependence of the ozone recombination reaction was studied experimentally for the reaction $^{16}O+^{16}O_2 \rightarrow {}^{16}O_3$ at various temperatures. Only at low temperatures (below 160 K) has the expected simple unimolecular reaction behavior been observed. At higher temperatures, however, there is a sudden rise on the log-log plot of the rate-pressure curves at very high pressures, which also corresponds to the negative temperature dependence being smaller at higher pressures.

C. Individual Recombination Rate Constants

Experiments at 300 K have shown a dramatic isotopic effect on the ratios of the individual recombination rate constants. The rate constant for the channel with a lower zero-point energy for the fragments is substantially larger than that for the other channel. This behavior can be explained by consequences of the difference of the two zero-point energies on the number of states $N_a^\dagger$ and $N_b^\dagger$, when a weak collision is assumed. However, if a strong collision limit is assumed, the expression given by Eq. (54) is used. This expression gives too small an effect[37] at 300 K for the differences in the various rate constant ratios: the reason is that states with high energies, where $N_a^\dagger/(N_a^\dagger + N_b^\dagger) \approx 1/2$, are accessible for recombination when a strong collision approximation is made. For example, the experimental results for the ratios of the

rate constants (compared with $^{16}O+^{16}O_2 \rightarrow {}^{16}O_3$) for $^{16}O+^{18}O^{18}O \rightarrow {}^{16}O\ {}^{18}O\ {}^{18}O$ is 1.53, and for $^{18}O+^{18}O^{16}O \rightarrow {}^{16}O\ {}^{18}O\ {}^{18}O$ is 0.46, while the use of the strong collision, Eq. (54), yields instead 1.27 and 0.58, respectively. The latter two figures barely differ from what one would expect from the η effect alone, namely 1.18 and 0.59.

However, in general, unimolecular reactions are best treated not in the strong collision deactivation form, according to extensive data,[44–49] and so the present treatment is consistent with that view. In the present study, since the weak collision assumption is used with a $\Delta E \sim 200$ cm^{-1}, highly energetic states of ozone are less important for the low pressure recombination reaction, and much better agreement with the experimental results for the individual rate constant ratios at room temperature (Table II, III, and IV) follows, using this ΔE.

An understanding of the effect of small difference in zero-point energies on the rate constant ratios is provided in Fig. 13. As seen there the small difference between the zero-point energies dramatically influences the ratio $N_a^\dagger/(N_a^\dagger + N_b^\dagger)$ even up to a relative high energy, i.e., ~ 200 cm^{-1}, and yields a large difference between the rate constants. For a better understanding of this unexpectedly large effect of the relative small zero-point energy difference, plots are given in Fig. 14 using a simple model for $N_a^\dagger$ and $N_b^\dagger$. The $N_a^\dagger$ ($N_b^\dagger$) is assumed to be either a linear or quadratic function of $E - E_a(E_b)$ with E_a (E_b) being the dissociation energy for channel a (b). The quadratic function gives a better agreement with the results for a real system (the points in Fig. 14), as indicated by the plots of $\sum_J N_a^\dagger(E,J)$ versus energy given in Fig. 4. For a quadratic case, the small difference of the zero-point energy contributes to a relatively large difference between the rate constants for the two channels even for energies up to 300 cm^{-1}, since it magnifies the effect on the differences in the partitioning factors Y_a and Y_b. The quadratic behavior of $N_a^\dagger$ and $N_b^\dagger$ above threshold is easily understood using a crude model.[94]

D. Pressure Effects

Various pressure effects have been investigated in these ozone systems: the effect of pressure on the formation rate constant of $^{48}O_3$,[30] on the enrichment of the isotopic combination $^{16}O^{16}O^{18}O$,[28] and on the rate constant ratios, $k_{16,1818}/k_{16,1616}$ and $k_{18,1616}/k_{18,1818}$.[28] All these calculated results were seen to be in reasonable agreement with the experimental results (Figs. 9, 10, and 11). We note, however, that there is some discrepancy between the calculated and experimental results for the pressure effect on the recombination rate constant for $^{16}O + ^{32}O \rightarrow ^{48}O$: the rate constants are too large at low pressures and too small at high pressures.

A better agreement between the experimental and calculated pressure effect, especially at the low pressure region, is expected if some additional non-RRKM effects, which reduce the effective density of states for both symmetric and asymmetric species, were included, or if the collisions less effective in deactivation (the effective $\rho(E,J)$ and some collisional term ω occur as a product $\rho(E,J)\omega$. Either effect above would serve to decrease k_{bi} at low pressures but, because of cancellation, would not affect the calculated low pressure results for individual rate constant ratios.

The present calculations using the weak collision approximation and the non-statistical factor $\eta = 1.18$ provide, as mentioned earlier, a reasonable fit to the various experimental results (Figs. 9, 10, and 11). One striking feature of these pressure effects is that the effect of pressure both on the enrichment and on the rate constant ratios $k_{16,1818}/k_{16,1616}$ is more sensitive than is that on the recombination rate constant for $^{16}O + ^{16}O^{16}O$. A large effect of pressure on the first two is evident at 10^2 torr, whereas that on the $k^{rec}_{6,66}$ becomes evident at 10^4 torr. This effect arises, at least in part, because the first two quantities are related to the slope of the pressure dependence of the rate constants, and the changes in a slope are more easily detected than changes in the "integrated" quantity, the k_{bi}. The effect is illustrated in Fig. 15. In this figure, a simple formalism is assumed for $N^{\dagger}_a$, which is assumed to be a quadratic function[94] of $E - E_{0,a}$ for $E - E_{0,a} \geq 0$, where E is the energy, $E_{0,a}$ is the zero-point energy for channel a. A similar function of $E - E_{0,b} \geq 0$ is

assumed for $N_b^\dagger$. Each function drawn in Fig. 15 is the quotient, as a function of ω, of $\int_0^\infty \omega(N_a^\dagger + N_b^\dagger)/[\omega + (N_a^\dagger + N_b^\dagger)/\eta\rho]$, where $E_{0,a} - E_{0,b} = 23$ cm^{-1}, $\eta = 1$, and a corresponding value where $N_a^\dagger = N_b^\dagger$ and $\eta = 1.18$, i.e., that for a symmetric molecule. The logarithm of the function $\int_0^\infty \omega N^\dagger/(\omega + N^\dagger/\rho)dE$, which represents a rate constant is also shown in arbitrary units in the same figure. It is seen from that figure that in this simple model the change of rate constant ratios with pressure is more easily detected than that of the rate constant itself, leading to a similar conclusion to that obtained using calculations for the real system.

An interesting effect of the non-RRKM parameter η is also seen using the above model system. The dashed line in Fig. 16 represents a function similar to that of the solid line, except that η is taken as unity there. In this case, only very weak pressure dependence of the rate constant ratios is seen: with increased pressure the importance of η is reduced, and so the presence of η makes the additional contribution to the effect of pressure.

It has been noted[28] that there is a marked difference between the pressure dependence of the rate constant ratios $k_{16,1818}/k_{16,1616}$ and $k_{18,1616}/k_{18,1818}$: when the pressure is varied from 100 to 3000 torr, while $k_{16,1818}/k_{16,1616}$ decreases from 1.53 to 1.27, $k_{18,1616}/k_{18,1818}$ is almost a constant. The present calculations show a trend similar to that for these experimental results (Fig. 11). Pressure effect on the enrichment of $^{16}O^{18}O^{18}O$ +^{18} $O^{16}O^{18}O$ and is also calculated in the present study, and is shown in Fig. 17 with a comparison to the pressure dependence of the enrichment of $^{16}O^{16}O^{18}O$ +^{16} $O^{18}O^{16}O$.

E. The Potential Energy Surface, η, and ΔE

We have noted earlier the need for an improved potential energy surface, and we have used, in the interim, a crude model potential instead. While calculations should be repeated with an improved potential energy surface when it becomes available, it is also true that fortunately most of the important results in the present study are obtained at the low pressure limit, and as noted earlier, these results are relatively

insensitive to the type of transition state and thus of the details of the potential energy surface, when a weak collision is assumed. In fact, the transition state tends to be rather loose for low energy states, which are the only important states in the weak collision case. The potential energy surface, however, does influence more strongly the results on the isotopic exchange reaction and the recombination reaction at high pressures. Since the temperature dependence of the isotopic exchange reaction rate constant is sensitive to the potential energy surface, and also since it does not suffer the complication of the high-pressure recombination rate constant, we have used a potential which is fitted to give reasonable results on the isotopic exchange reaction. It was then applied to all the other recombination reactions.

The η, as indicated earlier, in principle could be temperature dependent. Most of the experimental data treated in the present study were obtained at 300 K. The η and ΔE for this temperature were chosen to fit the two rate constant ratios, $^{16}O + ^{18}O^{18}O/^{16}O + ^{16}O^{16}O$ and $^{18}O + ^{16}O^{16}O/^{18}O + ^{18}O^{18}O$, and were applied to obtain the other reaction rate constants, and from them, the isotopic enrichments. It would be desirable to have similar data on these two rate constant ratios at other temperatures, which would provide information on the temperature dependence of η and ΔE. Currently, experimental results in the temperature range of 140 to 373 K, have been reported for the temperature dependence of the enrichment of $^{16}O^{16}O^{18}O$.[12] An η of 1.13 was obtained at 140 K by fitting the experimental enrichment $^{18}\delta$ and was then used, together with a $\Delta E = 210$ cm^{-1}, to calculate the rate constant ratios and isotopic enrichments for some other isotopic combinations. Predictions were made and are shown in Table VI.

To conclude, we would like to comment on the value of ΔE used in this study. As mentioned earlier, a value of $\Delta E = 210$ cm^{-1} and $\eta = 1.18$ were chosen at 300 K to fit the two experimental rate constant ratios, $^{16}O + ^{18}O^{18}O/^{16}O + ^{16}O^{16}O$ and $^{18}O + ^{16}O^{16}O/^{18}O + ^{18}O^{18}O$. These reactions are chosen because of their large difference in ratios. This ΔE and η were then used for the calculations for all the other properties and provide results that are in reasonable agreement with the experimental data for the various isotope arrangements. The use of 210 cm^{-1} for ΔE also gives reasonable

values for the rate constants for the recombination reaction of $^{16}O+^{16}O_2 \rightarrow {}^{16}O_3$ compared with the experimental results at both 130 K and 300 K and thus also provides the correct negative temperature dependence. When other values of ΔE were used for comparison in some of the calculations for $\eta = 1.18$, it was found that for ΔE in the range of 180 to 250 cm^{-1}, the calculations also gave results in reasonable agreement with the experimental values. Further, this value of ΔE is also not inconsistent with classical trajectory energy transfer studies for highly excited ozone molecules: In classical trajectory studies on the collisional energy transfer between highly energetic ozone molecules and Ar, He, and N_2, it was found that the averaged magnitude of the energy transferred per collision (both deactivation and activation collisions are counted) is about 0.4 k_BT at 2500 K ($\sim$ 600 cm^{-1}) and 0.5-0.6 k_BT at 500 K ($\sim$ 200 cm^{-1}).[95]

ACKNOWLEDGMENTS

It is a pleasure to acknowledge the support of this research by the National Science Foundation and helpful discussions in the early stage of this work with Dr. Bryan Hathorn.

APPENDIX A: DERIVATION OF EQ. (2.19)

We have (cf Eq. (2.18))

$$\omega(E', J' \rightarrow E, J) = \omega_d t(J' \rightarrow J)\delta(E' - E - \Delta E) \tag{A1}$$

and

$$\omega(E, J \rightarrow E', J') = \omega_a t(J \rightarrow J')\delta(E - E' + \Delta E). \tag{A2}$$

Microscopic reversibility yields

$$\sum_{J'J} \omega(E', J' \rightarrow E, J)\rho(E', J')e^{-E'/k_BT} = \sum_{J'J} \omega(E, J \rightarrow E', J')\rho(E, J)e^{-E/k_BT}, \tag{A3}$$

e.g., suppose $E' = E + \Delta E$, then $E' \rightarrow E$ is a deactivation and we have

$$\sum_{J'J} \omega_d \delta(E' - E - \Delta E)\rho(E + \Delta E, J')\frac{e^{-E_J/k_BT}(2J+1)}{Q_{rot}}e^{-(E+\Delta E)/k_BT} =$$

$$\sum_{J'J} \omega_a \delta(E' - E - \Delta E)\rho(E, J)\frac{e^{-E'_J/k_BT}(2J'+1)}{Q_{rot}}e^{-E/k_BT}, \qquad \text{(A4)}$$

i.e.,

$$\omega_d \delta(E' - E - \Delta E)\sum_{J'} \rho(E + \Delta E, J')e^{-(E+\Delta E)/k_BT} =$$

$$\omega_a \delta(E' - E - \Delta E)\sum_{J} \rho(E, J)e^{-E/k_BT}, \qquad \text{(A5)}$$

and so,

$$\omega_d \sum_{J'} \rho(E + \Delta E, J)e^{-\Delta E/k_BT} = \omega_a \sum_{J} \rho(E, J) \qquad \text{(A6)}$$

which yields Eq. (2.19) of the text when $\rho(E - \Delta E) = \sum_J \rho(E - \Delta E, J)$ and $\rho(E) = \sum_J \rho(E, J)$.

APPENDIX B: DERIVATION OF THE LOW PRESSURE RECOMBINATION RATE CONSTANT

In this Appendix, an expression for the ozone recombination rate constant is obtained by solving the rate equations for the population densities of ozone states. The stepladder model discussed in the text is applied. The states above the dissociation threshold are divided into open and closed states, the rate equations for open and closed states are given by Eqs. (23) and (27), respectively. The states below the dissociation threshold contain only closed states, and their population densities can be described by Eqs. (24)-(26). Combining these equations, for an N ladder system with M of them below the dissociation threshold, we have in matrix notation, $\mathbf{AC} = \mathbf{K}$, under the steady-state assumption, where $\mathbf{C}$ is a $1\times(N + M)$ matrix with elements $g^o_N, \cdots, g^o_{M+1}, g^c_N, \cdots, g^c_{M+1}, \cdots, g_2, g_1$, and $\mathbf{K}$ is also a 1×(N+M) matrix, with elements $-k^a_r(E_N), -k^a_r(E_{N-1}), \cdots, -k^a_r(E_{M+1}), 0, \cdots, 0$. The $\mathbf{A}$ is an $(N+M)\times(N+M)$ sparse matrix. For simplicity, an example is given for $N = 6, M = 3$

$$A = \begin{pmatrix} -k_d(E_3) & 0 & 0 & 0 & 0 & 0 & 0 & 0 & 0 \\ 0 & -k_d(E_2) & 0 & 0 & 0 & 0 & 0 & 0 & 0 \\ 0 & 0 & -k_d(E_1) & 0 & 0 & 0 & 0 & 0 & 0 \\ 0 & \omega_a P_3^c & 0 & -\omega_d & \omega_a P_3^c & 0 & 0 & 0 & 0 \\ \omega_d P_2^c & 0 & \omega_a P_2^c & \omega_d P_2^c & -\omega & \omega_a P_2^c & 0 & 0 & 0 \\ 0 & \omega_d P_1^c & 0 & 0 & \omega_d P_1^c & -\omega & \omega_a P_1^c & 0 & 0 \\ 0 & 0 & \omega_d & 0 & 0 & \omega_d & -\omega & \omega_a & 0 \\ 0 & 0 & 0 & 0 & 0 & 0 & \omega_d & -\omega & \omega_a \\ 0 & 0 & 0 & 0 & 0 & 0 & 0 & \omega_d & -\omega \end{pmatrix}. \quad \text{(B1)}$$

The k_d's in Eq. (B1) are defined by Eq. (29), and the k_r^a's in the expression for $\mathbf{K}$ is defined in Eq. (30).

The population density g_1 of the ladder $n = 1$ is then obtained as

$$g_1 = |\mathbf{B}|/|\mathbf{A}|, \quad \text{(B2)}$$

where the matrix $\mathbf{A}$ is given by Eq. (B1) and $\mathbf{B}$ is the same as $\mathbf{A}$ except that its last column is substituted by the elements of $\mathbf{K}$.

To evaluate $|\mathbf{A}|$, the determinant of the matrix $\mathbf{A}$, it is first noted that the terms containing ω are small compared to those of k_d's, at the low pressure limit. Thus the ω's in the rows that also have a k_d term can be replaced by zeros. The $|\mathbf{A}|$ is then decomposed to the product of the determinant of two matrices $\mathbf{K_d}$ and $\mathbf{D}$, the $\mathbf{K_d}$ containing only k_d's and determinant of $\mathbf{K_d}$ is the product of k_d's, and the $\mathbf{D}$ containing only collision terms. The matrix $\mathbf{D}$ is an $N \times N$ band matrix and its determinant is readily calculated. To calculate the determinant of $\mathbf{D}$, a series of matrices $\mathbf{D_i}$ can be constructed from the elements of $\mathbf{D}$. The $\mathbf{D_i}$ is an $i \times i$ matrix ($i = 1, 2, \cdots N$, thus $\mathbf{D_i} = \mathbf{D}$), it is formed by the last i rows and columns of the matrix $\mathbf{D}$. It is then readily obtained that

$$|\mathbf{D_1}| = -\omega_d(1 + \frac{\omega_a}{\omega_d}) \quad \text{(B3)}$$

$$|\mathbf{D_2}| = -\omega_d^2 \left[1 + \frac{\omega_a}{\omega_d} + \left(\frac{\omega_a}{\omega_d}\right)^2\right] \quad \text{(B4)}$$

$$|\mathbf{D_I}| = -(\omega_a + \omega_d)|\mathbf{D_{I-1}}| - \mathbf{D}_{N-I,N-I+1}\mathbf{D}_{N-I+1,N-I}|\mathbf{D_{I-2}}|, \quad \text{(B5)}$$

where $\mathbf{D}_{N-I,N-I+1}$ and $\mathbf{D}_{N-I+1,N-I}$ are the $(N-I, N-I+1)$ and $(N-I+1, N-I)$ elements of the matrix $\mathbf{D}$.

We first note that the use of Eq. (B5) leads to

$$|\mathbf{D}| \propto \omega_d^{M-1} \left[1 + \frac{\omega_a}{\omega_d} + \cdots + \left(\frac{\omega_a}{\omega_d}\right)^{M-1}\right]. \tag{B6}$$

Thus by increasing M but keeping $N - M$ constant, i.e., increasing the number of ladders below the dissociation threshold but keeping the number of ladders above constant, one has a convergent result $|\mathbf{D}| \propto \omega_d^{M-1}/(1 - \omega_a/\omega_d)$.

The determinant of the matrix $\mathbf{B}$ in Eq. (B2) can be evaluated similarly. Particularly, the ladder steps below the dissociation threshold contributes a factor of ω_d^{M-1} which cancels with the same factor in $|\mathbf{A}|$. We have then for the population g_1, for $N - M = 3$,

$$g_1 = (\omega_d - \omega_a)\left(\frac{k_r^a(E_{N-2})}{k_d(E_{N-2}}\frac{\omega}{\omega_d + \omega_a P_{N-2}^o} + \right.$$
$$\left.\frac{k_r^a(E_{N-1})}{k_d(E_{N-1})}\frac{\omega_d P_{N-1}^c}{\omega_d + \omega_a P_{N-1}^o} + \frac{k_r^a(E_N)}{k_d(E_N)}\frac{\omega_d^2 P_{N-1}^c P_N^c}{\omega(\omega_d + \omega_a P_N^o)} + \cdots\right). \tag{B7}$$

Since P_n^c is the sum of P(J), the occupation probability of states with total angular moment J, over the states that are nonreactive at the energy E_n, it is a decreasing function of E_n (Fig. 18. For a $\Delta_E \sim 200$ cm^{-1} used in this study, the third term in Eq. (B7) can be safely neglected. The rate constant is then obtained by summing g_1 over all sets of ladders, weighted by the distribution of X+YZ. The resulting expression of the rate constant is given by Eq. (31).

REFERENCES

[1] Y.Q. Gao and R.A. Marcus, submitted for publication.

[2] R.N. Clayton, L. Grossman, and T.K. Mayeda, Science. **182**, 485 (1973).

[3] J.E. Heidenreich III and M.H. Thiemens, J. Chem. Phys. **78**, 892 (1983).

[4] J.E. Heidenreich III and M.H. Thiemens, J. Chem. Phys. **84**, 2129 (1986).

[5] K. Mauersberger, Geophys. Res. Lett. **14**, 80 (1987).

[6] J. Yang and S. Epstein, Geochim. Cosmochim. Acta. **51**, 2011 (1987).

[7] J. Yang and S. Epstein, Geochim. Cosmochim. Acta. **51**, 2019 (1987).

[8] M.H. Thiemens and T. Jackson, Geophys. Res. Lett. **14**, 624 (1987).

[9] M.H. Thiemens and T. Jackson, Geophys. Res. Lett. **15**, 639 (1988).

[10] S.M. Anderson, J. Morton, and K. Mauersberger, Chem. Phys. Lett. **156**, 175 (1989).

[11] J. Morton, B. Schueler, and K. Mauersberger, Chem. Phys. Lett. **154**, 143 (1989).

[12] J. Morton, J. Barnes, B. Schueler, and K. Mauersberger, J. Geophys. Res. **95**, 901 (1990).

[13] M.H. Thiemens and T. Jackson, Geophys. Res. Lett. **17**, 717 (1990).

[14] B. Schueler, J. Morton, and K. Mauersberger, Geophys. Res. Lett. **17**, 1295 (1990).

[15] J. Wen and M.H. Thiemens, Chem. Phys. Lett. **172**, 416 (1990).

[16] J. Wen and M.H. Thiemens, J. Geophys. Res. **96**, 10911 (1991).

[17] S.M. Anderson, K. Mauersberger, J. Morton, and B. Schueler, ACS Symp. Ser. **502**, (1992).

[18] M.H. Thiemens, ACS Symp. Ser. **502**, (1992).

[19] K. Mauersberger, J. Morton, B. Schueler, and J. Stehr, Geophys. Res. Lett. **20**,

1031 (1993).

[20] D. Krankowsky, F. Bartecki, G.G. Klees, K. Mauersberger, and K. Schellenbach, Geophys. Res. Lett. **22**, 1713 (1995).

[21] J. Sehested, O.J. Nielsen, H. Egsgaard, N.W. Larsen, T. Pedersen, L.K. Christensen and M. Wiegell, J. Geophys. Res. **100**, 20979 (1995).

[22] D. Krankowsky and K. Mauersberger, Science. **274**, 1324 (1996).

[23] L.K. Christensen, N.W. Larsen, F.M. Nicolaisen, T. Pedersen, G.O. Sørensen, and H. Egsgaard, J. Mol. Spec. **175**, 220 (1996).

[24] J.C. Johnson and M.H. Thiemens, J. Geophys. Res. **102**, 25395 (1997).

[25] S.M. Anderson, D. Hüsebusch and K. Mauersberger, J. Chem. Phys. **107**, 5385 (1997).

[26] K. Mauersberger, B. Erbacher, D. Krankowsky, J. Günther, and R. Nickel, Science. **283**, 370 (1999).

[27] C. Janssen, J. Günther, D. Krankowsky, and K. Mauersberger, J. Chem. Phys. **111**, 7179 (1999).

[28] J. Guenther, B. Erbacher, D. Krankowsky, and K. Mauersberger, Chem. Phys. Lett. **306**, 209 (1999).

[29] J. Günther, D. Krankowsky, and K. Mauersberger, Chem. Phys. Lett. **324**, 31 (2000).

[30] H. Hippler, R. Rahn, and J. Troe, J. Chem. Phys. **93**, 6560 (1990).

[31] M.R. Wiegell, N.W. Larsen, T. Pedersen and H. Egsgaard, Int. J. Chem. Kinet. **29**, 745 (1997).

[32] M.H. Thiemens, Science. **283**, 341 (1999) and references cited therein.

[33] J. Farquhar, H.M. Bao, and M.H. Thiemens, Science. **289**, 756 (2000).

[34] H. Bao, M.H. Thiemens, J. Farquhar, D.A. Campbell, C.C.-W. Lee, K. Heine, and D.B. Loope, Nature. **406**, 176 (2000).

[35] M.H. Thiemens, T. Jackson, E.C. Zipf, P.W. Erdman, and C. van Egmond, Science, **270**, 969 (1995).

[36] B.C. Hathorn and R.A. Marcus, J. Chem. Phys. **111**, 4087 (1999).

[37] B.C. Hathorn and R.A. Marcus, J. Chem. Phys. **113**, 9497 (2000).

[38] J. Troe, J. Chem. Phys. **66**, 4745 (1977).

[39] J. Troe, J. Chem. Phys. **66**, 4748 (1977).

[40] J. Troe, J. Chem. Phys. **77**, 3485 (1982).

[41] J. Troe, J. Chem. Phys. **90**, 4745 (1986).

[42] W. Schranz and S. Nordholm, Int. J. Chem. Kinet. **13**, 1051 (1981).

[43] I. Oref, J. Chem. Phys. **77**, 5146 (1982).

[44] R.G. Gilbert and S.C. Smith, *Theory of Unimolecular and Recombination Reactions.* (Blackwell Scientific Publications, Boston, 1990) and references cited therein.

[45] P.J. Robinson and K.A. Holbrook, *Unimolecular Reactions.* (Wiley-Interscience, London, 1972) and references cited therein.

[46] D.C. Tardy and B.S Rabinovitch, J. Chem. Phys. **48**, 1282 (1968).

[47] D.C. Tardy and B.S Rabinovitch, J. Chem. Phys. **45**, 3720 (1966).

[48] I. Oref and D.C. Tardy, Chem. Rev. **90**, 1282 (1990).

[49] T. Baer and W.L. Hase, *Unimolecular Reaction Dynamics, Theory and Experiment.* (Oxford University Press, New York, 1996) and references cited therein.

[50] R.A. Marcus, J. Chem. Phys. **20**, 359 (1952).

[51] R.A. Marcus, J. Chem. Phys. **43**, 2658 (1965), **52**, 1108 (1970).

[52] S.C. Smith and R.G. Gilbert, Int. J. Chem. Kinet. **20**, 979 (1988).

[53] J.I. Steinfeld, S.M. Alder-Golden, and J.W. Gallagher, J. Phys. Chem. Ref. Data. **16**, 911 (1987) and references cited therein.

[54] S.M. Anderson, F.S. Klein and F. Kaufman, J. Chem. Phys. **83**, 1648 (1985).

[55] The $dg(E,J)/dt = -c(E,J)/([\mathrm{X}][\mathrm{YZ}])^2 d([\mathrm{X}][\mathrm{YZ}])/dt + dc(E,J)/dt/[\mathrm{X}][\mathrm{YZ}]$, where the second term gives rise to the righthand of Eq. (7), and the first term equals $-c(E,J)/[\mathrm{X}][\mathrm{YZ}]k_{bi}$. This first term is typically small and can be neglected. In fact, in the experiments for the measurement of the ozone formation rate constant, typically, only less than one thousandth of the reactants lead to the product.[19]

[56] R.W. Anderson, V. Aquilanti, S. Cavalli, and G. Grossi, J. Phys. Chem. **97**, 2443 (1993).

[57] R. E. Wyatt, J. Chem. Phys. **56**, 390 (1972).

[58] G. C. Schatz, A. Kuppermann, J. Chem. Phys. **65**, 4642 (1976).

[59] R.B. Walker, J.C. Light, Chem. Phys. **7**, 84 (1975).

[60] R.N. Zare, *Angular Momentum: Understanding Spatial Aspects in Chemistry and Physics.* (Wiley, New York, 1988) and references cited therein.

[61] R.A. Marcus and Y.Q. Gao, J. Chem. Phys. in press.

[62] The notation is different from and the expressions slightly less cumbersome than that used in Refs. 1 and 61, where N was used to denote the first active state (the state $M+1$ in the present article). The notation in Refs. 1 and 61 is retrieved by replacing the present M by $N-1$ and the present $N-1$ by M.

[63] We show here that the enrichment E defined by Eq. (4.13) of Ref. 36 reduces to the enrichment δ defined by Eq. (2.12) of Ref. 36 when $^{17}\mathrm{O}$ and $^{18}\mathrm{O}$ are present in trace amounts. We note that the $(^{M}\mathrm{O}_3)_{meas}$ in the former equals for trace isotope Q, OQO+QOO, and further that $(^{M}\mathrm{O}_3/^{48}\mathrm{O}_3)_{cal} = (3/2)\mathrm{QO}/\mathrm{O}_2$, since statistically, i.e., neglecting any isotopic effect, the equilib-

rium constant $(QO_2)_{tot}(O_2)/(O_3)(OQ)$=$(QOO+OQO)(O_2)/(O_3)(OQ)$= $1 + 1/2 = 3/2$, on introducing the symmetry factors. Thereby, Eq. (4.13) yields $E = \left({}^{M}O_3/{}^{48}O_3\right)_{meas}/(3QO/2O_2) - 1 = 2(QO)(OQO + QOO)/3(O_3)(O_2) - 1 = \delta$.

[64] K. Yamashita, K. Morokuma, F. Le Quere, and C. Leforestier, Chem. Phys. Lett. **191**, 515 (1992); C. Leforestier, F. Le Quere, K. Yamashita and K. Morokuma, J. Chem. Phys. **101**, 3806 (1994).

[65] A. Gross and G.D. Billing, Chem. Phys. **217**, 1 (1997).

[66] The modified *ab initio* potential[65] for the hindered rotation part of the diatomic fragment is fitted to a function $10.7\exp(-3.6(R - 1.667))\cos^2\theta$. The results obtained using this potential surface are 6.8×10^{-12} cm^{-3} s^{-1} at 300 K and 6.1×10^{-12} cm^{-3} s^{-1} at 130 K, which does not agree with the experimental temperature coefficient (Table I). The mimimum of the potential in Ref. 65 occurred at approximately an equilibrium angle of the stable ozone molecule even at large distances, and is shifted here to a linear configuration of the oxygen atom and the oxygen molecule.

[67] D.M. Wardlaw and R.A. Marcus, J. Chem. Phys. **83**, 3462 (1985).

[68] B. Brunetti, G. Liuti, E. Luzzatti, F. Pirani, and F. Vecchiocattvi, J. Chem. Phys. **74**, 6734 (1981).

[69] For $R \geq 2.6$Å, the $V_{bf}(R)$ is written as $-((1 - a(R))V_1 + a(R)V_2)$, where V_1 is the C_6/R^6 term and V_2 is the Morse potential, a is a function of R, $a = \exp(-6(R - 2.6))$.

[70] The β is obtained by $\beta = [f_{rr}/2D_{OO-O}]^{1/2}$, where f_{rr} is the diagonal quadratic stretching force constant and is 6.1164 mdyn Å^{-1} (Ref. 53) for ozone. (The number of significant figure is of course much less than this number would indicate.)

[71] A function of $\cos^2\theta$ type has been typically used.[67] In order to have a larger hindrance, to obtain a temperature dependence in reasonable agreement with the experimental results, a $\cos^4\theta$ function is used in this study. The effect of the hindered-rotor potential is seen in Fig. 4.

[72] W. Forst, *Theory of Unimolecular Reactions.* (Academic Press, New York, 1973) and references cited therein.

[73] B. Hathorn and R.A. Marcus, submitted for publication.

[74] V.G. Tyuterev, S. Tashkun, P. Jensen, A. Barbe and T. Cours, J. Mol. Spec. **198**, 57 (1999).

[75] C. Califano, *Vibrational States* (John Wiley and Sons, London, 1976), p. 215.

[76] The fitting parameters $hc\omega_i$'s and hcx_{ij}'s are given in the following in units of cm $^{-1}$: $hc\omega_1 = 716.6$, $hc\omega_2 = 1136.1$, $hc\omega_3 = 1071.4$, $hcx_{11} = -1.477$, $hcx_{22} = -4.497$, $hcx_{33} = -7.358$, $hcx_{12} = -8.087$, $hcx_{13} = -16.66$, $hcx_{23} = -37.87$.

[77] The vibrational states are, labeled from 1 to 35, (010), (100), (020), (110), (002), (030), (200), (120), (012), (040), (210), (102), (130), (300), (022), (050), (220), (112), (140), (310), (004), (032), (202), (060), (230), (400), (122), (150), (014), (320), (042), (212), (070), (240), (104).

[78] These rate constants differ slightly from those in Ref. 25, where in the definition of the rate constant an extra factor of 2 was added. In the present case, we have defined the rate constant so as not to include the factor of 2, in conformity with Ref. 26.

[79] For example, if $N_a^\dagger$ and $N_b^\dagger$ are both written as a function of its excess energy above threshold: $N_a^\dagger = (E - E_0^a)^n$ and $N_b^\dagger = (E - E_0^b)^n$. Then at energy E, where $E - E_a = \epsilon$, $E - E_0^b$ equals $\epsilon - \epsilon_0$, where $\epsilon_0 = E_b - E_a$. The ratio between the number of states becomes $(1 - \epsilon_0/\epsilon)^n$ and approaches unity more rapidly for a smaller value of n.

[80] W.L. Hase, J. Chem. Phys. **64**, 2442 (1976).

[81] M. Quack and J. Troe, Ber. Bunsenges. Phys. Chem. **81**, 329 (1977).

[82] G.P. Smith and D.M. Golden, Int. J. Chem. Kinet. **10**, 489 (1978).

[83] S.N. Rai and D.G. Truhlar, Int. J. Chem. Kinet. **79**, 6046 (1983).

[84] S.W. Benson, Can. J. Chem. **61**, 881 (1983).

[85] W.L. Hase and D.M. Wardlaw, in *Bimolecular Collisions*, edited by J.E. Baggott and M.N. Ashfold (Royal Society of Chemistry, Burlington House, London, 1989), p. 171.

[86] X. Hu and W.L. Hase, J. Phys. Chem. **93**, 6029 (1989).

[87] D.M. Wardlaw and R.A. Marcus, Adv. Chem. Phys. **70**, 231 (1988).

[88] S.J. Klippenstein and R.A. Marcus, J. Chem. Phys. **91**, 2281 (1989).

[89] S.J. Klippenstein and R.A. Marcus, J. Chem. Phys. **93**, 2418 (1990).

[90] S.J. Klippenstein, J. Chem. Phys. **94**, 6469 (1991).

[91] S.J. Klippenstein and Y.-W. Kim, J. Chem. Phys. **99**, 5790 (1993).

[92] S.J. Klippenstein, in *The Chemical Dynamics and Kinetics of Small Radicals, Part I*, edited by K. Liu and A. Wagner (World Scientific, Singapore, 1995) and references cited therein.

[93] Slightly better agreement is obtained for the temperature dependence of k_{bi}^0 by noting that η may increase with T, because of the shorter lifetimes of the high energy ozone molecules. This temperature dependence of η, however, is crucial for the temperature dependence of the enrichments. Indeed, the η at 140 K is obtained to be 1.13 (compared to 1.18 at 300 K), by fitting $^{16}\delta$ at that temperature.

[94] We consider the free rotor transition state to illustrate this approximately quadratic behavior: The number of rotational states of the diatomic molecule with energy less than or equal to ϵ is $\int_0^\epsilon (2j+1)(dj/dE)dE$, where $E = j(j+1)\hbar^2/2I$. This result equals $(2I/\hbar^2)\epsilon$, and the excess energy ϵ equals $E - E_c - E_0$, where E_c is the sum of the centrifugal potential and the loose transition state attractive potential for this channel, $l(l+1)\hbar^2/2\mu R^2 - C_6/R^6$, R being determined variationally by finding the maximum of this potential barrier. The E_c is then found to vary as l^3. If now we weight this number of states by $\rho(E, J)$, where ρ is approximately a constant

times $2J+1$, and let $J \approx l$ since $l >> j$, then we have an integral over $(2l+1)dl$. When the l^3 term is approximately replaced by an l^2 term with the same maximum magnitude and performing the integral, it is found that $N_a^\dagger$ is a quadratic function of $E - E_0^a$ and that $N_b^\dagger$ is a similar approximate function of $E - E_0^b$.

[95] A.J. Stace and J.N. Murrell, J. Chem. Phys. **68**, 3028 (1978).

TABLES

TABLE I. Calculated and experimental rate constants.

k	Reaction	T (K)	Expt.	Calc. (present)	Calc. (strong or loose)
k_{bi}^{0} [a]	$^{16}O + {}^{32}O_2 + N_2 \rightarrow {}^{48}O_3 + N_2$	130	4[b]	5.8[c]	7.0[d]
	$k_{bi} \propto T^{-n}$	130 – 300	$n = 2.6$	$n = 2.2$	$n = 0.77$
		300	0.5[b]	0.9[c]	3.7[d]
k_{ex} [e]	$^{16}O + {}^{18}O{}^{18}O \rightarrow {}^{16}O{}^{18}O + {}^{18}O$	130	5.6[f]	4.3[g]	9.2[h]
		300	2.9[f]	2.7[g]	9.5[h]
	$k_{ex} \propto T^{-m}$	130 – 300	$m = 0.88 \pm 0.26$	$m = 0.53$	$m = -0.07$
k_{bi}^{∞} [e]	$^{16}O + {}^{32}O_2 \rightarrow {}^{48}O_3$	130	18[b]	10.4[i]	21.7[j]
		300	> 4[b]	6.5[i]	20.6[j]

[a]Units are 10^{-33}cm^{6}s^{-1}.

[b]Experimental data from Hippler *et al.*, Ref. 30.

[c]Calculated from Eq. (31) using a value of 210 cm^{-1} for ΔE. When ΔE =180 cm^{-1} the values are 4.6, 0.7 and when ΔE =250 cm^{-1} the values are 6.1, 1.3. The results obtained for k_{bi}^{0} and n using a free rotor transition state are, for the weak collision case, the same to those given in the first three rows of the penultimate column in this Table.

[d]Calculated using the strong collision assumption.

[e]Units are 10^{-12}cm^{3}molecule^{-1}s^{-1}.

[f]Experimental data from Wiegell *et al.*, Ref. 31.

[g]Calculated from Eq. (18), using the hindered-rotor transition state theory.

[h]Calculated using the loose transition state theory.

[i]Calculated from Eq. (49), using the hindered-rotor transition state theory.

[j]Calculated from Eq. (49), using the loose transition state theory.

TABLE II. Relative rate coefficients of atom plus homonuclear diatomic formation channels ($X + YY \rightarrow XYY$ relative to $X + XX \rightarrow X_3$) at low pressure at 300 K.

Reaction	Expt.[a]	Cal.
$^{16}O + {}^{36}O_2/{}^{16}O + {}^{32}O_2$	1.53 ± 0.03	1.53
$^{17}O + {}^{36}O_2/{}^{17}O + {}^{34}O_2$	1.29 ± 0.07	1.36
$^{16}O + {}^{34}O_2/{}^{16}O + {}^{32}O_2$	1.23 ± 0.03	1.38
$^{17}O + {}^{32}O_2/{}^{17}O + {}^{34}O_2$	1.01 ± 0.05	1.01
$^{18}O + {}^{34}O_2/{}^{18}O + {}^{36}O_2$	1.00 ± 0.06	1.04
$^{18}O + {}^{32}O_2/{}^{18}O + {}^{36}O_2$	0.90 ± 0.03	0.90

[a]From Mauersberger *et al.*, Ref. 26.

TABLE III. Reaction rate coefficients for ozone formation processes relative to $^{16}O + {}^{32}O_2 \rightarrow {}^{48}O_3$ at low pressure.

Reaction	Expt.[a]	Calc.[b]
$^{16}O + {}^{16}O{}^{16}O$	1.00	1.00
$^{17}O + {}^{17}O{}^{17}O$	1.02	1.02
$^{18}O + {}^{18}O{}^{18}O$	1.03	1.03
$^{18}O + {}^{16}O{}^{16}O$	0.93	0.93
$^{17}O + {}^{16}O{}^{16}O$	1.03	1.03
$^{18}O + {}^{17}O{}^{17}O$	1.03	1.07
$^{17}O + {}^{18}O{}^{18}O$	1.31	1.39
$^{16}O + {}^{17}O{}^{17}O$	1.23	1.38
$^{16}O + {}^{18}O{}^{18}O$	1.53	1.53
$^{16}O + {}^{16}O{}^{17}O$[c]	1.17	1.19
$^{16}O + {}^{16}O{}^{18}O$[c]	1.27	1.25
$^{17}O + {}^{16}O{}^{17}O$[c]	1.11	1.04
$^{17}O + {}^{17}O{}^{18}O$[c]	1.21	1.20
$^{18}O + {}^{16}O{}^{18}O$[c]	1.01	0.99
$^{18}O + {}^{17}O{}^{18}O$[c]	1.09	1.05
$^{16}O + {}^{17}O{}^{18}O$[c]	—	1.43
$^{17}O + {}^{16}O{}^{18}O$[c]	—	1.21
$^{18}O + {}^{16}O{}^{17}O$[c]	—	1.01

[a]From Mauersberger *et al.* Ref. 26, at room temperature.

[b]The effective densities of states are reduced by a factor $\eta = 1.18$ for symmetric molecules. Results are obtained using the stepladder energy transfer model (Eq. (31)), with $\Delta E = 210$ cm^{-1}, and the hindered-rotor transition state theory. The results obtained using the loose transition state theory are essentially the same as when the hindered-rotor transition state theory is used, but there $\Delta E = 260$ cm^{-1}.

[c]The rate constant which appears here is the sum of both channels, i.e., both $X+YZ \rightarrow XYZ$ and $X + YZ \rightarrow XZY$. Each of the rate constants were determined separately, with the non-RRKM correction only applied to the symmetric channel, where applicable.

TABLE IV. Reaction rate coefficients for asymmetric and symmetric channels of recombination reactions, relative to $^{16}O + {}^{16}O_2 \rightarrow {}^{16}O_3$ at low pressure.

Reaction	Expt.[a]	Calc. [b]
Symmetric Products		
$^{16}O + {}^{17}O{}^{16}O \rightarrow {}^{16}O{}^{17}O{}^{16}O$	—	0.51
$^{16}O + {}^{18}O{}^{16}O \rightarrow {}^{16}O{}^{18}O{}^{16}O$	0.54±0.01	0.52
$^{17}O + {}^{16}O{}^{17}O \rightarrow {}^{17}O{}^{16}O{}^{17}O$	—	0.51
$^{17}O + {}^{18}O{}^{17}O \rightarrow {}^{17}O{}^{18}O{}^{17}O$	—	0.51
$^{18}O + {}^{16}O{}^{18}O \rightarrow {}^{18}O{}^{16}O{}^{18}O$	0.52±0.01	0.52
$^{18}O + {}^{17}O{}^{18}O \rightarrow {}^{18}O{}^{17}O{}^{18}O$	—	0.52
Asymmetric Products[c]		
$^{18}O + {}^{17}O{}^{16}O \rightarrow {}^{18}O{}^{17}O{}^{16}O$	—	0.47
$^{18}O + {}^{18}O{}^{16}O \rightarrow {}^{18}O{}^{18}O{}^{16}O$	0.46±0.03	0.47
$^{17}O + {}^{18}O{}^{16}O \rightarrow {}^{17}O{}^{18}O{}^{16}O$	—	0.52
$^{17}O + {}^{17}O{}^{16}O \rightarrow {}^{17}O{}^{17}O{}^{16}O$	—	0.53
$^{18}O + {}^{18}O{}^{17}O \rightarrow {}^{18}O{}^{18}O{}^{17}O$	—	0.53
$^{18}O + {}^{16}O{}^{17}O \rightarrow {}^{18}O{}^{16}O{}^{17}O$	—	0.53
$^{17}O + {}^{16}O{}^{18}O \rightarrow {}^{17}O{}^{16}O{}^{18}O$	—	0.70
$^{16}O + {}^{16}O{}^{17}O \rightarrow {}^{16}O{}^{16}O{}^{17}O$	—	0.68
$^{17}O + {}^{17}O{}^{18}O \rightarrow {}^{17}O{}^{17}O{}^{18}O$	—	0.70
$^{16}O + {}^{18}O{}^{17}O \rightarrow {}^{16}O{}^{18}O{}^{17}O$	—	0.69
$^{16}O + {}^{16}O{}^{18}O \rightarrow {}^{16}O{}^{16}O{}^{18}O$	0.73±0.02	0.74
$^{16}O + {}^{17}O{}^{18}O \rightarrow {}^{16}O{}^{17}O{}^{18}O$	—	0.74

[a]From Janssen *et al.*, Ref. 27. See also Ref. 78 for a definition of the value of k used.

[b]Calculated using the stepladder energy transfer model and the hindered-rotor transition state theory. ΔE is 210 cm^{-1}.

[c]Reactions for asymmetric products are ordered in sequence of increasing zero-point energy difference.

TABLE V. Calculated and experimental isotopic enrichments at 300 K.

Isotope Combination	Experiment[a]	Calc.[b] (%)
$^{16}O^{16}O^{16}O$	0.0	0.0
$^{17}O^{17}O^{17}O$	−1.8	−2.1
$^{18}O^{18}O^{18}O$	−4.6	−4.7
$^{16}O^{16}O^{17}O$[c]	11.3	12.3
$^{16}O^{16}O^{18}O$[c]	13.0	12.7
$^{17}O^{17}O^{16}O$[c]	12.1	12.2
$^{17}O^{17}O^{18}O$[c]	9.5	10.4
$^{18}O^{18}O^{16}O$[c]	14.4	12.7
$^{18}O^{18}O^{17}O$[c]	8.3	9.2
$^{16}O^{17}O^{18}O$[c]	18.1	17.4

[a]Experimental data at 300 K are from Mauersberger *et al.*, Ref. 26.

[b]Calculated from Eqs. (4.18a), (4.18b), and (4.26) of Part I. The definition of enrichment is given by Eq. (4.13) there. A value of 210 cm $^{-1}$ is used for the ΔE.

[c]Enrichment is for all possible isotopomers.

TABLE VI. Temperature effect on enrichments and rate constant ratios.

	Cal. (140 K)	Exp. (140K)[a]	Cal. (300 K)	Exp. (300K)[b]
η	1.13[c]	–	1.18[d]	–
$^{16}O + ^{16}O^{18}O/^{16}O + ^{16}O^{16}O$	0.75	–	0.74	0.73
$^{18}O + ^{16}O^{16}O/^{16}O + ^{16}O^{16}O$	0.83	–	0.93	0.93
$^{16}O + ^{18}O^{16}O/^{16}O + ^{16}O^{16}O$	0.52	–	0.52	0.54
enrichment of $^{16}O^{16}O^{18}O$	8.2%	8.3%	12.7%	13.0%
$^{16}O + ^{18}O^{18}O/^{16}O + ^{16}O^{16}O$	1.53	–	1.53	1.53
$^{18}O + ^{18}O^{16}O/^{16}O + ^{16}O^{16}O$	0.44	–	0.47	0.46
$^{18}O + ^{16}O^{18}O/^{16}O + ^{16}O^{16}O$	0.52	–	0.52	0.52
enrichment of $^{16}O^{18}O^{18}O$	3.0%	–	14.1%	14.4%
$^{18}O + ^{18}O^{18}O/^{16}O + ^{16}O^{16}O$	1.03	–	1.03	1.03
enrichment of $^{18}O^{18}O^{18}O$	−16.6%	–	−4.7%	−4.6%

[a]Experimental results are taken from Ref. 12.

[b]Experimental results are taken from Ref. 26.

[c]Obtained by fitting the experimental value of enrichment of $^{16}O^{16}O^{18}O$ at 140 K.

[d]Obtained by fitting the experimental value of two rate constant ratios, $^{16}O + ^{18}O^{18}O/^{16}O + ^{16}O^{16}O$ and $^{18}O + ^{16}O^{16}O/^{18}O + ^{18}O^{18}O$, at 300 K.

Figure Captions

Fig. 1 The stepladder model for the deactivation of XYZ* molecules formed by the recombination reaction.

Fig. 2 Examples of the energies for the eigenstate of a hindered rotor. The points are the calculated results. The horizontal line represents the height of the rotational barrier. The dashed line is the energy of a free rotor plus the averaged value of the potential energy.

Fig. 3 The total energy of a hindered rotor state (J, j, Ω) as a function of R. The maximum of the hindered rotor states (symbols) are shifted inward compared to that of a free rotor (J, j, K) (solid lines), increasingly shifted with increasing (J, j, ω).

Fig. 4 The number of states $N^{\dagger}$ as a function of R for the recombination reaction $^{16}O + ^{32}O_2 \rightarrow ^{48}O_3$. The top curve is obtained using free rotation in the transition and the other two curves are obtained using the hindered-rotor transition state: The middle curve, labeled by "Hindered Rotor TS 1," is obtained using a hindered-rotor potential $\cos^2\theta$, and the lowest curve is obtained using a $\cos^4\theta$ type potential.

Fig. 5 The fits of the known vibrational frequencies[77] (taken from Ref. 74) of $^{16}O^{16}O^{16}O$ using up to second-order anharmonicity corrections.

Fig. 6 Comparison of calculated and experimental[26] relative atom + diatomic rate constant ratios, k_{X+YY}/k_{X+XX}, at 300 K with $\eta = 1.18$.

Fig. 7 Comparison of calculated and experimental[26] relative atom + diatomic rate constant ratios, k_{X+YZ}/k_{6+66}, at 300 K with $\eta = 1.18$. Some of the experimental rate constants are "derived quantities"[26].

Fig. 8 Experimental[26] (grey bars) and calculated isotopic enrichments for scrambled systems heavily enriched in heavy isotopes at 300 K, with $\eta = 1.18$ (dark bars) and $\eta = 1.0$ (light bars) respectively.

Fig. 9 The pressure dependence of the recombination rate constant for $^{16}O + ^{32}O_2 \rightarrow ^{48}O_3$ at 130K and 300 K. The units are 10^{-12} cm^{-3} molecule^{-1} s^{-1}. The experimental data are taken from Ref. 30.

Fig. 10 The pressure dependence of the enrichment $^{18}\delta$. The filled diamonds are the experimental results[28] and the solid line gives the calculated results using the hindered-rotor transition state with a $\Delta E = 210\text{cm}^{-1}$.

Fig. 11 The pressure dependence of the individual rate constants. The filled circles are the experimental results[28] for the rate ratio between $^{18}O + ^{32}O_2 \rightarrow ^{18}O^{16}O^{16}O$ and $^{18}O + ^{36}O_2 \rightarrow ^{54}O_3$, and the triangles are the experimental results for the rate ratio between $^{16}O + ^{36}O_2 \rightarrow ^{18}O^{18}O^{16}O$ and $^{16}O + ^{32}O_2 \rightarrow ^{48}O_3$. The solid lines are the calculated results using the hindered-rotor transition state with a $\Delta E = 210\ \text{cm}^{-1}$.

Fig. 12 The effective density of states $\sum_J \rho(E,J)h(N^\dagger(E,J))$ as a function of R for the recombination reaction $^{16}O + ^{32}O_2 \rightarrow ^{48}O_3$, where h is the unit step function. The dashed curve is obtained using a free rotor transition state and the lower one is obtained using the hindered-rotor transition state. The E's are given relative to the lowest state of the separated O and O_2.

Fig. 13 The partitioning factors versus energy. The functions plotted in the figure are $\sum_J \rho(E,J)N^\dagger_{a,b}/(N^\dagger_a + N^\dagger_b)$ as a function of the excess energy. The zero of the energy is set to be D_0, the dissociation energy at $J = 0$ for the channel with the smaller zero point energy, in the present case $^{16}O + ^{18}O^{18}O \rightarrow ^{16}O^{18}O^{18}O$. The solid lines are obtained using a free rotor transition state, and the triangles are obtained using the hindered-rotor transition state. The upper solid line and points are for the channel a, the channel with a smaller zero-point energy, and the lower ones are for channel b.

Fig. 14 The partitioning factors versus energy. The functions plotted in the figure is $\sum_J \rho(E,J)N^\dagger_a(E,J)/[N^\dagger_a(E,J) + N^\dagger_b(E,J)]$ as a function of energy. The points are the same as in Fig. 13 for the channel with a large zero-point energy. The lines are for the function $N^\dagger_a(E)/(N^\dagger_a(E) + N^\dagger_b(E))$, with modeling $N^\dagger(E)$'s for an illustration of the partitioning between two channels. The upper line is obtained by assuming[94] $N^\dagger_{a,b}$ to be proportional to $E - E_{a,b}$ and the lower one assumes $N^\dagger_{a,b}$ to be proportional to $(E - E_{a,b})^2$. Here, E_a is the dissociation energy for channel a at $J = 0$, and the J dependence of the $N^\dagger$'s is neglected.

Fig. 15 A model for the pressure effects on the rate constant and the rate

constant ratios, $(k^{as}_{6,68} + k^{as}_{8,66})/k_{6,66}$. To represent the pressure effect on the enrichment, the rate constant for the formation of a symmetric molecule is modeled by $k_s = \int_E \omega N^\dagger/(N^\dagger/\eta\rho + \omega)$, and that for an asymmetric one is assumed to be $k_a = \int_E \omega(N^\dagger_a + N^\dagger_b)/[(N^\dagger_a + N^\dagger_b)/\rho + \omega]$, which corresponds to a k^{eff}_{bi} for a real system. $N^\dagger_{a,b}$ is assumed to be proportional to $(E - E_{a,b})^2$, where $E_{a,b}$ is the dissociation barrier of the channel a or b. The "Rate Ratio" curve is a plot of k_a/k_s with an $\eta = 1.18$, and the "log [Rate Constant]" curve is a plot of $\log k_s$. The units of k_s is 10^{-12} cm^{-3} s^{-1}. In the plot $\log k_s$ has been mutiplied by 1/33 and then shifted by 0.8 to fit in the same rectangle as the plot of the Rate Constant ratio vs log (pressure) without affecting the conclusion.

Fig. 16 The same as Fig. 15. The low curve is a plot of the same function as the top rate ratio curve, except that $\eta = 1$ for both symmetric and asymmetric cases.

Fig. 17 The comparison between the calculated pressure dependence of the enrichment of $^{16}O^{16}O^{18}O$ and $^{16}O^{18}O^{18}O$.

Fig. 18 The P^c as a function of energy.

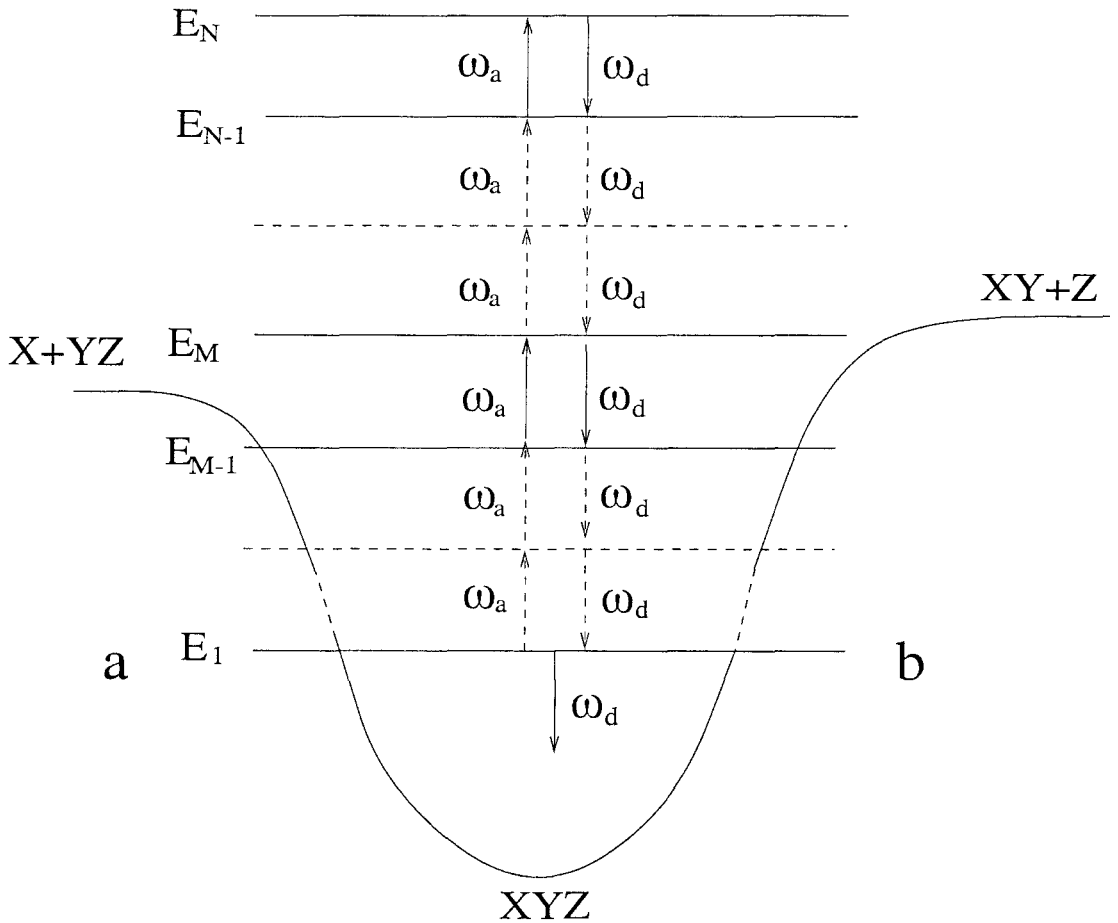

FIG. 1.

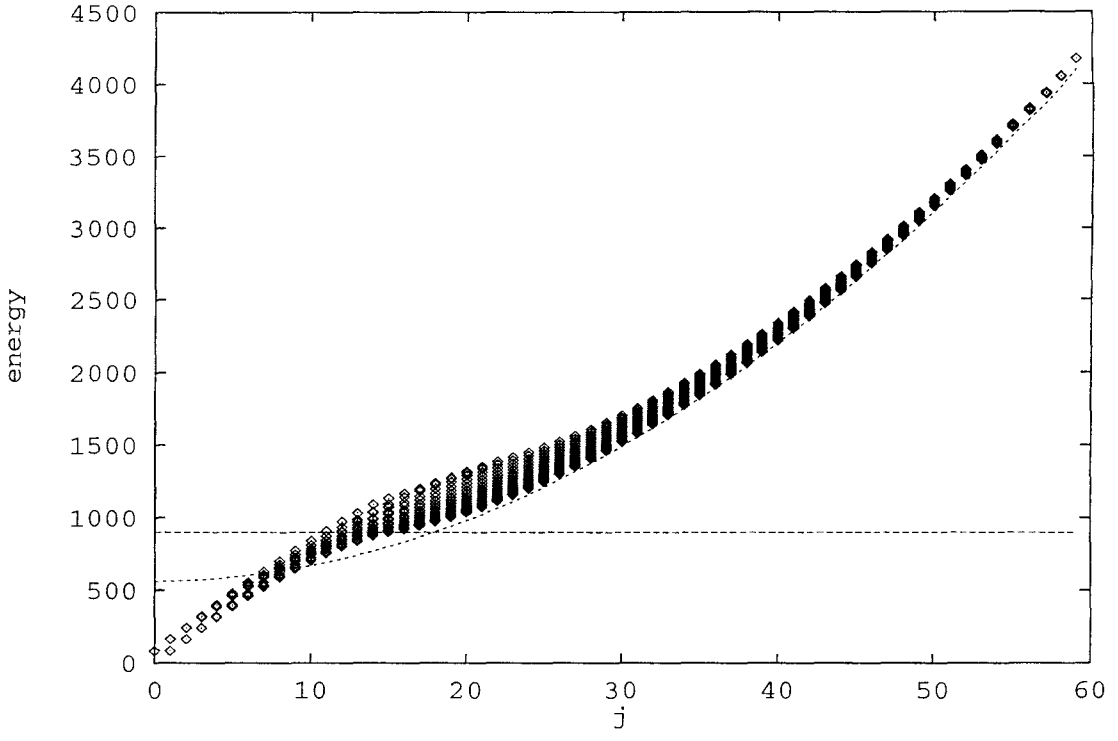
4500
4000
3500
3000
2500
2000
1500
1000
500
0
energy
0
10
20
30
40
50
60
j

FIG. 2.

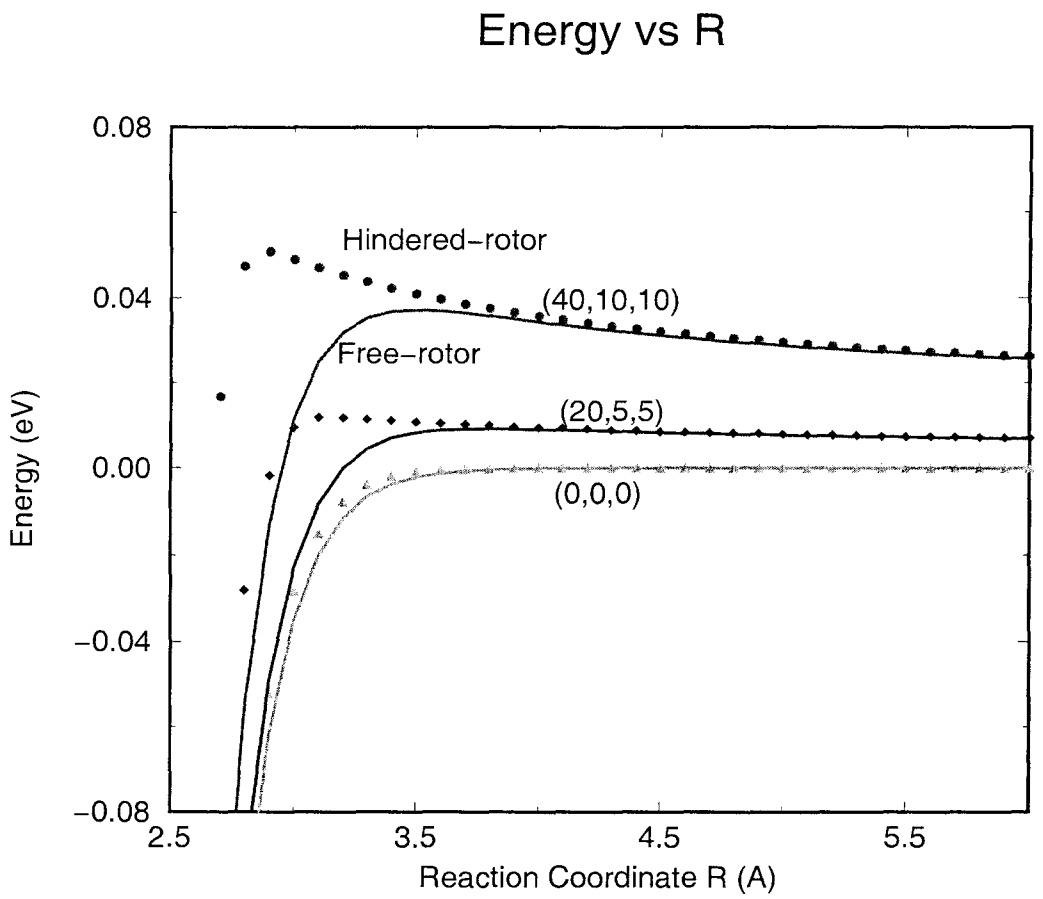
Energy vs R
0.08
0.04
0.00
−0.04
−0.08
Energy (eV)
Hindered−rotor
(40,10,10)
Free−rotor
(20,5,5)
(0,0,0)
2.5
3.5
4.5
5.5
Reaction Coordinate R (A)

FIG. 3.

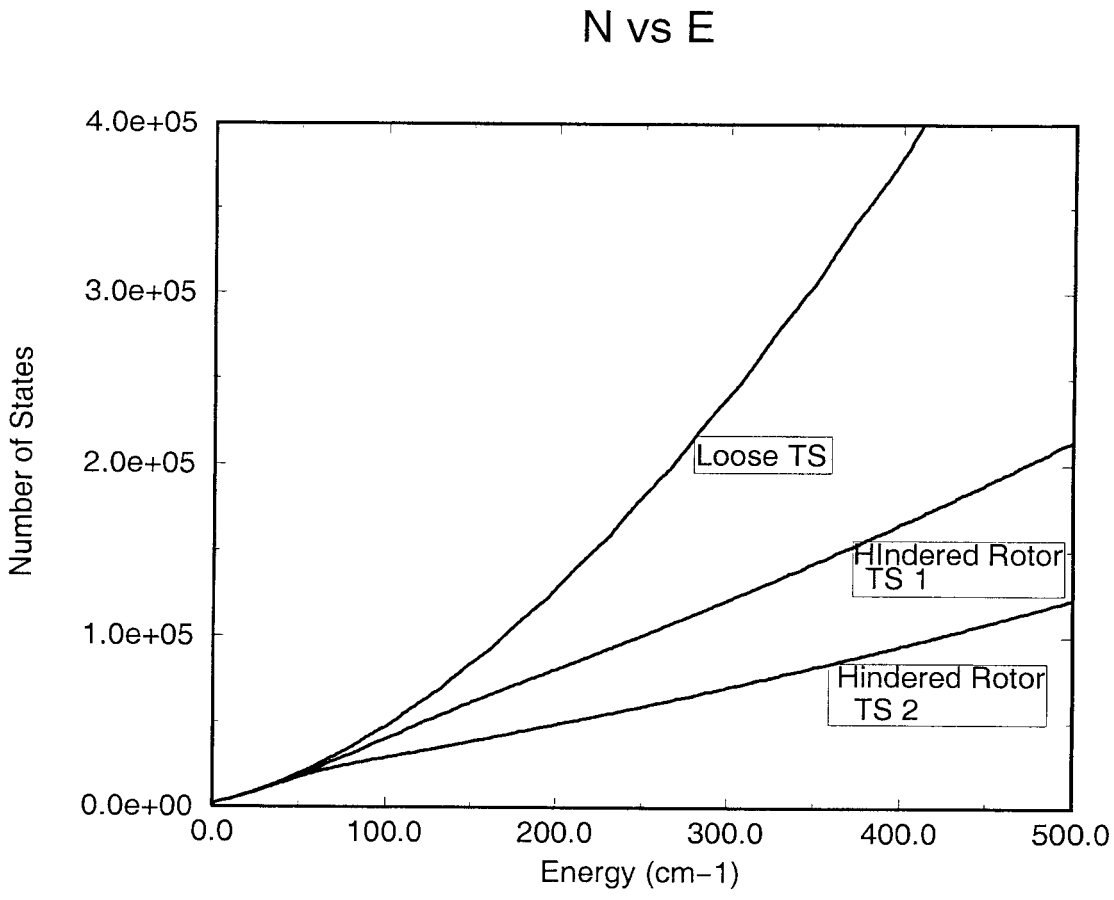
N vs E
4.0e+05
3.0e+05
2.0e+05
1.0e+05
0.0e+00
Number of States
0.0
100.0
200.0
300.0
400.0
500.0
Energy (cm-1)
Loose TS
Hindered Rotor TS 1
Hindered Rotor TS 2

FIG. 4.

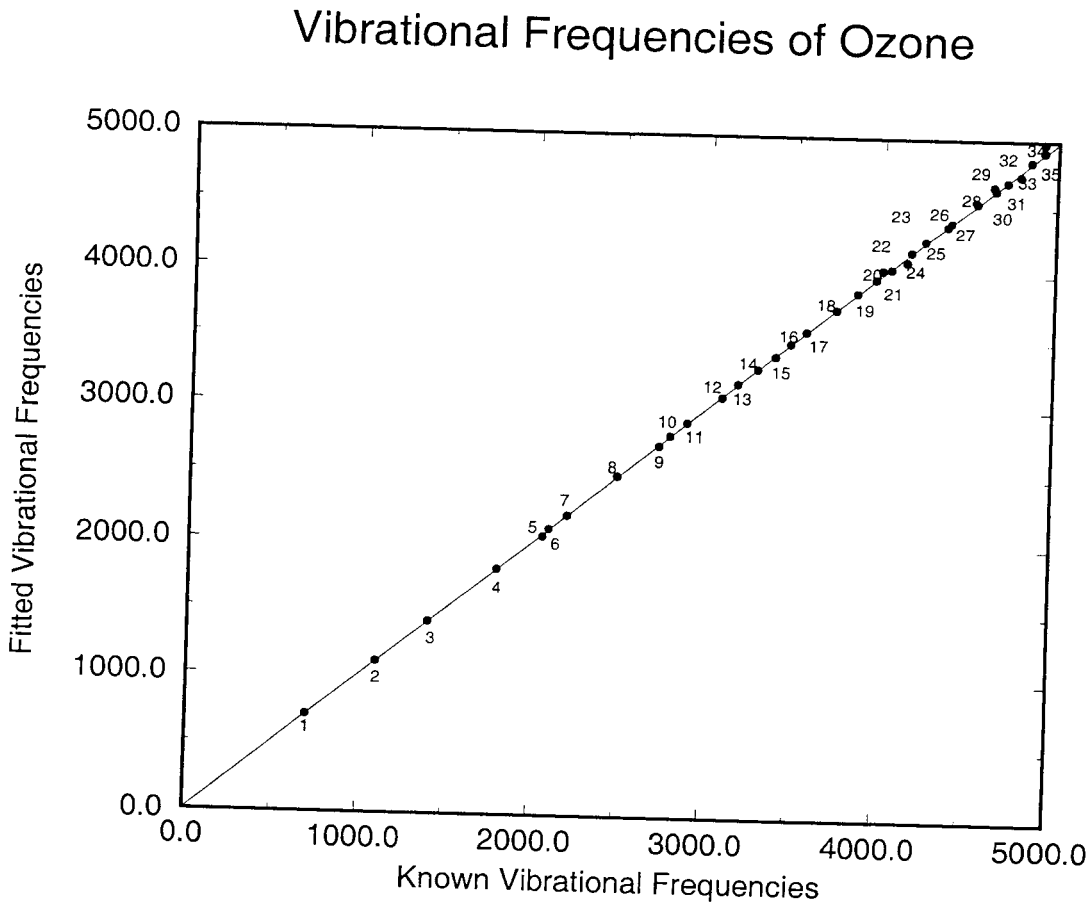
Vibrational Frequencies of Ozone
Fitted Vibrational Frequencies
Known Vibrational Frequencies
5000.0
4000.0
3000.0
2000.0
1000.0
0.0
0.0
1000.0
2000.0
3000.0
4000.0
5000.0

FIG. 5.

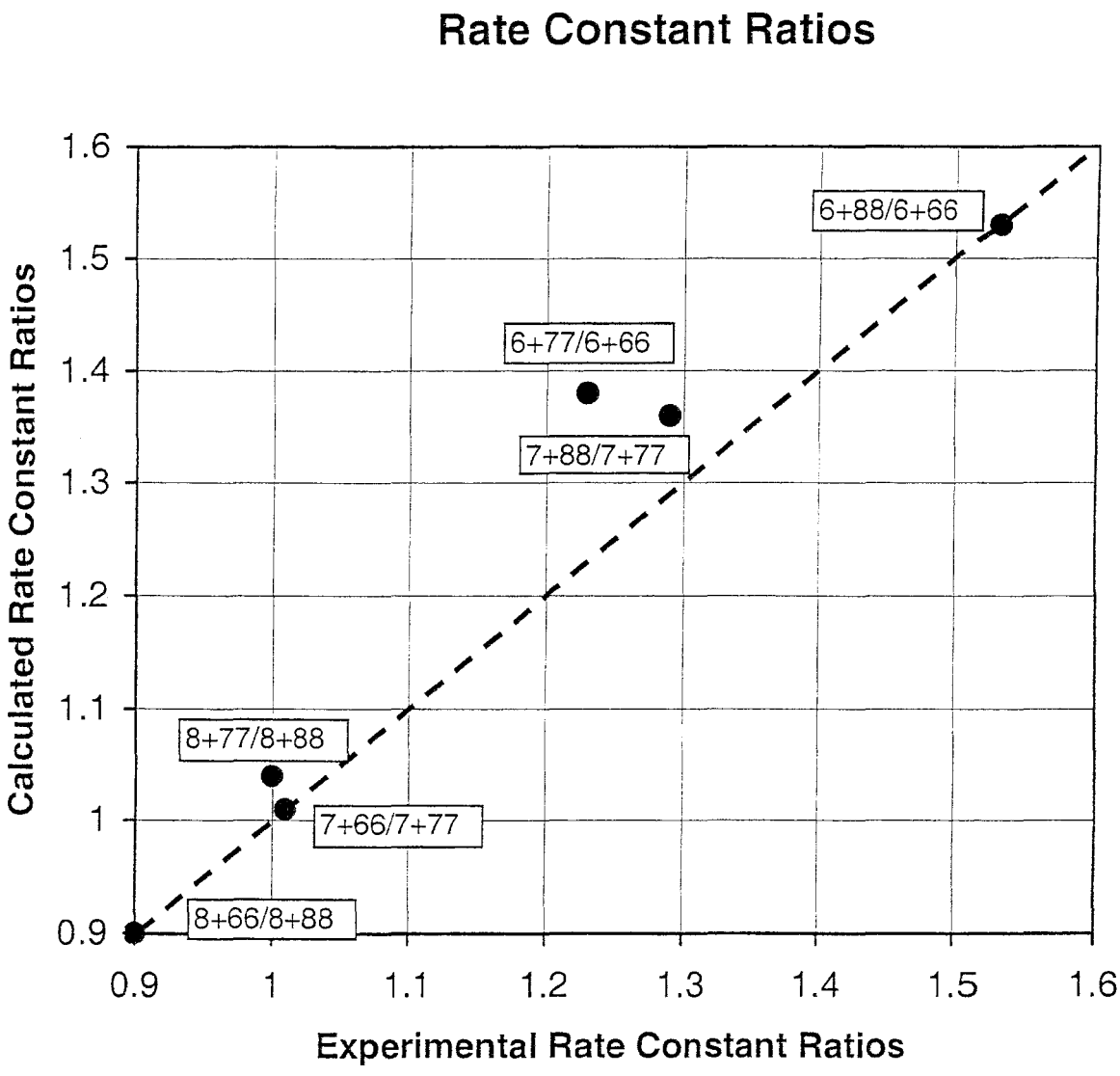
Rate Constant Ratios
Calculated Rate Constant Ratios
Experimental Rate Constant Ratios
1.6
1.5
1.4
1.3
1.2
1.1
1
0.9
0.9
1
1.1
1.2
1.3
1.4
1.5
1.6
6+88/6+66
6+77/6+66
7+88/7+77
8+77/8+88
7+66/7+77
8+66/8+88

FIG. 6.

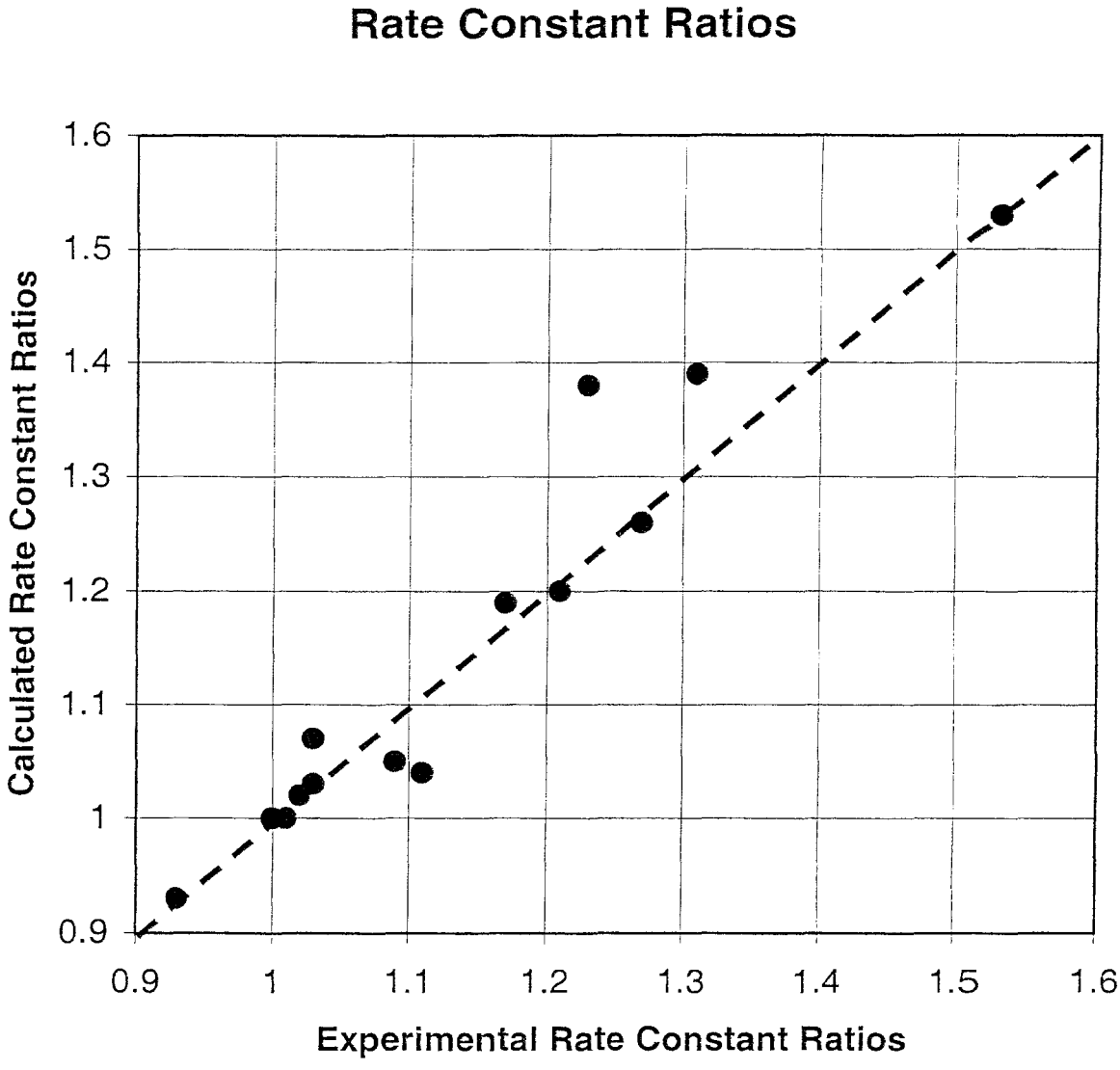
Rate Constant Ratios
Calculated Rate Constant Ratios
Experimental Rate Constant Ratios
1.6
1.5
1.4
1.3
1.2
1.1
1
0.9
0.9
1
1.1
1.2
1.3
1.4
1.5
1.6

FIG. 7.

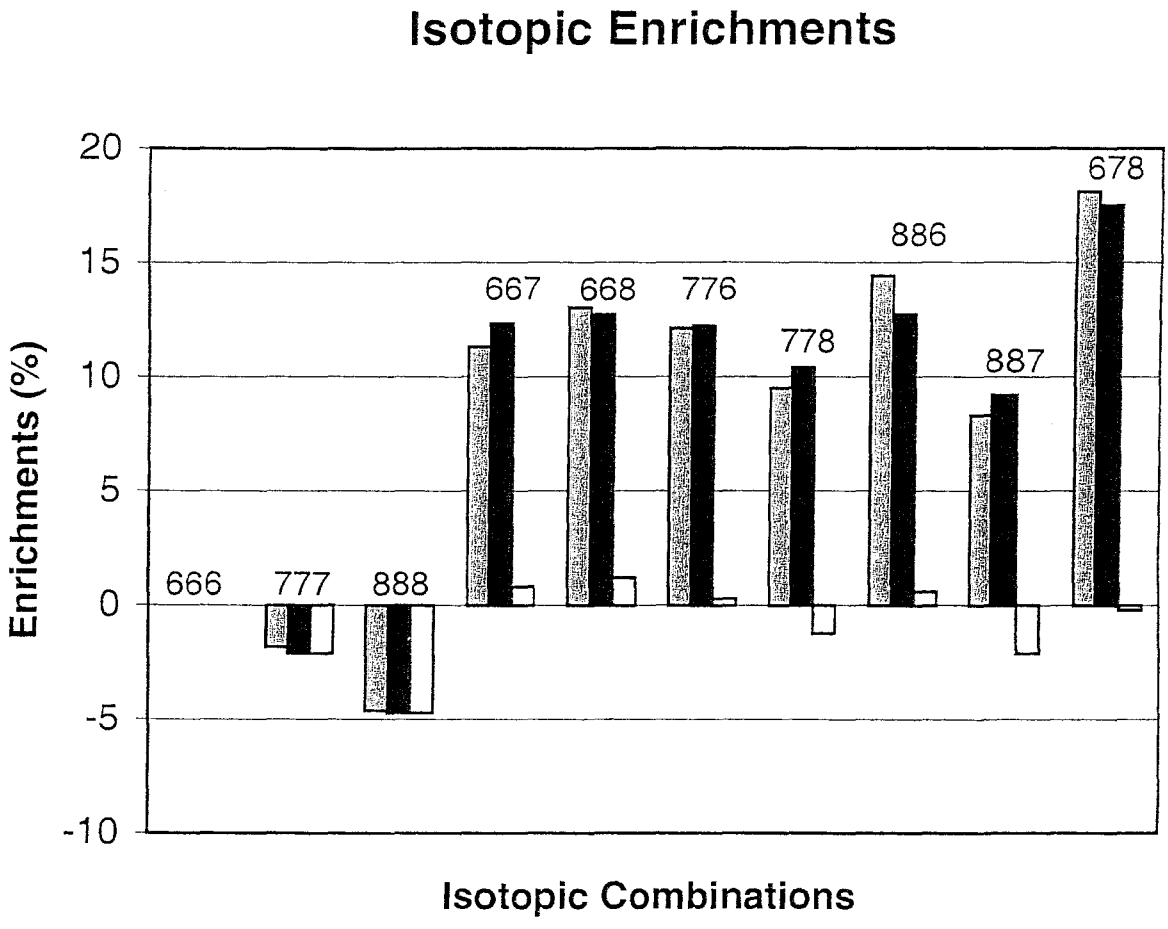
Isotopic Enrichments
20
15
10
5
0
-5
-10
Enrichments (%)
666
777
888
667
668
776
778
886
887
678
Isotopic Combinations

FIG. 8.

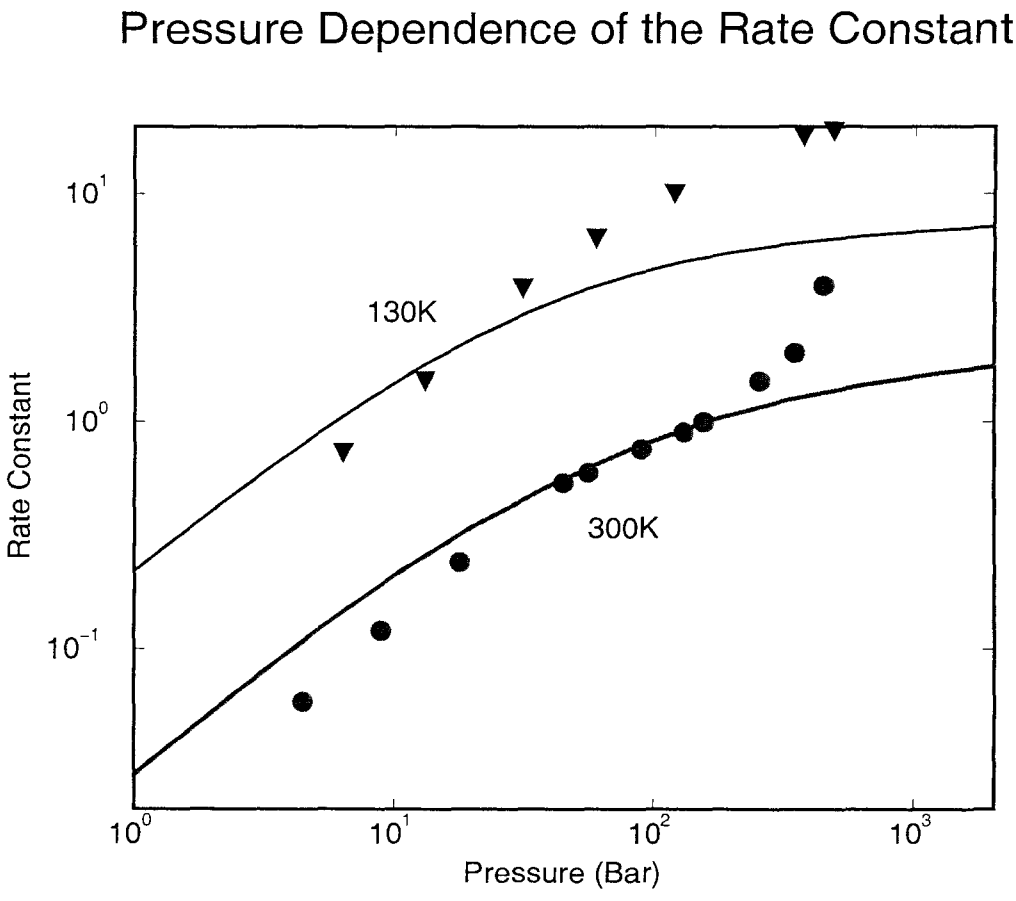
Pressure Dependence of the Rate Constant
Rate Constant
10^{1}
10^{0}
10^{-1}
130K
300K
10^{0}
10^{1}
10^{2}
10^{3}
Pressure (Bar)

FIG. 9.

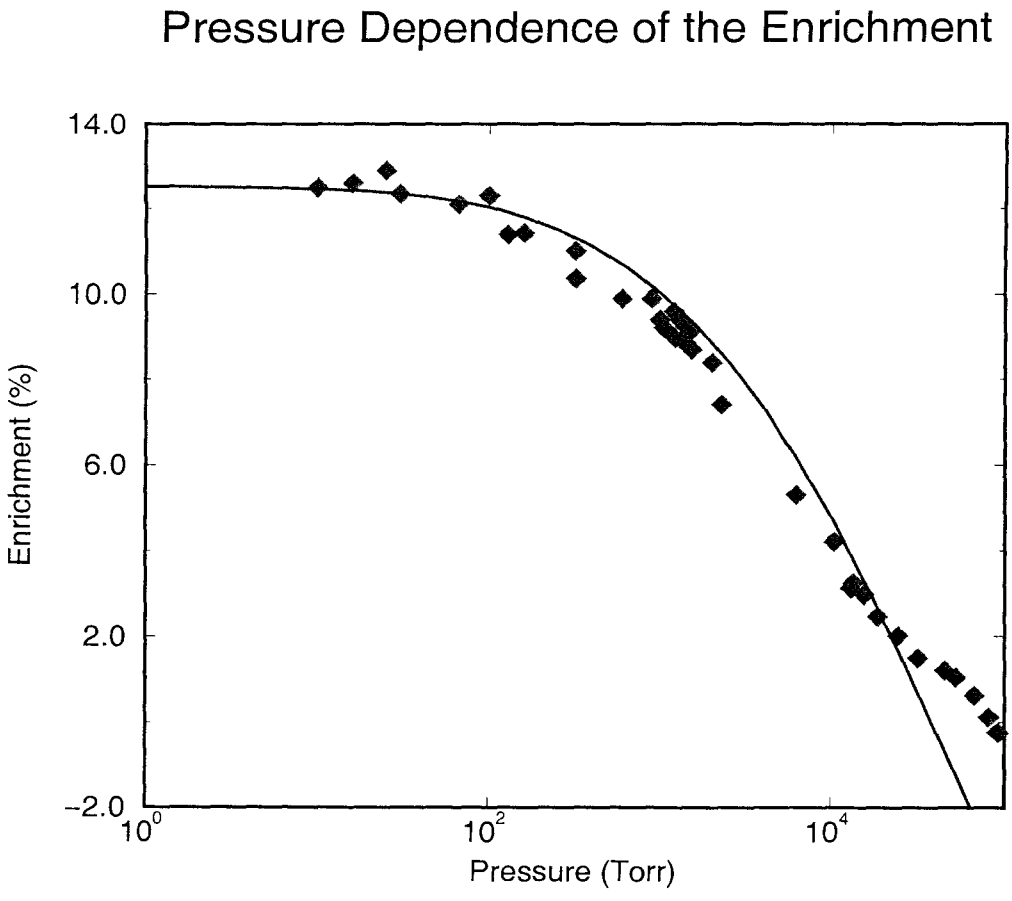
Pressure Dependence of the Enrichment
14.0
10.0
6.0
2.0
-2.0
Enrichment (%)
10^0
10^2
10^4
Pressure (Torr)

FIG. 10.

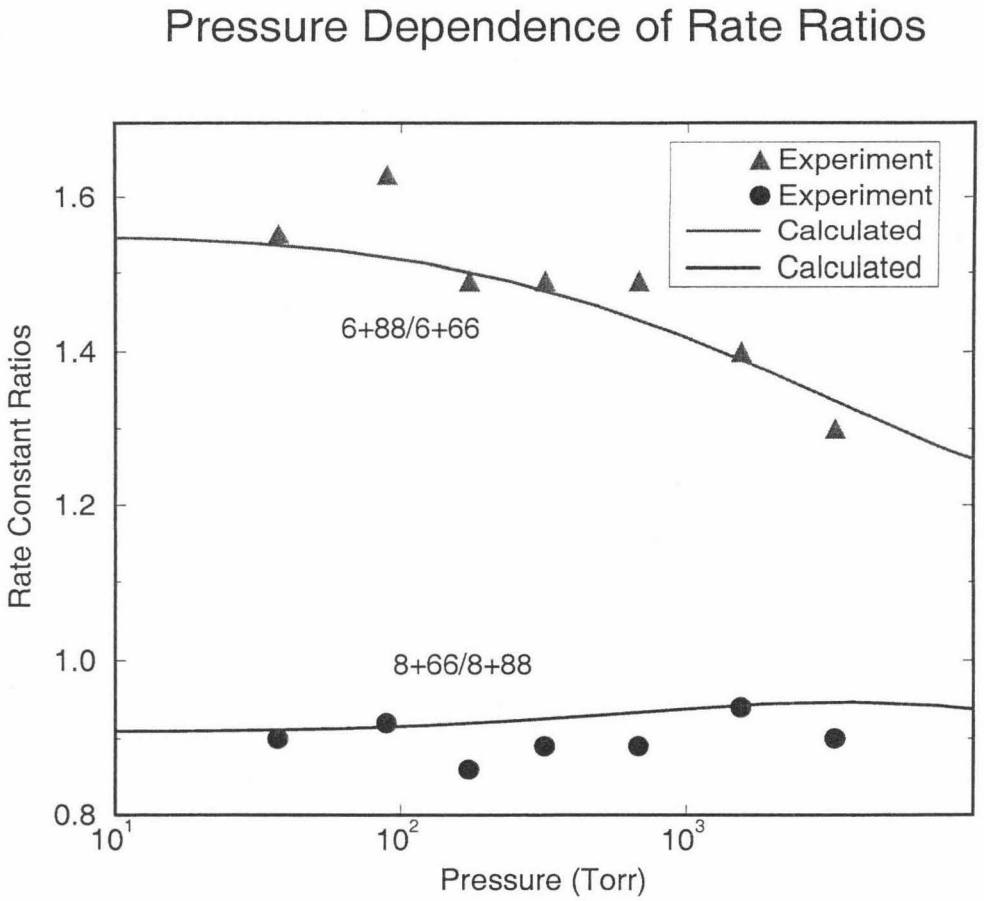
Pressure Dependence of Rate Ratios
Experiment
Experiment
Calculated
Calculated
6+88/6+66
8+66/8+88
Rate Constant Ratios
1.6
1.4
1.2
1.0
0.8
10^1
10^2
10^3
Pressure (Torr)

FIG. 11.

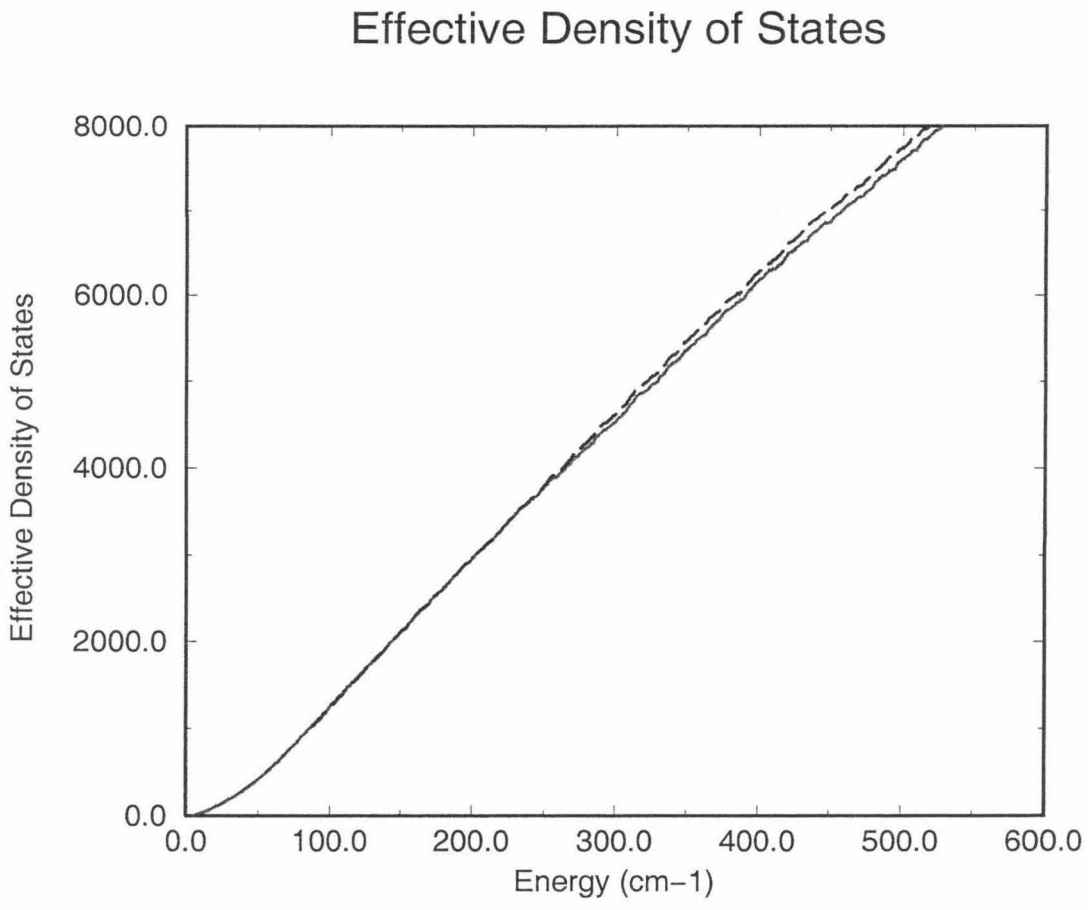
Effective Density of States
8000.0
6000.0
4000.0
2000.0
0.0
Effective Density of States
0.0
100.0
200.0
300.0
400.0
500.0
600.0
Energy (cm−1)

FIG. 12.

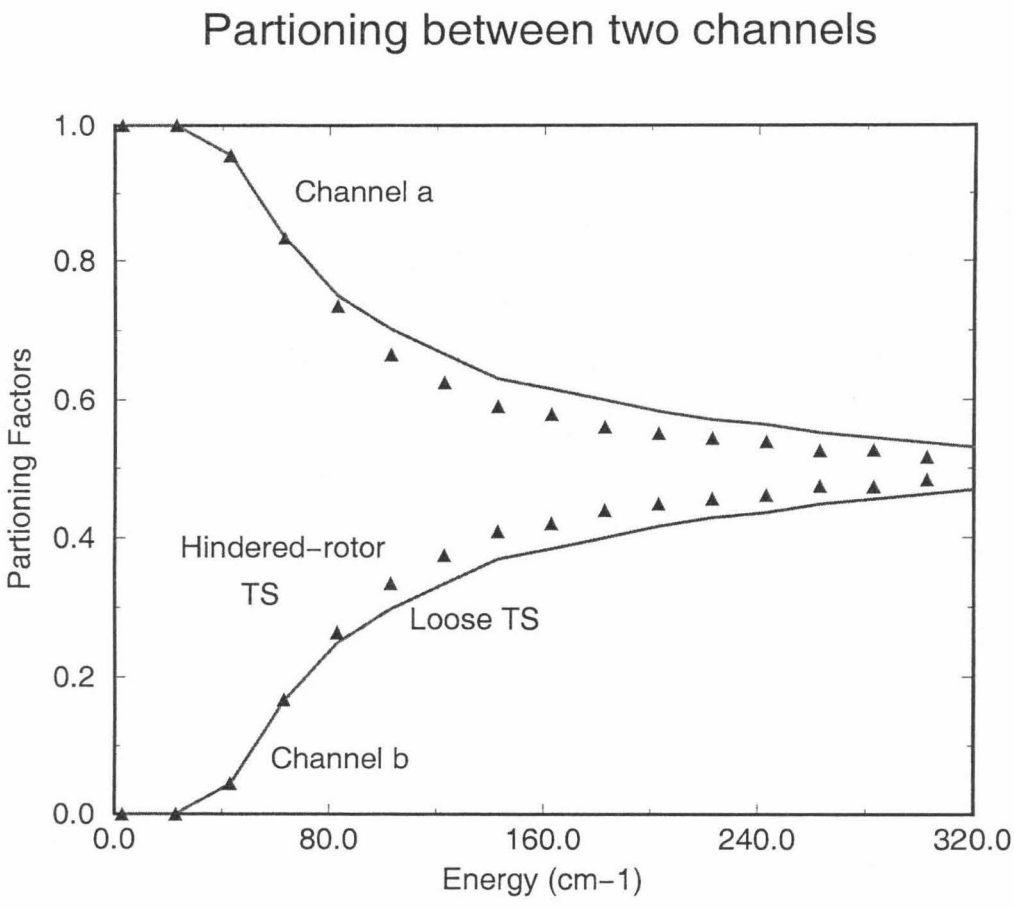
Partioning between two channels
Partioning Factors
1.0
0.8
0.6
0.4
0.2
0.0
Channel a
Hindered–rotor
TS
Loose TS
Channel b
0.0
80.0
160.0
240.0
320.0
Energy (cm–1)

FIG. 13.

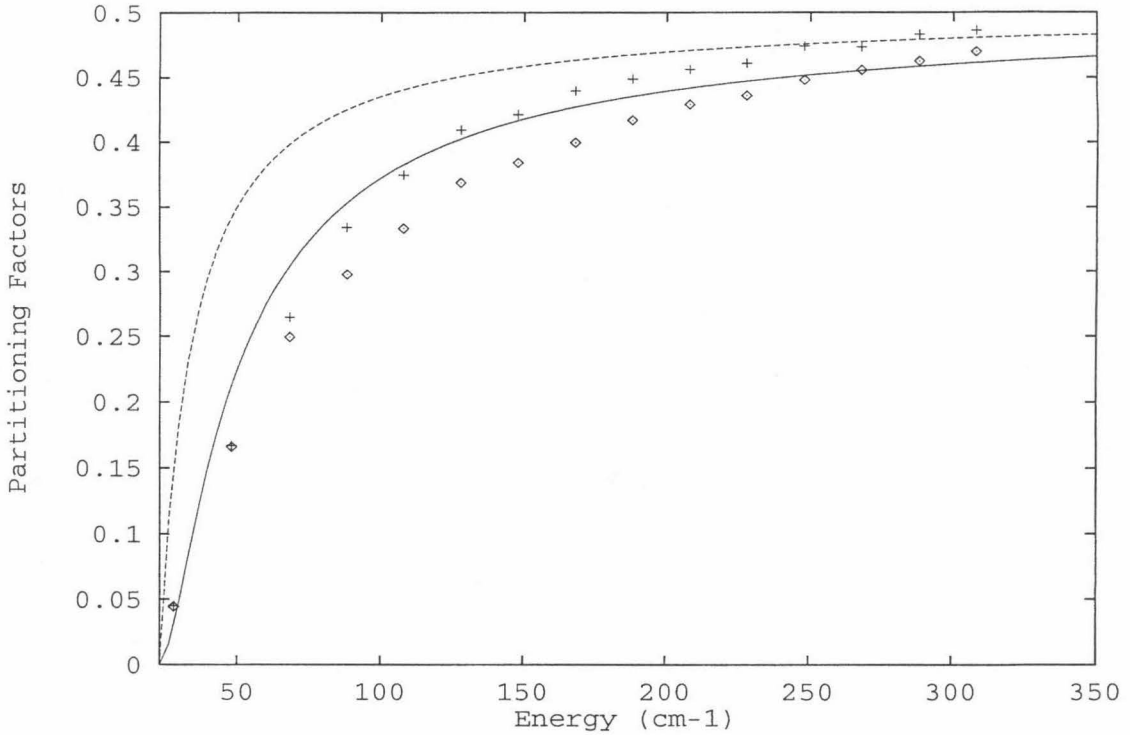
Partitioning Factors
0.5
0.45
0.4
0.35
0.3
0.25
0.2
0.15
0.1
0.05
0
50
100
150
200
250
300
350
Energy (cm-1)

FIG. 14.

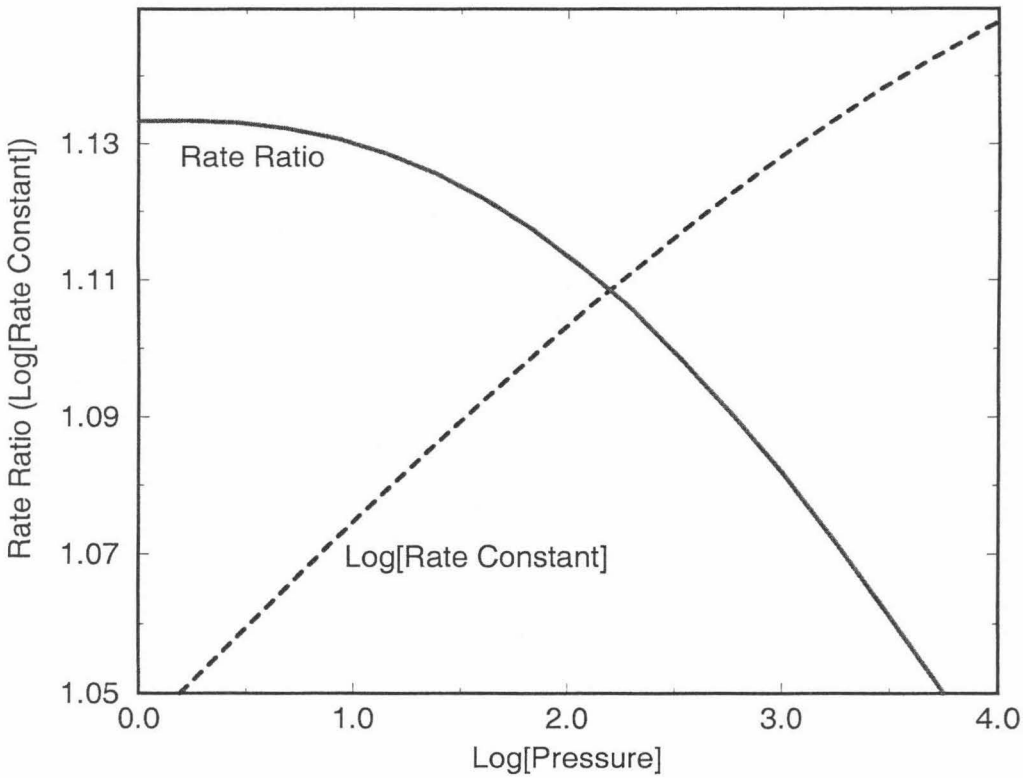
Rate Ratio (Log[Rate Constant])
1.13
1.11
1.09
1.07
1.05
Rate Ratio
Log[Rate Constant]
0.0
1.0
2.0
3.0
4.0
Log[Pressure]

FIG. 15.

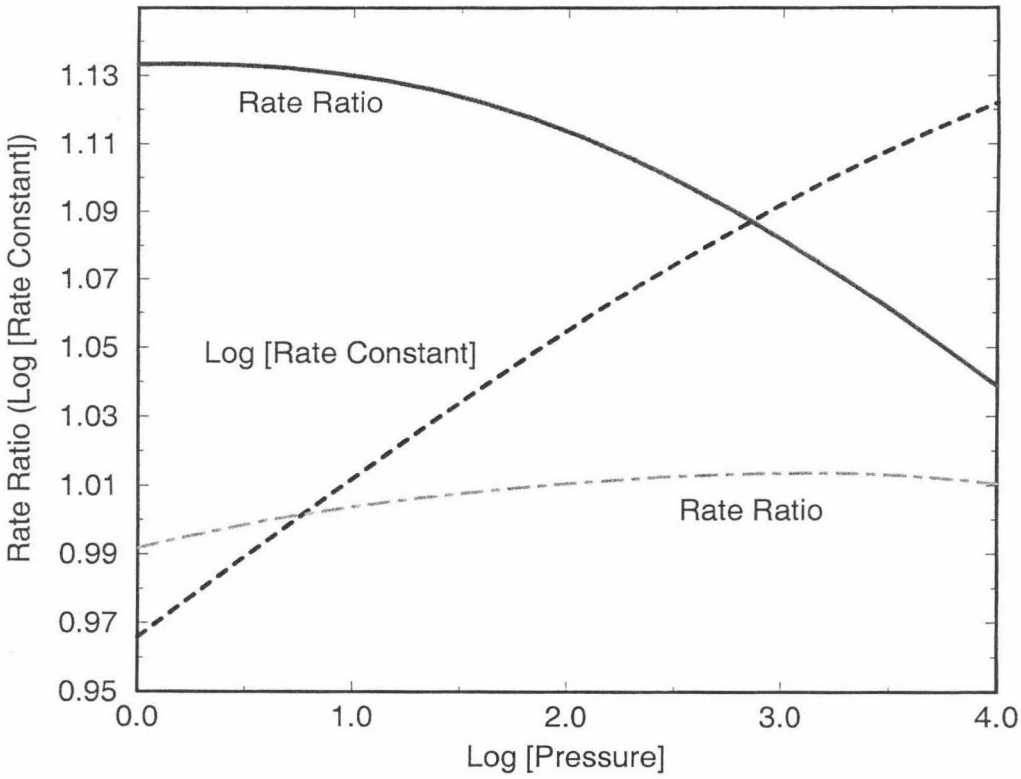
Rate Ratio (Log [Rate Constant])
1.13
1.11
1.09
1.07
1.05
1.03
1.01
0.99
0.97
0.95
0.0
1.0
2.0
3.0
4.0
Log [Pressure]
Rate Ratio
Log [Rate Constant]
Rate Ratio

FIG. 16.

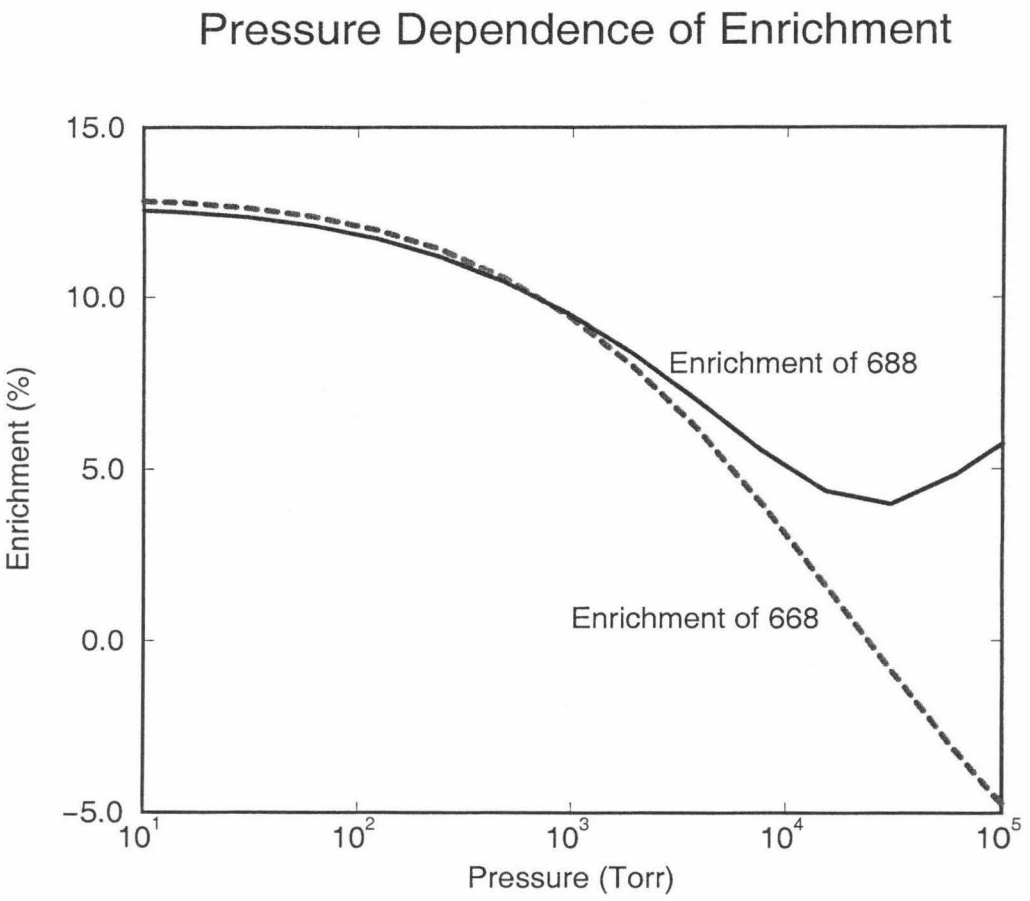
Pressure Dependence of Enrichment
15.0
10.0
5.0
0.0
−5.0
Enrichment (%)
Enrichment of 688
Enrichment of 668
10^1
10^2
10^3
10^4
10^5
Pressure (Torr)

FIG. 17.

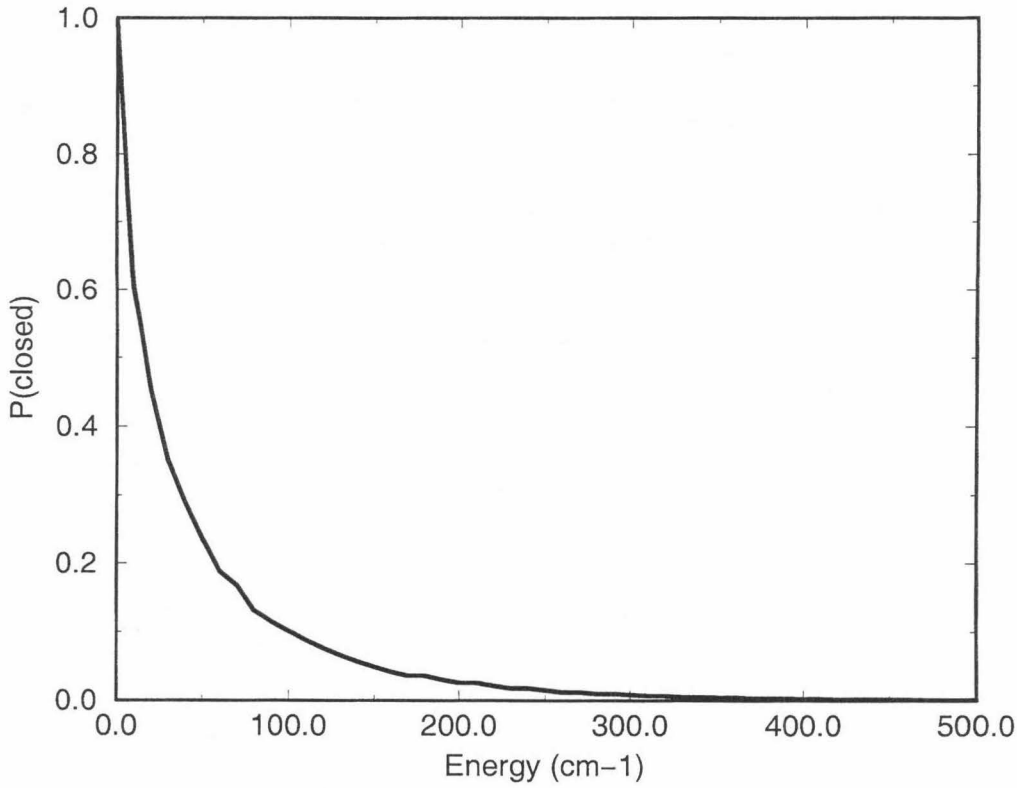
1.0
0.8
0.6
0.4
0.2
0.0
P(closed)
0.0
100.0
200.0
300.0
400.0
500.0
Energy (cm−1)

FIG. 18.

Chapter 3

Pressures effects on unimolecular dissociation
bimolecular recombination reactions
(J. Chem. Phys. in press)

Pressure Effects on Bimolecular Recombination and Unimolecular Dissociation Reactions

R. A. Marcus and Yi Qin Gao

Noyes Laboratory of Chemical Physics

California Institute of Technology

Pasadena, CA 91125

USA

Abstract

The treatment of pressure effects on bimolecular recombinations and unimolecular dissociations is discussed. The analysis of recombination and dissociation reactions is made by showing how the nonequilibrium energy (E) and angular momentum (J)-dependent steady-state population distribution functions for the two reactions are related to each other and to the equilibrium population distribution function at the given E and J. As a special case a strong collision model is then used for the collisional rotational angular momentum transfer, and a ladder model for the collisional energy transfer. An analytical result is obtained for states below the dissociation threshold. The extension to recombinations with two exit channels is described, for application to ozone formation and isotopic effects.

I. Introduction

Unimolecular dissociations and bimolecular associations have been intensively studied in the literature, and have been treated in well-known texts, monographs and articles.[1-5] It has been recognized for many years that weak collisions play a significant role in the activation-deactivation process and are needed to explain the detailed experimental results on pressure effects.[1,2,6-8] An important quantity in these collisions is the average energy of transfer ΔE, $\langle \Delta E \rangle$, for the deactivating collisions and, determined by microscopic reversibility, the average energy transfer in upward (activating) collisions. Studies have revealed that apart from rare "supercollisions"[9-11] the results for the energy transfer depend mainly on $\langle \Delta E \rangle$ (and the microscopic reversibility related upward average), and are relatively insensitive to the precise form of the collisional energy transfer function $\omega(E \rightarrow E')$.[1,2] In a recent study we have noted that an unusual "mass-independent" effect in recombination rates in "scrambled" systems and unconventional "mass-dependent" effects in unscrambled ones, may, in the interpretation given there, provide information on the dependence of $\langle \Delta E \rangle$ on temperature.[12] We discuss this particular aspect elsewhere,[13] using the formalism in the present paper, as well as using also an alternative "exponential-down" model for the collisional deactivation.[2] These applications of the present paper are to recombinations,[14] to their isotopic effects,[15,16] and to isotopic exchange reactions.[17]

The formalism is first given in Sec. II for the case of one *distinguishable* exit channel, i.e., for a system $X + YX \rightarrow XYX^* \rightarrow XY + X$, the asterisk denoting an energetic molecule. In Sec. II the relation of the steady-state distribution functions, as a function of the energy E and angular momentum J, is described for the recombination and dissociation reactions, both to each other and to the equilibrium distribution function. The treatment is specialized in Sec. III to include the strong collision approximation for rotations and a stepladder model for the collisional energy transfer, so leading to an analytical expression for the diffusion in "energy space" below the reaction threshold for dissociation. This model reduces significantly the number of quantum states needed in a numerical treatment. In Sec. IV the treatment is extended to the case of two distinguishable exit channels, e.g., $X + YZ \rightarrow XYZ^* \rightarrow X + YZ$ or $XY + Z$ ($X \neq Z$). The present equations, or their equivalent, are utilized elsewhere.[13] Isotopic exchange reactions are discussed in Sec. V.

II. A. Recombination

For the recombination of two particles X and YZ, where X may denote an atom or larger particle and YZ may denote a diatomic or larger particle, the reaction sequence for recombination can be written as

$$X + YZ \xrightarrow{k_a'(EJ)} XYZ\,(EJ) \tag{2.1}$$

$$XYZ\,(EJ) \xrightarrow{\omega(E\rightarrow E',J\rightarrow J')} XYZ\,(E'J') \tag{2.2}$$

$$XYZ\,(EJ) \xrightarrow{k_a(EJ)} X + YZ \tag{2.3}$$

$$XYZ\ (EJ) \xrightarrow{k_b(EJ)} XY + Z \tag{2.4}$$

where the energy E and the total angular momentum J of the colliding particles X and YZ are constants of the motion in (2.1), (2.3) and (2.4), and where, depending on (EJ), either or both $k_a(EJ)$ and $k_b(EJ)$ may vanish. Reactions (2.3) and (2.4) tacitly include XYZ$(E'J')$'s since the EJ in (2.1) can be an $E'J'$ and the double integration later in (2.7) and (2.13) is over all E, J, E' and J'.

In addition to the first step (2.1) a different reaction product XZY(EJ) may also be formed, with its own subsequent sequence of collisional and dissociation steps. It can be treated separately.[18,19]

The collisional frequency $\omega(E \rightarrow E', J \rightarrow J')$ for E and J transfer is typically proportional to the concentration of the ambient gas. The component K of the angular momentum of XYZ along a major symmetry or near-symmetry axis of XYZ may or may not be approximately constant during the lifetime of XYZ. We shall consider the latter case ("active rotation" K), and integrate over K in calculating the density of quantum states of an XYZ of given E and J. We first consider the case where there is only one distinguishable exit channel, i.e., where Z = X in Eqs. (2.1) – (2.4).

We let $c(EJ)$ be the concentration of XYZ(EJ) arising from reaction (2.1), abbreviate $\omega(E \rightarrow E', J \rightarrow J')$ by $\omega(EJ,E'J')$, and write

$$\int_{E'} \int_{J'} \omega(EJ,E'J')dE'dJ' = \omega \tag{2.5}$$

where ω is the total collision frequency. We define a population distribution function $g(EJ)$:

$$g(EJ) = c(EJ)/(X)\ (YZ) \tag{2.6}$$

where (X) and (YZ) denote concentrations. In a steady-state approximation for $g(EJ)$ we have[20]

$$0 = \frac{d}{dt} g(EJ) = k'_a\ (EJ) - [k_a(EJ) + \omega]\ g(EJ) + \int\int \omega(E'J',EJ)\ g(E'J')dE'dJ' \qquad (2.7)$$

This equation can be rewritten by defining an equilibrium population distribution function $g_{eq}(EJ)$, such that when introduced into Eq. (2.7) the forward and reverse reaction rate constants are equal

$$k_a(EJ)\ g_{eq}(EJ) = k'_a\ (EJ) \qquad (2.8)$$

(microscopic reversibility), while the collision terms are also equal (again, microscopic reversibility):

$$\omega\ g_{eq}(EJ) = \iint \omega(E'J',\ EJ)\ g_{eq}(E'J')\ dE'dJ' \qquad (2.9)$$

Equation (2.7) then becomes

$$[k_a(EJ) + \omega]\ [g_{eq}(EJ) - g(EJ)] = \iint \omega(E'J',\ EJ)[g_{eq}(E'J') - g(E'J')]\ dE'dJ' \qquad (2.10)$$

We denote the difference between the equilibrium population distribution function $g_{eq}(EJ)$ and $g(EJ)$ by $f(EJ)$,

$$f(EJ) = g_{eq}(EJ) - g(EJ) \qquad (2.11)$$

Thereby, Eqs. (2.10)-(2.11) yield a "master equation" for $f(EJ)$

$$[k_a(EJ) + \omega]\ f(EJ) = \iint \omega(E'J',\ EJ)\ f(E'J')\ dE'dJ' \qquad (2.12)$$

The bimolecular recombination rate constant k_{bi} is given by

$$k_{bi} = \iint [k'_a(EJ) - g(EJ)\ k_a(EJ)]\ dEdJ \qquad (2.13)$$

which with (2.8) and (2.11) yields

$$k_{bi} = \iint k_a(EJ)\, f(EJ)\, dEdJ \tag{2.14}$$

The rate constant k_{bi} is calculated by solving Eq. (2.12) for $f(EJ)$ and introducing it into Eq. (2.14), or alternatively by calculating the net collisional downward diffusion of the molecule XYZ in energy space to form a fully deactivated XYZ molecule.

B. Unimolecular dissociation

We denote by $C(EJ)$ the concentration of energetically excited XYZ molecules arising in the unimolecular dissociation and introduce a population distribution function $F(EJ)$ defined by

$$F(EJ) = C(EJ) / (\mathrm{XYZ}) \tag{2.15}$$

where (XYZ) is the concentration of XYZ. The unimolecular dissociation rate is given by

$$k_{uni}(\mathrm{XYZ}) = \iint k_a(EJ)\, C(EJ) dEdJ \tag{2.16}$$

and so

$$k_{uni} = \iint k_a(EJ)\, F(EJ) dEdJ \tag{2.17}$$

Before proceeding with the equations leading to the analog of Eqs. (2.12) and (2.14) for unimolecular reactions we first note that when there is an equilibrium between X + YZ and XYZ, the equilibrium concentration of excited XYZ at any (EJ), $c_{eq}(EJ)$, is the sum of two terms:

$$c_{eq}(EJ) = c(EJ) + C(EJ) \tag{2.18}$$

where $c(EJ)$ consists of marked XYZ molecules (labeled by a dagger †, say) which originated from X +YZ, and of differently marked XYZ molecules (labeled by ††) of concentration $C(EJ)$, which originated from XYZ. Each marked († or ††) molecule may either continue on to the reactants or products region. This progress is followed only until it has reached either destination, at which point it loses its label. If it leaves again, it is with a mark appropriate to the new departure point, † or ††. That is, the equilibrium population $c_{eq}(EJ)$ consists of molecules $XYZ^{\dagger}$ which arose from X + YZ and molecules $XYZ^{\dagger\dagger}$ which arose from XYZ, but where neither of them has yet arrived with its current label at a destination. In this way we consider in the equilibrium population, $c_{eq}(EJ)$, the point of origin of the XYZ (EJ) and so include in our considerations the forward and reverse reactions.

We have introduced expressions for the concentrations in terms of population distribution functions and note that at equilibrium the ratio (XYZ)/(X) (YZ) equals $K^{XYZ}_{X,YZ}$, the equilibrium constant. From Eq. (2.6) we have $c_{eq}(EJ)/(X)(YZ) = g_{eq}(EJ)$. Then, upon dividing both sides of (2.18) by the product of the concentrations (X) (XY), then introducing the equilibrium constant to relate (X) (YZ) to (XYZ) and using the definition (2.15) of $F(EJ)$, we have

$$g_{eq}(EJ) = g(EJ) + F(EJ)\, K^{XYZ}_{X,YZ} \tag{2.19}$$

Inasmuch as $f(EJ)$ is given by Eq. (2.11), it is seen from (2.19) that the population distribution function $F(EJ)$ for the unimolecular dissociation is given by

$$F(EJ) = f(EJ) / K^{XYZ}_{X,YZ}, \tag{2.20}$$

a result used below.

We consider next for unimolecular reactions the analog of Eq. (2.6) and the subsequent equations. In the steady-state we have[21]

$$0 = \frac{d}{dt} F(EJ) = [k_a(EJ) + \omega] F(EJ) - \iint \omega(E'J', EJ) F(E'J') dE'dJ' \tag{2.21}$$

That is,

$$[k_a(EJ) + \omega] F(EJ) = \int\int \omega(E'J', EJ) F(E'J') dE'dJ' \tag{2.22}$$

It is seen from Eqs. (2.12) and (2.22) that $f(EJ)$ and $F(EJ)$ obey the same equation relating values at one EJ to those at the other EJ's. Indeed, they should, in virtue of (2.20).

The unimolecular rate constant k_{uni} given by Eq. (2.17) thus also equals

$$k_{uni} = \iint f(EJ)\, k_a(EJ)\, dEdJ / K^{XYZ}_{X,YZ} \tag{2.23}$$

Thereby,

$$k_{uni} = k_{bi} / K^{XYZ}_{X,YZ}, \tag{2.24}$$

as expected. The k_{bi} or k_{uni} can equally be obtained by solving master equations for $f(EJ)$ or $F(EJ)$, since the latter two functions differ only by a factor $K^{XYZ}_{X,YZ}$.

III. Solution of the master equation

A. Master equation and stepladder model

In the master equation for $f(EJ)$ we first introduce a strong collision approximation for rotation by writing

$$\omega(E'J',EJ) = \omega(E',E)\ P_J^{eq} \tag{3.1}$$

where P_J^{eq} denotes the equilibrium distribution of J's. Equation (2.12) now reads

$$[k_a(EJ)+\omega]f(EJ) = P_J^{eq}\int \omega(E',E)f(E'J')dE'dJ' \tag{3.2}$$

We next introduce a stepladder model for the collisional energy transfer, the steps being of energies E_n (n = 0 to ∞) of stepsize ΔE. We note that in the stepladder model $\langle\Delta E\rangle$ becomes ΔE. If E_n is an energy in a deactivation/activation collision stepladder, then $E_n = E_N - (N-n)\,\Delta E$, where we choose N as the value corresponding to E_N lying in an interval of ΔE whose lower limit is at the threshold for dissociation. Later we integrate over each E_n in its relevant energy interval ΔE. For the distribution function $f(E_nJ)$, obtained from Eq. (2.12), Eq. (3.2), and the stepladder model we have

$$f(E_nJ) = \frac{P_J^{eq}(\omega_{a,n-1}f_{n-1} + \omega_{d,n+1}f_{n+1})}{k_a(E_nJ)+\omega} \tag{3.3}$$

where

$$f_n = \int f(E_nJ')dJ', \tag{3.4}$$

ω_d is the deactivation collision frequency $\omega(E_n,E_{n-1})$, which will be assumed to be independent of n in the region of interest (n close to N),[22] and $\omega_{a,\,n-1}$ is the collision frequency for the reverse (activation) step (the a in $\omega_{a,n-1}$ denotes activation). The two are related by microscopic reversibility, as in Eq. (3.13) given later.

Summed over the steps of energies $E_0, E_1, \ldots,$ the total net incoming flux S_J for a given J is

$$S_J = \sum_{n=N}^{\infty} S_{nJ}, \quad S_{nJ} = k_a(E_n, J) f(E_n, J) \tag{3.5}$$

the lower summation limit arising since the $k_a(E_nJ)$'s vanish for $n < N$. To obtain k_{bi} one then integrates the E_n in each S_{nJ} over an energy interval ΔE and sums (or integrates) over J. We then have

$$k_{bi} = \sum_{n=N}^{\infty} \int\int S_{nJ}\, dE_n\, dJ \tag{3.6}$$

Alternatively, k_{bi} is obtained from the net downward diffusional flux in energy space for $n < N$ via Eq. (3.15) below.

A master equation is obtained for the f's upon integrating (3.3) over J:

$$f_n = A_n(\omega_{a,n-1} f_{n-1} + \omega_{d,n+1} f_{n+1}) \tag{3.7}$$

where

$$A_n = \int_J [k_a(E_nJ) + \omega]^{-1} P_J^{eq}\, dJ \tag{3.8}$$

and f_n is defined by (3.4). This A_n becomes ω^{-1} for $n < N$.

When the master equation (3.7) is solved for the f_n's, subject to the appropriate boundary conditions, $f(E_nJ)$ is obtained from (3.3), and k_{bi} is then obtained. Two boundary conditions are needed since (3.7) is a second-order difference equation. One boundary condition is to take the population distribution function at the lowest step g_0 to be zero. The second condition is the conservation of flux S_J. We first show in the following Section that the equation relating the f_n's for $n \leq N$ can be solved analytically.

B. Flux below the dissociation threshold

For energies E_n below E_N the net downward flux S_J^{diff} of the energetic XYZ's along the energy stepladder can be written as

$$S_J^{diff} = P_J^{eq}[\omega_d g_n - \omega_{a,n-1} g_{n-1}] \quad (n \leq N) \tag{3.9}$$

where

$$g_n \equiv \int g(E_nJ)dJ \tag{3.10}$$

The microscopic reversibility equation is

$$\omega_d g_n^{eq} \equiv \omega_d \int g_{eq}(E_n, J)dJ \equiv \omega_{a,n-1} \int g_{eq}(E_{n-1}, J)dJ \equiv \omega_{a,n-1} g_{n-1}^{eq} \tag{3.11}$$

where it can be shown that[23]

$$P_J^{eq} g_n^{eq} = g_{eq}(E_nJ) = \rho(E_nJ)e^{-E_n/k_BT} / Q_{X,YZ} \equiv e^{-G_n^J/k_BT} \tag{3.12}$$

The J-dependent part of the energy of XYZ is included in E_n and $Q_{X,YZ}$ is the partition function for X + YZ. (The actual energy of this molecule is $E_n + D$, where D is the dissociation energy. To simplify the notation we have denoted this $\rho(E_n + D,J)$ by $\rho(E_nJ)$.) In the last equality in (3.12) we have defined a free energy term G_n^J, a function of E_n and J.

We next rewrite (3.11) in terms of the free energy difference, $G_{n-1}^J - G_n^J$:

$$\omega_{a,n-1} = \omega_d \, e^{(G_{n-1}^J - G_n^J)/k_BT} \tag{3.13}$$

Thereby, using (3.9),

$$S_J^{diff} = P_J^{eq}\omega_d(g_n - g_{n-1}e^{(G_{n-1}^J - G_n^J)/k_BT}) \qquad (n \le N) \tag{3.14}$$

On multiplying (3.14) by exp (G_n^J/k_BT) and summing over n from $n = 1$ to $n = N$ we have

$$S_J = P_J^{eq}\, k_{diff}^N(g_N - g_0 e^{(G_0^J - G_N^J)/k_BT}) = P_J^{eq} k_{diff}^N g_N \tag{3.15}$$

where k_{diff}^N is defined by

$$k_{diff}^N = \omega_d / \sum_{n=1}^{N} e^{(G_n^J - G_N^J)/k_BT} \tag{3.16}$$

and where we have treated the $n = 0$ state as a sink by setting $g_0 = 0$. The P_J^{eq} cancels in the difference $G_n^J - G_N^J$, and so the k_{diff}^N in (3.16) does not depend on J.

C. Case of only one reactive step N in the ladder

We first consider for simplicity the case where only one recombination step N in the ladder for the XYZ formation in reaction (2.1) contributes significantly. In this case there is no need to solve the master equation (3.7), since there is only one reactive state N and a solution for all other states $n < N$ was obtained analytically in terms of g_N, namely, via Eq. (3.15).

The net incident flux S_J from reactants X and YZ for this E_N and J, using (3.5) and (3.3), is given by

$$S_J \equiv S_{NJ} = k_a(E_N J) f(E_N, J) = \frac{\omega_{a,N-1} P_J^{eq} f_{N-1} k_a(E_N J)}{k_a(E_N J) + \omega} \tag{3.17}$$

where the term $\omega_{d,N+1} f_{N+1}$ in (3.3) is now absent, since state N is the highest state considered in this one-reactive state model.

Equations (3.9) (for $n = N$), (3.15), and (3.17) contain the unknowns g_N and g_{N-1}. Equating these expressions for S_J yields two equations. Since there are two unknowns, g_{N-1} and g_N, one can solve for g_N. Use of Eq. (3.15) then yields an

$$g_N = g_N^{eq} \omega_d k_a / (\omega_d k_a + \omega k_{diff}^N), \; k_a \equiv k_a(EJ) \tag{3.18}$$

Further, for this model of only one reactive state N, $\omega_{a,N}$ must vanish and so ω, which equals $\omega_d + \omega_{a,N}$, equals ω_d. Equations (3.6), (3.15), (3.18) and the first equality in Eq. (3.12), then yield

$$k_{bi} = \int_{E_N} \int_{J} \frac{k_a(E_N J) k_{diff}^N g_{eq}(E_N J)}{k_a(E_N J) + k_{diff}^N} dE_N dJ \tag{3.19}$$

where the E_N integration is over an interval ΔE.

In the strong collision limit k_{diff}^N equals its first term in a series expansion of (3.16), namely ω_d, which in turn now equals ω. Equation (3.19) then reduces to the usual strong collision expression, on taking ΔE to be very large.

D. Case of any number of reactive steps

We consider next the case where there are reactive states N, $N + 1$, $N + 2$, ... ∞, where E_N lies in $(0,\Delta E)$ and E_{N+n} in $[n\,\Delta\,E,(n + 1)\Delta E]$. The contribution of these particular energies to the flux S at a given J is given by (3.5), and Eq. (3.6) – (3.16) also apply. Equations (3.5), (3.3), and (3.7) yield

$$S_J = \sum_{n=N}^{\infty} \frac{k_a(E_n J) P_J^{eq} f_n}{A_n[k_a(E_n J) + \omega]} \tag{3.20}$$

noting that $\omega_{d,n+1}$ equals ω_d in the present approximation. The f_n's for $n > N$ can be expressed in terms of f_N by solving the master Eq. (3.7). Upon then equating the S_J in (3.20) to the S_J in (3.15), g_N is obtained. The k_{bi} equals the downward flux S_J in Eq. (3.15), integrated over ΔE and summed (or integrated) over J:

$$k_{bi} = \int \sum_J P_J^{eq} k_{diff}^N g_N dE_N \tag{3.21}$$

IV. Two Reaction Exit Channels *a, b*

A. Master Equation

We consider now the reactions (2.1) – (2.4) where Z ≠ X. Equation (2.8) now serves as a definition of a quantity which we again write as $g_{eq}(EJ)$:

$$g_{eq}(EJ) = k'_a(EJ) \;/\; k_a(EJ) \tag{4.1}$$

This $g_{eq}(EJ)$ is thereby an equilibrium population distribution function.

Equation (2.7) is replaced by

$$0 = k'_a(EJ) - [k_a(EJ) + k_b(EJ) + \omega]\, g(EJ) + \int\int \omega(E'J', EJ) g(E'J') dE' dJ' \tag{4.2}$$

and so with (2.8) and (2.11) we then have, instead of (2.12),

$$[k_a(EJ) + k_b(EJ) + \omega] f(EJ) - k_b(EJ) g^{eq}(EJ) = P_J^{eq} \int \omega(E', E) f(E'J') dE' dJ' \tag{4.3}$$

where we have again introduced (3.1). The bimolecular recombination rate constant for X + YZ → XYZ is given, following (2.11) and (2.13), by

$$k_{bi}^a = \int\int k_a(EJ) f(EJ) dE dJ \tag{4.4}$$

where $f(EJ)$ now satisfies the master Eq. (4.3).

Upon introducing the stepladder model for the collisional energy transfer, Eq. (4.3) becomes

$$f(E_n J) = P_J^{eq} \frac{(\omega_{a,n-1} f_{n-1} + \omega_d f_{n+1}) + k_b(E_n J) g^{eq}(E_n J)}{k_a(E_n J) + k_b(E_n J) + \omega} \tag{4.5}$$

where f_n is again given by (3.4). The bimolecular rate constant is again obtained from the downward diffusional probability flux given by (3.5), integrated over E_N and summed over J. Thereby, the bimolecular rate constant, which we now

denote by k_{bi}^{a} to indicate that the entrance channel in the example is a, is again given by (3.6), namely

$$k_{bi}^{a} = \sum_{J} \int P_J^{eq} k_{diff}^{N} g_N dE_N \tag{4.6}$$

A master equation for the f_n's obtained by integrating $f(E_nJ)$ in (4.4) over J, is now

$$f_n = B_n(\omega_{a,n-1} f_{n-1} + \omega_d f_{n+1}) + C_n \tag{4.7}$$

where

$$B_n = \int \frac{P_J^{eq} dJ}{k_a(E_nJ) + k_b(E_nJ) + \omega}, \quad C_n = \int \frac{k_b(E_nJ) g^{eq}(E_nJ) dJ}{k_a(E_nJ) + k_b(E_nJ) + \omega} \tag{4.8}$$

We note that the two exit channels will have slightly different energy thresholds, because of a difference in zero-point energies of YZ and XY, and the integration in (4.6) over E_N is intended to begin at the lower threshold of the two. The master Eq. (4.7) is first solved for the f's in terms of f_N and hence of g_N. Then, as before, g_N can be obtained from the boundary condition describing flux conservation. We proceed as follows:

The net flux entering via channel a for a given J, S_J^a, is the same as (3.5) and so we have

$$S_J^a = \sum_{n=N}^{\infty} S_{nJ}^a, \; S_{nJ}^a = k_a(E_n, J) f(E_nJ) \tag{4.9}$$

The flux outgoing in channel b, S_J^b, is given by

$$S_J^b = \sum_{n=N}^{\infty} S_{nJ}^b, \; S_{nJ}^b = k_b(E_n, J) g(E_nJ) \tag{4.10}$$

The downward diffusional flux S_J^{diff} is again given by (3.15) and conservation of flux yields

$$S_J^a = S_J^b + S_J^{diff} \tag{4.11}$$

which serves as a boundary condition for solution of the master equation, by providing an equation for g_N. Equation (4.6) then yields k_{bi}^a.

This material balance Eq. (4.11) can also be written equivalently as

$$\sum_{n=N}^{\infty}[k_a(E_nJ)+k_b(E_nJ)+k_{diff}^N]g(E_nJ)=\sum_{n=N}^{\infty}k_a(E_nJ)g^{eq}(E_nJ) \tag{4.12}$$

The present equations, or their equivalent, are utilized elsewhere in a treatment of isotopic effects.[12,13]

D. Special Case of One Reactive Step N

An expression for g_N is obtained from Eqs. (3.9), (3.12), (3.15), (4.5), and (4.9)-(4.11) . From Eq. (4.6) and the first equality in (3.12), one then obtains

$$k_{bi}^a = \int_{E_N}\int_J \frac{k_a(E_NJ)k_{diff}^N g_{eq}(EJ)}{k_a(E_NJ)+k_b(E_NJ)+k_{diff}^N}dE_NdJ \tag{4.13}$$

On letting ΔE become very large k_{diff}^N reduces to ω_d and hence to ω as before, and the result obtained in Ref. 18 is recovered. Further, Eq. (4.13) reduces to (3.22) when $k_b(E_NJ)$ vanishes. The equation for k_{bi}^b is obtained from (4.13) by interchanging a's and b's.

V. Isotopic Exchange Reactions

The isotopic exchange reactions

$$X + YZ \rightarrow XY + Z, \tag{5.1}$$

where X, Y, Z are isotopes, are typically studied at low pressures, where the newly formed vibrationally hot XYZ^* typically dissociates before it can undergo a collision with the bath gas. The results are then independent of whether the deactivating collisions are strong or weak, and so the equations given in Refs. 18 and 19 apply.

Acknowledgment

It is a pleasure to acknowledge the support of this research by the National Science Foundation. We thank the reviewer for helpful comments.

References

1. R. G. Gilbert and S. C. Smith, *Theory of Unimolecular and Recombination Reactions* (Blackwell Scientific, Boston, 1990), and references cited therein. Section (6.10) for unimolecular reactions prompted the *J*-averaging used in (3.2).
2. K. A. Holbrook, M. J. Pilling, and S. H. Robertson, *Unimolecular Reactions*, John Wiley & Sons, New York, (1996), 2nd ed. and references cited therein.
3. T. Baer and W. L. Hase, *Unimolecular Reaction Dynamics, Theory and Experiments*. (Oxford University Press, New York, 1996) and references therein.
4. D. M. Wardlaw and R. A. Marcus, Adv. Chem. Phys. **70**, 231 (1988).

5. S. J. Klippenstein, in *The Chemical Dynamics and Kinetics of Small Radicals, Part I*, ed. K. Liu and A. Wagner (World Scientific, Singapore, 1995) and references therein.
6. D. C. Tardy and B. S. Rabinovitch, *J. Chem. Phys.* **48**, 1282 (1968).
7. D. C. Tardy and B. S. Rabinovitch, *J. Chem. Phys.* **45,** 3720 (1966).
8. I. Oref and D. C. Tardy, *Chem. Rev.* **90**, 1407 (1990).
9. H. G. Löhmannsröben and K. Luther, *Chem. Phys. Lett.*, **144**, 173 (1988).
10. A. Pashutski and I. Oref, *J. Phys. Chem.*, **92**, 178 (1988).
11. Ref. 2 Chap. 9.
12. Y.-Q. Gao and R. A. Marcus, submitted for publication.
13. Y.-Q. Gao and R. A. Marcus, to be submitted for publication.
14. H. Hippler, R. Rahn, and J. Troe, *J. Chem. Phys.* **93**, 6560 (1990); Ref. 2, Chap. 7, and references cited therein.
15. E.g., M. H. Thiemens and T. Jackson, *Geophys. Res. Lett.* **17,** 717 (1990).
16. E.g., K. Mauersberger, B. Erbacher, D. Krankowsky, J. Günther, and R. Nickel, *Science*, **283**, 370 (1999).
17. M. R. Wiegell, N. W. Larsen, T. Pedersen, and H. Egsgaard, *Int. J. Chem. Kinet.* **29**, 745 (1997).
18. B. C. Hathorn and R. A. Marcus, *J. Chem. Phys.* **111**, 4087 (1999).
19. B. C. Hathorn and R. A. Marcus, *J. Chem. Phys.* **113**, 9497 (2000).
20. There is very little difference whether one sets $dg(EJ)/dt = 0$, as in Eq. (2.7), or sets $dc(EJ)/dt = 0$. This fact is most easily seen for the unimolecular reaction and we return to this point in Ref. 21.
21. Given $dF(EJ)/dt = 0$ in (2.21), we can explore its consequences for $dC(EJ)/dt$. We have, using (2.15), $0 = -[C(EJ)/(XYZ)^2]d(XYZ)/dt + (dC(EJ)/dt)/(XYZ)$.

But the first term equals $-[C(EJ)/(XYZ)]k_{uni}$, i.e., $k_{uni}F_{EJ}$, which is typically small relative to the individual terms enhancing or decreasing $F(EJ)$ in the rate expression (2.21). Accordingly, $dC(EJ)/dt$ typically equals zero to a good approximation.

22. The total collision frequency ω of an ozone molecule in state n is $\omega_d + \omega_{a,n} + \omega_o$, where the o label indicates the possibility that there is no net energy transfer. We note in passing that the approximation that in the neighborhood of $n = N$, ω_d can be treated as constant while $\omega_{a,n}$ obeys (3.4) can have some implications for the behavior of ω.

23. We have $P_J^{eq} g_n^{eq} = P_J^{eq} \int g_{eq}(E_n, J')dJ'$. We write $g_{eq}(E_n,J')$ as $(2J' + 1)\ \rho_{vib}(E_n - E_{J'})$ C, where C = exp $(-E_n/k_BT)/Q_{X,YZ}$. Here, $E_n - E_{J'}$ (in turn, a shorthand for $D + E_n - E_N - E_{J'}$) is the vibrational energy E_{vib}^n, and so $\rho_{vib}(E_n - E_{J'})$ is the vibrational density of states. Then writing E_n as $E_n - E_{J'} + E_{J'}$ and integrating over J' one obtains $P_J^{eq}\rho_{vib}(E_{vib}^n)\exp(-E_{vib}^n / kT)/Q_{X,YZ}$, which can be rewritten as $\rho(E_n, J)\exp(-E_n / k_BT)/Q_{X,YZ}$, i.e., as $g_{eq}(E_n,J)$, as in the text.

Chapter 4

On the theory of electron transfer reaction at semiconductor/liquid interfaces

(Appeared in J. Chem. Phys. **112**, 3358 (2000))

JOURNAL OF CHEMICAL PHYSICS VOLUME 112, NUMBER 7 15 FEBRUARY 2000

On the theory of electron transfer reactions at semiconductor electrode/liquid interfaces

Yi Qin Gao, Yuri Georgievskii, and R. A. Marcus
Noyes Laboratory of Chemical Physics, California Institute of Technology, Pasadena, California 91125

(Received 5 October 1999; accepted 23 November 1999)

Electron transfer reaction rate constants at semiconductor/liquid interfaces are calculated using the Fermi Golden Rule and a tight-binding model for the semiconductors. The slab method and a z-transform method are employed in obtaining the electronic structures of semiconductors with surfaces and are compared. The maximum electron transfer rate constants at Si/viologen$^{2+/+}$ and InP/$Me_2Fc^{+/0}$ interfaces are computed using the tight-binding type calculations for the solid and the extended-Hückel for the coupling to the redox agent at the interface. These results for the bulk states are compared with the experimentally measured values of Lewis and co-workers, and are in reasonable agreement, without adjusting parameters. In the case of InP/liquid interface, the unusual current vs applied potential behavior is additionally interpreted, in part, by the presence of surface states. © *2000 American Institute of Physics.* [S0021-9606(00)70507-1]

I. INTRODUCTION

Insight into the dynamics of the electron transfer reactions at semiconductor/liquid interfaces can be helpful in constructing efficient and stable photoelectrochemical cells and other applications, and is of interest in understanding the basic chemical reactions. Due to the instability and the nonideal behavior of most semiconductor electrodes in contact with liquids, only recently have reliable kinetic measurements been performed at semiconductor/electrolyte interfaces.[1–6] In these experiments the flux from the conduction band edge of a semiconductor to a molecular electron acceptor species dissolved in the solution can be expressed as

$$J_f(E)=ek_{et}n_s(E)[A], \tag{1}$$

where J_f (current per unit area) is the current density due to the direct electron transfer, e is the elementary charge, $n_s(\mathrm{cm}^{-3})$ is the electron concentration at the surface of the semiconductor and is a function of E, the applied potential, and $[A](\mathrm{cm}^{-3})$ is the concentration of the acceptors in the solution. An analogous expression can also be written for hole transfer from the valence band of the semiconductor. The units of k_{et} defined by Eq. (1) are cm^4 $\mathrm{molecule}^{-1}$ s^{-1} and it contains the energy distribution of the electrons.

The electron transfer reactions at n-type Si(100)/viologen$^{2+/+}$(CH_3OH) and n-type InP(100)/$Me_2Fc^{+/0}$(CH_3OH) interfaces were studied systematically by Lewis group.[1,4] The built-in voltage (the voltage drop inside the semiconductor) and the concentration of the semiconductor conduction band electrons were obtained by differential capacitance vs potential measurements. The current densities were also measured as a function of the applied potential for different concentrations of acceptors and donors. The first-order dependence of current density on concentration of surface electrons n_s in the semiconductor and concentration of electron acceptors $[A]$ in the solution was verified for a series of Si/viologen$^{2+/+}$(CH_3OH) interfaces.[4] In this study[4] the authors chose a series of viologen ions with very similar molecular structures and thus presumably similar reorganization energies, but with very different free energy changes for the electron transfer reactions. The electron transfer rate constants obtained experimentally served also to measure the maximum of the electron transfer rate constant. The measured maximum rate constant for the electron transfer reaction across such an interface was in the range of 10^{-17}–10^{-16} cm^4 s^{-1}. The experimental studies of the electron transfer reaction at InP/$Me_2Fc^{+/0}$(CH_3OH) interfaces provided similar maximum rate constant results but less ideal voltage–current behavior.

By applying a treatment[7] for liquid/liquid interfacial electron transfer reactions to semiconductor/liquid interfaces and by assuming an "electron ball" model for the electron in the semiconductor, Lewis[2,8] provided a theoretical estimate of the maximum rate constant which is close to the experimental value. The treatment is closely related to the model suggested by Gerischer[9] who used a half-sphere instead of a sphere, and is a nonadiabatic approach. In the model of Lewis the electron in the semiconductor is represented by a spherical donor with radius around 10 Å, and any reorganization around the electron in the semiconductor was neglected. The electron transfer rate constant was then calculated using the formula derived for the electron transfer reactions at liquid/liquid interface,

$$k_{D,A}=\nu_n[2\pi(r_D+r_A)\beta_s^{-3}] \times e^{-(\lambda_A+\lambda_D+\Delta G^0)^2/4k_BT(\lambda_A+\lambda_D)}, \tag{2}$$

where ν_n is typically expected to be around 10^{13} s^{-1} for a process which is adiabatic when the reactants are in contact, and where the decay of rate with distance through the solvent, assumed to be exponent with a decay length β_s, r_D and r_A are the radii of the donor and the acceptor, λ_D and λ_A are the reorganization associated to the donor and acceptor, and ΔG^0 is the standard free energy of the reaction in the pre-

 © 2000 American Institute of Physics

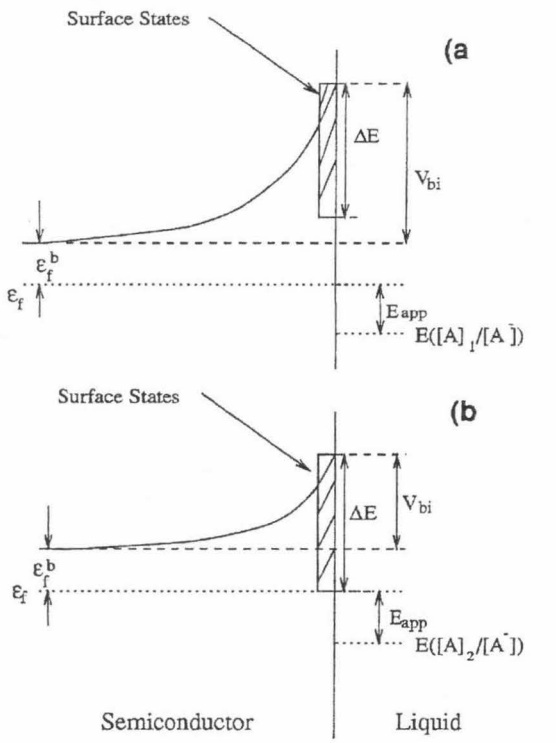

FIG. 1. The energetics at semiconductor/liquid interfaces with surface states homogeneously distributed in the energy range $(-\Delta E,0)$ referred to the conduction band edge at the surface (a) with a larger $[A]/[A^-]$ ratio and the Fermi level is far below the surface states; (b) with a smaller $[A]/[A^-]$ ratio and the occupancy of the surface states must be described by a Fermi–Dirac distribution. In (a) and (b), the same potential vs $E(A/A^-)$ is applied but (a) has a larger built-in voltage.

vailing medium. Royea, Fajardo, and Lewis[10] also investigated the relation between the electron transfer reactions at metal/liquid and semiconductor/liquid interfaces using Fermi Golden Rule. The coupling between the semiconductor and the redox molecules was not calculated for an actual system.[10]

Dogonadze and Kuznetsov[11] studied both nonadiabatic and adiabatic electron transfer reactions at semiconductor/liquid interfaces by analogy with the metal/liquid interfacial electron transfer reactions. The reorganization energy of the redox molecules at semiconductor/liquid interfaces was investigated by one of us[12] and was shown to be different from the reorganization energy for the same molecules in a homogeneous situation. Smith and Nozik[13,14] studied the semiconductor/liquid interfacial adiabatic electron transfer reactions by extending Schmickler's treatment[15] for metal/liquid electron transfer reactions, choosing an Anderson-type Hamiltonian, and by molecular dynamic calculations.[16]

In the present paper, the electron transfer reactions at semiconductor/liquid interfaces are treated nonadiabatically. Extended-Hückel calculations are performed to estimate the electronic coupling between the donor/acceptor level of the redox agent and the solid electronic states of the semiconductor. The electronic structure of the solid is treated by

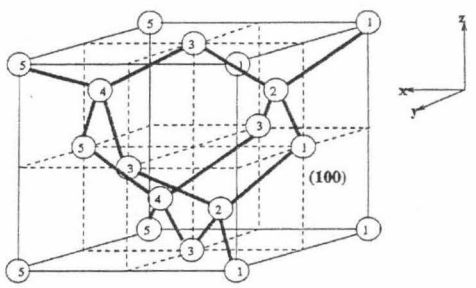

FIG. 2. View of the Si and InP semiconductor with (100) surfaces. For a Si electrode, all circles represent silicon atoms; for an InP electrode, 1,3,5,... =P and 2,4,... =In. The numbers indicate the two-dimensional layer to which the atoms belong. Every two layers of atoms form a superlayer.

tight-binding calculations using existing solid state parameters in literature, parameters that had been chosen to fit the band structure. Each semiconductor electrode is treated both as a slab and as a semi-infinite crystal for comparison. For a slab, the direct diagonalization of the Hamiltonian matrix is performed as usual to obtain the eigenvalues as well as the eigenstates,[17] while for a semi-infinite crystal, a transform method introduced earlier by one of us for this purpose[18] is employed. The procedure is applied to two semiconductor/liquid interfaces, Si/viologen$^{2+/+}$ and InP/$Me_2Fc^{+/0}$, InP/$PV^{2+/+}$. In addition, surface states are included for the current vs applied potential behavior observed at InP/$Me_2Fc^{+/0}$, $PV^{2+/+}$ interfaces, as one way for accounting for the nonideal behavior observed for this system. The maximum rate mentioned earlier, which is the principal focus of our attention, is calculated under conditions where surface states are unimportant.

The paper is organized as follows: The theoretical basis for the electron transfer rate constant calculation and solid state calculation is described in Sec. II. The application of the theoretical methods to the actual systems are given in Secs. III and IV, and the results are discussed there.

II. THEORETICAL MODELS

A. General comment

The net current density J due to the electron transfer reaction at a semiconductor S/liquid interface,

$$A+e(S)\rightleftharpoons A^-+S, \tag{3}$$

can be written as

$$J=J_f-J_r, \tag{4}$$

where J_f is the current density due to the electron transfer from the semiconductor to the molecule and J_r is the current density corresponding to the reverse process. J_f and J_r depend on the concentrations of A and A^-, respectively, at the interface,

$$J_f=ek_f[A], \tag{5}$$

$$J_r=ek_r[A^-], \tag{6}$$

where k_f and k_r are the first-order rate constants. In the following only the forward reaction is considered, unless otherwise stated. When it is assumed that the electron transfer from the electrode to the acceptors is proportional to the concentration of the electrons n_s at the electrode surface, in the case of an n-type semiconductor, the forward electron transfer rate constant is expressed as

$$k_f = n_s k_{et}. \tag{7}$$

Here, k_{et}, a rate constant for a reaction that is second-order with respect to the concentrations, is the quantity obtained in Lewis' experiments.

The rate of a nonadiabatic electron tunneling from one electronic state to another is frequently described by the Landau–Zener formula. Under the weak-coupling assumption, the Golden Rule expression for the nonadiabatic electron transfer rate constant, which includes both the electron tunneling and the "nuclear reorganization," contains implicitly the Landau–Zener expression,[19]

$$k_f^s = \frac{2\pi}{\hbar}|V|^2 \mathrm{FC}, \tag{8}$$

where FC is the Franck–Condon factor, V is the electronic coupling matrix element, and $\hbar$ is Planck's constant. A common classical expression for the Franck–Condon factor is[19]

$$\mathrm{FC} = \frac{1}{\sqrt{4\pi\lambda k_B T}} \exp\left(\frac{-(\lambda+\Delta G)^2}{4\lambda k_B T}\right), \tag{9}$$

where λ is the reorganization energy, and ΔG is a free energy of reaction under the prevailing conditions of temperature, electrode–solution potential difference and environment. We return later to this quantity for the present systems.

The electron transfer at the semiconductor/liquid interfaces involves the continuum of electronic states in the semiconductor, whose theory, strictly speaking, requires solving a many-electronic state problem. Quantum mechanical studies of many-state crossing problems show that the Landau–Zener formula is applicable to a large variety of such problems, when the splitting of the states caused by crossing is small.[20] The major charge carriers in a semiconductor have very low concentrations and can be treated individually in interfacial reactions.[9] In accordance with a weak-coupling approximation[20] transitions can be treated as occurring between pairs of states, and a "two-level" approximation can then be considered, in which the electron transfer current between the electrode and an acceptor state is treated as the sum of the currents from each electronic state of the electrode to the acceptor state. Considering first the acceptor as being at position $\mathbf{r}$ in the solution, the rate constant is

$$k_f^t(\mathbf{r}) = \sum_{\mathbf{k}} k_f^s(\mathbf{k},\mathbf{r}). \tag{10}$$

Here, $k_f^t(\mathbf{r})$ is the rate constant for the total current from the semiconductor to the molecule, expressed as a sum of the currents from all the electronic states of the semiconductor, $\mathbf{k}$ denotes the electronic state of the semiconductor with the wave vector $\mathbf{k}$, and $k_f^s(\mathbf{k},\mathbf{r})$ varies with the position $\mathbf{r}$ of the acceptor relative to the electrode. It can be further written as[10,11,21]

$$k_f^t(\mathbf{r}) = \frac{2\pi}{\hbar}\int_\epsilon \mathrm{FC}(\epsilon) f(\epsilon) \sum_{\mathbf{k}} |V(\mathbf{k},\mathbf{r})|^2 2\pi\delta(\epsilon_{\mathbf{k}} - \epsilon) d\epsilon, \tag{11}$$

where the coupling matrix element V is defined later and $f(\epsilon)$ is the probability that a state in the semiconductor with energy ϵ is occupied, while ΔG in Eq. (9) is related to ϵ by

$$\Delta G = \Delta G^0 - \epsilon. \tag{12}$$

Here, ΔG^0 is defined as the standard free energy of the reaction when the donor state in the electrode is at the conduction band edge at the semiconductor surface. ΔG^0 can be obtained from electrochemical measurements. After denoting by $\bar{V}(\epsilon,\mathbf{r})$ the averaged coupling of all the states with energy ϵ, Eq. (11) can be written as

$$k_f^t(\mathbf{r}) = \frac{2\pi}{\hbar}\int_\epsilon f(\epsilon)\rho(\epsilon)\mathrm{FC}(\epsilon)|\bar{V}(\epsilon,\mathbf{r})|^2 d\epsilon, \tag{13}$$

where $\rho(\epsilon)$ is the density of states, i.e., $\Sigma_{\mathbf{k}} 2\pi\delta(\epsilon_{\mathbf{k}} - \epsilon)$ (Ref. 22) and $|\bar{V}(\epsilon,\mathbf{r})|^2$ denotes $\Sigma_{\mathbf{k}}|V(\mathbf{k},\mathbf{r})|^2\delta(\epsilon_{\mathbf{k}} - \epsilon)/\Sigma_{\mathbf{k}}\delta(\epsilon_{\mathbf{k}} - \epsilon)$.

The current density at the electrode is obtained by summing over the current from the electrode to all the acceptors A in the solution and dividing the sum by the area of the electrode surface σ,

$$J_f = \frac{e}{\sigma}\int_{\mathbf{r}} A(\mathbf{r}) k_f^t(\mathbf{r}) d^3\mathbf{r}, \tag{14}$$

where $A(\mathbf{r})$ is the concentration of A at $\mathbf{r}$. When the reaction is not diffusion-controlled, and when the change of electrical potential inside the liquid can be neglected, $A(\mathbf{r})$ can be taken as constant. A first-order electron transfer rate constant, which is independent of the concentration of acceptors in the solution but dependent on the concentration of electrons in the semiconductor, can be defined,

$$k_f = \frac{1}{\sigma}\int_{\mathbf{r}} k_f^t(\mathbf{r}) d^3\mathbf{r}. \tag{15}$$

When $k_f(\mathbf{r})$ depends exponentially on distance with a decay constant β_s, the k_f becomes

$$k_f = \frac{1}{\beta_s} k_f^t(\text{contact}), \tag{16}$$

where $k_f^t(\text{contact})$ is the value of $k_f^t(\mathbf{r})$ at the van der Waals' contact distance, averaged over orientations as discussed later in Sec. III A.

B. Tight-binding model

For obtaining the electronic states of the semiconductors, we consider the tight-binding method, which has been used extensively in treating the electronic properties of solids and their surfaces and has been useful and efficient in approximately solving solid state physics problems.[23–27] As noted earlier,[18,21,28] because it involves a linear combination of

atomic orbitals, the tight binding method for the electronic structure calculations for the solid is readily combined with the extended-Hückel treatment to estimate the electronic coupling at the interface.

In this approach the one-electron wave function of an infinite solid is expressed as a linear combination of Bloch functions, $\Sigma_{\mathbf{R}_i}\exp(i\mathbf{k}\cdot\mathbf{R}_i)\psi_n(\mathbf{r}-\mathbf{R}_i)$,

$$\Psi_{\mathbf{k}}(\mathbf{r})=\sum_n c_n(\mathbf{k})\sum_{\mathbf{R}_i}\exp(i\mathbf{k}\cdot\mathbf{R}_i)\psi_n(\mathbf{r}-\mathbf{R}_i), \tag{17}$$

where $c_n(\mathbf{k})$'s are coefficients, $\psi_n(\mathbf{r}-\mathbf{R}_i)$'s are atomic orbitals centered at the position $\mathbf{R}_i$, and the n's denote different bands of orbitals.

Substitution of the wave function into the Schrödinger equation, $\mathbf{H}\Psi_{\mathbf{k}}(\mathbf{r})=E_k\Psi_{\mathbf{k}}(\mathbf{r})$, produces the well known set of linear algebraic equations, with the standard result for non-trivial solutions that[23]

$$|\mathbf{H}-E\mathbf{S}|=0, \tag{18}$$

where $\mathbf{H}$ and $\mathbf{S}$ are matrices of the Hamiltonian and overlap with elements H_{nm} and S_{nm}. The elements of the matrices are readily obtained by the consideration of the symmetry of the solid and by choosing appropriate interaction and overlap parameters for the neighboring atoms, H_{nm} and S_{nm}. We have

$$H_{nm}=\sum_{\mathbf{R}_j}\exp(i\mathbf{k}\cdot(\mathbf{R}_j-\mathbf{R}_i))\int\psi_n^*(\mathbf{r}-\mathbf{R}_i)\times H\psi_m(\mathbf{r}-\mathbf{R}_j)d^3\mathbf{r}, \tag{19}$$

$$S_{nm}=\sum_{\mathbf{R}_j}\exp(i\mathbf{k}\cdot(\mathbf{R}_j-\mathbf{R}_i))\int\psi_n^*(\mathbf{r}-\mathbf{R}_i)\times\psi_m(\mathbf{r}-\mathbf{R}_j)d^3\mathbf{r}. \tag{20}$$

In practice the parameters are adjusted in the band structure calculation so as to fit experimental data on the band structure.[24] If an orthonormal basis is chosen, the $\mathbf{S}$ matrix becomes the unit matrix and Eq. (18) becomes[29]

$$|\mathbf{H}-E\mathbf{I}|=0, \tag{21}$$

where $\mathbf{I}$ is the unit matrix. The solution of the electronic structure is provided by the direct diagonalization of the Hamiltonian matrix.

An infinite solid can also be viewed as being formed by an infinite number of layers of atoms. Each of the layers has the full two-dimensional translational symmetry. In this scheme, the wave function is expressed as

$$\Psi_{\mathbf{k}}(\mathbf{r}_\parallel)=\sum_{n,m}c_{nm}(\mathbf{k}_\parallel)\sum_{\mathbf{R}_{\parallel,i}}\exp(i\mathbf{k}_\parallel\cdot\mathbf{R}_{\parallel,i})\psi_{nm}(\mathbf{r}_\parallel-\mathbf{R}_{\parallel,i}), \tag{22}$$

where $\mathbf{k}_\parallel$ and $\mathbf{r}_\parallel$ are the wave vector and the space vector in the two-dimensional layer. Here, $\psi_{nm}(\mathbf{R}_{\parallel,i})$ is the mth type atomic orbital at the position $\mathbf{R}_{\parallel,i}$ in the nth layer. This wave function is easily generalized to the case where the solid is not infinite, e.g., has one (semi-infinite) or two (slab) surfaces. For a semi-infinite crystal, n, the number of the layer counted from the surface, varies from 1 to ∞. For a slab, n varies from 1 to some finite number.

In the slab method, the model of the solid is constructed using a finite number of infinite planes parallel to the surface. Each plane is composed of lattice atoms and the electronic motion in it can be described by Bloch plane waves. The one-electron wave functions of a slab consisting of N atomic layers are expanded in $M\times N$ LCAO-type Bloch functions, where M is the number of different atomic orbitals per layer for each value of $\mathbf{k}_\parallel$. The overlap and Hamiltonian matrix elements are expressed in terms of the overlap and interaction integrals between the atomic orbitals. Again, an orthonormal atomic basis can be chosen and the eigenvalues and eigenvectors can be obtained by direct diagonalization of the Hamiltonian matrix.

For a semi-infinite semiconductor, the z-transform method, which was introduced earlier for the tight-binding study of a semi-infinite solid, is applied to the present study. The detailed derivation is given in Ref. 18. In the following we consider a semi-infinite solid having M coupled bands, which arises either when an atom has several different orbitals or when each layer of the solid is a superlayer, i.e., consisting more than one layer, or both. Substitution of the wave function Eq. (22) into the Schrödinger equation yields an infinite set of difference equations. In matrix notation, the difference equations can be written as

$$\mathbf{B}^\dagger\mathbf{c}_{n+2}+(\mathbf{A}-E\mathbf{I})\mathbf{c}_{n+1}+\mathbf{B}\mathbf{c}_n=0, \quad (n\geq 1), \tag{23}$$

$$\mathbf{B}_1^\dagger\mathbf{c}_2+(\mathbf{A}_1-E\mathbf{I})\mathbf{c}_1=0, \tag{24}$$

where $\mathbf{c}_n$ is a column vector whose elements c_{mn} describe the coefficients of the bands in the nth layer, and where

$$B_{ml}\delta(\mathbf{k}_\parallel-\mathbf{k}_\parallel')=\langle\psi_{mn}|H|\psi_{l,n-1}\rangle, \quad (n\neq 1), \tag{25a}$$

$$A_{ml}\delta(\mathbf{k}_\parallel-\mathbf{k}_\parallel')=\langle\psi_{mn}|H|\psi_{ln}\rangle, \quad (n\neq 1), \tag{25b}$$

$$A_{1,ml}\delta(\mathbf{k}_\parallel-\mathbf{k}_\parallel')=\langle\psi_{m1}|H|\psi_{l1}\rangle, \quad (n\neq 1), \tag{25c}$$

$$B_{1,ml}\delta(\mathbf{k}_\parallel-\mathbf{k}_\parallel')=\langle\psi_{m2}|H|\psi_{l1}\rangle, \quad (n\neq 1). \tag{25d}$$

Introducing the z-transform for the coefficients, defined by

$$F_m(z)=\sum_1^\infty c_{mn}z^{1-n}, \quad (m=1 \text{ to } M), \tag{26}$$

its inversion formula is

$$c_{mn}=\frac{1}{2\pi i}\oint_C F_m z^{n-2}dz, \quad (m=1 \text{ to } M). \tag{27}$$

Applying them to the set of difference equations Eq. (23), and writing the result in the matrix form, we obtain

$$[z^2\mathbf{B}^\dagger+z(\mathbf{A}-E\mathbf{I})+\mathbf{B}]\mathbf{F}=[z^2\mathbf{B}^\dagger+z(\mathbf{A}-E\mathbf{I})+\mathbf{B}-\mathbf{B}_1]\mathbf{c}_1+z\mathbf{B}^\dagger\mathbf{c}_2, \tag{28}$$

with the boundary condition relating $\mathbf{c}_2$ to $\mathbf{c}_1$ given by Eq. (24).

The vector $\mathbf{F}$, whose elements are F_m, can then be obtained from Eqs. (24) and (28),

$$\mathbf{F}=\mathbf{I}c_1-[z^2\mathbf{B}^\dagger+z(\mathbf{A}-E\mathbf{I})+\mathbf{B}]^{-1}\times[\mathbf{B}_1+z\mathbf{B}^\dagger\mathbf{B}_1^{\dagger-1}(\mathbf{A}_1-E\mathbf{I})]\mathbf{c}_1. \quad (29)$$

As can be seen from Eq. (29), the poles of the integrand in Eq. (27) are found by locating the zeros of the polynomial

$$\det[z^2\mathbf{B}^\dagger+z(\mathbf{A}-E\mathbf{I})+\mathbf{B}], \quad (30)$$

and are used in the inversion formula to yield the coefficients c_{mn}'s in terms of c_{m1}'s. The boundary condition at the surface is included in the expression for $\mathbf{F}$, and in Eq. (29) the requirement that the wave functions do not become infinite as $n\to\infty$ is satisfied by choosing c_{m1}'s which make the terms with $|z|>1$ in Eq. (24) for c_{mn}'s vanish.

A numerically simpler way of solving the preceding problem is proposed and used here and is illustrated as follows. Since

$$\mathbf{A}^\dagger=\mathbf{A}, \quad (31)$$

in Eq. (30), z and z^{*-1} are both the zeros of the polynomial in that equation. As a result, the number of zeros inside the unit circle must equal the number of zeros outside the unit circle. By denoting the roots of z by z_l, $l=1$ to $2M$, the integral in Eq. (27) can be evaluated using Cauchy's residue theorem,

$$c_{mn}=\sum_{l=1}^{2M} z_l^{n-2}\,\mathrm{Res}\,F_m(z_l)\equiv\sum_{l=1}^{2M}\tilde{c}_{lm}z_l^{n-1}, \quad (32)$$

where

$$\tilde{c}_{lm}=z_l^{-1}\,\mathrm{Res}\,F_m(z_l). \quad (33)$$

In order to satisfy the outgoing boundary condition at $n\to\infty$, the zeros outside the unit circle are discarded by setting the corresponding $\tilde{\mathbf{c}}_l$, the column vector whose elements are $\tilde{c}_{lm}$, equal to zero.

Substitution of Eq. (32) into Eq. (23) yields

$$\sum_l z_l^{n+2}\mathbf{B}^\dagger\tilde{\mathbf{c}}_l+\sum_l z_l^{n+1}(\mathbf{A}-E\mathbf{I})\tilde{\mathbf{c}}_l+\sum_l z_l^{n+1}\mathbf{B}\tilde{\mathbf{c}}_l=0. \quad (34)$$

The above equation holds for all $n\geq 1$, which can be satisfied by setting

$$z_l^{n+2}\mathbf{B}^\dagger\tilde{\mathbf{c}}_l+z_l^{n+1}(\mathbf{A}-E\mathbf{I})\tilde{\mathbf{c}}_l+z_l^n\mathbf{B}\tilde{\mathbf{c}}_l=0, \quad (35)$$

for all z_l's. Thereby, $\tilde{\mathbf{c}}_l$ is the solution of the linear system,

$$(z_l^2\mathbf{B}^\dagger+z_l(\mathbf{A}-E\mathbf{I})+\mathbf{B})\tilde{\mathbf{c}}_l=0, \quad (36)$$

with boundary condition given by Eq. (24). When it can be assumed that

$$\mathbf{A}_1=\mathbf{A},\quad \mathbf{B}_1=\mathbf{B}, \quad (37)$$

the boundary condition can be rewritten as

$$\mathbf{B}^\dagger\mathbf{c}_2+(\mathbf{A}-E\mathbf{I})\mathbf{c}_1+\mathbf{B}\mathbf{c}_0=0, \quad (38)$$

with

$$\mathbf{c}_0=\sum_l \tilde{\mathbf{c}}_l z_l^{-1}=0. \quad (39)$$

Upon obtaining the roots z and the corresponding coefficient vectors $\tilde{\mathbf{c}}_l$, the coefficients in the wave function are readily obtained using Eq. (32). Since the system is semi-infinite, although these c_{mn}'s constitute both propagating and decaying components, the decaying wave functions go to zero as n goes to infinity and so they do not contribute to the normalization, the normalization of the wave functions only needs to be performed on the propagating ones. The wave functions are normalized to give correct number of orbitals per unit cell. For example, for a semi-infinite silicon semiconductor, there are eight $\mathbf{c}_n$'s satisfying the boundary condition. For a bulk state, each $\mathbf{c}_n$ is the linear combination of eight wave functions, at least two of which are propagating ones, and each of these wavefunctions is a linear combination of the eight atomic orbitals of the unit cell. The normalization of the $\mathbf{c}_n$'s, after taking into account the spin of the electrons, is performed in such a way that $\Sigma_m c_{mn}c_{mn}^*=2$, where the sum is over the propagating components of $\mathbf{c}_n$. The eight orthogonal wave functions satisfying the boundary conditions then give 16 orbitals per unit cell. Given the condition in Eq. (37) the final equations used in this method become equivalent to those used by Gosavi and Marcus[30] in their treatment of electron transfer at metal electrodes, although their appearance differs.

Although the above formulation of the z-transform method was derived by considering the first nearest neighbor interactions between the solid atoms, the z-transform method can be applied to the tight-binding model with interactions involving as many atoms as desired. When the interactions include more than the nearest neighbors, one can simply increase the thickness of the superlayer so that only the nearest neighboring superlayers interact with each other.

When the one-electron wave functions are expressed in an orthonormal atomic basis set, the coupling $V(\mathbf{k},\mathbf{r})$ between a solid electronic state $|\Psi_\mathbf{k}\rangle$ and the acceptor state $|\Phi\rangle$,

$$V(\mathbf{k},\mathbf{r})=\langle\Psi_\mathbf{k}|H(\mathbf{r})|\Phi\rangle, \quad (40)$$

can be expressed in terms of the couplings between the atomic states,

$$V(\mathbf{k},\mathbf{r})=\sum_{n,a,m,i,j} e^{i\mathbf{k}_\parallel\cdot\mathbf{r}_{\parallel,a}}c_{nm}(\mathbf{k})^*C_{ij}\langle\psi_{nam}|H(\mathbf{r})|\phi_{ij}\rangle, \quad (41)$$

where the ϕ_{ij} is the jth orbital of the ith atom in the molecular acceptor state, and C_{ij} is the coefficient of the this orbital in forming the acceptor state, ψ_{nam} is the mth type of atomic orbital which belongs to the ath semiconductor atom in the nth layer. $\mathbf{r}_{\parallel,a}$ in Eq. (41) is the position of the atom a in a semiconductor layer. We may illustrate the notation by considering a semi-infinite silicon semiconductor. Each superlayer of silicon consists of two layers of silicon atoms, and each silicon atom contains 4 relevant orbitals(e.g., $3s$, $3p_x$, $3p_y$, $3p_z$) and so m varies from 1 to 8. The first layer is formed by atoms denoted by $(1,a)$, where a is only odd numbered, 1, 3, 5,..., the orbitals of which are then denoted by $(1, a, m)$, where $m=1$, 2, 3, 4. The second layer also belongs to the first superlayer and thus $n=1$, $a=2$, 4, 6,... and $m=5$, 6, 7, 8. (We note that the $a=2$, $a=4$, etc. atoms

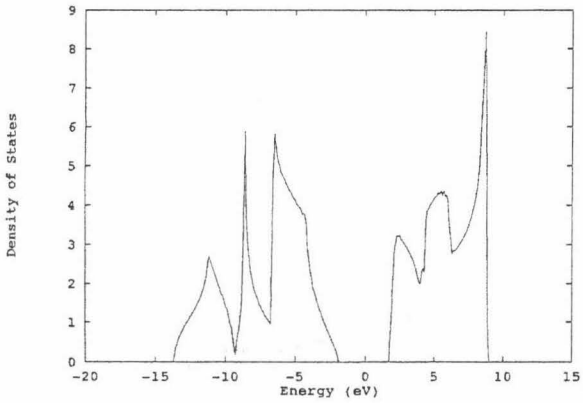

FIG. 3. Calculated density of states ρ for the bulk of Si semiconductor. The unit of the density of states is per unit cell (2 atoms) per eV. The Fermi level is located at 0 eV.

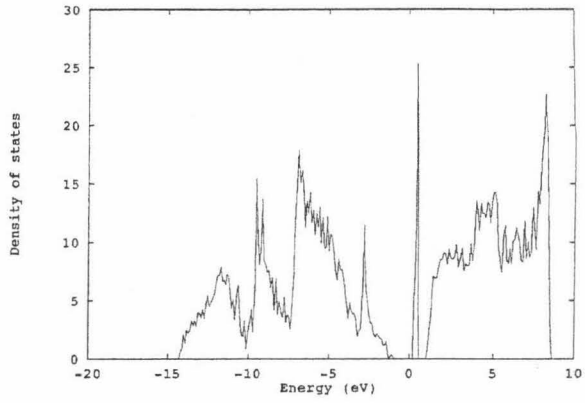

FIG. 4. Calculated density of states ρ for a slab of Si semiconductor. The unit of the density of states is per eV per unit cell. There are 20 atoms per unit cell, which has one atom on each face of the slab and so is 20 atoms thick. The Fermi level is located at 0 eV.

interact differently with the molecule, because of their different positions with respect to it.) The c_{nm} in Eq. (41) are obtained by the tight-binding calculations described earlier and are functions of $\mathbf{k}_{\|}$ but are independent of $\mathbf{r}_{\|,a}$. The coupling matrix elements $\langle \psi_{nam} | H(\mathbf{r}) | \phi_{ij} \rangle$ are obtained by the extended-Hückel calculations for the acceptor atomic orbital (i,j) and the semiconductor atomic orbital m at the position (n, a).

III. APPLICATIONS

A. Silicon/viologen system

1. Band structure calculations of silicon

The LCAO ("tight-binding") method has provided a good description for the semiconductor valence band and conduction band edge for silicon even when only the nearest-neighbor interactions are considered and an orthogonal basis is used.[31] In this calculation, the nearest-neighbor interaction parameters are taken from a table of solid state parameters in Ref. 25. The density of states is obtained by randomly choosing a certain number of wave vectors in the calculation which show a statistical number of the energy eigenvalues. The computed density of states for a bulk silicon is normalized to give 16 orbitals per unit cell (including the spin of the electrons) and is shown as a function of the orbital energy in Fig. 3.

The surface studied experimentally for silicon was, as noted earlier, the (100) surface. In the slab method, the silicon (100) surface bands were calculated using models of infinite silicon slabs with ideal (100) surfaces, i.e., a finite number of layers, each consisting of an infinite number of (100) silicon atoms as a two-dimensional array, are placed as in a perfect silicon crystal (Fig. 2). The one-electron wave functions are written as linear combinations of Bloch functions as in Eq. (22), where the sums are over the layers and the $3S, 3P_x, 3P_y, 3P_z$ orbitals, respectively. The (100) surface is treated as ideal and the matrix elements between a Bloch function of the surface plane and one plane inside the slab is treated as the same as the corresponding elements between two Bloch functions well inside the slab. The wave functions are determined by solving the eigenvalue problem represented by Eq. (18).

The Hamiltonian matrix elements were computed as functions of a two-dimensional wave vector (k_y, k_z) by choosing the same parameters as in the bulk calculation. The energy eigenvalues and the eigenstates were obtained by diagonalizing the Hamiltonian matrix, and the density of states as a function of energy is calculated using a statistical number of the eigenvalues. The density of states was normalized to give the proper number of orbitals per unit cell (which contains N silicon atoms for the unit cell in an N layer slab). Except for the intrinsic surface states, which lie in the band gap, the density of states calculated for a slab of a Si semiconductor (Fig. 4) is similar to the one obtained for the bulk silicon.

Since each primary unit cell of a bulk silicon crystal has two silicon atoms, one should include at least two layers of (100) plane in a superlayer in the application of the z-transform to a semi-infinite system. The **B** and **A** matrices, obtained by using the same solid state parameters as in the bulk and slab calculations, are all 8×8 matrices. The bulk and surface states of the semi-infinite semiconductor can both be obtained using the z-transform. A bulk state contains at least two propagating components and a surface state has only decaying wave functions.

In the experiments,[4] the electrode surfaces were occupied by hydrogen atoms to saturate the dangling bonds of surface silicon atoms, removing thereby the surface states resulted from the dangling bonds of the surface silicon atoms. According to previous calculations in the literature on a hydrogen-terminated Si (111) surface[32] all surface states were removed and the silicon–hydrogen interaction forms two bands deep inside the silicon bulk bands. Although the band structure of the hydrogen-terminated Si (100) slab is different, it seems reasonable to suppose that there will be no intrinsic surface states left for a perfect hydrogen-terminated Si (100) surface.

2. The electronic structure of the redox molecule

For the calculation of the rate constant of the electron transfer reaction at the silicon/viologen$^{2+/+}$ interfaces, N,N'-dimethyl-4,4′-bipyridylium^{2+} was chosen as the electron acceptor. Using the structural data of this cation in a crystal,[33] the most stable structure of the ion was obtained by the EHMACC (extended-Hückel molecular and crystal calculations program).[34] The two pyridyl planes formed thereby a 50^0 angle. However, since the calculation was performed without the consideration of the interactions between the acceptor and the solvent molecules, some differences may occur for the structure of this ion in solution. The LUMO of the ion, i.e., the acceptor state was obtained as a linear combination of the atomic orbitals,

$$\Phi=\sum_{i,j} C_{ij}\phi_{ij}, \tag{42}$$

where the sum is over the atoms i and the valence orbitals j of each atom with C_{ij}'s obtained from the extended-Hückel calculation.

3. Calculation of the electron transfer rate constant

To be consistent with the experiments where the only rate-limiting step is the electron transfer process the acceptors are considered homogeneously distributed in the solution. The orientations are taken as random, using 125 different orientations, each translated so as to have the closest pair of atoms, of the molecule and of the semiconductor surface, in van der Waals' contact, i.e., they have a separation distance equal to the sum of the atomic van der Waals' radii. The square of the electronic coupling is averaged over these orientations. In the calculations, the semiconductor is assumed to be uniform and is represented by the surface $x=0$, and the 125 orientations of the molecule are created by the rotations of the molecule in the three-dimensional space each with a set of randomly chosen Eulerian angles. The geometric center of the molecule with each selected orientation has 16 randomly chosen (y, z) coordinate relative to the closest Si surface atom. Because of the symmetry of the Si semiconductor surface, y and z vary between 0 and half a lattice constant. Under the assumption that the coupling decays exponentially with distance with a decay exponent β_s, the range of contributing distances is $1/\beta_s$, and we note that $\beta_s \approx 1$ Å^{-1}.[19] The averaged quantity of coupling matrix element, denoted by $\langle|V(\mathbf{k})|^2\rangle$ at the van der Waals' contact mentioned earlier was obtained by an extended-Hückel[34] calculation. For the hydrogen-terminated silicon surface, $\langle|V(\mathbf{k})|^2\rangle$ is calculated assuming a direct van der Waals' contact between the hydrogen atom on the Si surface and the closest atom of the redox species[35] for each given orientation. A certain number of states at each energy ϵ is randomly chosen to give the average of the square of the coupling, $\langle|\bar{V}(\epsilon)|^2\rangle$, which is then multiplied by the density of states to yield the total coupling at that energy.

Combining Eqs. (9), (13), and (16) an expression is obtained for the first-order electron transfer reaction rate constant,

TABLE I. Experimental and calculated $k_{et}^{\max}$.[a]

System	$k_{et}^{\max}$ (expt.)	$k_{et}^{\max}$ (*z-trans.*)	$k_{et}^{\max}$ (slab)
Si/viologen$^{2+/+}$	0.6[b]	1.3	1.6
InP/$Me_2Fc^{+/0}$	1–2[c]	0.084	0.086

[a]Units are 10^{-16} cm^4 s^{-1}, and the theoretical $k_{et}^{\max}$ includes only bulk states.
[b]From Ref. 4.
[c]From Ref. 1.

$$k_f=\frac{2\pi}{\hbar}\frac{1}{\sqrt{4\pi\lambda k_B T}}\frac{1}{\beta_s}\int_0^\infty \exp\left(-\frac{(\lambda+\Delta G^0-\epsilon)^2}{4\lambda k_B T}\right)$$
$$\times\langle|\bar{V}(\epsilon)|^2\rangle f(\epsilon)\rho(\epsilon)d\epsilon, \tag{43}$$

where $\rho(\epsilon)$ and $\langle|\bar{V}(\epsilon)|^2\rangle$ are normalized to the unit cell. Because of the low occupancy of the semiconductor conduction band, and reflecting the Boltzmann factor the electron transfer can be regarded as occurring only near the edge of the conduction band, i.e., nearly at $\epsilon=0$. In Eq. (43) and hereinafter for convenience of discussion the energy ϵ of the electrons in the semiconductor will be referred to the conduction band edge at the semiconductor surface as zero.

For a semiconductor/electrolyte interface as in the electron transfer reaction studies in Refs. 1–6, the change of electrostatic potential across a semiconductor/liquid interface exists mainly within the semiconductor, because of the low concentration of the charge carriers in the semiconductor. In this case, the change of applied potential changes only the concentration of carriers at the interface and does not change the free energy ΔG^0 of the electron transfer reaction. As shown in the Appendix, the maximum second-order electron transfer rate constant can then be expressed as

$$k_{et}^{\max}=\frac{2\pi}{\hbar}\frac{1}{\sqrt{4\pi\lambda k_B T}}\frac{\nu}{\beta_s}\langle|\bar{V}|^2\rangle, \tag{44}$$

where $\langle|\bar{V}|^2\rangle$ is defined in the Appendix [cf. Eq. (A6)]. The maximum rate constant computed using the above equation is shown in Table I.

B. Indium phosphide/ferrocene interfaces

1. Band structure of indium phosphide

The bulk band structure of the InP semiconductor was calculated using the Hamiltonian and the interaction parameters given by Chadi *et al.*[24,36,37] The density of states computed for the bulk and a slab of the InP semiconductor are shown in Figs. 5 and 6, respectively. The electronic structure of Me_2Fc^+ was obtained from the extended-Hückel calculation[34] using the molecular structure given in Ref. 38. The electronic structure calculations were again performed for a slab and for a semi-infinite crystal model of the InP semiconductor with a (100) surface. The maximum second-order electron transfer rate constant (per unit area) was computed and the results are given in Table I.

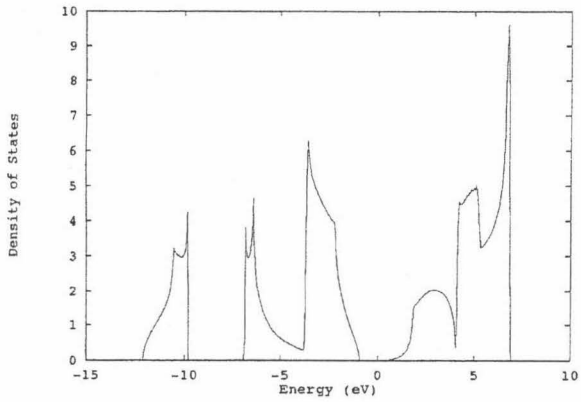

FIG. 5. Calculated density of states ρ for the bulk of InP semiconductor. The unit of the density of states is per unit cell (2 atoms) per eV. The Fermi level is located at 0 eV.

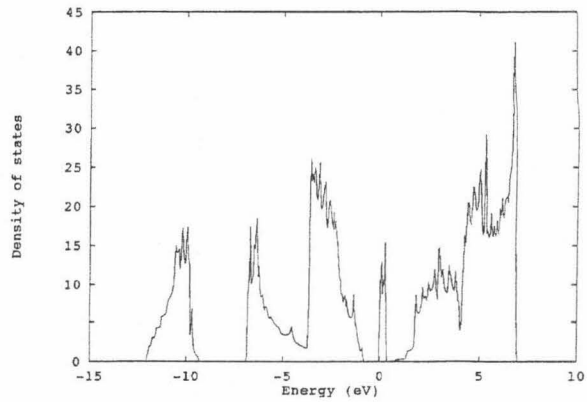

FIG. 6. Calculated density of states ρ for a slab of InP semiconductor. The unit of the density of states is per eV per unit cell. There are 20 atoms per unit cell, which has one atom on each face of the slab and so is 20 atoms thick. The Fermi level is located at 0 eV.

2. Contribution of surface states

Using considerations similar to those used in the treatment of bulk states we shall also assume that the electron transfer between a surface state and the bulk state is much faster than the electron transfer between the surface state and the molecular acceptor. In the preceding treatment we neglected the interactions which might lead to such a coupling, e.g., radiationless transitions. The resulting expression for the current density corresponding to the electron transfer from the surface states of the semiconductor to the acceptor is

$$J_f^{ss}=e[A]\frac{2\pi}{\hbar}\frac{1}{\sqrt{4\pi\lambda k_BT}}\frac{1}{\beta_s}\times\int_{\epsilon}|V_{ss}(\epsilon)|^2e^{-[(\lambda+\Delta G)^2/4\lambda k_BT]}f(\epsilon)\rho_{ss}(\epsilon)d\epsilon, \quad (45)$$

where ρ_{ss} is the density of surface states, and

$$\Delta G=\Delta G^0-\epsilon, \quad (46)$$

is the driving force for the electron transfer from a surface state with energy ϵ to the acceptor. If, for simplicity, it is further assumed that the surface states are distributed homogeneously in an energy range from $-\Delta E$ to 0, i.e., in an interval ΔE below the conduction band edge, then

$$\rho_{ss}=\frac{N_{ss}}{\Delta E}, \quad (47)$$

where N_{ss} is the total number of surface states.

The occupancy of these states obeys the Fermi–Dirac distribution,

$$f(\epsilon)=\frac{1}{1+e^{(\epsilon-\epsilon_f)/k_BT}}, \quad (48)$$

where ϵ_f is the Fermi level, and depends linearly on the applied potential E_{app},

$$\epsilon_f=eE_{app}+\epsilon_f^0=eE_{app}+V_{bi}^0+\epsilon_f^b. \quad (49)$$

Here, ϵ_f^0 is the value of ϵ_f when $E_{app}=0$, V_{bi}^0 is the built-in voltage, the potential drop within the semiconductor, when $E_{app}=0$, and ϵ_f^b is the energy difference between the Fermi level and the conduction band edge inside the semiconductor (Fig. 1). When any dependence of the coupling between the surface states and the acceptor state on the energy ϵ is neglected, an expression for the surface states contribution to the current density from the semiconductor to the acceptor state J_f^{ss} is

$$J_f^{ss}=e[A]\frac{2\pi}{\hbar}\frac{1}{\sqrt{4\pi\lambda k_BT}}\frac{1}{\beta_s}\frac{N_{ss}|V_{ss}|^2}{\Delta E}\times\int_{-\Delta E}^{0}e^{-[(\lambda+\Delta G)^2/4\lambda k_BT]}f(\epsilon)d\epsilon, \quad (50)$$

where ΔG is given by Eq. (46). Similarly, the current density due to the electron transfer from the donor to the surface states can be expressed as

$$J_b^{ss}=-e[A^-]\frac{2\pi}{\hbar}\frac{1}{\sqrt{4\pi\lambda k_BT}}\frac{1}{\beta_s}\frac{N_{ss}|V_{ss}|^2}{\Delta E}\times\int_{-\Delta E}^{0}e^{-[(\lambda-\Delta G)^2/4\lambda k_BT]}(1-f(\epsilon))d\epsilon. \quad (51)$$

The sum $J_f^{ss}+J_b^{ss}$ is next used to interpret the current-applied potential behavior obtained in the experiments. The $N_{ss}|V_{ss}|^2$ is treated as a single parameter which can be adjusted to fit the experimental data, in the absence of any other complicating factors.

3. Current vs applied potential behavior

As we have noted earlier, the total current can be written as the sum of two components,

$$J=J^{ss}+J^{bk}. \quad (52)$$

In the present treatment J^{ss} is computed using Eqs. (50) and (51) and J^{bk}, the current from the bulk states, is calculated using the tight-binding method.

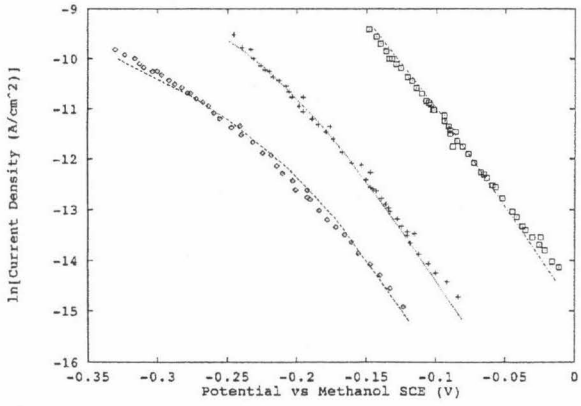

FIG. 7. Current-applied potential behavior at the InP/$Me_2Fe^{+/0}$ interfaces. The experimental data are taken from Ref. 1. From left to right, the concentrations of Me_2Fe^+ are 0.001 M, 0.01 M, 0.1 M, respectively. The concentration of Me_2Fe is 0.1 M. To fit the experimental data, $N_{ss}|V_{ss}|^2$ is taken as 1.25, 0.31, 0.44×10^{-8} eV^2, respectively.

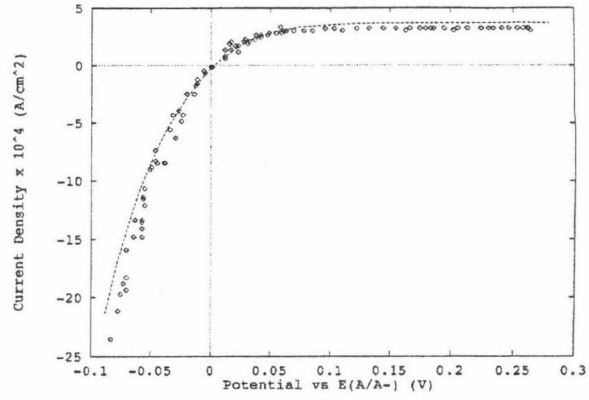

FIG. 8. Current-applied potential behavior at the InP/$PV^{2+/+}$ interfaces. The experimental data are taken from Ref. 1. $N_{ss}|V_{ss}|^2$ is taken as 3.2×10^{-8} eV^2.

When the current via the surface states dominates, namely, when the surface states are much more occupied than the conduction band or when the density of surface states is high, one has approximately for the forward and reverse current density,

$$J_f^{ss}+J_b^{ss}=0, \tag{53}$$

at equilibrium. In the case of the InP/$Me_2Fc^{+/0}$ interface, using Eqs. (48), (49), (50), (51), and (53) to fit the built-in voltage V_{bi}^0 of the semiconductor at zero applied potential, which leads to a equality between the integrals in Eqs. (50) and (51), a value for ΔE is obtained as 0.4 eV. This value of ΔE agrees with results from surface state studies of the (100) surface of lightly doped n-InP semiconductors in vacuum both experimentally[39] and theoretically,[40] where the surface states were shown to be located at (1/3) E_g below the conduction band minimum.[41] Here, E_g is the band gap of the semiconductor and is around 1.35 eV.

Similarly, the electrochemical studies at p-InP/electrolyte interfaces[42] also lead to surface states distributed mostly near the conduction band edge. Other parameters used in this calculation are as follows: the reorganization energy λ is 0.8 eV, as suggested in Ref. 1, ΔG^0 is 0.79 eV;[1] the parameter $N_{ss}|V_{ss}|^2$ is chosen as 10^{-8} $(eV)^2$ to fit the net current density obtained in the experiments[1] using Eqs. (50) and (51). The current density is then obtained as a function of the applied potential for different $[A]/[A^-]$ ratios and is compared with the experimental data. The curvature of the plot is determined by the relative position of the energy of the surface states and the Fermi level, and so depends on E_{app} and ΔG^0, as shown in Fig. 1. When the Fermi energy is much lower than the energies of the surface states, the occupancy of these states can be treated as obeying a Boltzmann distribution, and the $\ln[J]$ vs E_{app} curve is a straight line.[43] When the energy difference between the lowest surface states and the Fermi level is less than k_BT, the Fermi–Dirac distribution must be employed. The $\ln[J]$ vs E_{app} plot then deviates from a straight line, as shown in Fig. 7. In order to fit the experimental results different densities of states are used for different InP/liquid interfaces. This assumption is not necessarily correct, since the deviation of the horizontal distance between the neighboring curves in Fig. 7 from the value of 0.059 V may also result from experimental uncertainties.[44]

In order to fit the experimental current vs applied potential data obtained at the InP/$PV^{2+/+}$ interface by the diode equation,[1]

$$J=J_0(e^{-eE_{app}/Ak_BT}-1), \tag{54}$$

the A in Eq. (54) should be greater than 1.8, which indicates that the current vs applied potential behavior at this interface is far from ideal ($A=1$). A better fit is obtained by including surface states in the calculation, using the following parameters: $\Delta E=0.4$ eV, $\Delta G^0=-0.34$ eV,[1] $\lambda=0.5$ eV,[1] and $N_{ss}|V_{ss}|^2=2\times10^{-8}$ $(eV)^2$. Here, ΔE is taken the same as in the InP/$Me_2Fc^{+/0}$ case and $N_{ss}|V_{ss}|^2$ is chosen to fit the measured net current density. The calculated result is shown in Fig. 8 together with the experimental results.

IV. DISCUSSION

The nonadiabatic description and the two-level approximation applied in our theoretical studies of electron transfer reactions at semiconductor/liquid interfaces provide a consistent value for the reaction rate constant when compared with the experimental results. Semiconductors differ from metals because of their band gap, which, as pointed out by Dogonadze,[11] makes the electron transfer reactions more likely to be nonadiabatic. This effect is associated with the low occupancy of the semiconductor conduction band, which allows the electron transfer to occur mainly nearly the edge of the conduction band. For a metal/liquid interface, the electron transfer reaction happens largely at the Fermi energy, and the coupling strength between the metal electrode and the molecular acceptor can be characterized by[15,22]

$$\Delta(\epsilon)=2\pi\sum_{\mathbf{k}}|V_{\mathbf{k}}|^2\delta(\epsilon_{\mathbf{k}}-\epsilon), \tag{55}$$

where $\Delta(\epsilon)$ is evaluated at the Fermi energy. $\Delta(\epsilon_f)/\hbar\omega_{\max}$ has been then taken[15,45] as the criterion for distinguishing nonadiabatic from adiabatic reactions for a metal/liquid interface,[15] where $\omega_{\max}$ is the "fastest phonon mode" contributing to the electron transfer reaction. For an $\omega_{\max}/2\pi$ of the order of 10^{13} s^{-1} this $\hbar\omega_{\max}$ is about 0.03 eV. At a semiconductor/liquid interface, the electron transfer reaction occurs mainly near the edge of the conduction band. The interaction strength between the continuum states of a semiconductor and the acceptor state is better characterized by[20]

$$\Delta^I=\frac{1}{k_BT}\int_{\epsilon}\Delta(\epsilon)d\epsilon, \tag{56}$$

where the limit "ϵ" denotes a narrow interval of an amount k_BT at the semiconductor conduction band edge. Because of the low occupancy of the electronic states in the semiconductor conduction band, the electron transfer happens only at a small energy range near the conduction band edge, and then the important integration regime only covers a narrow interval of the order of k_BT. As pointed out by Harrison,[25] band energy is proportional to the square of $k-k_0$ near the conduction band edge, where k_0 is the value of k at the conduction band edge (conduction band minimum). The value of k_0 depends on the nature of the interaction of different bands. For InP k_0 is zero,[46] while for Si it is quite large.[46] For Si and InP, the density of states is very low near the conduction band edge,[25,46] the total coupling between these semiconductors and the molecular acceptor is typically weak. The Δ^I is the counterpart of the usual matrix element that appears in the two-state Landau-Zener formula. The present approximate calculations lead to a value of Δ^I of the order of 10^{-5} eV. In that case, with $\hbar\omega_{\max}\sim 0.03$ eV, the reactions can be regarded as nonadiabatic.

Since the double layer at the interface of semiconductor/liquid interfaces is neglected and the redox molecules are also allowed to penetrate to the electrode surface, the present calculations more likely represent an upper bound of the maximum rate constant. Although the approach in this study is intended to be a pragmatic one, the calculated result for the maximum rate constant at the Si/viologen$^{2+/+}$ interfaces is in a surprisingly reasonable agreement with the experimental data. The agreement for InP/$Me_2Fc^{+/0}$ is less satisfactory, the calculated value being approximately an order of magnitude smaller than the experimental one. Nevertheless, considering the approximation of using the extended-Hückel treatment to obtain the coupling, this extent of agreement is, in our opinion, encouraging.

The difference between the calculated results for Si/viologen$^{2+/+}$ and InP/$Me_2Fc^{+/0}$ systems[47] may be due to several effects. One factor is the difference in size of the acceptor state, since the LUMO of a viologen$^{2+/+}$ ion is calculated in the present work to be delocalized over the whole ring system, and the LUMO of a $Me_2Fc^{+/0}$ ion is localized mainly on the Fe^{3+} ion (here and in Ref. 48) and so distant from the periphery of the molecule. This effect would yield a larger electronic coupling between the semiconductor and the first redox species, other things being equal. However, there are factors which would make InP more effective than Si, e.g., a smaller effective electron mass,[25,46] and so tend to counter the above molecular effect. It would be useful therefore to study the two semiconductor systems with the same molecular species, if possible. In an effort to resolve this question using calculations we have compared the calculated maximum rate constant for the Si/viologen$^{2+/+}$ system, 1.6×10^{-16} cm^4 s^{-1}, as in Table I, with a maximum rate constant which we subsequently calculated for the Si/$Me_2Fc^{+/0}$ system, 0.17×10^{-16} cm^4 s^{-1}. Thus, it is seen that the viologen$^{2+/+}$ pair has a closer effective contact with the Si interface than does the $Me_2Fc^{+/0}$ pair. Accordingly, the experimental result in Table I, in contrast with the calculated results in that table, that the InP/$Me_2Fc^{+/0}$ has a higher rate than Si/viologen$^{2+/+}$, cannot be attributed to a more effective contact. For this reason we attribute the higher experimental rate for InP to the presence of surface states in the InP, as discussed earlier. We note also that the calculated (bulk state) result for InP/$Me_2Fc^{+/0}$ (0.086×10^{-16} cm^4 s^{-1}) is comparable with the calculated (bulk state) result for Si/$Me_2Fc^{+/0}$ (0.17×10^{-16} cm^4 s^{-1}).

Under some conditions, surface states may play a role in the electron transfer reactions at semiconductor/liquid interfaces, because of their localization at the electrode surfaces, as noted by previous authors.[9,16] Although the density of bulk states of the InP conduction band is large, of the order of 10^{17} cm^{-3}, the decay length of their coupling to the molecule of about 1 Å yields an effective surface density of states of the conduction band of the order of only 10^9 cm^{-2}. We note further that in a free-electron model a surface state has a wave function which can be expressed as

$$\varphi\propto e^{-\beta_{ss}x}\cos(k_xx). \tag{57}$$

The $1/\beta_{ss}$ is about 8 Å for the InP semiconductor.[49] As a result, a large fraction of surface states can be effective in contributing to the electron tunneling event. In treating the electron transfer at InP/$Me_2Fc^{+/0}$ interfaces, the possibility of surface states was subsequently included in Sec. III B, as one interpretation of the nonideal current vs applied potential behavior in the experiments. A coupling strength between the surface states and the acceptor required to account for the discrepancy between the theoretical and experimental results was then estimated. We have not included any such contribution in Table I, the discrepancy in the rate constant of a factor of 10 between experimental and calculated results for the InP system in Table I could also have other sources.

While the inclusion of the surface states helps to explain the current vs applied potential behavior obtained in the experiments, the nonideal behavior being explained by the Fermi–Dirac occupancy of the surface states, the nonideal behavior can also result from many other mechanisms, such as the recombination of charge carriers in the solid bulk. The latter can produce a diode plot with a slope larger than unity.[50,51] We have noted earlier that the part of the present calculation which includes surface states is based on the assumption that the electron transfer between the bulk states and the surface states is much faster than the interfacial charge transfer, and is also based on a simplified model for the density of surface states. A deeper understanding of the mechanism would require the investigation of other pro-

cesses at the semiconductor/liquid interface and inside the semiconductor, as Anz and Lewis[50] have concluded from their recent simulation.

We turn next to a comparison of the electronic structure calculations of semiconductors with surfaces using the direct diagonalization vs using the z-transform. The direct diagonalization uses a slab of the crystal and mathematically is more straightforward, but because the computing time increases rapidly with the size of the slab, it is a less practical way to treat a very "thick slab". On the other hand, as noted in the literature,[52] usually a 20-layer slab is enough to produce a correct band structure for the crystal. The slab method is also a convenient method for obtaining the band structure and the density of states, and is practical for our purpose. With the z-transform method, a semi-infinite crystal is treated. Its mathematical formula is more complicated than that of the slab method, in that its solution requires the location of the roots of a high order and in many cases complex polynomial. Although it is time-consuming to obtain the whole band structure, in the application of the z-transform the energy is an input, the computing time can be considerably reduced if only states of some specific energies are required. The two methods provide similar results when they are applied to the calculations of the electron transfer reaction rate constants at semiconductor/liquid interfaces (Table I).

ACKNOWLEDGMENTS

It is a pleasure to acknowledge the support of the National Science Foundation and the Office of Naval Research. We thank Professor Nathan S. Lewis, Dr. Arnel M. Fajardo, and Samir J. Anz for valuable discussions, and Professors Mark Ratner and Harry Finklea for their especially helpful comments. We also thank Shachi S. Gosavi for discussions on the application of the z-transform method.

APPENDIX A: THE EXPRESSION FOR THE MAXIMUM ELECTRON TRANSFER RATE CONSTANT

As discussed in the text, in the integral in Eq. (43) $f(\epsilon)$ is the only term which depends on the applied potential $E_{\rm app}$,

$$f(\epsilon)=\exp\left(-\frac{\epsilon-\epsilon_f^0-eE_{\rm app}}{k_BT}\right), \tag{A1}$$

where the quantities in Eq. (A1) were defined earlier in the text [cf. Eq. (49)]. ϵ_f^0 is a constant for a semiconductor/liquid interface. Equation (43) can then be written as

$$k_f(E_{\rm app})=e^{eE_{\rm app}/k_BT}\frac{2\pi}{\hbar}\frac{1}{\sqrt{4\pi\lambda k_BT}}\frac{1}{\beta_s}\times\int_0^\infty\exp\left(-\frac{(\lambda+\Delta G^0-\epsilon)^2}{4\lambda k_BT}\right)\times\langle|\bar V(\epsilon)|^2\rangle f_0(\epsilon)\rho(\epsilon)d\epsilon, \tag{A2}$$

where $f_0(\epsilon)$ is the occupancy, $\exp[-(\epsilon-\epsilon_f^0)/k_BT]$, of the conduction band states at the semiconductor surface at zero applied potential. The number density of electrons n_s at the semiconductor surface is also a function of the applied potential,

$$n_s=n_0\exp\left(-\frac{eV_{\rm bi}^0-eE_{\rm app}}{k_BT}\right), \tag{A3}$$

where n_0 is the number density of conduction band electrons in the semiconductor bulk, and $V_{\rm bi}^0$ is the potential drop within the semiconductor at zero applied potential, i.e., at $E_{\rm app}=0$.

Comparison of Eqs. (A2) and (A3) then illustrates that $k_f(E_{\rm app})$ is proportional to the density of surface electrons n_s. An expression of a second-order electron transfer rate constant that is independent of the applied potential, and thus of the density of surface electrons of the semiconductor, can be written as

$$k_{et}=\frac{2\pi}{n_0e^{-V_{bi}^0/k_BT}\hbar}\frac{1}{\sqrt{4\pi\lambda k_BT}}\frac{1}{\beta_s}\times\int_0^\infty\exp\left(-\frac{(\lambda+\Delta G^0-\epsilon)^2}{4\lambda k_BT}\right)\times\langle|\bar V(\epsilon)|^2\rangle f_0(\epsilon)\rho(\epsilon)d\epsilon. \tag{A4}$$

The $n_0e^{-V_{bi}^0/k_BT}$ in Eq. (A4) is readily evaluated, being equal to $\int\rho(\epsilon)f_0(\epsilon)d\epsilon/v$, with $\epsilon=0$ to $\epsilon=\infty$ as integration limits.[53] The v is the volume of the unit cell, and in the calculations using Eq. (A4) the wave functions are normalized to a unit cell.

Since we are interested in the maximum rate constant for the electron transfer, where $\lambda+\Delta G^0$ is nearly zero, in the exponent term of the free energy one can set $\epsilon=0$, since $\epsilon\ll\lambda$, and remove it from the integral, one then has

$$k_{et}=\frac{2\pi}{\hbar}\frac{1}{\sqrt{4\pi\lambda k_BT}}\frac{v}{\beta_s}\exp\left(-\frac{(\lambda+\Delta G^0)^2}{4\lambda k_BT}\right)\times\frac{\int_0^\infty\langle|\bar V(\epsilon)|^2\rangle f_0(\epsilon)\rho(\epsilon)d\epsilon}{\int_0^\infty f_0(\epsilon)\rho(\epsilon)d\epsilon}\cdot(\Delta G^0\simeq-\lambda). \tag{A5}$$

In the experiments,[4] the maximum rate constants were obtained by choosing a series of acceptors in the liquid with different reaction free energy but with similar reorganization energy around 0.7 eV.[4] Here, by setting $\Delta G^0+\lambda=0$, and by introducing an averaged coupling matrix element square,[53] $\langle|\bar V|^2\rangle$, where

$$\langle|\bar V|^2\rangle=\frac{\int_0^\infty\langle|\bar V(\epsilon)|^2\rangle f_0(\epsilon)\rho(\epsilon)d\epsilon}{\int_0^\infty f_0(\epsilon)\rho(\epsilon)d\epsilon}, \tag{A6}$$

an expression of the second-order electron transfer rate constant is then obtained as in Eq. (44).

[1] K. E. Pomykal and N. S. Lewis, J. Phys. Chem. B **101**, 2476 (1997).
[2] K. E. Pomykal, A. M. Fajardo, and N. S. Lewis, J. Phys. Chem. **100**, 3652 (1996).
[3] A. M. Fajardo and N. S. Lewis, Science **274**, 969 (1996).
[4] A. M. Fajardo and N. S. Lewis, J. Phys. Chem. B **101**, 11136 (1997).
[5] B. R. Horrocks, M. V. Mirkin, and A. J. Bard, J. Phys. Chem. **98**, 9106 (1994).

[6] I. Uhlendorf, R. Reineke-Kock, and R. Memming, J. Phys. Chem. **100**, 4390 (1996).
[7] R. A. Marcus, J. Phys. Chem. **95**, 1050 (1991).
[8] N. S. Lewis, Annu. Rev. Phys. Chem. **42**, 543 (1991).
[9] H. Gerischer, J. Phys. Chem. **95**, 1356 (1991).
[10] W. J. Royea, A. M. Fajardo, and N. S. Lewis, J. Phys. Chem. B **101**, 11152 (1997).
[11] R. R. Dogonadze and A. M. Kuznetsov, Prog. Surf. Sci. **6**, 42 (1975).
[12] R. A. Marcus, J. Phys. Chem. **94**, 1050 (1990).
[13] B. B. Smith and A. J. Nozik, Chem. Phys. **205**, 47 (1996).
[14] B. B. Smith, J. W. Halley, and A. J. Nozik, Chem. Phys. **205**, 245 (1996).
[15] W. Schmickler, J. Electroanal. Chem. **204**, 31 (1986).
[16] B. B. Smith and A. J. Nozik, J. Phys. Chem. B **101**, 2459 (1997).
[17] For examples, S. G. Davison and J. D. Levine, Solid State Phys. **25**, 1 (1970); D. J. Chadi and M. L. Cohen, Phys. Status Solidi B **68**, 405 (1975); Y. R. Yang and C. B. Duke, Phys. Rev. B **36**, 2763 (1987).
[18] R. A. Marcus, J. Chem. Phys. **98**, 5604 (1993).
[19] R. A. Marcus and N. Sutin, Biochim. Biophys. Acta **811**, 265 (1985).
[20] Y. D. Demkov and V. I. Osherov, Sov. Phys. JETP **26**, 916 (1968).
[21] H. Ou-Yang, B. Källebring, and R. A. Marcus, J. Chem. Phys. **98**, 7565 (1993).
[22] J. P. Muscat and D. M. Newns, Prog. Surf. Sci. **9**, 1 (1978).
[23] J. C. Slater and G. F. Koster, Phys. Rev. **94**, 1498 (1954).
[24] D. J. Chadi, Phys. Rev. B **16**, 790 (1977).
[25] W. A. Harrison, *Electronic Structure and the Properties of Solids* (Dover, New York, 1989).
[26] G. Allan, Surf. Sci. **299/300**, 319 (1994).
[27] D. H. Lee and D. Joannopoulos, Phys. Rev. B **23**, 4988 (1981).
[28] H. Ou-Yang, R. A. Marcus, and B. Källebring, J. Chem. Phys. **100**, 7814 (1994).
[29] D. A. Papaconstantopoulos, *Handbook of the Band Structure of Elemental Solids* (Plenum, New York, 1986).
[30] S. Gosavi and R. A. Marcus, J. Phys. Chem. B (to be published).
[31] S. T. Pantelides and J. Pollmann, J. Vac. Sci. Technol. **16**, 1349 (1979).
[32] F. Bechstedt and R. Enderlein, *Semiconductor Surfaces and Interfaces* (Akademie-Verlag, Berlin, 1988).
[33] J. H. Russell and S. C. Wallwork, Acta Crystallogr., Sect. B: Struct. Crystallogr. Cryst. Chem. **28**, 1527 (1971).
[34] M. H. Whangbo *et al.*, Extended Hückel Molecular, Crystal, and Properties Package, QCPE Program No. 571.
[35] The van der waals radii used in this study are taken from D. Freifelder, *Physical Chemistry for Students of Biology and Chemistry* (Science Books International, Boston, 1982), p. 60: H (1.2 Å), O (1.4 Å), and C (1.5 Å). The SiH (1.55 Å) and PO (1.84 Å) bond lengths are taken from D. F. Shriver, P. W. Atkins, and C. H. Langford, *Inorganic Chemistry* (Freeman and Company, New York, 1990), p. 68.
[36] D. J. Chadi, Phys. Rev. B **19**, 2074 (1979).
[37] D. J. Chadi and M. L. Cohen, Phys. Status Solidi B **68**, 405 (1975).
[38] J. D. Dunitz, L. E. Orgel, and A. Rich, Acta Crystallogr. **9**, 373 (1955).
[39] J. M. Moison, M. Van Rompay, and M. Bensoussan, Appl. Phys. Lett. **48**, 1362 (1986); J. M. Moison and M. Bensoussan, Surf. Sci. **168**, 68 (1986); S. S. Hullavarad, S. V. Bhoraskar, and D. N. Bose, J. Appl. Phys. **82**, 5597 (1997).
[40] B. C. Chan and C. K. Ong, J. Phys. Chem. Solids **52**, 699 (1991); W. G. Schmidt, Appl. Phys. A: Mater. Sci. Process. **65**, 581 (1997).
[41] Occupied surface states were also found at energy about 0.2 eV above the valence band maximum at 4×2 and 2×2 reconstructed *n*-InP (100) surfaces.[39,40] These surface states are energetically unfavorable in the electron transfer reactions considered in this study and are neglected in the calculations.
[42] H. J. Lewerenz, J. Electroanal. Chem. **356**, 121 (1993).
[43] When the Fermi energy is far below the energy of the surface states, the occupation of the surface states can be written as $f(\epsilon)=e^{-(\epsilon-\epsilon_f)/k_BT}$, where ϵ_f is given by Eq. (49). Since the $e^{-(\lambda+\Delta G)^2/4\lambda k_BT}$ term can be taken as a constant, Eq. (50) becomes $J_f^{ss}=e[A](2\pi/\hbar)(1/\sqrt{4\pi\lambda k_BT})(1/\beta_\epsilon)\ (N_{ss}|V_{ss}|^2/\Delta E)\exp\{-[(\lambda+\Delta G_0+\Delta E)^2/4\lambda k_BT]\}\exp(-e(V_{bi}^0+\epsilon_f^b)/k_BT)\exp(-eE_{app}/k_BT)$. If J_f^{ss} is much lager than J_b^{ss}, ln J is linearly dependent on the applied potential E_{app} with a unit diode factor A, in Eq. (54).
[44] Lewis group (private communication),
[45] T. Iwasita, W. Schmickler, and J. W. Schultze, B. Bunsenges, Ber. Bunsenges. Phys. Chem. **89**, 138 (1985).
[46] Karl W. Böer, *Survey of Semiconductor Physics* (VNR, New York, 1990).
[47] The self-exchange electron transfer rate constant for the viologen system (S. Dai, thesis, University of Tennessee, 1990) is about one order higher than that of the Fc system [R. M. Neilson, G. E. MacManis, L. K. Safford, and M. J. Weaver, J. Chem. Phys. **93**, 2152(1989)]. Since no temperature-dependence measurement was done for the viologen system, the reorganization energy is unknown and thus no conclusion can be drawn by comparing the self-exchange reactions.
[48] G. L. Miessler and D. A. Tarr, *Inorganic Chemistry* (Prentice–Hall, New Jersey, 1999); A. Haaland, Acc. Chem. Res. **12**, 415 (1979); J. Giordan, J. H. Moore, and J. A. Tossel, *ibid.* **19**, 281 (1979); E. Rühl and A. P. Hitchcock, J. Am. Chem. Soc. **111**, 5069 (1989).
[49] W. Monch, *Semiconductor Surfaces and Interfaces* (Springer-Verlag, Berlin, 1993).
[50] S. J. Anz and N. S. Lewis, J. Phys. Chem. B **103**, 3908 (1999).
[51] S. J. Fonash, *Solar Cell Device Physics* (Academic, New York, 1981).
[52] I. Alstrup, Surf. Sci. **42**, 335 (1969).
[53] There is some arbitrariness of this definition of the surface density of electrons and the averaged coupling matrix element because the applied potential on different atom layers of the semiconductor are different. But because the coupling between the semiconductor atoms and the redox species decays fast with their distance (with a decay length in the order of 1 Å), and the applied potential varies slowly (with the band bending in the order of 100 nm), it is a good approximation to assume that the density of electrons is the same in the semiconductor surface region of present interest.

Chapter 5

On the theory of electron transfer reaction at semiconductor/ liquid interfaces II: a free electron model

(Appeared in J. Chem. Phys. **113**, 6351 (2000))

JOURNAL OF CHEMICAL PHYSICS VOLUME 113, NUMBER 15 15 OCTOBER 2000

On the theory of electron transfer reactions at semiconductor/liquid interfaces. II. A free electron model

Yi Qin Gao and R. A. Marcus
Noyes Laboratory of Chemical Physics, Mail Code 127-72, California Institute of Technology, Pasadena, California 91125

(Received 10 March 2000; accepted 24 July 2000)

Electron transfer reactions at semiconductor/liquid interfaces are studied using the Fermi Golden rule and a free electron model for the semiconductor and the redox molecule. Bardeen's method is adapted to calculate the coupling matrix element between the molecular and semiconductor electronic states where the effective electron mass in the semiconductor need not equal the actual electron mass. The calculated maximum electron transfer rate constants are compared with the experimental results as well as with the theoretical results obtained in Part I using tight-binding calculations. The results, which are analytic for an s-electron in the redox agent and reduced to a quadrature for p_z- and d_{z^2}-electrons, add to the insight of the earlier calculations. © *2000 American Institute of Physics.* [S0021-9606(00)70739-2]

I. INTRODUCTION

The electron transfer reactions at the Si/viologen$^{2+/+}$ and InP/$Me_2Fc^{+/0}$ interfaces were studied recently by Lewis and co-workers.[1–3] The experiments yielded a maximum electron transfer rate constant in the range of 10^{-17}–10^{-16} cm^4 s^{-1}. To compare with the experimental results, the maximum rate of interfacial electron transfer reactions between a redox agent in solution and InP and Si semiconductors was calculated in Part I, the InP surface, as is believed, being terminated with O's and the Si surface with H's.[4] A tight-binding model was used for the semiconductor and extended Hückel calculations were performed for the molecule and for the electronic coupling, in conjunction with z-transform[5] and slab methods.[6] Since a free electron model for the problem provides a simple description which can add to the physical insight, the present treatment was undertaken, by adapting Bardeen's method to this study. It is known that with an effective mass the free electron model describes many properties of bulk semiconductors[7–12] and that the free electron model with the actual electron mass describes various properties associated with the LCAO molecular wave functions of aromatics and polyenes, such as electron densities and bond orders[13] (and so even the coefficients).

The paper is organized as follows: The theoretical model is given in Sec. II. The expression for the electron transfer rate constant and its application is given in Sec. III, and the results are compared with those in Part I and are discussed in Sec. IV.

II. THEORY

A. Preliminary remarks

The electrons in the semiconductor are treated here as free electrons in a semi-infinite potential well with a constant potential inside the well and a known effective mass. The potential well has a surface normal to the z direction and is infinite in extent in the x and y directions. The electronic wave function of the molecule is obtained by solving a Schrödinger equation whose potential is constant inside a spherical potential well and is zero outside. Analogous models for molecules were applied in earlier studies of the orientation effect on the electron transfer reactions by Siders *et al.*[14,15]

The wave functions for the semiconductor electrode and the molecule obtained using the free electron model are then used to calculate the electronic coupling matrix element, and from it the maximum electron transfer rate constant. The electron transfer between a semiconductor electronic state and the molecular state is treated as nonadiabatic and Fermi Golden Rule is applied, and the electronic coupling matrix element is calculated by adapting the method introduced by Bardeen.[16] The application of Bardeen's method, with an adaptation to the present case where the effective electron mass in a semiconductor differs from the actual electron mass, provides an analytical or quadrature expression for the coupling matrix element between the semiconductor and the molecular state.

The total electron transfer current between the semiconductor and the molecule is obtained as the sum of the currents between each semiconductor electronic state and the molecular state. This procedure was discussed and applied earlier in Part I to the study of electron transfer reactions at semiconductor/liquid interfaces using a tight-binding model.[4] It has also been used by various groups in the study of electron transfer reactions at metal[17–20] and semiconductor surfaces.[18,21]

The formula for the maximum rate constant is then applied to two semiconductor/liquid interfaces (Si/viologen$^{2+/+}$ and InP/$Me_2Fc^{+/0}$). These two interfaces were studied experimentally by Lewis and co-workers,[1–3] and conditions were obtained for the former and partly for the latter which satisfied ideal current vs applied potential behavior. In these studies, the current density J_f due to electron transfer from the semiconductor to the molecule is proportional to both the

 © 2000 American Institute of Physics

concentration $[A]$ of the molecules in the liquid and the density of electrons n_s at the semiconductor surface,[2]

$$J_f = e k_{et} n_s [A], \tag{1}$$

where e is the elementary charge and k_{et} is the electron transfer rate constant. These studies also provided experimental values for the maximum rate constant, which were around $10^{-16}\,\mathrm{cm}^4\,\mathrm{s}^{-1}$, for the electron transfer reaction at the two interfaces. The free electron model used in the present study provides rate constants for the two systems in reasonable agreement with the results of tight-binding calculations and with the experimental maximum rate constants.

B. Kinetics at semiconductor/liquid interfaces

The net current density J due to the electron transfer reaction at a semiconductor (S)/liquid interface,

$$A + e(S) \rightleftharpoons A^- + S, \tag{2}$$

can be written as

$$J = J_f - J_r, \tag{3}$$

where J_f is the current density due to the electron transfer from the semiconductor to the molecule and J_r is the current density corresponding to the reverse process. J_f and J_r depend on the concentration of A and A^-, respectively, at the interface,

$$J_f = e k_f [A], \tag{4}$$

$$J_r = e k_r [A^-], \tag{5}$$

where k_f and k_r are pseudo-first-order rate constants, and, from Eq. (1),

$$k_f = n_s k_{et}. \tag{6}$$

In the following, we obtain an expression for k_f using a standard result[22] on electron transfer reactions: Under the weak coupling assumption, the rate constant k_f^s for the electron transfer from a single electronic state of the semiconductor described by a superscript s, which includes both the effect of electron tunneling or hole and "nuclear reorganization," can be expressed using the Fermi Golden Rule,[22] for an electronic state to electronic state transition,

$$k_f^s = \frac{2\pi}{\hbar} |V|^2 \mathrm{FC}, \tag{7}$$

where FC is the Franck–Condon factor, V is the electronic coupling matrix element, and $\hbar$ is Planck's constant. A common classical expression for the Franck–Condon factor is[22]

$$\mathrm{FC} = \frac{1}{\sqrt{4\pi\lambda k_B T}} \exp\left(\frac{-(\lambda + \Delta G)^2}{4\lambda k_B T}\right), \tag{8}$$

where λ is the reorganization energy, and ΔG is the free energy change of the reaction under the prevailing conditions of temperature, electrode-solution potential difference and environment.

Electron transfer at the semiconductor/liquid interface involves a continuum of electronic states in the semiconductor, whose solution, strictly speaking, requires solving a many-electronic state problem. A quantum mechanical study of the many-state crossing problem shows that when the splitting of the states caused by crossing is small the Landau–Zener formula is applicable to a large variety of such problems.[23]

The major charge carriers in these semiconductors have very low concentration and can be treated individually in interfacial reactions.[24] As in the tight-binding calculations[4] for the semiconductor/liquid interfacial electron transfer rate constant, it is assumed in the present study that only transitions between each pair of semiconductor/molecule states are important, and we restrict ourselves to this two-level approximation. Under this approximation the electron transfer current between the electrode and an acceptor state is the sum of the current from each electronic state of the semiconductor electrode to the molecular state, and a total rate constant (total denoted by t) $k_f^t(\mathbf{r})$ can be written as $k_f^t(\mathbf{r}) = \sum_{\mathbf{k}} k_f^s(\mathbf{k},\mathbf{r})$. Here, $\mathbf{k}$ denotes a semiconductor electronic state whose wave vector is $\mathbf{k}$. The $k_f^t(\mathbf{r})$ varies with the position $\mathbf{r}$ of the acceptor molecule relative to the electrode, and can be further written as[18]

$$k_f^t(\mathbf{r}) = \frac{2\pi}{\hbar} \sum_{\mathbf{k}} \mathrm{FC}(\epsilon_{\mathbf{k}}) f(\epsilon_{\mathbf{k}}) |V_{\mathbf{k}}(\mathbf{r})|^2, \tag{9}$$

where $\epsilon_{\mathbf{k}}$ is the energy of the state $\mathbf{k}$, $f(\epsilon_{\mathbf{k}})$ is the probability that the state $\mathbf{k}$ is occupied and $V_{\mathbf{k}}(\mathbf{r})$ is the coupling matrix element between the electronic state $\mathbf{k}$ of the semiconductor and the molecule. The FC and $|V_{\mathbf{k}}(\mathbf{r})|^2$ have units of energy^{-1} and energy^2, and $k_f^t(\mathbf{r})$ has units of s^{-1}. When $\epsilon_{\mathbf{k}}$ denotes the energy of state $\mathbf{k}$ relative to the edge of the conduction band, the ΔG in Eq. (8) is related to $\epsilon_{\mathbf{k}}$ by

$$\Delta G = \Delta G^0 - \epsilon_{\mathbf{k}}, \tag{10}$$

where ΔG^0 is defined as the standard free energy of the reaction when the donor state in the semiconductor electrode is at the conduction band edge at the interface ($\epsilon_{\mathbf{k}} = 0$). ΔG^0 can be obtained from electrochemical measurements.

An expression for the current density is given next in the terms of $k_f^t(\mathbf{r})$. The forward current density through the electrode is obtained by first summing over currents from the electrode to all the acceptors in the solution and then dividing the sum by the area of the electrode surface σ,

$$J_f = \frac{e}{\sigma} \int_{\mathbf{r}} [A(\mathbf{r})] k_f^t(\mathbf{r}) d^3\mathbf{r}. \tag{11}$$

When the reaction is not diffusion-controlled, and when the change of electrical potential inside the liquid can be neglected, as apparently it is under the condition in Lewis' experiments,[1–3] $[A(\mathbf{r})]$ can be taken as constant. The electron transfer rate constant in Eq. (4), which is independent of the concentration of acceptors in the solution but is implicitly dependent on the concentration of electrons in the semiconductor is then

$$k_f = \frac{1}{\sigma} \int_{\mathbf{r}} k_f^t(\mathbf{r}) d^3\mathbf{r}. \tag{12}$$

It has units of $\mathrm{cm\,s}^{-1}$.

In particular, when $k_f(\mathbf{r})$ is only a function of R, the distance between the redox species and the electrode surface, Eq. (12) becomes

$$k_f = \int_{R_0}^{\infty} k_f^t(R)\,dR. \tag{13}$$

This equation, together with Eq. (9), will be used later in deriving an expression for the maximum electron transfer rate constant at a semiconductor/liquid interface.

C. Electronic coupling matrix element

In this section, the electronic coupling matrix element is obtained using the semiconductor and molecular electronic wave functions given in Appendices A and B as the zeroth-order orbitals for the interacting system.

For an electron donor (D) and acceptor (A) system, if treated as a two-state problem, the coupling matrix element can be obtained by solving a secular equation $\det(\mathbf{H}-E\mathbf{S})=0$, where $\mathbf{H}$ and $\mathbf{S}$ are the Hamiltonian and overlap matrices for the two-level system. When the two zeroth-order states have the same energy, or in the context of Eq. (14) below, $\langle D|H|D\rangle = \langle A|H|A\rangle$, the matrix element T_{DA} is then half of the value of the difference between the two eigenvalues of the above secular problem, and can be expressed as[25,26]

$$T_{DA} = \frac{\langle D|H|A\rangle - \langle D|H|D\rangle\langle D|A\rangle}{1-|\langle D|A\rangle|^2}, \tag{14}$$

where $\langle D|A\rangle$ is the electronic overlap integral of the donor and the acceptor state. The electron transfer between each semiconductor state and the molecular state will be treated as a two-state problem with the coupling matrix element obtained using Eq. (14). For a free electron model the Hamiltonian of such an interacting system is $H=-\hbar^2/2m\nabla^2+V$, where $V=V_1$ within the semiconductor, $V=V_2$ within the molecule, and $V=0$ everywhere else. In this case, the coupling matrix element denoted by $V_{\mathbf{k}}$ between the semiconductor state with wave vector $\mathbf{k}$ and the molecule, can be written as[14,15,27,28]

$$V_{\mathbf{k}} = \frac{V_1\langle\psi|\Psi_{\mathbf{k}}\rangle_1 - V_1\langle\psi|\psi\rangle_1\langle\psi|\Psi_{\mathbf{k}}\rangle}{1-|\langle\psi|\Psi_{\mathbf{k}}\rangle|^2}$$

$$\cong V_1\langle\psi|\Psi_{\mathbf{k}}\rangle_1 - V_1\langle\psi|\psi\rangle_1\langle\psi|\Psi_{\mathbf{k}}\rangle, \tag{15}$$

where $\langle\cdots\rangle_1$ means the integration over the space occupied by the semiconductor. The term $|\langle\psi|\Psi_{\mathbf{k}}\rangle|^2$ in the denominator of the first equality can be neglected relative to unity as the volume of the semiconductor region becomes large.

To apply Bardeen's method to calculate $V_{\mathbf{k}}$, it is necessary to extend it to the present system where the electron mass m_2 in the molecule differs from the effective mass m of the electron in the semiconductor. Further, the effective mass for an electron of the semiconductor has been defined only for the bulk properties, and yet an electron mass in the wave function just outside the semiconductor is needed also. With these observations in mind, we introduce the following procedure.

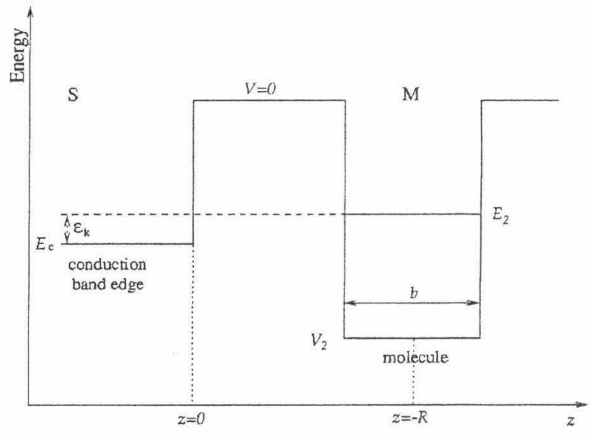

FIG. 1. Profile of potential wells of the semiconductor and of the spherical molecule. There is an electron tunneling through the intervening environment.

A typical fall-off factor of an electron transfer coupling matrix element with distance is $\exp(-\beta R/2)$, where R is distance from the relevant edge of one reactant to the relevant edge of the second reactant and $\beta \cong 1$ Å^{-1}.[22] We can achieve this distance dependence in the free electron model as follows: we write $R=R_1+R_2$, where R_1 is the distance from a field point along $\mathbf{R}$ to the edge of one reactant and R_2 is the distance from that point to the edge of the other reactant. In a free electron description each wave function then decreases as $\exp(-\beta R_i/2)$, $i=1,2$. For the semiconductor, denoting β by β_1, we have $\beta_1/2=\sqrt{-2m(E_c+\epsilon_{\mathbf{k}})}/\hbar$, where E_c is the conduction band edge relative to the energy in the solvent, taken as zero. [The $E_{\mathbf{k}}$ given later in Eq. (16) is this $E_c+\epsilon_{\mathbf{k}}$.] Since E_c is about 1–2 eV and $\epsilon_{\mathbf{k}}$ is about k_BT, we have $\epsilon_{\mathbf{k}} \ll |E_c|$ and so $\beta_1/2 \cong \sqrt{-2mE_c}/\hbar$. For any choice for m, e.g., choosing it to equal to the effective mass in the bulk semiconductor, we can choose E_c to yield the chosen $\beta_1(\sim 1$ Å$^{-1})$.

For the molecule the wave function and energy of the electron depends on the relevant molecular radius b, on the electron mass m_2, and on the position of the molecular energy level E_2 relative to the solvent, again taken as zero. Inasmuch as the relevant β, written as β_2, equals $2\sqrt{-2m_2E_2}/\hbar$, and we wish to have $\beta_2 \cong \beta_1 = \beta$. In the interests of simplicity, we can choose the pair (m_2, E_2) so as to produce the desired β_2. If we take, for example, $m_2 = m$, the effective mass in the bulk semiconductor, we can adjust E_2 to achieve this β_2. The adjusted E_2 equals $E_c + \epsilon_{\mathbf{k}}$ (and hence $\cong E_c$). Indeed, for electron transfer we have $E_c+\epsilon_{\mathbf{k}}=E_2$ in the transition state and so this selection of m for the electron mass outside the molecule is consistent with this energy requirement (see Fig. 1).

It remains to consider the behavior of the molecular wave function inside the molecule. We have already fixed the energy E_2, a mass m, and a radius b. To achieve this E_2 for the given b and m we merely choose the appropriate depth of the potential energy well V_2. Accordingly, we now have a system which has the same electron mass m through-

out and yields the desired decrease of the wave function with distance.

The method due to Bardeen,[16] used here for the evaluation of the value of $V_{\mathbf{k}}$, is only applicable when the donor and acceptor states have the same energy, which is the case for the electron transfer reaction obeying the Franck–Condon principle and considered in this study. Since $\langle\psi|\psi\rangle_1\langle\psi|\Psi_{\mathbf{k}}\rangle$ is typically small as compared to $\langle\psi|\Psi_{\mathbf{k}}\rangle_1$,[29] the $V_{\mathbf{k}}$ in Eq. (15) can be approximated by $V_1\langle\psi|\Psi_{\mathbf{k}}\rangle_1$. Following Bardeen,[16] this quantity can be written as an integral over the space occupied by one of the reactants, here the semiconductor S, we note that

$$\langle\psi|T+V_1|\Psi_{\mathbf{k}}\rangle_1=E_{\mathbf{k}}\langle\psi|\Psi_{\mathbf{k}}\rangle_1, \tag{16}$$

where $E_{\mathbf{k}}$ is the eigenvalue corresponding to $|\Psi_{\mathbf{k}}\rangle$ and T denotes the kinetic energy operator, $-(\hbar^2/2m)\nabla^2$, in coordinate space. But we also have $T|\psi\rangle=E_2|\psi\rangle$ in the region outside the molecule, where E_2 is the eigenvalue for the molecule. Thereby,

$$\langle\Psi_{\mathbf{k}}^*|T|\psi^*\rangle_1=E_2\langle\Psi_{\mathbf{k}}^*|\psi^*\rangle_1=E_2\langle\psi|\Psi_{\mathbf{k}}\rangle_1. \tag{17}$$

We have from Eqs. (16) and (17),

$$-\frac{\hbar^2}{2m}\int_1(\psi^*\nabla^2\Psi_{\mathbf{k}}-\Psi_{\mathbf{k}}\nabla^2\psi^*)d^3\mathbf{r}=(E_{\mathbf{k}}-E_2-V_1)\times\langle\psi|\Psi_{\mathbf{k}}\rangle_1. \tag{18}$$

When $\langle D|H|D\rangle$ and $\langle A|H|A\rangle$ are set equal in the transition state, $E_{\mathbf{k}}$ and E_2 are not quite equal, but the difference between them[30] is neglected.[27,28] We thus obtain, on neglecting the terms mentioned earlier,

$$V_{\mathbf{k}}=-\frac{\hbar^2}{2m}\int\mathbf{n}\cdot(\psi^*\nabla\Psi_{\mathbf{k}}-\Psi_{\mathbf{k}}\nabla\psi^*)ds, \tag{19}$$

where $\mathbf{n}$ is a unit vector normal to the surface of well S and pointing outward from S, i.e., in the direction of negative z, and ds is the area element of the surface of well S. Setting $z=0$ at the semiconductor surface, Eq. (19) then becomes,

$$V_{\mathbf{k}}=-\frac{\hbar^2}{2m}\int_{z=0}\{\psi(\partial\Psi_{\mathbf{k}}^*/\partial z)-\Psi_{\mathbf{k}}^*(\partial\psi/\partial z)\}ds. \tag{20}$$

In the following the implementation of Bardeen's method is illustrated by an evaluation of the electronic coupling matrix element between a semiconductor state and an s-type state of the molecular acceptor. The expressions used for p_z-like and d_{z^2}-like molecular wave functions are given in Appendix B. The integrand in Eq. (20) is evaluated at the semiconductor surface. We have

$$\Psi_{\mathbf{k}}(x,y,z=0)=a_1e^{i(k_xx+k_yy)}, \tag{21}$$

$$\partial\Psi_{\mathbf{k}}/\partial z(x,y,z=0)=\beta_1a_1e^{i(k_xx+k_yy)}, \tag{22}$$

and when an s-type orbital is used for the molecular acceptor, we have

$$\psi(x,y,z=0)=\frac{2A_0}{\sqrt{4\pi}}\frac{e^{-\beta_2(\sqrt{\rho^2+R^2}-b)/2}}{\beta_2\sqrt{\rho^2+R^2}}, \tag{23}$$

$$\partial\psi/\partial z(x,y,z=0)=-\frac{2A_0R}{\sqrt{4\pi}}\frac{1+(\beta_2/2)\sqrt{\rho^2+R^2}}{\beta_2(\rho^2+R^2)^{3/2}}e^{-\beta_2(\sqrt{\rho^2+R^2}-b)/2}. \tag{24}$$

The normalization of $\Psi_{\mathbf{k}}$ will be made with respect to a large volume v, most of which encompasses the semiconductor surface. The a_1 in Eqs. (21) and (22) has units of $1/\sqrt{v}$, and is given by Eq. (27) below, and the A_0 in Eqs. (23) and (24) has units of $\mathrm{cm}^{-1/2}$. A normalization to a delta function could have been introduced instead if we had introduced a z-dependent electric field inside the semiconductor similar to the actual field. However, the present procedure is simpler and should suffice for our purpose.

Equations (23) and (24) are obtained using Eq. (B7) and setting the coordinate of the center of the spherical potential well as $(0, 0, -R)$, R being the distance between the center of the molecule and the semiconductor surface, ρ being $\sqrt{x^2+y^2}$, and ds being $2\pi\rho d\rho$.

Equations (21)–(24) are next used for the evaluation of the coupling matrix element. For a semiconductor conduction band, the occupation of the electronic states is low enough to be considered as obeying Boltzmann statistics. Thus, only states within an energy range of k_BT above the conduction band edge are important in the electron transfer reaction. Since $k=|\mathbf{k}|$ is only about $0.1\ \text{Å}^{-1}$ at room temperature, it is a good approximation to replace the term $e^{i(k_xx+k_yy)}$ by unity in Eqs. (21) and (22). A final expression for the coupling matrix element is then obtained by performing the integral in Eq. (20), yielding

$$V_{\mathbf{k}}(R)=-A_0\frac{2\sqrt{\pi}\hbar^2}{\beta_2m}a_1\left(1+\frac{1}{\beta_2R}\right)e^{-\beta_2(R-b)/2}. \tag{25}$$

In obtaining the above expression, the approximation that $\int_{u_0}^{\infty}(e^{-u}/u^2)du\approx e^{-u_0}/u_0^2$, and $\int_{u_0}^{\infty}(e^{-u}/u)du\approx e^{-u_0}/u_0$, when $u_0\gg1$, are used. Here, $u=(\beta_2/2)\sqrt{\rho^2+R^2}$, and $u_0=\beta_2R/2$, the value of u at $\rho=0$. Because of a_1, $V_{\mathbf{k}}(R)$ is seen to be proportional to $1/\sqrt{v}$.

The term $1/\beta_2R$ is small compared to the other term in the parenthesis in Eq. (25) when R is large. In the problems treated in this paper, R is always greater than 4 Å, and the term $1/\beta_2R$ can then be neglected. In this case, Eq. (25) becomes,

$$V_{\mathbf{k}}(R)=-\sqrt{\pi}A_0a_1\frac{2\hbar^2}{\beta_2m}e^{-(\beta_2/2)(R-b)},\quad(\psi=s), \tag{26}$$

and so $V_{\mathbf{k}}(R)$ depends exponentially on the edge to edge distance $R-b$ between the semiconductor and the molecule. A_0 is given by Eq. (B8) or approximately by Eq. (B11).

The quantity a_1 in Eq. (26) is estimated as in Appendix A to be

$$a_1=\sqrt{\frac{2}{v}}\frac{k_z}{\sqrt{k_z^2+(\beta_1/2)^2}}\approx\sqrt{\frac{2}{v}}\frac{2k_z}{\beta_1}, \tag{27}$$

the second equality arising because $k_z\ll\beta_1$.

Using the relation that $\beta_1=\beta_2$, and the above expression for a_1, the expression for $V_{\mathbf{k}}(R)$ then becomes

$$V_{\mathbf{k}}(R) = -\sqrt{\frac{2\pi}{v}} A_0 \frac{4k_z\hbar^2}{\beta_2^2 m} e^{-\beta_2(R-b)/2}, \quad (\psi = s). \quad (28)$$

The procedure discussed above for the s-type orbital can also be applied to a system with other types of molecular orbitals. In the present study, when a p_z-like or d_{z^2}-like orbital is used for the molecular orbital, as it should be for the molecules considered here, the approximation that $1/\beta_2 = 1/\beta_1 \approx 1$ Å is also used. The wave function ψ is given by Eqs. (B1) and (B2), with $l=1$, $m=0$ for a p_z-like orbital, and $l=2$, $m=0$ for a d_{z^2}-like orbital, and their normalization constants are given by Eqs. (B3)–(B5). The electronic coupling matrix elements for these orbitals are then calculated using Eq. (20).

III. ESTIMATE OF THE MAXIMUM ELECTRON TRANSFER RATE CONSTANT

We next obtain the expression for the maximum rate constant k_{et}^{max} of the electron transfer reaction at a semiconductor/liquid interface, based on the free electron model given in the preceding section. We first discuss the $f(\epsilon_{\mathbf{k}})$ term in Eq. (9) and then derive an expression for k_f^t using Eqs. (9) and (28).

For a low-doped semiconductor of the zincblende type, the occupation of its conduction band at the surface is low enough that the occupancy probability, $f(\epsilon_{\mathbf{k}})$, of the state $\mathbf{k}$, the kinetic energy of which is $\hbar^2k^2/2m$,[11] can be treated as obeying Boltzmann statistics. The sum $\Sigma_{\mathbf{k}} \cdots f(\epsilon_{\mathbf{k}})$ in Eq. (9) can be written as an integral over $\mathbf{k}$-states, when properly normalized. The number of electrons in the semiconductor conduction band in the volume v is $n_s v$, and the probability of finding one of these electrons in $dk_x dk_y dk_z$ is the Boltzmann factor $\exp(-\epsilon_{\mathbf{k}}/k_BT)dk_x dk_y dk_z / \int_{-\infty}^{\infty}\int_{-\infty}^{\infty}\int_{-\infty}^{\infty} \exp(-\epsilon_{\mathbf{k}}/k_BT)dk_x dk_y dk_z$. When multiplied by $n_s v$ it becomes the probability that a state is occupied. The sum in Eq. (9) thus becomes

$$\sum_{\mathbf{k}} \mathrm{FC}(\epsilon_{\mathbf{k}})|V_{\mathbf{k}}(\mathbf{r})|^2 f(\epsilon_{\mathbf{k}}) = \frac{n_s v \iiint \mathrm{FC}(\epsilon_{\mathbf{k}})|V_{\mathbf{k}}(\mathbf{r})|^2 e^{-\epsilon_{\mathbf{k}}/k_BT} dk_x dk_y dk_z}{\iiint e^{-\epsilon_{\mathbf{k}}/k_BT} dk_x dk_y dk_z}. \quad (29)$$

Since $|V_{\mathbf{k}}|^2$ is inversely proportional to v, the v cancels. Equation (9) yields

$$k_f^t(\mathbf{r}) = n_s v \frac{2\pi}{\hbar} \frac{\iiint \mathrm{FC}(\epsilon_{\mathbf{k}})|V_{\mathbf{k}}(\mathbf{r})|^2 e^{-\epsilon_{\mathbf{k}}/k_BT} dk_x dk_y dk_z}{(2\pi m k_B T)^{3/2}/\hbar^3}, \quad (30)$$

where $V_{\mathbf{k}}$ for an s-like electron is given by Eq. (28), and for p_z-like and d_{z^2}-like electrons in the molecule is given by Eq. (B12) in Appendix B.

Integration over k_x, k_y, and k_z is intermediately performed, and one obtains

$$k_f^t(R) = n_s \frac{2\pi\hbar}{m(\beta_2/2)^4} A_0^2 \left(\frac{2\lambda}{\lambda - \Delta G^0}\right)^{5/2} \sqrt{\frac{\pi k_B T}{\lambda}} \times e^{-[(\lambda+\Delta G^0)^2/4\lambda k_B T]} e^{-\beta_2(R-b)}, \quad \lambda - \Delta G^0 \gg 0, \quad (31)$$

where ΔG^0 is the same as defined earlier and $\beta_1 \approx \beta_2$ has been used. Equation (31) was obtained under the condition that $\lambda - \Delta G^0 \gg 0$.

The k_f^t given by Eq. (31) is then introduced into Eq. (13) to yield an expression for k_f. The maximum electron transfer rate constant k_f^{max} is obtained by setting $\lambda + \Delta G^0 = 0$ in Eq. (31) to obtain

$$k_f^{max} = n_s \frac{\pi\hbar}{m(\beta_2/2)^5} A_0^2 \sqrt{\frac{\pi k_B T}{\lambda}} e^{-\beta_2(R_0-b)}, \quad (s \text{ electron}). \quad (32)$$

It is seen to be linearly dependent on n_s, the electron density near the surface of the semiconductor electrons. Here, R_0 is the smallest distance between the center of the molecule and the semiconductor surface. We then have an expression for the maximum second-order electron transfer rate constant written as

$$k_{et}^{max} = \frac{32\pi\hbar}{m\beta_2^5} A_0^2 \sqrt{\frac{\pi k_B T}{\lambda}} e^{-\beta_2(R_0-b)}, \quad (s \text{ electron}), \quad (33)$$

where A_0 is given by Eqs. (B8) and (B9).

The above equation is then applied in the following to the two systems studied by Lewis and co-workers for a comparison with the experimental results. Following the discussion in the earlier section, β_2 is taken as 1 Å^{-1}.

The rate constant of the electron transfer reaction at the silicon/viologen$^{2+/+}$ interface is estimated using Eq. (33) for a (hypothetical) s-like electron. At the Si/N,N'-dimethyl-4,4′-bipyridylium^{2+} interface, one of the Si/viologen systems studied by Fajardo and Lewis,[1,3] the radius of the spherical potential b is estimated as 3 Å,[31] which gives approximately the size of the LUMO of the molecular acceptor. The m was obtained from self-consistent band structure calculations to be 0.191 m_e,[32] where m_e is the mass of a free electron. Since the surface of the silicon semiconductor in the experiments is terminated by a single layer of hydrogen atoms to remove the dangling Si bonds, the value of R_0 is chosen as the value corresponding to the direct contact of the adsorbed hydrogen atoms and the acceptors and is about 5 Å.[33] The value of λ obtained from a fit in Ref. 12 to the experimental data,[1] is about 0.7 eV and the calculated maximum rate constant is relatively insensitive to λ. When the maximum rate constant for this s-electron model is calculated using Eq. (33), the result in Table I is obtained, and compared there with the experimental results as well as the theoretical results obtained in Part I by the tight-binding method.

We turn next to the estimate of the electron transfer reaction rate constant at the InP/$Me_2Fc^{+/0}$ interface. For this system, b is taken as 0.6 Å,[34] the radius of a Fe^{2+}, because of the localization of the LUMO at Fe atom.[35] The (100) surface InP semiconductor used in the experiments is believed[36] to be terminated by a layer of oxygen atoms which saturate the dangling P bonds. The smallest distance R_0 between the center of the acceptor and the electrode is chosen to be 5 Å which corresponds to the direct contact of the molecular acceptor (the whole ferrocene molecule) and the oxygen atom.[33] The experimental effective mass m of an

TABLE I. Experimental and calculated maximum electron transfer rate constant.[a]

System	k_{et}^{max} (expt.)	k_{et}^{max} (z-trans.)[d]	k_{et}^{max} (slab)[d]	k_{et}^{max} (free e)[e]	k_{et}^{max} (free e)
Si/viologen$^{2+/+}$	0.6[b]	1.3	1.6	1.2(p_z)	1.9(''s'')
Si/$Me_2Fc^{+/0}$	...	...	0.17	0.024(d_{z^2})	1.2(''s'')
InP/$Me_2Fc^{+/0}$	1–2[c]	0.084	0.086	0.017(d_{z^2})	1.1(''s'')

[a]Units are 10^{-16} cm^4 s^{-1}.
[b]From Ref. 12.
[c]From Ref. 10.
[d]From Ref. 4.
[e]The result for viologen$^{2+/+}$ was obtained using a p_z-like orbital and the result for $Me_2Fc^{+/0}$ was obtained using a d_{z^2}-like orbital. The results in the last column were obtained using a hypothetical s-like orbital and Eq. (33).

electron in the InP conduction band is 0.077 m_e.[11,37] The reorganization energy λ of the system is about 0.8 eV,[2] but k_{et}^{max} is again relatively insensitive to λ. The estimated rate constant for the s-electron model is then given in Table I.

However, to compare with the real systems studied by Lewis and co-workers,[1,2] a p_z-like orbital should be used for the viologen to be more consistent with the symmetry of the LUMO of the viologen ions. For the InP/$Me_2Fc^{+/0}$ system, since the LUMO of Me_2Fc^+ has primarily d_{z^2} character,[35] the d_{z^2}-like orbital is used for the acceptor state of Me_2Fc^+. When a p_z- or d_{z^2}-like orbital is used, we average the rate constant[38] over the orientation of the orbital respect to the semiconductor surface, yielding the results in Table I.

For comparison, the maximum electron transfer rate constant at the Si/$Me_2Fc^{+/0}$ interface is also calculated, although the data on the maximum rate constant for this system are absent. The effective electron mass for the Si conduction band is again taken as 0.191 m_e, the reorganization energy is 0.8 eV, the radius of $Me_2Fc^{+/0}$ LUMO is 0.6 Å, and R_0 is taken as 4 Å. The results obtained using an s-type orbital and a d_{z^2}-like orbital are both given in Table I.

IV. DISCUSSION AND CONCLUSION

A. Discussion

In the present paper, the free electron model is applied to the study of electron transfer reactions at semiconductor electrode/liquid interfaces. The electronic wave functions of the semiconductor are obtained in terms of plane waves in a semi-infinite potential well and the wave function of the acceptor is approximated to be a p_z-like or d_{z^2}-like orbital and for comparison results for an s-like orbital are also given, all for a spherical potential well. An analytic formula for the coupling matrix element is obtained for an s-like orbital using Bardeen's method, and then an expression for the electron transfer rate constant is obtained using this formula of the coupling matrix element.

The maximum electron transfer rate constants for Si/viologen$^{2+/+}$ and InP/$Me_2Fc^{+/0}$, the two systems studied experimentally by Lewis *et al.*, are then estimated using Eq. (33). The maximum rate constants of both systems are compared with the experimental result, which is of order of 10^{-17} to 10^{-16} cm^{-4} s^{-1}. The agreement is reasonable, considering the approximations involved, and the result is also in reasonable agreement with the theoretical results obtained in Part I using tight-binding calculations. As mentioned earlier, to mimic the experiments and the tight-binding calculations, a p_z-like orbital and a d_{z^2}-like orbital were used for the viologen$^{2+/+}$ and $Me_2Fc^{+/0}$ ions, respectively, in the calculations of the coupling matrix elements for these two systems. The error is greater for $Me_2Fc^{+/0}$ ions, where the LUMO is assumed to be localized on the Fe atom. For comparison, an s-like orbital was also used for the calculation of the maximum rate constant. However, this s-like orbital is hypothetical, since the LUMO of these systems is not an s-orbital.

The difference between the theoretical maximum rate constants at Si/viologen$^{2+/+}$ and InP/$Me_2Fc^{+/0}$ interfaces in these calculations is partly due to the different size of the molecular orbitals. The LUMO, the electron acceptor state, of a viologen molecule is more delocalized than that of the Me_2Fc molecule, which is essentially localized on the Fe atom.[35] Although the centers of the two spherical potential wells representing the two molecules are at approximately the same distance from the semiconductor surface, the calculated electron transfer rate constant for the Si/viologen$^{2+/+}$ interface is larger than that for the InP/$Me_2Fc^{+/0}$. The coupling matrix element as a function of the size of the acceptor orbital is shown in Fig. 2. The distance between the center of the spherical orbital and the semiconductor surface is kept constant in obtaining this figure. Another factor responsible for the larger calculated maximum rate constant at the Si/viologen$^{2+/+}$ interface is the character of the acceptor orbital. The use of a p_z-like orbital yields more efficient coupling between the semiconductor and the acceptor for the Si/viologen$^{2+/+}$ interface than does the d_{z^2}-like orbital that used for the InP/$Me_2Fc^{+/0}$ interface, both for the tight-binding and for the free electron calculations. The relative inefficiency of d-electron in electron transfer was described in an earlier paper.[40]

It is interesting that a model as simple as the free electron model yields a result for the electron transfer matrix element in reasonable agreement with the tight-binding calculation and with experiments. In these applications, the wave functions of the semiconductor or a reactant are needed outside the molecular potential well and on the surface of the semiconductor. For both wave functions boundary conditions are imposed (continuity of the respective wave function and of their derivatives at the relevant boundary). For the region outside the semiconductor and outside the molecule we introduce a distance dependence of the wave function which yielded the expected distance dependence of the electronic matrix element. Since the expected distance dependence is also reproduced quite well by extended-Hückel calculations,[39] with no adjustable parameters, perhaps the agreement of the matrix element calculated using the free electron model with the obtained tight-binding/extended-Hückel calculations or from experiments is also consistent with this earlier work. The analytical expression Eq. (28) serves to bring out some of the sources of error: when the molecule and the semiconductor are more or less in edge-to-edge contact, as in the methyl viologen case, the exponential factor in Eq. (28) is of the order of unity, and so is not a major source of error. However, when the orbital in the mol-

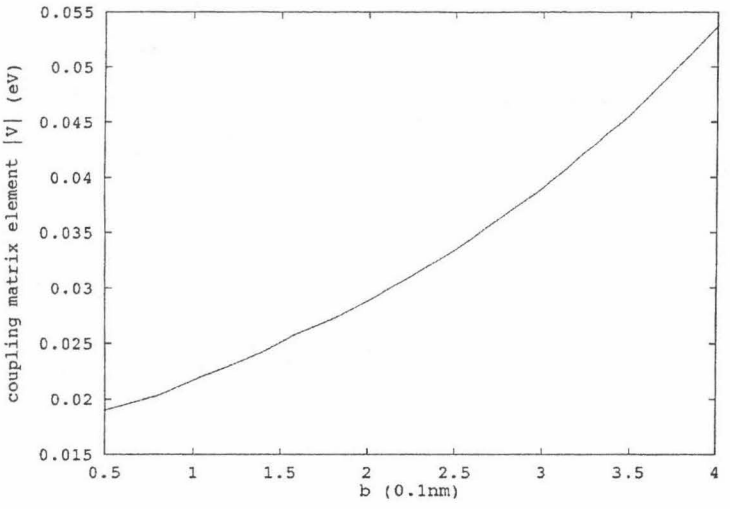

FIG. 2. The coupling matrix element between the semiconductor state $\mathbf{k}=(0, 0, 0.02)$ and an s-like molecular orbital as a function of the size of the acceptor state. The distance between the center of the molecule and the semiconductor surface is kept as a constant 5 Å.

ecule is localized, as in the ferrocene and so is buried, the orbital distance $R-b$, is large. Because of the exponential, the corresponding free electron model matrix element is subject to a substantially large error, as seen in Table I, using orbitals of the appropriate symmetry. Errors in the other quantities, e.g., for A_0 in Eq. (B11), appear to be more minor.

We explore further in the next section the relation between the free electron and the tight-binding models.

B. Relation of free electron and tight-binding models

We make this comparison initially for a one-dimensional chain of length l. For this chain the free electron value of a_1 is still given by Eq. (27), but with $\sqrt{v}$ replaced by $\sqrt{l}$. The tight-binding coefficients C_M^K for a chain of N atoms can be written as[41]

$$C_M^K=\sqrt{2/(N+1)}\,\sin\pi MK/(N+1), \tag{34}$$

where M is a lattice atom index ($M=1,\ldots,n$), K is an electronic state index ($K=1,\ldots,N$), and $M=1$ is a surface atom. Since the wave number $k_z=2\pi/\lambda\cong\pi K/(N+1)a$, where a is the lattice distance parameter, we can write

$$C_M^K=\sqrt{2a/l}\,\sin Mk_za. \tag{35}$$

Inasmuch as the C_M^K's are normalized to unity ($\Sigma_M|C_M^K|^2=1$) and the individual atomic wave functions are normalized over a length a, the $C_M^K/\sqrt{a}$ for $M=1$ is the quantity to compare with the one-dimensional analog of a_1 in Eq. (27), $\sqrt{2/l}2k_z/\beta_1$. Since k_z is small, Eq. (35) yields $C_1^K/\sqrt{a}\cong\sqrt{2/l}k_za$. When the tight-binding model is extended to the x and y directions, infinite in both directions, normalized to periodic boundary conditions (area l^2) using complex exponential wave functions, which are the discrete analogs of the $\exp ik_xx+ik_yy$ in Eq. (A2), Eq. (35) again applies but with $\sqrt{2a/l}$ replaced by $\sqrt{2a^3/v}$,

$$C_M^K=\sqrt{2a^3/v}\,\sin Mk_za. \tag{36}$$

Omitted for brevity in the right-hand side of Eq. (36) are the discrete analogs of $\exp ik_xx+ik_yy$. For $M=1$ and with k_za being small, we can write

$$a_1\cong 2C_1^K/\beta_1a\sqrt{a^3}, \tag{37}$$

where C_1^K is the same for each surface atom (for small k_xx and k_yy). Thereby, $2/\beta_1a\sqrt{a^3}$ can be regarded as the factor in a_1 contributing to the atom/atom exchange integral between the semiconductor and the adjacent solvent.

The contribution C^2 to $\int|\psi|^2 4\pi r^2dr$ outside $r=b$ is, from Eq. (B7), $4A_0^2/\beta_2^3$. Taking the coefficient C of the molecule as unity, we can now rewrite $V_{\mathbf{k}}$ in Eq. (25) as

$$V_{\mathbf{k}}\cong-\sqrt{\pi}\frac{4A_0\hbar^2}{m\beta_2a^{5/2}}CC_1^K, \tag{38}$$

where $C\cong 1$. Now the lowest energy of an electron in a cubic box of edge length a is $\epsilon=3\hbar^2/8a^2m$. In terms of ϵ, Eq. (38) becomes

$$V_{\mathbf{k}}=-\sqrt{\frac{\pi}{\beta a}}\frac{4}{3\pi^2}\epsilon CC_1^K. \tag{39}$$

For a value of $\beta=1$ Å^{-1}, $m=0.1\ m_e$, and the lattice constant $a=3$ Å, the factor multiplying CC_1^K is about 2.5 eV. Not all of C can contribute to $V_{\mathbf{k}}$, but more than one semiconductor atom, and its C_1^K, can contribute. To some extent these neglected aspects approximately cancel. The coefficient of CC_1^K is seen to have (approximately) the value expected for an atom/atom exchange integral.

C. Conclusion

Although the free electron model is highly approximate, it does provide a reasonable description for the semiconductor electronic structure at the conduction band edge.[11,32,42,43] The present model also incorporates the actual molecular orbital size and symmetry and the experimental coupling decay length, and perhaps for these reasons gives a reasonable zeroth-order approximation for treating the electron transfer

at semiconductor/liquid interfaces. Although one cannot generalize from only two cases, we suspect on comparing the tight-binding and free electron results in Table I that the free electron model is better for a delocalized orbital like that of viologen than for a highly localized one like that of ferrocene. In this paper, for simplicity, the molecular orbital was first taken as an s-like orbital with a certain size, leading to an analytic result. However, the symmetry of the molecular orbital was taken into account instead by choosing orbitals with appropriate quantum numbers l and m in Eqs. (B6) and (B7).

In summary, it appears that the free electron model provides a reasonable and simple though crude description of the electron transfer reaction at semiconductor/liquid interfaces. Since this method uses Bardeen's method of estimating the coupling matrix element, it is not applicable to two overlapping potential wells[16] and thus it is only applicable to relatively weak couplings. Also it is only applicable to the electron transfer reaction near the semiconductor conduction/valence band edge, because of the use of the free electron model. This method of estimating the electron transfer rate constant can be readily applied to other semiconductor/liquid interfaces.

ACKNOWLEDGMENTS

It is a pleasure to acknowledge the support of the National Science Foundation and the Office of Naval Research. We thank Professor Nathan S. Lewis, William J. Royea, and Dr. Yuri Geogievskii for valuable discussions. We would like to dedicate this article to our esteemed colleague, Royce Murray, on the occasion of his forthcoming 65th birthday.

APPENDIX A: FREE-ELECTRON MODEL FOR THE SEMICONDUCTOR ELECTRODE

We treat the semiconductor electrode first and then the molecular electron acceptor in the solution using the potential wells. The electrons in the semiconductor are treated as free electrons in a potential well in the three-dimensional space, with a constant potential V_1 inside the well ($V_1<0$). The potential well is infinite in the x and y directions and has a surface at $z=0$, and the potential is taken as zero outside the potential well. The wave functions are then obtained using the one-electron Schrödinger equation,

$$-\frac{\hbar^2}{2m}\nabla^2+V(\mathbf{r})|\Psi_{\mathbf{k}}\rangle=E_{\mathbf{k}}|\Psi_{\mathbf{k}}\rangle, \tag{A1}$$

where $V(\mathbf{r})=V_1$ when $z\geqslant 0$ and $V(\mathbf{r})=0$ when $z<0$. The $\mathbf{k}$ again denotes the wave vector of the electronic state $\Psi_{\mathbf{k}}$ and m is the effective mass of the electron.

The relevant solution of Eq. (A1) is

$$\Psi_{\mathbf{k}}(\mathbf{r})=e^{i(k_x x+k_y y)}(a_2 e^{ik_z z}+a_3 e^{-ik_z z}), \quad \text{(inside well)}, \tag{A2}$$

for $z\geqslant 0$, and

$$\Psi_{\mathbf{k}}(\mathbf{r})=a_1 e^{i(k_x x+k_y y)}e^{\beta_1 z/2}, \quad \text{(outside well)}, \tag{A3}$$

where β_1 is a positive number, for $z\leqslant 0$. Here, k_x, k_y, and $k_z(\beta)$ are the components of the wave vector $\mathbf{k}$ in x, y, and z directions, respectively, with

$$\frac{\hbar^2}{2m}(k_x^2+k_y^2+k_z^2)=E-V_1, \quad \frac{\hbar^2}{2m}(k_x^2+k_y^2-\beta_1^2/4)=E, \tag{A4}$$

where E is the energy of the electron.

In Eqs. (A2) and (A3), a_2, a_3, and a_1 are constants which can be obtained by satisfying the boundary condition at the surface of the semiconductor and by the normalization of the wave function. The boundary condition at $z\to\infty$ requires that $\beta_1>0$. The amplitude of $\Psi_{\mathbf{k}}^*(\mathbf{r})$ outside the potential well is considerably smaller than inside, a normalization of the wave function, $\langle\Psi_{\mathbf{k}}|\Psi_{\mathbf{k}}\rangle=1$, yields $|a_2|^2+|a_3|^2=1/v$ to a good approximation, where v is the volume of the semiconductor as discussed in the text.

As usual, the relations between a_2 and a_3, and between a_2 and a_1 are obtained using the continuity of the wave function and its first derivative with respect to z at $z=0$, and can be written as

$$a_3=\frac{k_z-i\beta_1/2}{k_z+i\beta_1/2}a_2, \quad a_1=\frac{2k_z}{k_z+i\beta_1/2}a_2. \tag{A5}$$

These two equalities combined with the normalization equation, $|a_2|^2+|a_3|^2=1/v$, determine the three constants a_2, a_3, and a_1 up to an arbitrary phase factor. These quantities will be used later in calculate the coupling matrix element between the $\Psi_{\mathbf{k}}$ and the wave function of the molecule. From Eq. (A5) one can verify that $|a_3|^2=|a_2|^2$, and if, without loss of equality we choose a_1 to be real, then $a_2^*=a_3$ and Eq. (27) is obtained.

APPENDIX B: THE ELECTRONIC WAVE FUNCTION OF THE ACCEPTOR MOLECULE

For simplicity, we treat the electronic wave function of the molecule in liquid as an electron moving in a finite spherical potential well with a radius b. The potential $V_2(\mathbf{r})$ within the potential well is a constant V_2 and is zero outside. The problem is well known[44] and the results will be used as follows.

The solution of the Schrödinger equation in the spherical polar coordinate (r,θ,ϕ) gives the normalized wave functions which are continuous at $r=b$,[14]

$$\psi_{ml}(r,\theta,\phi;E)=A_l N_{ml}\Phi_m(\phi)P_l^m(\cos\theta)j_l(\alpha r)k_l(\beta_2 b/2)/j_l(\alpha b)e^{\beta_2 b/2} \quad \text{(inside well)}, \tag{B1}$$

when $r\leqslant b$, and

$$\psi_{ml}(r,\theta,\phi;E)=A_l N_{ml}\Phi_m(\phi)P_l^m(\cos\theta)k_l(\beta_2 r/2)e^{\beta_2 b/2}, \quad \text{(outside well)}, \tag{B2}$$

when $r\geqslant b$. For use in Eqs. (B1) and (B2) we have defined the A_l's In Eqs. (B3) and (B5) below by introducing there a factor $e^{-\beta_2 b/2}$, so as to make the A_l's less sensitive to β_2. Here, m and l are the usual quantum numbers, $\alpha=\sqrt{2m(E-V_2)}/\hbar$, $\beta_2/2=\sqrt{-2mE}/\hbar$, $\Phi_m(\phi)$ is $e^{im\phi}/\sqrt{2\pi}$, P_l^m is an associated Legendre polynomial, and j_l

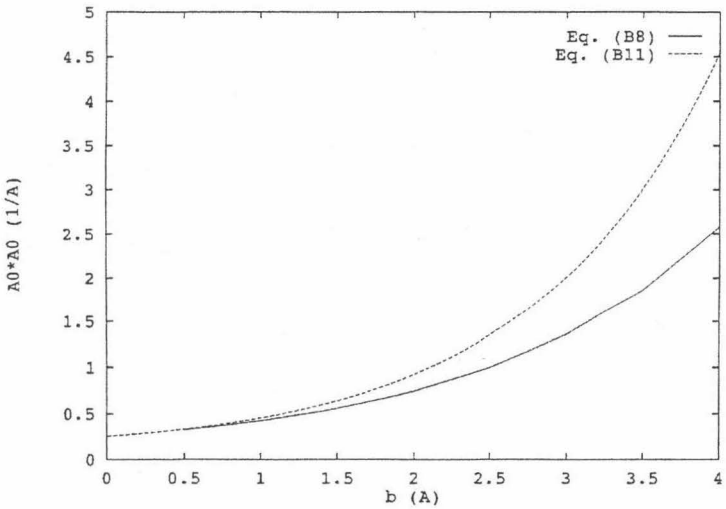

FIG. 3. The comparison for A_0^2 being calculated using Eq. (B8) (exact) and using Eq. (B11) (approximate).

and k_l are spherical Bessel and Hankel functions. The normalization constants A_l and N_{ml} are given by

$$A_l=\left\{\frac{k_l^2(\beta_2 b/2)}{j_l^2(\alpha b)}\int_0^b j_l^2(\alpha r)r^2dr + \int_b^\infty k_l^2(\beta_2 r/2)r^2dr\right\}^{-1/2} e^{-\beta_2 b/2}, \tag{B3}$$

and

$$N_{ml}=\left\{\frac{2\pi}{2l+1}\frac{(l+m)!}{(l-m)!}\nu\right\}^{-1/2}. \tag{B4}$$

A_l can be further evaluated to be

$$A_l=(2/b^3)^{1/2}\left\{k_{l-1}(\beta_2 b/2)k_{l+1}(\beta_2 b/2) - \frac{k_l^2(\beta_2 b/2)}{j_l^2(\alpha b)}j_{l-1}(\alpha b)j_{l+1}(\alpha b)\right\}^{-1/2} e^{-\beta_2 b/2}. \tag{B5}$$

The ν in Eq. (B4) is 2 for $m=0$, and 1 for $m\neq 0$. In particular, $m=l=0$ corresponds to an s state with a wave function denoted by ψ,

$$\psi=\frac{2A_0}{\sqrt{4\pi}}\frac{\sin(\alpha r)}{\beta_2 r\sin(\alpha b)}, \quad r\leqslant b \tag{B6}$$

and

$$\psi=\frac{2A_0}{\sqrt{4\pi}}\frac{e^{-\beta_2(r-b)/2}}{\beta_2 r}, \quad r\geqslant b. \tag{B7}$$

The constant A_0 obtained by setting $l=0$ in Eq. (B3) is given by

$$A_0=\frac{\beta_2}{2}\left\{\frac{2\alpha b-\sin(2\alpha b)}{4\alpha\sin^2(\alpha b)}+\frac{1}{\beta_2}\right\}^{-1/2}. \tag{B8}$$

Clearly A_0 varies with the radius b of the spherical potential well. The relation between α and β_2 in the last three equations, obtained by making $\partial\psi/\partial r$ continuous at $r=b$, gives

$$\tan(\alpha b)=-2\alpha/\beta_2. \tag{B9}$$

For a given β_2 and b, the eigenvalue of the energy E of the systems are then determined by the above equation and the relation between β_2 and E.

Using Eq. (B9), Eq. (B8) can be expressed as

$$A_0=\frac{\beta_2}{2}\left\{\frac{\alpha^2+(\beta_2/2)^2}{\alpha^2}\frac{2\alpha b-\sin(2\alpha b)}{4\alpha}+\frac{1}{\beta_2}\right\}^{-1/2}. \tag{B10}$$

One notes from Eq. (B9) that $\tan(\alpha b)<0$, thus $2\alpha b>\pi>\sin(2\alpha b)$. When α^2 is sufficiently large, Eq. (B8) can be approximated by

$$A_0=\frac{(\beta_2)^{3/2}}{2}[1/(1+b\beta_2/2)]^{1/2}. \tag{B11}$$

The α decreases monotonically when b increases and is $0.73\,\text{Å}^{-1}$ when $b=3$ Å. The A_0^2 calculated using Eqs. (B8) and (B11) are compared in Fig. 3. In the text and in Table I only Eq. (B8) is used. We note that $\int|\psi|^2 4\pi r^2 dr$ outside of the well of radius b equals $4A_0^2/\beta_2^3$, and we wish $4A_0^2/\beta_2^3$ to be small. The value from Eq. (B11) is $[2/(2+b\beta_2)]^{1/2}$.

As discussed in the text, the coupling matrix element between a molecular and a semiconductor state can be evaluated using

$$V_{\mathbf{k}}=-\frac{\hbar^2 a_1}{2m}\int_{\rho=0}^\infty e^{i(k_x x+k_y y)}(\beta_1\psi_{ml}-\partial\psi_{ml}/\partial z)2\pi\rho d\rho, \tag{B12}$$

where the wave function ψ_{ml} given by Eq. (B2) is a p_z-like orbital when $l=1$, $m=0$ and is a d_{z^2}-like orbital when $l=2$, $m=0$, and where we have written the area element as $\rho d\rho d\phi$ and integrated the ϕ from 0 to 2π, noting that the integrand is independent of ϕ.

[1] A. M. Fajardo and N. S. Lewis, J. Phys. Chem. B **101**, 11136 (1997).
[2] K. E. Pomykal and N. S. Lewis, J. Phys. Chem. B **101**, 2476 (1997).
[3] A. M. Fajardo and N. S. Lewis, Science **274**, 969 (1996).
[4] Y. Q. Gao, Y. Georgievskii, and R. A. Marcus, J. Chem. Phys. **112**, 3358 (2000).
[5] R. A. Marcus, J. Chem. Phys. **98**, 5604 (1993).
[6] For example, S. G. Davison and J. D. Levine, Solid State Phys. **25**, 1 (1970); D. J. Chadi and M. L. Cohen, Phys. Status Solidi B **68**, 405 (1975); Y. R. Yang and C. B. Duke, Phys. Rev. B **36**, 2763 (1987).
[7] B. Sapoval and C. Hermann, *Physics of Semiconductors* (Springer-Verlag, New York, 1993).
[8] S. M. Sze, *Physics of Semiconductor Devices*, 2nd ed. (Wiley, New York, 1981).
[9] B. K. Ridley, *Quantum Processes in Semiconductors* (Clarendon, Oxford, 1988).
[10] K. W. Böer, *Survey of Semiconductor Physics* (Van Nostrand Reinhold, New York, 1990).
[11] W. A. Harrison, *Electronic Structure and the Properties of Solids* (Dover, New York, 1989).
[12] C. Kittel, *Introduction to Solid State Physics*, 6th ed. (Wiley, New York, 1981), p. 193 or Fig. 9, p. 176. There it is seen that the curvature d^2E/dk^2, which is inversely proportional to the effective mass, is much larger at a band gap edge than is the curvature for a free electron. A $\mathbf{k}\cdot\mathbf{p}$-based formula for the effective mass m is derived in Ref. 11 and illustrates the factors influencing m.
[13] For example, J. R. Platt, K. Ruedenberg, C. W. Scherr, N. S. Ham, H. Labhart, and W. Lichten, *Free-Electron Theory of Conjugated Molecules: A Source Book* (Wiley, New York, 1964) (papers of the Chicago group 1949–1961), and references cited therein.
[14] P. Siders, R. J. Cave, and R. A. Marcus, J. Chem. Phys. **81**, 5613 (1984).
[15] R. J. Cave, P. Siders, and R. A. Marcus, J. Phys. Chem. **90**, 1436 (1986).
[16] J. Bardeen, Phys. Rev. Lett. **6**, 57 (1961).
[17] W. Schmickler, J. Electroanal. Chem. **204**, 31 (1986).
[18] R. R. Dogonadze and A. M. Kuznetsov, Prog. Surf. Sci. **6**, 42 (1975).
[19] H. Ou-Yang, B. Källebring, and R. A. Marcus, J. Chem. Phys. **98**, 7565 (1993).
[20] H. Ou-Yang, R. A. Marcus, and B. Källebring, J. Chem. Phys. **100**, 7814 (1994).
[21] W. J. Royea, A. M. Fajardo, and N. S. Lewis, J. Phys. Chem. B **101**, 11152 (1997).
[22] R. A. Marcus and N. Sutin, Biochim. Biophys. Acta **811**, 265 (1985).
[23] Y. D. Demkov and V. I. Osherov, Sov. Phys. JETP **26**, 916 (1968).
[24] H. Gerischer, J. Phys. Chem. **95**, 1356 (1991).
[25] N. R. Kestner, J. Logan, and J. Jortner, J. Phys. Chem. **78**, 2148 (1974).
[26] A. A. Stuchebrukhov, Chem. Phys. Lett. **265**, 643 (1997).
[27] To obtain Eq. (15) from Eq. (14), we write the acceptor wave function as Ψ_k, and the donor wave function as ψ. Using the Hamiltonian described in the text, we write it as $H=-\hbar/2m\nabla^2+V_2h_2+V_1h_1$, where h_1 is unity inside the semiconductor and zero everywhere else, while h_2 is unity inside the molecule and zero everywhere else. We can thus write H as $H_2+V_1h_1$, where H_2 is the Hamiltonian for the molecule, $-\hbar^2/2m\nabla^2+V_2h_2$. We then have $\langle\psi|H|\Psi_k\rangle=\langle\psi|H_2|\Psi_k\rangle+V_1\langle\psi|h_1|\Psi_k\rangle=E_2\langle\psi|\Psi_k\rangle+V_1\langle\psi|\Psi_k\rangle_1$, the 1 subscript indicating that the integration is over the volume of the semiconductor, and E_2 denoting the eigenvalue for the molecule, $\langle\psi|H_2|\Psi_k\rangle=E_2\langle\psi|\Psi_k\rangle$. Further, $\langle\psi|H|\psi\rangle=\langle\psi|H_2+h_1V_1|\psi\rangle=E_2+V_1\langle\psi|\psi\rangle_1$, since $\langle\psi|\psi\rangle=1$. Thus the numerator in the right-hand side of Eq. (14) becomes that of Eq. (15).
[28] A. A. Stuchebrukhov, J. Chem. Phys. **105**, 10819 (1996), which also, in effect, extends Bardeen's method.
[29] The calculated $\langle\psi|\psi\rangle_1\langle\psi|\Psi_k\rangle/\langle\psi|\Psi_k\rangle_1$ for s, p, and d orbitals are less than 0.007 for the cases considered in this paper.
[30] We note that E_k and E_2 are related as follows $E_2=\langle\psi|T+h_2V_2|\psi\rangle=\langle\psi|H|\psi\rangle-\langle\psi|h_1V_1|\psi\rangle$ and the last term equals $-V_1\langle\psi|\psi\rangle_1$. Further, $E_k=\langle\Psi_k|T+h_1V_1|\Psi_k\rangle=\langle\Psi_k|H|\Psi_k\rangle-\langle\Psi_k|h_2V_2|\Psi_k\rangle$ and the last term equals $-V_2\langle\Psi_k|\Psi_k\rangle_2$, the 2 indicating that it is integrated over the volume of the molecule. Since $\langle\psi|H|\psi\rangle=\langle\Psi_k|H|\Psi_k\rangle$, it then follows that $E_k-E_2=-V_2\langle\Psi_k|\Psi_k\rangle_2+V_1\langle\psi|\psi\rangle_1$. However, terms such as $\langle\psi|\psi\rangle_1$ and $\langle\Psi_k|\Psi_k\rangle_2$ are neglected, tacitly or explicitly (Refs. 27,28).
[31] The LUMO of the viologen^{2+} ion is obtained by an extended Hückel calculation using M. H. Whangbo *et al.*, Extended Hückel Molecular, Crystal and Properties Package, QCPE Program No. 571.
[32] The minima of $E(\mathbf{k})$ for Si shows ellipticity and two different effective masses can be distinguished, parallel and orthogonal to the axis (100). Since we are interested in the electron transfer across the (100) surface, the mass parallel to the (100) axis is used.
[33] Because of the asymmetry of the molecules studied in the experiments, there is some arbitrariness in estimating their radii and their closest distance to the semiconductor surface. This could bring in some error in estimating the electron transfer rate constant. The van der Waals' radii used in this study are taken from D. Freifelder, *Physical Chemistry for Students of Biology and Chemistry* (Science Books International, Boston, 1982), p. 60: H (1.2 Å), O (1.4 Å), and C (1.5 Å). The SiH (1.55 Å) and PO (1.84 Å) bond lengths are taken from D. F. Shriver, P. W. Atkins, and C. H. Langford, *Inorganic Chemistry* (Freeman, New York, 1990), p. 68.
[34] R. D. Shannon and C. T. Prewitt, Acta Crystallogr., Sect. B: Struct. Crystallogr. Cryst. Chem. **25**, 925 (1969).
[35] G. L. Miessler and D. A. Tarr, *Inorganic Chemistry* (Prentice–Hall, New Jersey, 1999); A. Haaland, Acc. Chem. Res. **12**, 415 (1979); J. Giordan, J. H. Moore, and J. A. Tossel, *ibid.* **19**, 281 (1979); E. Rühl and A. P. Hitchcock, J. Am. Chem. Soc. **111**, 5069 (1989).
[36] N. Lewis group (private communication).
[37] W. J. Turner, W. E. Reese, and G. D. Pettit, Phys. Rev. **136**, 157 (1964).
[38] When a p_z-like orbital ($l=1, m=0$) or a d_{z^2}-like orbital ($l=2, m=0$) is used, the coupling matrix element between the molecule and the semiconductor depends on the orientation of the orbital with respect to the semiconductor surface. Denoting the angle between the z axis, which is normal to the semiconductor surface, and the body fixed z axis of the molecule, which is along a maximum of the orbital, α, the angular function of the oriented orbital can be written as $P_l^0[\cos\theta\cos\alpha+\sin\theta\sin\alpha]=P_l^0(\cos\theta)P_l^0(\cos\alpha)+2\Sigma_{m=1}^{l}[(l-m)!/(l+m)!]\,P_l^m(\cos\theta)P_l^m(\cos\alpha)$; [H. Hochstadt, *Special Functions of Mathematical Physics* (Holt, Rinehart, and Wintson, New York, 1961), p. 35.] Here, P_l^m again denotes the Legendre polynomial. Because of symmetry, the contribution of the terms P_l^m with $l=1$, $m=1$ or $l=2$, $m=1,2$ to the coupling between the oriented orbital and the semiconductor vanishes. The coupling between an oriented orbital and the semiconductor can be expressed as $P_l^0(\cos\alpha)\langle\psi_{0l}|H|\Psi_k\rangle$. The $\langle\psi_{0l}|H|\Psi_k\rangle$ denotes the coupling matrix element between the wave function ψ_{0l}, defined by Eq. (B1), and the semiconductor wave function Ψ_k and can be evaluated using Bardeen's method described in Sec. II C. The average for the rate constant over the angle α then yields a factor $\int_0^\pi(P_1^0(\cos\theta))^2d\alpha/\pi=\int_0^\pi\cos^2\alpha d\alpha/\pi=0.5$ for a p_z-like orbital, and a factor $\int_0^\pi(P_2^0(\cos\alpha))^2d\alpha/\pi=(\int_0^\pi(3\cos^2\alpha-1)^2/4d\alpha)/\pi=0.34$ for a d_{z^2}-like orbital.
[39] P. Siddarth and R. A. Marcus, J. Phys. Chem. **94**, 2985 (1990).
[40] S. Gosavi and R. A. Marcus, J. Phys. Chem. B **104**, 2067 (2000).
[41] For example, T. A. Hoffman and A. Konya, Acta Phys. Acad. Sci. Hung. **1**, 5 (1951), Eq. (5.16).
[42] J. Bardeen, J. Chem. Phys. **6**, 367 (1938).
[43] F. Bechstedt and R. Enderlein, *Semiconductor Surfaces and Interfaces* (Akademie-Verlag, Berlin, 1988).
[44] For example, L. I. Schiff, *Quantum Mechanics*, 3rd ed. (McGraw-Hill, New York, 1968).

Chapter 6

Temperature dependence of the electronic factor
in the nonadiabatic electron transfer at metal
and semiconductor electrodes
(Appeared in J. Electroanal. Chem. **500**, 71 (2001))

ELSEVIER

Journal of Electroanalytical Chemistry 500 (2001) 71–77

Journal of Electroanalytical Chemistry

www.elsevier.nl/locate/jelechem

Temperature dependence of the electronic factor in the nonadiabatic electron transfer at metal and semiconductor electrodes

Shachi Gosavi, Yi Qin Gao, R.A. Marcus *

Arthur Amos Noyes Laboratory of Chemical Physics, Division of Chemistry and Chemical Engineering, California Institute of Technology, Pasadena, CA 91125, USA

Received 14 September 2000; received in revised form 23 October 2000; accepted 24 October 2000

Dedicated to Professor R. Parsons on the occasion of his retirement from the postion of the Editor in Chief of the Journal of Electroanalytical Chemistry and in recognition of many contributions to electrochemistry

Abstract

The temperature dependence of the electronic contribution to the nonadiabatic electron transfer rate constant (k_{ET}) at metal electrodes is discussed. It is found in these calculations that this contribution is proportional to the absolute temperature T. A simple interpretation is given. We also consider the nonadiabatic rate constant for electron transfer at a semiconductor electrode. Under conditions for the maximum rate constant, the electronic contribution is also estimated to be proportional to T, but for different reasons than in the case of metals (Boltzmann statistics and transfer at the conduction band edge for the semiconductor versus Fermi–Dirac statistics and transfer at the Fermi level, which is far from the band edge, of the metal). © 2001 Elsevier Science B.V. All rights reserved.

Keywords: Heterogeneous electron transfer rate constant; Metal electrode; Semiconductor electrode; Temperature dependence of electronic coupling matrix element

1. Introduction

In this article, the temperature dependence of the electronic factor in the expression for the nonadabatic rate constant (k_{ET}) is discussed, both for metals and for semiconductors. In the case of the electrochemical exchange current at metal electrodes the temperature dependence of k_{ET} is due to two parts: one part arises from the well known variation with temperature of the Franck–Condon factor. It has an exponential term and a pre-exponential term which, classically, is proportional to $T^{-1/2}$. The second part of the temperature variation arises from the increasing range of energies of electronic states in the metal near the Fermi level that can contribute significantly to the rate constant with increasing temperature. An experimental system of an alkanethiol monolayer adsorbed on two different metals, Au and Pt, is considered to investigate how this temperature dependence of the Fermi–Dirac distribution affects the rate. The metal electronic state dependence of the metal–reagent electronic coupling matrix element is included in the calculation. To a good approximation, the averaged electronic factor for the exchange current rate constant is calculated below to be proportional to T, the known proportionality when the electronic coupling element is energy-independent.

The temperature dependence of the electronic factor for nonadiabatic electron transfer at semiconductor electrodes is also discussed. For the present purpose, in lieu of detailed calculations, this factor is estimated using the free electron model. It is found to be proportional to the temperature T under conditions for the maximum of the rate constant, but the origin of the proportionality is quite different from that in the case of the electrochemical exchange current at metal electrodes.

* Corresponding author. Tel.: +1-626-3956566; fax: +1-626-7928485.

E-mail address: ram@caltech.edu (R.A. Marcus).

0022-0728/01/$ - see front matter © 2001 Elsevier Science B.V. All rights reserved.
PII: S0022-0728(00)00452-6

In the following sections the theoretical model used and the predictions that can be made from this model are described.

2. Theory

2.1. Metals

The rate constant for nonadiabatic electron transfer from a metal to a reactant at the interface (k_{ET}) is given by [1]

$$k_{ET} = \frac{2\pi}{\hbar}\int d\varepsilon FC|V(\varepsilon)|^2 f(\varepsilon) \quad (1)$$

where $f(\varepsilon)$ is the Fermi–Dirac distribution with ε measured relative to μ, the chemical potential of the electrons in the electrode,

$$f(\varepsilon) = \frac{1}{1+e^{\varepsilon/k_BT}} \quad (2)$$

FC is the Franck–Condon factor, which in its classical form is

$$FC = \frac{e^{-(\lambda - e\eta - \epsilon)^2/4\lambda k_BT}}{(4\pi\lambda k_BT)^{1/2}} \quad (3)$$

Here, λ is the reorganization energy, e the electronic charge, η the overpotential, and $|V(\varepsilon)|^2$ the square of the electronic coupling matrix element, integrated over the distribution of the electronic states at the given ε:

$$|V(\varepsilon)|^2 = \int d^3k |H_{kA}|^2 \delta(\varepsilon(k) - \varepsilon) \quad (4)$$

where $|H_{kA}|$ denotes $\langle \Psi_k|H|\Psi_A\rangle$ and describes the electronic coupling between the redox agent (A) and each electronic state of wave vector k of the electrode.

Eqs. (1)–(4) are given for the reduction rate constant. The rate constant for the reverse reaction, which we will denote by k^r_{ET} is obtained by replacing ε by $-\varepsilon$ and η by $-\eta$. One can verify, for example, that the equilibrium constant k_{ET}/k^r_{ET} is then given by $\exp(e\eta/k_BT)$, as expected.

From Eqs. (1)–(3) we have

$$k_{ET} = \frac{2\pi}{\hbar}\frac{e^{-\lambda/4k_BT}}{(4\pi\lambda k_BT)^{1/2}}\int_{-\infty}^{\infty} e^{\frac{-\varepsilon^2 + h(\varepsilon,\eta)}{4k_BT}} g(\varepsilon)|V(\varepsilon)|^2 d\varepsilon \quad (5)$$

where $g(\varepsilon)$ is given by

$$g(\varepsilon) = \frac{1}{2}\mathrm{sech}\left(\frac{\varepsilon}{2k_BT}\right) \quad (6)$$

and

$$h(\varepsilon,\eta) = 2(\lambda - \varepsilon)e\eta - (e\eta)^2 \quad (7)$$

In applications, the dependence of $|V(\varepsilon)|^2$ is normally neglected. The reorganization energy λ is then obtained in two different ways, one from a plot of $\ln k_{ET}$ versus η [2–13], and the other from a plot (noted below) involving $\ln(k^0/T^{1/2})$ versus $1/T$, or both [14–19]. While the effect of neglecting the dependence of $V(\varepsilon)$ on ε is expected to be small, it is estimated in the present paper. Results for finite η can also be estimated from the calculations, with appropriate additions, as discussed later.

When $\eta = 0$, Eq. (5) becomes k^0, the standard rate constant

$$k^0 = \frac{2\pi}{\hbar}\frac{e^{-\lambda/4k_BT}}{(4\pi\lambda k_BT)^{1/2}}\int_{-\infty}^{\infty} e^{-\varepsilon^2/4\lambda k_BT}(\varepsilon)|V(\varepsilon)|^2 d\varepsilon \quad (8)$$

We first consider, for comparison, the simplest case: both the dependence of $V(\varepsilon)$ on ε and the $\varepsilon^2/4\lambda k_BT$ term Eq. (8) are neglected. In that case the integral in Eq. (8) is a standard integral [20][1] yielding

$$k^0 \cong \frac{2\pi}{\hbar}\frac{e^{-\lambda/4k_BT}}{(4\pi\lambda k_BT)^{1/2}}\pi k_BT|V(0)|^2 \quad (9)$$

When the value of λ is obtained from Eq. (9) and a plot of the experimental rate constant k^0, $\ln(k^0/T^{1/2})$ versus $1/T$, we have

$$\lambda/k_B = -4\partial \ln(k^0 T^{-1/2})/\partial(1/T) \quad (10)$$

We next consider the case where the dependence of $|V(\varepsilon)|^2$ is neglected, as before, but where the $\varepsilon^2/4k_BT$ in Eq. (8) is included. In this case we have

$$k^0 \cong \frac{2\pi}{\hbar}\frac{e^{-\lambda/4k_BT}}{(4\pi\lambda k_BT)^{1/2}}\pi k_BT|V(0)|^2\langle e^{-\varepsilon^2/4\lambda k_BT}\rangle \quad (11)$$

where we have used [20] $\pi k_BT = \int_{-\infty}^{\infty} g(\varepsilon)d\varepsilon$ and where $\langle\rangle$ denotes an average over the distribution function, $g(\varepsilon)d\varepsilon/\int_{-\infty}^{\infty} g(\varepsilon)d\varepsilon$. The exponent is so small that the exponential in $\langle\rangle$ can be expanded, retaining only the first two terms. Use of standard integrals [20][1] then yields

$$k^0 = \frac{2\pi}{\hbar}\frac{e^{-\lambda/4k_BT}}{(4\pi\lambda k_BT)^{1/2}}\pi k_BT|V(0)|^2\left(1 - \frac{\pi^2 k_BT}{4\lambda}\right) \quad (12)$$

For a value [15] of $\lambda \cong 0.8$ eV and $k_BT \cong 0.025$ eV, the last factor in the parentheses, due to $\langle\exp(-\varepsilon^2/4\lambda k_BT)\rangle$ term, is 0.923, and so is close to unity. In the following the $\exp(-\varepsilon^2/4\lambda k_BT)$ in Eq. (8) will be replaced by unity.

In passing, we note that from Eq. (11) that the slope of $\ln(k^0(\lambda/k_BT)^{1/2})$ versus λ/k_BT equals $-(1/4)(1 - \pi^2(k_BT/\lambda)^2)$, because of the smallness of k_BT/λ. The reciprocal of this quantity can, because of the smallness

[1] $\int_{-\infty}^{\infty} g(\varepsilon/2)^2 g(d\varepsilon) = (\pi k_BT)^3/4$, $\int_{-\infty}^{\infty} g(\varepsilon/2)^4 g(d\varepsilon) = (\pi k_BT)^5(5/16)$
$\int_{-\infty}^{\infty} g(\varepsilon/2)^6 g(d\varepsilon) = (\pi k_BT)^6(61/64)$

of the correction, be written, as -4.04. A numerical evaluation of the integral [15] gave -4.03, which is within the round off error. The difference of -4.03 from -4 is 1% and so can be neglected relative to other sources of error in λ.

The integral in Eq. (8) can now be written as

$$I(k_BT) = \int_{-\infty}^{\infty} g(\varepsilon)|V(\varepsilon)|^2 d\varepsilon \tag{13}$$

We have written the limits as $\pm\infty$, but of course the lower limit is finite. It equals the lower limit of the energy of the band, which is very negative. More than adequate for our purpose is changing the limits of integration to ± 1.1 eV.

The temperature dependence of $I(k_BT)$ arises from the weighting function, $g(\varepsilon)$, which becomes broader with increasing temperature. The $|V(\varepsilon)|^2$ depends only on ε and so is independent of temperature. However, because of the broadening of $g(\varepsilon)$ with increasing T, parts of $|V(\varepsilon)|^2$ at larger and smaller ε contribute more in the integral when the temperature is increased. For a $|V(\varepsilon)|^2$ replaced by $|V(0)|^2$, the integral in Eq. (12), is as already noted $|V(0)|^2\pi k_BT$.

For flat and broad bands, such as s and p bands, one expects $|V(\varepsilon)|^2$ to remain constant with ε. In that case, the temperature dependence arises mainly from the width of the weighting function, $g(\varepsilon)$, given in Eq. (6). For narrow bands such as d bands the density of states, ρ, changes fairly rapidly over a short energy range. If this feature leads to a large change in $|V(\varepsilon)|^2$ then widely varying values of $I(k_BT)$ become increasingly included in $I(k_BT)$ when the temperature is increased, and some deviation of the temperature dependence of $I(k_BT)$ from $|V(0)|^2\pi k_BT$ is expected. However, the d states do not couple as well into the donor/acceptor species in solution [21][2]; the large change in the density of d states with ε is diminished by the small coupling of these states, so leading again to an approximately constant $|V(\varepsilon)|^2$. In this case, the temperature dependence would remain about the same as in the case of the s and p bands, i.e., depending only on the width of the weighting function.

The accessible number of participating electronic states near the Fermi level ($\varepsilon = 0$) increases linearly with temperature, a result well known from the proportionality of the electronic specific heat of the metals to the temperature. However, this observation offers no information on the average strength of $|H_{kA}|^2$ as a function of ε. The question of the behavior of the matrix element, suitably averaged, is addressed in calculations in a later section.

Numerical results of the calculations based on Eqs. (4) and (8) (both with and without $\varepsilon^2/4\lambda k_BT$ neglected), are given in Section 3.1.

2.2. Semiconductors

In the case of electron transfer from a semiconductor to a reactant species in solution, the rate is first-order in the concentration of electrons in the semiconductor at the surface and first-order in the reactant. An expression for the second-order nonadiabatic rate constant k_{ET} was given earlier [22][3]

$$k_{ET} = \frac{2\pi}{\hbar}\frac{v}{\sqrt{4\pi k_BT}}\frac{1}{\beta_s} \frac{\int_0^{\infty} e^{-(\lambda+\Delta G^0-\varepsilon)^2/\lambda 4k_BT}\langle|\overline{V}(\varepsilon)|^2\rangle e^{-\varepsilon/k_BT}\rho(\varepsilon)d\varepsilon}{\int_0^{\infty} e^{-\varepsilon/k_BT}\rho(\varepsilon)d\varepsilon} \tag{14}$$

where $\langle|\overline{V}(\varepsilon)|^2\rangle$ is an electronic matrix element [22]

$$|\overline{V}(\varepsilon)|^2 = \frac{|V(\varepsilon)|^2}{\rho(\varepsilon)} \tag{15}$$

and

$$\rho(\varepsilon) = \int d^3\boldsymbol{k}\,\delta(\varepsilon(\boldsymbol{k}) - \varepsilon) \tag{16}$$

The average $\langle\rangle$ was over all orientations of the reactant at the contact distance [2]. In Eq. (14), v is the volume of the unit cell in the semiconductor (the wave functions appearing in $V(\varepsilon)$ are normalized to that volume), and β_s is the exponent for the decay of the square of the matrix element with distance.

We note, in passing, that in the experiments [23] ΔG° is varied by varying the redox reagent in solution. The maximum k_{ET}, k_{ET}^{max} determined in this way, corresponds to $\lambda + \Delta G^\circ = 0$.

The exponent of the first factor in the integral in the numerator of Eq. (14) can be written as

$$\frac{(\lambda+\Delta G^0-\varepsilon)^2}{4\lambda k_BT} = \frac{(\lambda+\Delta G^0)^2}{4\lambda k_BT} - \frac{(\lambda+\Delta G^0)2\varepsilon}{4\lambda k_BT} + \frac{\varepsilon^2}{4\lambda k_BT} \tag{17}$$

The first term in the r.h.s. of the above equation is independent of ε and can be removed from the integral. The second term varies much more slowly with ε than the ε/k_BT in the exponent of the third term in the

[2] In this reference and the present paper the surface of the metal is a (111) face. For some simpler surfaces with more symmetry elements the Z-transform method that we use is not necessary and the wavefunctions can be described in these cases by a simple sine-like function. We use extended Hückel (EH) theory to calculate the bridge coupling matrix elements in both the above article and the present paper. The EH method gives more accurate results for relative matrix elements and rates than it does for absolute values.

[3] The V_k in this article is denoted in the present paper by H_{kA}. Since the form of the electronic matrix element is the same for both semiconductors and metals Eqs. (4), (15) and (16) remain valid for both types of electrodes.

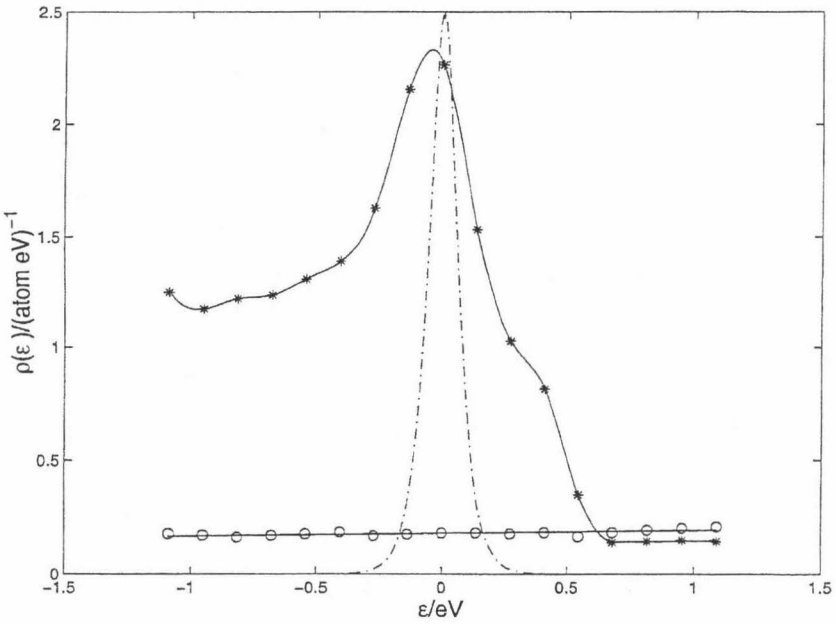

Fig. 1. Band structure of Au and Pt with the Fermi energies of each set to 0. ✱ is for Pt and ○ is for Au. $\rho(\varepsilon)$ is in units of number of states per atom per eV. The weighting function $g(\varepsilon) \times 5$ at $k_B T = 0.025$ eV i.e. $T = 300$ K is also plotted (–·) to show the density of states which contribute to the integral in the rate constant k_{ET}. For simplicity a 'splined' fit is drawn through the points for $\rho(\varepsilon)$ for Pt.

integral in Eq. (14), when $\lambda + \Delta G^\circ \approx 0$ (the important region for k_{ET}^{max}, as noted above). The ratio of the third term in Eq. (17) to $\varepsilon/k_B T$ is $\varepsilon/4\lambda$, which is very small since $\varepsilon \approx k_B T$, i.e., 0.025 eV, and λ is typically 1 eV. The dependence of $(\lambda + \Delta G^\circ - \varepsilon)^2$ on ε in Eq. (17) can then be ignored, yielding

$$k_{ET} = \frac{2\pi}{\hbar} \frac{v}{\sqrt{4\pi\lambda k_B T}} \frac{1}{\beta_s} e^{-(\lambda + \Delta G^0 - \varepsilon)^2/4\lambda k_B T} \frac{\int_0^\infty \langle |\overline{V}(\varepsilon)|^2 \rangle e^{-\varepsilon/k_B T} \rho(\varepsilon) d\varepsilon}{\int_0^\infty e^{-\varepsilon/k_B T} \rho(\varepsilon) d\varepsilon} \quad (18)$$

as in eq. (A5) of Ref. [22]. Of particular interest is k_{ET}^{max}, which, obtained from Eq. (18) is

$$k_{ET}^{max} = \frac{2\pi}{\hbar} \frac{v}{\sqrt{4\pi\lambda k_B T}} \frac{1}{\beta_s} \frac{\int_0^\infty \langle |\overline{V}(\varepsilon)|^2 \rangle e^{-\varepsilon/k_B T} \rho(\varepsilon) d\varepsilon}{\int_0^\infty e^{-\varepsilon/k_B T} \rho(\varepsilon) d\varepsilon} \quad (19)$$

When $|\lambda + \Delta G^\circ|/\lambda$ becomes different from zero, say, $\approx 1/2$, then the ratio of the second term in Eq. (17) to $\varepsilon/k_B T$ becomes 1/4, which on integration, including a slowly varying $\overline{V}(\varepsilon)$ will affect the pre-exponential factor a little. The ratio of the last term in Eq. (17) to $\varepsilon/k_B T$ becomes $\varepsilon/4\lambda$, which for an averaged value of $\varepsilon \approx \lambda/4$ in the sampling of εs for the exothermic direction, is still a relatively small though not negligible quantity. Accordingly, Eq. (18) is expected to suffice for typical conditions. When it does not suffice Eq. (14) could be used instead. However, our main interest here is in k_{ET}^{max} and so in Eq. (19).

3. Applications

3.1. Metals

A particular system, an alkanethiol monolayer with 15 CH_2 units and with the redox agent $Ru(NH_3)_5Py^{2+}$ tethered to it is considered here. Only one alkanethiol molecule adsorbed on a metal electrode is used in our calculation, since it has been found that this approximation is reasonable, and adding more molecules does not have a large effect on the rate [24]. Two metals, gold (Au) and platinum (Pt) are considered, the method of Z-transforms and a tight binding Hamiltonian are used to obtain the wavefunctions of the metal. The details of the calculation are given elsewhere [21]. For the purpose of the calculations we use Eqs. (4), (15) and (16).

The metal Au has no d states near the Fermi level while the d band of Pt lies close to its Fermi level. The $\rho(\varepsilon)$ given by Eq. (16) is plotted in Fig. 1 for both these metals, as well as the $g(\varepsilon)$ at $T = 300$ K. The Fermi levels of both metals are used as the zeros for their respective εs.

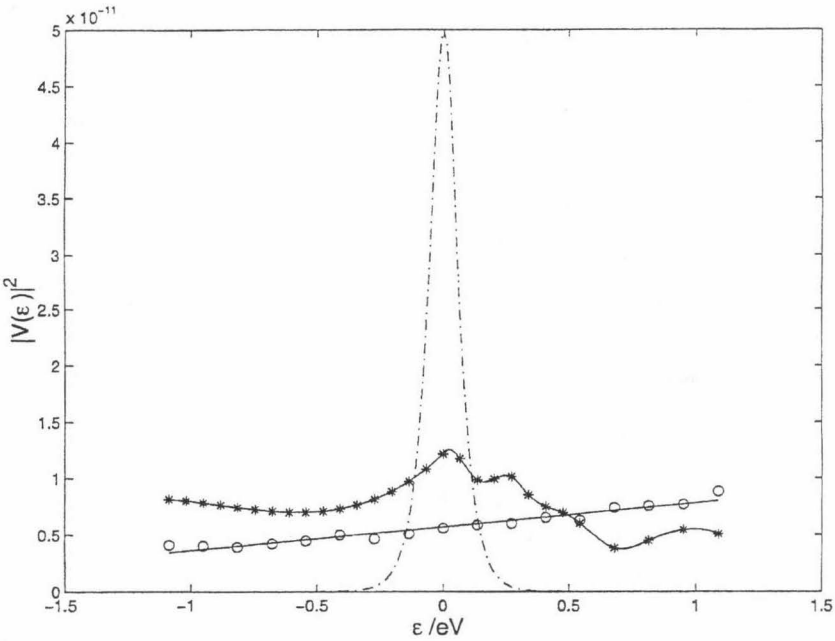

Fig. 2. A plot of $|V(\varepsilon)|^2$ vs. ε. ○ gives the plot for Au and ✱ gives the plot for Pt. A plot of $g(\varepsilon) \times 10^{-10}$ (–·) is also given. The Au curve is a best fit to the points, the Pt curve is a 'splined' fit.

The $|V(\varepsilon)|^2$ is plotted in Fig. 2 for the two metals as a function of ε. It is seen that even though the $|V(\varepsilon)|^2$ for Pt does change somewhat with the energy ε, the effect is considerably less than the change in $\rho(\varepsilon)$. Although the extent of ε is nonzero is $\sim \pm 0.3$ eV (Fig. 2) the validity of the $\lambda \ll \varepsilon$ approximation and the neglect of the ε^2 term should be checked against the full width at half maximum of the $g(\varepsilon)$ curve. The half-width is $\varepsilon \sim 0.066$ eV. Thus, with the usual values of $\lambda = 0.6$ to 1.2 eV the approximation is still valid.

Although only a narrow range of ε is needed for our purpose of calculating the standard reduction rate constant k^0, we have given in Fig. 2 a substantially larger range of ε. When large overpotentials $\pm e\eta$ are considered, electronic energy levels with a correspondingly large range of ε are needed for the evaluation of the integral. Accordingly, this larger range of εs is given in Fig. 2, should k_{ET} (or the reverse rate constant k_{ET}^r at larger $|\eta|$s, rather than just at $\eta = 0$, be needed. However, when large overpotentials are considered, the effect of the energy denominators should be included, e.g., Ref. [25].

The $\ln(I(k_BT))$ is plotted in Fig. 3 versus $\ln(k_BT)$ from $T \cong 120$–325 K with and without $\varepsilon^2/4\lambda k_BT$. A value of 0.8 eV is used for λ. The slope is close to unity without the $\varepsilon^2/4\lambda k_BT$ correction (1.00 for Au and 0.97 for Pt) and deviates a little from it with the correction (0.96 for Au and 0.93 for Pt). Thus, in both cases $I(k_BT) \propto k_BT$ is valid for the nonadiabatic electron transfer to Au and Pt. Accordingly, the temperature dependence of the electronic factor in Eq. (13) is proportional to T and so the k_{ET} in Eqs. (1)–(3) (apart from the exponential part of the Franck–Condon factor) is proportional to $T/T^{1/2}$, i.e. $T^{1/2}$. With the classical formulation for the Franck–Condon factor for the electrochemical exchange current $k_{ET} \propto T^{1/2} e^{-\lambda/4k_BT}$ for both metals and thus we expect it to apply for other metals at these temperatures.

The slopes from Fig. 3 can be used to evaluate the value of the prefactor in Eq. (10). We proceed by writing the integral in Eq. (8) as $C(k_BT)^{1+\Delta n}$, where Δn is the deviation of the slope from unity and C is some constant. Eq. (8) can then be written as

$$k^0 = \frac{2\pi}{\hbar} \frac{e^{-\lambda/4k_BT}}{(4\pi\lambda k_BT)^{1/2}} C(k_BT)^{1+\Delta n} \tag{20}$$

The above equation can then be used to find the value of $\partial \ln(k^0 T^{-1/2})/\partial(1/T)$. It equals $-\lambda/k_B[1/4 + \Delta n k_BT/\lambda]$, which gives instead of the factor of 4 in Eq. (10) a factor of $4/(1 + 4\Delta n k_BT/\lambda)$. For the slopes from Fig. 3, with $\lambda = 0.8$ eV and $k_BT = 0.025$ eV we get values of 4.02 and 4.04 for Pt (with and without $\varepsilon^2/4\lambda k_BT$ correction) and 4.00 and 4.02 for Au (with and without correction).

The slopes of the $\ln(I(k_BT))$ versus $\ln(k_BT)$ given above $(1 + \Delta n)$ could also have been obtained from an

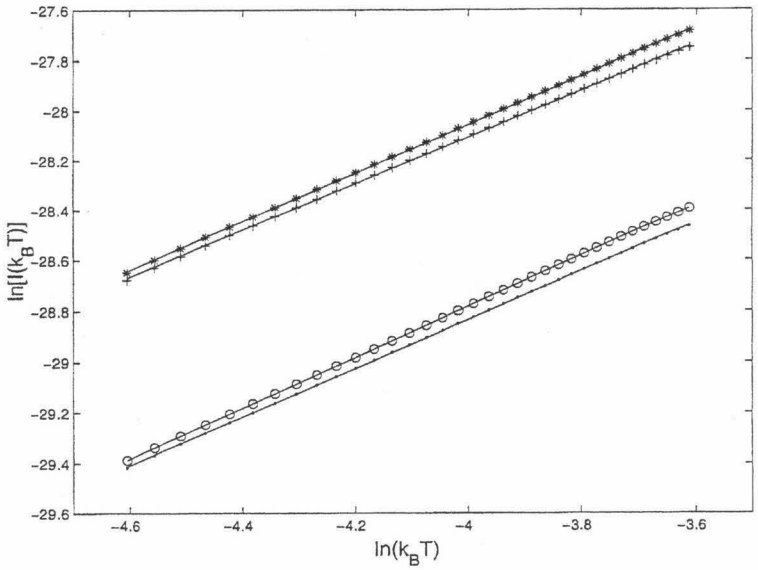

Fig. 3. A plot of ln $[I(k_BT)]$ vs. ln (k_BT). The slope gives the exponent of k_BT in $I(k_BT)$. The ✱ and + (with the $\varepsilon^2/4\lambda k_BT$ correction) points are for Pt and ○ and · (with correction) points are for Au. The slope for Au is 1.00 and 0.96 (with correction) and the slope for Pt is 0.97 and 0.93 (with correction).

expansion of $|V(\varepsilon)|^2$ in the vicinity of $\varepsilon = 0$, using the data in Fig. 2.

$$|V(\varepsilon)|^2 = |V(0)|^2(1 + a\varepsilon + b\varepsilon^2 + c\varepsilon^3 + d\varepsilon^4 \ldots) \quad (21)$$

The terms having odd powers of ε do not contribute, and so we have

$$I(k_BT) = |V(0)|^2 \pi k_BT[1 + (\pi k_BT)^2 b + 5(\pi k_BT)^4 d + \ldots] \quad (22)$$

Since the $|V(\varepsilon)|^2$ for Au is linear in ε at $\varepsilon = 0$, Fig. 2, b vanishes and it is clear why a plot of ln $(I(k_BT))$ versus ln (k_BT) was 1.00 for Au. Expanding $|V(\varepsilon)|^2$ around $\varepsilon = 0$ for Pt by fitting the Pt curve in Fig. 2 with various polynomial functions it was found that the calculated slope varied from 0.9 to 1.0, thus yielding an almost linear plot[4].

3.2. Semiconductors

To treat the T dependence for semiconductor electrodes using Eq. (18) or Eq. (19), calculations such as those given in Ref. [22] would need to be repeated at various temperatures. In the absence of those particular results we use here the free electron model [26][5] in which the matrix element H_{kA} (i.e. $\langle \Psi_k | H | \Psi_A \rangle$) at small ε is found to be proportional to k_z [27][6] (because Ψ_k is proporational to k_z), and so $|H_{kA}|^2 \propto k_z^2 \propto k^2/3 \propto \varepsilon$, where ε is the energy. Since $\rho(\varepsilon)$ varies as some (known) power of ε, one finds that the electronic factor, $\langle|\bar{V}(\varepsilon)|^2\rangle$ in Eq. (4), is proportional to k_BT. A consequence is that k_{ET}^{max} varies as $T/T^{1/2}$, i.e., $T^{1/2}$.

4. Discussion

Two differences between metals and the present nondegenerate semiconductors may be noted: (1) In the former the Fermi–Dirac distribution is needed, while the Boltzmann distribution suffices for the semiconductor. (2) As a first approximation the H_{kA} in Eq. (4),

[4] For a particular fit function we find a value of $b = -10.84$ and $d = 203.47$ which gives an average correction of 0.96 for a k_BT range of ~ 0.01 to 0.027 eV, i.e., $120 \leq T \leq 325$ K. Because of the peak of the Pt curve in Fig. 2 at the Fermi energy, the slopes of the Pt plots in Fig. 3 are sensitive to the fitted polynomial used.

[5] If in other cases, H_{kA} were proportional to a linear combination of k_x k_y and k_z, then $|H_{kA}|^2$ averaged near the conduction band edge would still be proportional to ε. In general, Ψ_k and thus the matrix element is proportional to $\sin(k_z)$, which becomes k_z only at a band-edge (small k_z). Like k_z, the distribution of $\sin(k_z)$ is hardly changed when ε is changed in the case of a metal since $\Delta \gg \varepsilon$.

[6] In the case of indirect bandgap semiconductors the k_x, k_y and k_z are replaced by $k_x - k_0$, $k_y - k_0$ and $k_z - k_0$ throughout and the same conclusion applies.

appearing via Eq. (15) in Eq. (19) or k_{ET}^{max}, is approximately proportional to k_z in the free electron model for the semiconductor [26]. Since $\langle|\bar{V}(\varepsilon)|^2\rangle$ is, as seen from above, proportional to k_z^2 and since the transfer is from the edge of the conduction band, it is also proportional to ε. In the case of the metal, however, the distribution of the ks is hardly changed when the energy ε relative to the Fermi level is changed. Thus, now $\langle|\bar{V}(\varepsilon)|^2\rangle$ is essentially independent of ε. Specifically, at the high energies associated with ks near the Fermi level in free electron metals, k_z^2 would be proportional to $(\Delta + \varepsilon)$, where Δ is the energy of the Fermi level relative to that of the bottom of the band, namely about 2 or more eV. Thus, as ε is varied, the distribution of the k_zs is hardly changed, since $\Delta \gg \varepsilon$. This behavior is in marked contrast to that of the semiconductor at its band edge, where $k_z^2 \propto \varepsilon$.

These two effects, seen to be different for the semiconductor and the metal, never the less, for different reasons, gave rise to a proportionality of the electronic factor to k_BT for k_{ET} for the exchange current in the case of the metal and for k_{ET}^{max} in the case of the maximum rate constant for the semiconductor.

Acknowledgements

We are pleased to acknowledge discussions with Professors Harry Finklea and Nate Lewis, who called our attention to this question for metals and semiconductors, respectively. It is a pleasure to acknowledge the support of this research by the Office of Naval Research and the National Science Foundation, and to dedicate this article to Professor Roger Parsons. As one of us mentioned in an earlier article honoring Roger, RAM is very much indebted to him for the illuminating chapter he wrote many decades ago in Modern Aspects of Electrochemistry. This chapter facilitated considerably RAM's entry into the field of electron transfer in electrochemistry.

References

[1] R.A. Marcus, J. Chem. Phys. 43 (1965) 679 and references cited therein.
[2] C.E.D. Chidsey, Science 251 (1991) 919.
[3] C. Miller, M. Grätzel, J. Phys. Chem. 95 (1991) 5225.
[4] H.O. Finklea, D.D. Hanshew, J. Am. Chem. Soc. 114 (1992) 3173.
[5] A.M. Becka, C.J. Miller, J. Phys. Chem. 96 (1992) 2657.
[6] H.O. Finklea, M.S. Ravenscroft, D.A. Snider, Langmuir 9 (1993) 223.
[7] M.S. Ravenscroft, H.O. Finklea, J. Phys. Chem. 98 (1994) 3843.
[8] L.M. Tender, M.T. Carter, R.W. Murray, Anal. Chem. 66 (1994) 3173.
[9] K. Weber, S.E. Creager, Anal. Chem. 66 (1994) 3164.
[10] G.K. Rowe, M.T. Carter, J.N. Richardson, R.W. Murray, Langmuir 11 (1995) 1797.
[11] K. Weber, L. Hockett, S. Creager, J. Phys. Chem. Sect. B 101 (1997) 8286.
[12] H.O. Finklea, M.S. Ravenscroft, Israel J. Chem. 37 (1997) 179.
[13] S. Sek, A. Misicka, R. Bilewicz, J. Phys. Chem. Sect. B 104 (2000) 5399.
[14] J.N. Richardson, G.K. Rowe, M.T. Carter, L.M. Tender, L.S. Curtin, S.R. Peck, R.W. Murray, Electrochim. Acta 40 (1995) 1331.
[15] J.F. Smalley, S.W. Feldberg, C.E.D. Chidsey, M.R. Linford, M.D. Newton, Y.-P. Liu, J. Phys. Chem. 99 (1995) 13141.
[16] M.T. Carter, G.K. Rowe, J.N. Richardson, L.M. Tender, R.H. Terrill, R.W. Murray, J. Am. Chem. Soc. 117 (1995) 2896.
[17] J.N. Richardson, S.R. Peck, L.S. Curtin, L.M. Tender, R.H. Terrill, M.T. Carter, R.W. Murray, G.K. Rowe, S.E. Creager, J. Phys. Chem. 99 (1995) 766.
[18] H.O. Finklea, in: A.J. Bard, I. Rubinstein (Eds.), Electroanalytical Chemistry, vol. 19, Marcel Dekker, New York, 1996, p. 109.
[19] K.S. Weber, S.E. Creager, J. Electroanal. Chem. 458 (1998) 17.
[20] I.S. Gradshteyn, I.M. Ryzhik, Tables of Integrals, Series and Products, Academic Press, New York, 349.
[21] S. Gosavi, R.A. Marcus, J. Phys. Chem. Sect. B 104 (2000) 2067.
[22] Y.Q. Gao, Y. Georgievskii, R.A. Marcus, J. Chem. Phys. 112 (2000) 3358.
[23] N.S. Lewis, Z. Phys. Chem. 212 (1999) and references cited therein.
[24] C.-P. Hsu, R.A. Marcus, J. Chem. Phys. 106 (1997) 584.
[25] R.A. Marcus, J. Chem. Soc., Faraday Trans. 92 (1996) 3905.
[26] Y.Q. Gao, R.A. Marcus, J. Chem. Phys. 113 (2000) 6351.
[27] K.W. Böer, Survey of Semiconductor Physics, VNR, New York, 1990, p. 215.

Chapter 7

Application of z-transform to composite materials
(Submitted to J. Chem. Phys.)

Application of the z-transform to composite materials

Yi Qin Gao and R. A. Marcus

Noyes Laboratory of Chemical Physics,
Mail code 127-72, California Institute of Technology,
Pasadena, CA 91125

Abstract

Applications of the z-transform were made earlier to interfacial electron transfer involving semi-infinite solids, e.g., semiconductor/liquid and metal/liquid interfaces and STM. It is shown how this method is readily adapted to treat composite materials, such as solid/solid interfaces or "molecular wire"/solid interfaces.

I. INTRODUCTION

The electronic structure of solids having surfaces has been of much interest in a variety of physical and chemical studies.[1–4] Among the simple theoretical methods used for treating the electronic properties of solids the tight-binding approach is considered the simplest that is also reliable for approximate calculations.[1,3] In the implementation of this method to solids with surfaces, the solids can be considered as consisting of coupled atomic layers parallel to the surface. The system can then be simplified as a one-dimensional chain, with each unit representing a principal layer.[5,6] The principal layers are then treated separately using the two-dimensional space group symmetry.

Various methods have been developed in tight-binding studies of solids having surfaces. In the 'slab' method[7] the solid is treated as consisting of a finite number of principal layers parallel to the surface and the electronic structure of such a 'slab' is usually obtained by direct diagonalization of the Hamiltonian. The elements of the Hamiltonian are expressed in terms of atomic or molecular orbitals and their interactions within and between layers. Other methods for semi-infinite solids include the transfer matrix[6,8] and scattering-theoretic[9] formalisms, which usually employ Green function techniques.

Instead of the Green function method, a z-transform method has also been used to treat the electronic structure of a semi-infinite solid.[10] The z-transform, also known as the discrete Laplace transform,[11] had been applied earlier in electrical engineering and allied fields. The transform reduces the problem of solving an infinite set of linear difference equations to an algebraic equation. This transform method can be applied to multi-band and/or complex interacting systems and still be transparent in its mathematical results. It was recently used to obtain the electronic wave functions of single element (Si) and compound element (InP) semiconductors.[12] The calculated electronic wave functions were then used to calculate the electronic coupling matrix element for electron transfer reactions at semiconductor/liquid interfaces. The z-transform method proved to be efficient and the results showed good agreement with

those of the slab method in those studies.

The Green function approach lends itself quite naturally to focusing on local regions,[13,14] such as defects or surfaces. It is adaptable to thermal averaging, and there are well defined procedures for treating Green functions and summing over formal expansions. The wave function approach has been more commonly used in chemical studies, particularly in the form of a slab or cluster approach, since it has permitted very detailed electronic structure calculations. The Green function has been extensively used in recent years in the treatment of "molecular wires" and related systems.[14]

In earlier studies, the application of the z-transform has been used in the treatment of semi-infinite solids,[10] including electron transfer reactions for STM,[15] semiconductor/liquid[12] and metal/attached monolayer systems.[16] In the present article the method is extended to composite systems, such as solid/solid interfaces. The extension also applies to "molecular wire"/solid interfaces, as a particular example of a composite system. Interfaces between a metal and a semiconductor and that between two semiconductors have been studied extensively in the literature,[17–19] and reflect the scientific and technological interest in such systems. Their electronic structures have been studied by Green function techniques, using tight-binding[3,17] or pseudopotential methods.[2] In the present paper the electronic wave function of such systems is obtained by introducing separate z-transforms for the coefficients of both solids and using the interaction parameters between the two solids. Both bulk and interfacial states can be studied in this manner.

II. THE Z-TRANSFORM METHOD FOR TREATING SEMI-INFINITE SOLIDS AND SOLID/SOLID INTERFACES

A. z-transform

We have noted earlier the use of "principal layers," which are parallel to the surface, and the subsequent treatment of the system is one-dimensional, each unit being a principal layer.[5] In the following, we first consider the tight-binding wave functions for a one-dimensional solid-solid interface, and show how the z-transform method can be applied to it. For its application to solid/solid interfaces, it is useful to first illustrate the z-transform method by applying it to electronic wave functions of a semi-infinite solid. A more detailed derivation is given in Ref. 10. In this approach the tight-binding type electronic wave functions can be written as

$$|\Psi_k\rangle = \sum_{n=1}^{\infty} c_n(k)|\psi_n\rangle, \tag{1}$$

where the coefficient $c_n(k)$ in Eq. (1) is the solution of an infinite set of linear equations,

$$c_{n+1}\beta^* + c_n(\alpha - E) + c_{n-1}\beta = 0, \quad n \geq 2, \tag{2}$$

with the boundary condition

$$c_2\beta^* + c_1(\alpha_1 - E) = 0. \tag{3}$$

Here, $\alpha = \langle\psi_n|H|\psi_n\rangle$ $(n \geq 2)$, $\beta = \langle\psi_{n+1}|H|\psi_n\rangle$ $(n \geq 1)$, and $\alpha_1 = \langle\psi_1|H|\psi_1\rangle$. The notation for the k-dependence of the c_n is suppressed for brevity.

To solve the linear equations given by Eq. (2), the z-transform for c_n is defined by

$$\mathcal{Z}(c_n) = \sum_{n=1}^{\infty} c_n z^{1-n} \equiv F(z), \tag{4}$$

which, using Eqs. (2) and (3), can be shown to yield[10]

$$F(z) = c_1 \frac{(\alpha - \alpha_1)z - \beta^* z^2}{\beta^* z^2 + (\alpha - E)z + \beta}. \tag{5}$$

The coefficients c_n are recovered using the inverse z-transform of $F(z)$,

$$c_n = \mathcal{Z}^{-1}[F(z)] = \frac{1}{2\pi i}\oint_C F(z)z^{n-2}dz, \tag{6}$$

that is

$$c_n = \frac{c_1}{2\pi i}\oint_C \frac{(\alpha-\alpha_1)-\beta^* z}{\beta^* z^2+(\alpha-E)z+\beta} z^{n-1}dz. \tag{7}$$

The latter is readily integrated using Cauchy's residue theorem. The z-transform is applied to solid/solid interfaces in the next section. For simplicity, the solid/solid interfaces will be studied using mainly one-dimensional models, but the results are immediately generalized to the 3-D case. Ideal interfaces and reconstructed interfaces are treated separately in the following. The constant c_1 is evaluated by normalizing the wave function to a delta function.[10]

B. Ideal interface between two one-dimensional one-band systems

The one-dimensional model of the composite interface is illustrated in Fig. 1(a). The wave function of such a system can be written in terms of localized atomic orbitals

$$|\Psi_k\rangle = \sum_{n=-\infty}^{\infty} c_n|\psi_n\rangle, \quad (n \neq 0) \tag{8}$$

where ψ_n again denotes the orbital localized at the nth site.

The tight-binding Hamiltonian of this system can be written as

$$\begin{aligned} H = & \sum_{n=-\infty}^{-1} \alpha_2|\psi_n\rangle\langle\psi_n| + \left(\sum_{n=-\infty}^{-1} \beta_2|\psi_n\rangle\langle\psi_{n-1}| + c.c.\right) \\ & + \sum_{n=1}^{\infty} \alpha_1|\psi_n\rangle\langle\psi_n| + \left(\sum_{n=1}^{\infty} \beta_1|\psi_n\rangle\langle\psi_{n+1}| + c.c.\right) \\ & + (\gamma|\psi_{-1}\rangle\langle\psi_1| + c.c.)\,, \end{aligned} \tag{9}$$

where β_1 and β_2 are the interaction parameters between the neighboring sites within each of the two semi-infinite chains, denoted by positive and negative numbers, respectively, α_1 and α_2 are the corresponding coulombic parameters, and γ is the interaction parameter between the two adjacent sites 1 and -1 of the two chains. As can be seen from the Hamiltonian, it is assumed here for simplicity that the interface consists of

only two sites (-1 and 1), and at first the coulombic parameter α for each of the two sites at the interface is given the same value as that in each semi-infinite solid. When the interfacial potential parameters α_1 and α_{-1} are different from their bulk values and/or when the interaction involves more than the nearest neighbors, the same derivation is applicable, but the final formulae are more complicated.

Using the same strategy as that used in the semi-infinite solid case a set of difference equations is obtained for the coefficients c_n's, $n = 1, 2, ...\infty$ and a set for the other coefficients, $n = -1, -2, ... - \infty$, instead of just one set of equations. These two sets are coupled by the coefficients c_{-1} and c_1,

$$\beta_1^* c_{n+1} + (\alpha_1 - E)c_n + \beta_1 c_{n-1} = 0, \qquad n = 2, 3, 4, ..., \qquad \text{(solid 1)} \tag{10}$$

$$\beta_1^* c_2 + (\alpha_1 - E)c_1 + \gamma c_{-1} = 0, \tag{11}$$

and

$$\beta_2 c_{n+1} + (\alpha_2 - E)c_n + \beta_2^* c_{n-1} = 0, \qquad n = -2, -3, -4, ..., \qquad \text{(solid 2)} \tag{12}$$

$$\gamma^* c_1 + (\alpha_2 - E)c_{-1} + \beta_2^* c_{-2} = 0. \tag{13}$$

The z-transforms for solid 1 ($n \geq 1$) and solid 2 ($n \leq -1$) are, respectively,

$$F^+(z) = \sum_{n=1}^{\infty} c_n z^{1-n}, \quad F^-(z) = \sum_{n=-1}^{-\infty} c_n z^{1+n}. \tag{14}$$

With these definitions, $F^+(z)$ and $F^-(z)$ converge when $|z| \leq 1$ and $n \to \infty$ and $n \to -\infty$, respectively. Application of the z-transform to the two sets of difference equations, Eqs. (10) and (12) separately, yields the z-transform for c_n $(n > 0)$ as $F^+(z)$ and that for c_n $(n < 0)$ as $F^-(z)$,

$$F^+(z) = \frac{\beta_1^* z^2 c_1 + (\alpha_1 - E)z c_1 + z\beta_1^* c_2}{\beta_1^* z^2 + (\alpha_1 - E)z + \beta_1}, \qquad \text{(solid 1)} \tag{15}$$

$$F^-(z) = \frac{\beta_2^* z^2 c_{-1} + (\alpha_2 - E)z c_{-1} + z\beta_2 c_{-2}}{\beta_2^* z^2 + (\alpha_2 - E)z + \beta_2}. \qquad \text{(solid 2)} \tag{16}$$

Equations (11) and (13)-(16) yield

$$F^+(z) = \frac{c_1 \beta_1^* z^2 - c_{-1}\gamma z}{\beta_1^* z^2 + (\alpha_1 - E)z + \beta_1}, \qquad \text{(solid 1)} \tag{17}$$

$$F^-(z) = \frac{c_{-1}\beta_2^* z^2 - c_1 \gamma^* z}{\beta_2^* z^2 + (\alpha_2 - E)z + \beta_2}. \qquad \text{(solid 2)} \tag{18}$$

The coefficients obtained by the inverse z-transform are

$$c_n = \frac{1}{2\pi i}\oint_C \frac{(c_1\beta_1^* z - c_{-1}\gamma)z^{n-1}}{\beta_1^* z^2 + (\alpha_1 - E)z + \beta_1} dz, \qquad \text{(solid 1, n > 0)} \tag{19}$$

$$c_n = \frac{1}{2\pi i}\oint_C \frac{(c_{-1}\beta_2^* z - c_1\gamma^*)z^{-(n+1)}}{\beta_2^* z^2 + (\alpha_2 - E)z + \beta_2} dz. \qquad \text{(solid 2, n < 0)} \tag{20}$$

For $n = 1$ and $n = -1$, integration of the above equations yields $c_1 = c_1$ and $c_{-1} = c_{-1}$, as they should.

To obtain solutions which are propagating to infinity in both sides of the solid, c_n and c_{-n} should neither vanish nor become infinite as $n \to \infty$. (We treat bound interfacial states later.) We thus require that the poles of the integrand in Eqs. (19) and (20) lie on the unit circle, a result which implies that the solution $z = z_1$ of

$$\beta_1^* z^2 + (\alpha_1 - E)z + \beta_1 = 0 \tag{21}$$

and the solution $z = z_2$ of

$$\beta_2^* z^2 + (\alpha_2 - E)z + \beta_2 = 0 \tag{22}$$

both lie on the unit circle. In a simple case where β_1 and β_2 are real, the solutions of Eqs. (21) and (22) are both of the type $e^{\pm i\theta}$, but each typically has a different value of θ. We then have

$$E - \alpha_1 = \beta_1(e^{i\theta} + e^{-i\theta}) = 2\beta_1 \cos\theta_1 \tag{23}$$

and

$$E - \alpha_2 = 2\beta_2 \cos\theta_2, \tag{24}$$

which also serve to relate θ_2 to θ_1 at each E.

The c_n for $n > 0$, as discussed earlier, is given by Eq. (19). The poles of the integrand of the right hand side of Eq. (19) are at $z = \exp(i\theta_1)$ and $z = \exp(-i\theta_1)$. The former gives a term $\exp(in\theta_1)$ and the latter $\exp(-in\theta_1)$. After evaluating the residues in Eq. (19), we have

$$c_n = \frac{(c_1\beta_1 e^{i\theta_1} - c_{-1}\gamma)e^{i(n-1)\theta_1}}{2i\beta_1 \sin\theta_1} + \frac{(c_1\beta_1 e^{-i\theta_1} - c_{-1}\gamma)e^{-i(n-1)\theta_1}}{-2i\beta_1 \sin\theta_1}, \qquad (n > 0, \text{ solid 1}). \tag{25}$$

Similarly, from Eq. (20), we have

$$c_n = \frac{(c_{-1}\beta_2 e^{-i\theta_2} - c_1\gamma^*)e^{-i(n+1)\theta_2}}{2i\beta_2 \sin\theta_2} + \frac{(c_{-1}\beta_2 e^{i\theta_2} - c_1\gamma^*)e^{i(n+1)\theta_2}}{-2i\beta_2 \sin\theta_2}, \qquad (n < 0, \text{ solid } 2). \tag{26}$$

The constants c_1 and c_{-1} are obtained by a normalization and by satisfying a boundary condition at infinity. For example, if a traveling wave is incident in solid 1, partially reflected at the interface, and a purely outgoing wave, $e^{-in\theta_2}$, occurs in solid 2, n becoming progressively more negative, then the boundary condition is to set the coefficient of the $\exp(in\theta)$ term ($n < 0$) in Eq. (26) equal to zero. Thereby,

$$c_{-1}\beta_2 e^{i\theta_2} = c_1\gamma^*, \tag{27}$$

and so from Eq. (26)

$$c_n = c_{-1}e^{-i(n+1)\theta_2} \qquad (n < 0). \tag{28}$$

The c_n in Eq. (25) can also be expressed in terms of c_{-1} using Eq. (27), and the c_{-1} can be evaluated from whatever normalization that is used. (e.g., unit incident wave in solid 1, or normalization to a delta function.)

Two limiting cases are readily retrieved from these equations: In the limiting case where $\gamma = 0$, the two semi-infinite solids are uncoupled, and the above expressions yield wave functions which are those of semi-infinite chains.[1,10] The other limiting case is where the two semi-infinite chains are the same, so that $\gamma = \beta_1 = \beta_2$, $\alpha_1 = \alpha_2$, and $\theta_1 = \theta_2 = \theta$. We then have an infinite one-dimensional chain of sites, and $c_n = e^{i(n-1)\theta}c_1$, for $n > 0$, $c_{-1}e^{i\theta} = c_1$, and $c_n = c_{-1}e^{-i(n+1)\theta}$, for $n < 0$.

At both metal-semiconductor[20] and semiconductor-semiconductor interfaces,[18] bound interfacial states are common and are known to play an important role in determining physical features such as conduction behavior[17] and the Schottky barrier height.[18] The bound interfacial states have been studied extensively using the Green function method.[21] In the following it is seen that the z-transform method similarly provides an examination of conditions and energy values for these interfacial states.

To illustrate the use of the z-transform method for this purpose, we again model such a situation by a one-dimensional chain. In this case, the solutions of Eqs. (21)

and (22) are both of the form $z = e^{-\theta_{1,2}}$, where the real parts of θ_1 and θ_2 are positive. Since e^{θ_1} is also a solution of Eq. (21), in order to avoid c_n increasing as n increases, the integrand of Eq. (19) is such that the numerator has $z - e^{\theta_1}$ as a factor to cancel a corresponding term in the denominator. Thus we require that

$$c_1\beta_1 z + c_{-1}\gamma \propto z - e^{\theta_1} \tag{29}$$

which yields

$$\frac{c_1}{c_{-1}} = -\frac{\gamma}{\beta_1}e^{-\theta_1}. \tag{30}$$

Similarly, we have that

$$\frac{c_{-1}}{c_1} = -\frac{\gamma^*}{\beta_2}e^{-\theta_2} \tag{31}$$

from the requirement that c_n $(n < 0)$ decreases as n decreases. Comparison of Eqs. (30) and (31) finally yields

$$e^{\theta_1+\theta_2} = \frac{\gamma\gamma^*}{\beta_1\beta_2} \tag{32}$$

The interfacial states can exist only if Eq. (32) is satisfied, and thus $\gamma\gamma^*/\beta_1\beta_2$ must exceed unity. These results are readily extended to three-dimensional cases and the z-transform method proves to be a simple method for obtaining the existing condition of interfacial states.

C. One-dimensional one-band systems with a reconstructed and/or coated interface

When two solids form a heterojunction, the interface is frequently reconstructed. In many cases one of the solids is coated by some other material beforehand. Such systems have usually been treated by the Green function technique.[19] This situation is readily modeled by treating the interface as a different unit from the two bulk phases, as illustrated in Fig. 1(b). One type of atom occupies sites from 1 to ∞, those of the other type occupy -1 to $-\infty$, and the interface occupies site 0. Using the same parameters α_1, α_2, β_1 and β_2 tacitly defined in Eq. (10) and introducing

$$\alpha_0 = \langle\psi_0|H|\psi_0\rangle, \qquad \gamma_1 = \langle\psi_0|H|\psi_1\rangle, \qquad \gamma_2 = \langle\psi_{-1}|H|\psi_0\rangle, \tag{33}$$

the following linear equations are obtained for this system by the same method as that described earlier,

$$\beta_1^* c_{n+1} + (\alpha_1 - E)c_n + \beta_1 c_{n-1} = 0, \qquad n = 2, 3, 4, ..., \tag{34}$$

$$\beta_1^* c_2 + (\alpha_1 - E)c_1 + \gamma_1 c_0 = 0, \tag{35}$$

and

$$\beta_2 c_{n+1} + (\alpha_2 - E)c_n + \beta_2^* c_{n-1} = 0, \qquad n = -2, -3, -4, ..., \tag{36}$$

$$\gamma_2 c_0 + (\alpha_2 - E)c_{-1} + \beta_2^* c_{-2} = 0. \tag{37}$$

Electronic wave functions of such a system can again be obtained using the z-transform method described in the previous section. Using the boundary condition,

$$c_0 = \frac{c_1\gamma_1^* + c_{-1}\gamma_2^*}{E - \alpha_0}, \tag{38}$$

the tight-binding coefficients are obtained as

$$c_n = \frac{1}{2\pi i}\oint_C \frac{\{c_1(\beta_1^* z - \frac{\gamma_1\gamma_1^*}{E-\alpha_0}) - c_{-1}\frac{\gamma_1\gamma_2^*}{E-\alpha_0}\}z^{n-1}}{\beta_1^* z^2 + (\alpha_1 - E)z + \beta_1} dz \tag{39}$$

$$c_n = \frac{1}{2\pi i}\oint_C \frac{\{c_{-1}(\beta_2^* z - \frac{\gamma_2\gamma_2^*}{E-\alpha_0}) - c_1\frac{\gamma_2\gamma_1^*}{E-\alpha_0}\}z^{-(n+1)}}{\beta_2^* z^2 + (\alpha_2 - E)z + \beta_2} dz \tag{40}$$

The condition for the existence of bound interfacial states can be found in a way similar to that discussed in the previous section. For bound interfacial states there should only be terms of exponentially decaying waves in the expression for c_n. Accordingly, terms that increase as n increases are made to vanish. As in the previous section, one obtains

$$c_1(\frac{\gamma_1\gamma_1^*}{E - \alpha_0} - \beta_1 e^{\theta_1}) = c_{-1}\frac{\gamma_1\gamma_2^*}{\alpha_0 - E}, \tag{41}$$

$$c_{-1}(\frac{\gamma_2\gamma_2^*}{E - \alpha_0} - \beta_2 e^{\theta_2}) = c_1\frac{\gamma_2\gamma_1^*}{\alpha_0 - E}. \tag{42}$$

In order for there to be a nontrivial solution for c_1 and c_{-1}, the determinant of the coefficients in Eqs. (41) and (42) vanishes, yielding

$$\frac{\gamma_1\gamma_1^*}{\beta_1}e^{-\theta_1} + \frac{\gamma_2\gamma_2^*}{\beta_2}e^{-\theta_2} = E - \alpha_0. \tag{43}$$

The requirement that the wave functions decay in both sides of the solid yields the following condition for the existence of bound interfacial states, obtained by requiring that the poles in Eqs. (39) and (40) be of the form $z = e^{\theta_1}$ and e^{θ_2}, respectively,

$$E = \alpha_1 + 2\beta_1 \cosh\theta_1 = \alpha_2 + 2\beta_2 \cosh\theta_2, \quad \theta_1 > 0, \quad \theta_2 > 0. \tag{44}$$

It is readily verified that the expected results can be obtained for several limiting situations.

For simplicity, in the following all the interaction parameters are treated as real. A simple semi-infinite system is achieved by setting

$$\gamma_1 = \beta_1, \quad \gamma_2 = \beta_2 = 0, \quad \alpha_2 = 0. \tag{45}$$

The condition for the existence of bound surface states can be obtained by applying the above equalities to Eqs. (43) and (44),

$$\alpha_1 - \alpha_0 = \beta_1 e^{\theta_1}, \quad \theta_1 > 0. \tag{46}$$

which can be rewritten as

$$\frac{\alpha_1 - \alpha_0}{\beta_1} > 1, \tag{47}$$

and is in agreement with the known result.[1,10]

Another limiting case occurs when two identical semi-infinite linear chains form an interface,

$$\beta_1 = \beta_2 = \gamma_1 = \gamma_2, \quad \alpha_1 = \alpha_2. \tag{48}$$

It then readily follows that the condition for the existence of bound interfacial states is

$$\alpha_1 - \alpha_0 > 0, \tag{49}$$

i.e., that the surface states below the allowed band of the infinite chain can exist only if the α_0 is more negative than α_1.

III. CONCLUDING REMARKS

In the present study the z-transform method has been applied to composite materials, such as solid/solid interfaces. The existing condition for bound interfacial states is obtained in terms of tight-binding solid state parameters, treating both reconstructed and ideally non-reconstructed interfaces. The z-transform and the models introduced in the present paper can be applied to systems of experimental interest, including charge transfer through diodes and molecular wires. In particular, it can be applied, using the tight-binding wave functions, to study the interface between a "molecular wire" and a metallic surface,[22] and the contact between nanotubes and metals.[23]

ACKNOWLEDGMENTS

It is a pleasure to acknowledge the support of this research by the National Science Foundation and the Office of Naval Research.

REFERENCES

[1] S. G. Davison and M. Steslicka, *Basic theory of surface states* (Clarendon Press, Oxford, 1996).

[2] F. Garcia-Moliner and V. R. Velasco, *Theory of single and multiple interfaces* (World Scientific Publishing, 1992).

[3] F. Bechstedt and R. Enderlein, *Semiconductor Surfaces and Interfaces* (Akademie-Verlag, Berlin, 1988).

[4] M. Lannoo and P. Friedel, *Atomic and Electronic Structure of Surfaces* (Springer-Verlag, Berlin Heidelberg, 1991).

[5] E.g., Ref. 3, pp131-133.

[6] D. H. Lee and D. Joannopoulos, Phys. Rev. B **23**, 4988 (1981).

[7] E.g., K. Hirabayashi, J. Phys. Soc. Japan, **27**, 1475 (1969), C. Calandra, F. Manghi, and C. M. Bertoni, J. Phys. C **10**, 1911 (1977), D. J. Chadi, Phys. Rev. B **18**, 1800(1978), K. C. Pandey and J. C. Philips, Phys. Rev. Lett. **34**, 1450 (1975).

[8] E. J. Mele and J. D. Joannopoulos, Phys. Rev. B **17**, 1816 (1978).

[9] E.g., J. Koutecky and M. Tomasek, Phys. Rev. **120**, 1212 (1960); I. Ivanov and J. Pollmann, Solid State Commu. **36**, 361 (1980). A scattering formalism for STM and related "molecular wire" problems has been used in M. Magoga and C. Joachim, Phys. Rev. B **56**, 4722 (1997) and references to P. Sautet and C. Joachim cited therein; also E. G. Emberly and G. Kirczenow, Phys. Rev. B **58**, 10911 (1998).

[10] R. A. Marcus, J. Chem. Phys. **98**, 5604 (1993).

[11] E.g., J. R. Ragazzi and L. A. Zadeh, Trans. A.I.E.E. **71**, Pt. II, 225 (1952); E. I. Jury, A.I.E.E. **73**, Pt. II, 332 (1954).

[12] Y. Q. Gao, Y. Georgievskii, and R. A. Marcus, J. Chem. Phys. **112**, 3358 (2000).

[13] Extensive references to the use of Green function methods are given in Ref. 1, Chap.

7, as well as in J.E. Inglesfield, Progr. Surf. Sci. **25**, 57 (1978) and in J. Pollman and S. T. Pantelides, Phys. Rev. B **18**, 5524 (1978), articles which describe advantages of a Green function approach.

[14] E.g., S. N. Yaliraki, M. Kemp, and M. A. Ratner, J. Am. Chem. Soc. **121**, 3428 (1999) and references cited therein; S. Datta, W. Tian, S. Hong, R. Reifenberger, J. I. Henderson, and C. P. Kubiak, Phys. Rev. Lett. **79**, 2530 (1997) and references cited therein; C. P. Hsu and R. A. Marcus, J. Chem. Phys. **106**, 584 (1997); L. E. Hall, J. F. Reimers, N. S. Hush, and K. Silverbrook, J. Chem. Phys. **112**, 1510 (2000).

[15] H. Ouyang and R. A. Marcus, J. Chem. Phys. **100**, 7814 (1994).

[16] S. Gosavi and R. A. Marcus, J. Phys. Chem. B, **104**, 2067 (2000).

[17] E.g., S. G. Davison and J. D. Levine, Sol. Stat. Phys. **25**, 1(1970); D. J. Chadi and M. L. Cohen, Phys. Stat. Solid B, **68**, 405 (1975); Y. R. Yang and C. B. Duke, Phys. Rev. B **36**, 2763 (1987).

[18] E.g., W. Schottky, Z. Phys. **113**, 367 (1939); A. Zur, T. C. McGill, and D. L. Smith, Phys. Rev. B **28**, 2060 (1983); E. J. Mele and J. D. Joannopolous, Phys. Rev. B **17**, 1528 (1978); J. Tersoff, Phys. Rev. Lett. **52**, 465 (1984); Phys. Rev. B **30**, 4874 (1984).

[19] E.g., W. Moench, J. Vac. Sci. Technol. B **14**, 2985 (1996); A. K. Agrawal, Phys. Rev. B **23**, 2995 (1981); D. N. Lowy, A. Madhukar, Phys. Rev. B **17**, 2995 (1978).

[20] V. Heine, Phys. Rev. A **138**, 1689 (1965).

[21] E.g., N. V. Dandekar, A. Madhukar, and D. N. Lowy, Phys. Rev. B **21**, 5687 (1980); B. Djafari-Rouhani, L. Dobrzynski, and M. Lannoo, Surf. Sci. **78**, 24 (1978); R. N. Nucho and A. Madhukar, J. Vac. Sci. Technol. **15**, 1530 (1978).

[22] S.N. Yaliraki, A.E. Roitberg, C. Gonzalez, V. Mujica, and M.A. Ratner, J. Chem. Phys. **111**, 6997 (1999); S.N. Yaliraki and M.A. Ratner, J. Chem. Phys. **109**, 5036

(1998).

[23] M.P. Anantram, S. Datta, and Y. Xue, Phys. Rev. B **61**, 14219 (2000).

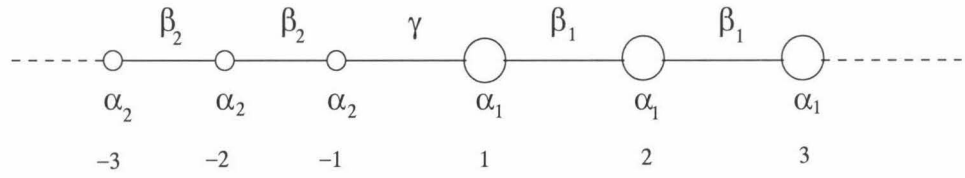

(a)

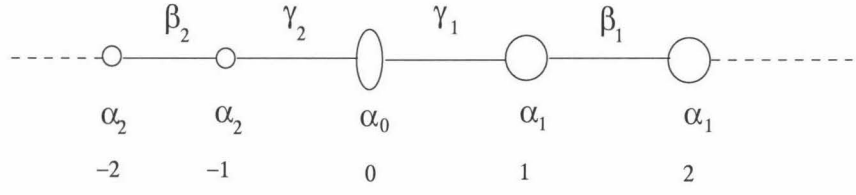

(b)

FIG. 1. Schematic picture of the interface formed by two semi-infinite linear chain: (a) an ideal interface, (b) a reconstructed (coated) interface. α, β and γ are the interaction parameters. The sites in the left-hand side are denoted by negative numbers and the sites in the right-hand side are denoted by positive numbers.

Chapter 8

Theoretical investigation of the directional electron transfer in a small supramolecular system
(Submitted to J. Phys. Chem.)

Theoretical investigation of the photoinduced electron transfer in 4-aminonaphthalimide compounds

Yi Qin Gao and R. A. Marcus

Noyes Laboratory of Chemical Physics,
Mail code 127-72, California Institute of Technology,
Pasadena,CA 91125

Abstract

Photoinduced electron transfer reactions in small supramolecular systems, such as the 4-aminonaphthalimide compounds, are interesting in that there are two alternative directions for the electron transfer to occur. Nevertheless, the electron transfer is unidirectional, as deduced from pH-dependent fluorescence quenching studies of selected compounds. The role of the electronic coupling matrix element, and the effect of the charges accompanying protonation, are considered so as to explain the directionality of the electron transfer and other results. A related mechanism is suggested for interpreting the behavior of similar molecules which serve as fluorescent sensors of metal ions.

I. INTRODUCTION

In recent years the 4-aminonaphthalimide compounds have been the subject of many studies,[1–8] in part because of their fluorescence properties and their serving as sensors. Recently, the photoinduced electron transfer reactions in synthesized supramolecular systems, consisting of various 4-aminonaphthalimide compounds, were studied by de Silva and coworkers.[1,2] The pH-dependent fluorescence spectrum was investigated for the compounds depicted in Fig. 1. Each of these molecules contains a fluorescent 4-aminonaphthalimide as the core and different amino groups in the side chains serving as the electron donors. The electronic absorption and fluorescence emission spectra were measured as a function of the pH of the solution, the solvent being water : methanol in a ratio of 1 :1. Some of the observed optical properties[1,2] are given in Table I. A strong pH-dependence of the fluorescence quantum yield is displayed by **3**,[1] **4**,[2] and **5**,[2] but not by **1** or **2**:[1] The fluorescence quantum yield of **1** and **2** remains relatively low (~ 0.2) in the pH range of experiments (4 to 11), while the fluorescence quantum yield for **3**, **4** and **5** is very low (< 0.1) in base but high in acid (> 0.5). The recovery of the fluorescence of **3**,[1] **4**,[2] and **5**[2] occurs at a pH that corresponds to the pK_a of the distal nitrogen of the 4-substituent.

Of particular interest was the pH-dependent fluorescence experiment for **4** and **5**.[2] Each of these two compounds consists of a fluorophore with two side chains, each containing an amino electron donor. With the pH-dependent fluorescence spectroscopy studies, two possible electron transfer directions responsible for the fluorescence quenching could be investigated. In their experiments,[2] de Silva and Rice made the striking discovery that the electron transfer is unidirectional: The fluorescence is recovered only when the distal nitrogen on the 4-substituent is protonated, while the protonation of the distal nitrogen in the 9-substituent has negligible influence on the fluorescence quantum yield. Thus, only the electron transfer from the distal nitrogen in the 4-substituent occurred.

In their explanation of their striking observations on the unidirectional behavior of **4** and **5**, de Silva *et al.* suggested[2] that the excitation first produces a charge-

separated state, namely a charge $+\delta$ on the 4-N and a charge $-\delta$ on the dicarboximide (-CO-N-CO-) group, the 4-N being the amino group at the 4-position. The resulting internal electric field then directs the hole to the distal nitrogen in the 4-substituent. A similar mechanism was assumed later by Tian *et al.* to explain the pH-dependence of the fluorescence of a 4-amino-1,8-naphthalimide compound.[9]

Indeed, as de Silva *et al.* noted, there is an effect of a ground state dipole on the direction of electron transfer in an α-helical polypeptide.[13] However, there is a striking contrast in the two phenomena: in the 4-aminonaphthalimide, the hole-electron pair $(+\delta, -\delta)$ (in the excited state denoted by $|\mathbf{e}\rangle$ later) changes after its initial formation. It is part of the dipolar field itself, rather than moving in an external field, and the concept was not developed further in the form of an actual calculation. In the present paper a different but simple explanation of the results is proposed, one based on the calculations of the relevant electronic coupling matrix elements between the orbitals.

The paper is organized as follows: Further experimental results are described in Sec. II. The electronic states involved in the present mechanism are given in Sec. III. In Sec. IV a crude estimate of the electronic coupling matrix elements is given for the two electron transfer directions. The electronic coupling matrix elements for the two pathways are calculated and used to interpret the directionality of the electron transfer in Sec. V, and explanations of various other experimental results are given in Sec. VI and VII. A concluding discussion is given in Sec. VIII.

II. FURTHER EXPERIMENTAL RESULTS

In the experiments,[1,2] a noticeable difference was observed between the pH-dependence of the wavelength of absorption maxima λ_{abs}^{max} for **1** and **2** and that for **3**, **4** and **5** (Table I): The λ_{abs}^{max} undergoes very little change with pH for compounds **1** and **2**, while there was about a 20 nm blue shift of the absorption spectra of **3**, **4**, and **5** when measured in acid relative to the spectra in base.[10] These changes of the λ_{abs}^{max}'s of **3**, **4**, and **5** occur at pH's corresponding to the pK_a's of the distal nitrogens in the 4-substituents.

In a related study, other 4-aminonaphthalimide compounds (**6**, and **7** in Fig. 2) were investigated by Mitchell *et al.* as fluorescent sensors for metal ions,[6,11] where the compounds are again believed to undergo intramolecular quenching by the distal nitrogen of the 4-substituent. For comparison, the fluorescence of **8**, a molecule similar to **6** and **7** but with a much longer 4-substituent side chain, was also studied in the presence of metal ions.[6] This quenching of **6** and **7** disappeared with the complexation of the metal ions with the distal nitrogen of the 4-substituent. The electron transfer from this distal nitrogen is thus again believed to be responsible for the fluorescence quenching of **6** and **7**. The fluorescence decay profile of **6** and **7** shows that the addition of metal ions which form amino complexes increases both the intensity and the lifetime of the fluorescence, while such effects have not been observed for **8**.

Experiments also confirmed that when a 4-substituent is moved to the 9-position it has, Mitchell *et al.* noted,[6] much less influence on the fluorescence quenching and on the fluorescence recovery mechanism of **6** and **7**.[7,12] It was also observed that the addition of metal ions, which can readily form complexes with the 4-distal nitrogen of all three molecules, causes the absorption maxima of **6** and **7** to undergo a 10-30 nm blue shift, while the addition of the same metal ions to the solution of **8** has no effect on absorption wavelength. The addition of metal ions that do not form amino complexes causes no change in the spectrum of any of the three molecules, **6** , **7** and **8**.

III. THE ELECTRONIC STATES

We consider a mechanism for the fluorescence quenching and for its recovery for the 4-aminonaphthalimide compounds in which there are the ground state, $|\mathbf{g}\rangle$, and at least two excited states, one of which, $|\mathbf{e}\rangle$, is less charge-separated and is fluorescent. The other, labeled $|\mathbf{e}_{\mathrm{CT1}}\rangle$ in Fig. 3, is more charge-separated and relatively non-fluorescent. The state $|\mathbf{e}\rangle$ is created by the excitation of a HOMO of the fluorophore and consists of a HOMO and a LUMO of the fluorophore (Fig. 4). The $|\mathbf{e}_{\mathrm{CT1}}\rangle$ is coupled to $|\mathbf{e}\rangle$ and arises from the electron transfer from the distal nitrogen. It has a

positive charge on that nitrogen, and the electron transfer quenches the fluorescence. This quenching mechanism is removed if this charge transfer is inhibited, and then the fluorescence increases. For the present systems, the attached amino groups act as electron donors and the ring system as an electron acceptor. The assumption of having a locally excited state and a charge-separated state is common for similar systems.[17] The various states discussed above are shown in Fig. 4 with the relevant orbitals given as follows:

$$|\mathbf{g}\rangle : (\mathrm{HOMO})_2(\mathrm{LUMO})_0(\mathrm{N4})_2(\mathrm{ND})_2,$$

$$|\mathbf{e}\rangle : (\mathrm{HOMO})_1(\mathrm{LUMO})_1(\mathrm{N4})_2(\mathrm{ND})_2,$$

$$|\mathbf{e}_{\mathrm{CT1}}\rangle : (\mathrm{HOMO})_2(\mathrm{LUMO})_1(\mathrm{N4})_2(\mathrm{ND})_1,$$

$$|\mathbf{e}_{\mathrm{CT2}}\rangle : (\mathrm{HOMO})_2(\mathrm{LUMO})_1(\mathrm{N4})_1(\mathrm{ND})_2,$$

where, as indicated in Fig. 4, N4 is an orbital localized on the 4-amino group and ND is an orbital localized on a distal nitrogen. The possible role of $|\mathbf{e}_{\mathrm{CT2}}\rangle$, which is higher in energy than $|\mathbf{e}_{\mathrm{CT1}}\rangle$ because of the very electrophilic nature of the 4-N, is discussed later.

IV. CRUDE THEORETICAL ESTIMATE OF THE ELECTRONIC COUPLING MATRIX ELEMENTS

We first consider a very approximate estimate of the difference in coupling to the two distal nitrogens by noting that the distal N on the 4-substituent is three bonds removed from the 4-N, which is found in the calculations given later to make a significant contribution to the HOMO of the system, and is part of the initial acceptor state $|\mathbf{e}\rangle$ for the electron transfer reactions (Fig. 4). Using as an approximate figure a decrease of the square of the coupling matrix element V of a factor of 3 per bond of an alkyl chain,[14] this $|V|^2$ is about 1/27 of the contact value. If the contact value is of the order of 2 eV, the V then would be of the order of $2/\sqrt{27}$, i.e., $\sim$ 0.4 eV. On the other hand, the distal nitrogen in the 9-substituent is three single bonds and 6 double bonds away from that 4-N. If one takes the decay of the coupling matrix

element for electron transfer via double bonds as $e^{-\beta R}$, where β is a distance decay parameter and R is the total length of the double bonds, about 8.5 Å in this case, the coupling matrix element for the electron transfer from the distal nitrogen of the 9-substituent would be $(2/\sqrt{27})e^{-8.5\beta/2}$. If β is taken as 0.36 $Å^{-1}$ (although strictly speaking this β refers to a direct distance),[15] this coupling matrix element would be about 0.08 eV, and if β is instead 0.57 $Å^{-1}$,[16] it would be about 0.03 eV.

The energy barrier to electron transfer at the crossing point is lowered by an amount equal to V, and so the activation energy for the electron transfer from the distal N of the 4-substituent would be significantly less than that for the electron transfer from the distal N of the 9-substituent. If these crude "back of the envelope" figures were taken literally, the electron transfer from the distal N on the 9-substituent would be $\sim e^{0.37/0.025}$ (0.025 being k_BT in eV) or 10^7 times slower than the electron transfer from the distal N on the 4-substituent.

In the following section, we give a more detailed estimate, using an extended Hückel theory, with similar results also being obtained using a Hartree-Fock calculation.

V. CALCULATIONS: DIRECTIONALITY AND $|E_{CT1}\rangle$

We focus first on a comparison between the electron transfer from the distal nitrogens in the 4- and 9-substituents of **4** and **5**, where $|e\rangle$ and $|e_{CT1}\rangle$ are the principal states involved. Calculations for the electronic coupling matrix elements between $|e_{CT1}\rangle$ and $|e\rangle$ were performed, as noted earlier, using an extended Hückel and, separately, using an *ab initio* Hartree-Fock method.

A model system, compound **9** in Fig. 5 was used instead of **4** and **5** in the calculations, to reduce the computational time and so the two distal amino groups of **9** were both chosen to be a NH_2 group in the extended Hückel and Hartree-Fock calculations. The molecular structure given in ref. 18 was used after an optimization by a Hartree-Fock calculation using the basis set 6-31G*. In both calculations, the acceptor state was chosen to be the HOMO of the molecule and the donor states

were identified as the states having electron localized at the distal amino groups. The coordinates are given in the supplementary material in Table I S.

For convenience in the extended Hückel calculations the relative energies of the donor and acceptor diabatic states were changed by placing at different distances an F^- anion near the nitrogen of the donor group under consideration, as far as possible from all the other atoms, to increase mainly the energy of the state $|\mathbf{e}\rangle$ and to minimize the change of the stable molecular structure. The energies of the two states, in one of which the orbital is delocalized in the fluorophore and in the other it is localized on the distal amino group, were then plotted as a function of the distance between the nitrogen of the amino group and the anion. In this way, the two adiabatic curves were obtained and the coupling matrix element was obtained from their avoided crossing as one half of the least splitting of the adiabatic curves. That avoided intersection occurred when the distance between the distal group in the 4-substituent and the F^- was about 1.9 Å.

Ab initio Hartree-Fock calculations were performed in a way similar to the extended Hückel calculations, except that in these calculations the change of the energies of the states of interest was achieved by applying an electric field, which is a built-in function of the Gaussian 98, along the direction of the electron transfer. The avoided crossing of the energy curves occurred at an applied field of 8.5×10^6 in the units in Gaussian 98.

The calculated electronic coupling matrix element between $|\mathbf{e}\rangle$ and $|\mathbf{e}_{CT1}\rangle$ for the electron transfer from the distal N in the 4-substituent is 0.25 eV for the extended Hückel calculation and 0.39 eV in the Hartree-Fock calculation. For the electron transfer from the distal nitrogen in the 9-substituent it is 0.030 and 0.035 eV, respectively. The calculated electronic coupling matrix elements for electron transfer reactions from both 4- and 9-substituents are large enough for the reactions to be considered as adiabatic, and the coupling matrix element for the electron transfer from the 4-distal nitrogen is about 10 k_BT larger than that for the electron transfer reaction from the 9-distal nitrogen. Since this difference in the electronic coupling matrix elements makes the energy barrier about 10 k_BT smaller at the avoided cross-

ing for the electron transfer from the 4-distal nitrogen than that from the 9-distal nitrogen, on this basis the electron transfer from the 4-distal nitrogen would be much faster ($\sim e^{10}$ or 10^4, if the calculations were literally correct) than that via the competing pathway, from the 9-distal nitrogen. The fluorescence of the fluorophore is then mainly quenched by the electron transfer from the distal amino group in the 4-substituent.

When this distal nitrogen is protonated, the electron transfer reaction is inhibited because the protonation of that nitrogen should considerably stabilize electrons on it and, in terms of Fig. 3, increase the energy of the charge-separated state ($|e_{CT1}\rangle$) relative to the fluorescent excited state ($|e\rangle$), reflecting in part the role of coulombic repulsion. The fluorescence recovery is then observed at pH's equal to and lower than the pK_a values of the distal nitrogens, because of this inhibition of the electron transfer.

VI. FLUORESCENCE QUENCHING IN 1 AND 2 AND THE ROLE OF 4-N

We turn next to the differences between the pH-dependence of the fluorescence of **1** and **2**, and that of **3**, **4** and **5**. As noted earlier, the experimental[1,2] fluorescence quantum yields of molecules **1** and **2** are relatively low at all pH values compared to those of **3**, **4**, and **5** in acid (Table I). The main structural difference between them is that there exists a distal nitrogen in the 4-substituent of **3**, **4** and **5** but not in that of **1** or **2**.

The fluorescence of the 4-aminonaphthalimide, due to an $|e\rangle \rightarrow |g\rangle$ transition, is in competition with a radiationless transition, even in the absence of any distal amino group. The quantum yield of the fluorescence is low (~ 0.2) for **1** and **2** because of that competition. This radiationless transition is enhanced when the $(HOMO)_1(LUMO)_1$ and $(HOMO)_2(LUMO)_0$ surfaces are more displaced in coordinate space from each other. The presence of the 4-amino substituent on the ring presumably enhances this displacement (by concentrating the charge in a smaller region near the 4-N) and so enhances the radiationless transition rate and hence decreases the fluorescence

quantum yield.

Upon the protonation of the 4-distal nitrogen, not only is the energy of the HOMO is raised, but also its electron distribution is less concentrated in the small region near 4-N, and so the $(HOMO)_1(LUMO)_1$ state is expected to be less shifted in coordinate space from the $(HOMO)_2(LUMO)_0$ state. This change results in a corresponding decrease in the radiationless transition rate and so in an enhancement of the fluorescence quantum yield. Accordingly, the protonation of the 4-distal nitrogen increases the fluorescence quantum yields of **3**, **4** and **5** to values (> 0.5) greater than that of **1** or **2** (~ 0.2), which do not contain a distal nitrogen in the 4-substituent.

The energy of a state $|e_{CT2}\rangle$ (Fig. 4) is expected to be appreciably higher than that of $|e_{CT1}\rangle$ (Fig. 4), because of the electrophilic nature of the 4-N. This difference is reflected in the pK_a's of the 4-N and and the distal nitrogen, e.g., -0.5 as contrasted with 6 or 8, depending on the nature of the distal group. This difference is about 0.39 eV. Accordingly the state $|e_{CT2}\rangle$ may not be directly involved in the present electron transfer, but its presence would only enhance the pathway to the 4-distal nitrogen. The latter pathway could make use of $|e_{CT2}\rangle$ via a superexchange mechanism, whereas the pathway from distal nitrogen in the 9-substituent could not.

The above discussion also applies to the pH-dependence of the absorption spectra of **1** to **5**. Compounds **1** and **2** cannot be protonated in the pH range of the experiments, because of the absence of the distal nitrogen in the amino position and the low pK_a of the 4-N. Correspondingly, their λ_{abs}^{max} should be pH-independent. For compounds **3**, **4**, and **5**, however, the protonation of the distal nitrogen increases the energy of the fluorescent state $|e\rangle$ (which is slightly charge-separated), leading to a blue shift of the λ_{abs}^{max} in acid compared with that in base.

VII. FLUORESCNCE OF 6, 7, AND 8 IN THE PRESENCE OF METAL IONS

The spectra of systems **6**, **7**, and **8**[6,10] can be interpreted in a similar way. The electron transfer is faster from the distal nitrogen of the 4-substituent than that

from the distal nitrogen of the 9-substituent, for the reason discussed above. The fluorescence is quenched by the distal amino group on the 4-substituent and recovery occurs when a complex between this nitrogen and some metal ion is formed, both the intensity and the lifetime being increased with the increase of the ion concentration.[6] This complexation between the distal nitrogen and metal ions, which has a charge effect on the fluorophore, also provides a possible explanation of the blue shift of the absorption spectra[19] of **6** and **7** in the presence of metal ions which can form an amino complex. The molecule **8**, however, has a much longer side chain at the 4-substituent position and the distal nitrogen and 4-N are separated by 8 other atoms. Accordingly, the metal ion attached to this distal nitrogen has a much smaller effect on the fluorophore and there is negligible influence of the metal ions on the observed absorption and fluorescence wavelength of **8**.[20]

VIII. CONCLUDING DISCUSSION

Summarizing the calculations, the fast electron transfer from the distal nitrogen in the 4-substituent, versus slow charge transfer from the 9-substituent, is mainly due to the difference in the electronic coupling matrix elements for the two reactions. Both the extended Hückel and the *ab initio* Hartree-Fock calculations yield a much larger electronic coupling matrix element for the electron transfer from the distal nitrogen attached to the 4-position than that from the distal nitrogen attached to the 9-position. This result is consistent with the "back of the envelope" argument given in Sec. IV.

It would be desirable for further pH-dependent fluorescence studies of similar systems to be performed to test the mechanism of the fluorescence quenching and the corresponding recovery. For example, the electron transfer from the distal nitrogen on the 4-substituent can be reduced by lengthening the carbon chain of that substituent. The question of assessing the role of a possible hydrogen-bond interaction in the protonated form of **4** and **5**, as in Fig. 6, to the 4-N also arises. Reducing the carbon chain length will enhance the coulombic repulsion of the protonic charge, so decrease

the formation of a $+\delta$ on the 4-N and reduce this source of quenching of the fluorescence. It would also reduce the formation of a hydrogen bond to the 4-N by requiring a 4-member hydrogen-bonded ring. The protonation of the distal nitrogen then would not reduce the quenching by the 4-N if the formation of an intramolecular bond were needed for recovering the fluorescence. This experiment would distinguish the relative importance of the coulombic repulsion and of the hydrogen bonding caused by the protonation of the distal N to the 4-N. Nuclear magnetic resonance experiments might also permit the detection of a hydrogen bond. Real-time experiments on the decay of the fluorescence under the condition of the experiments in refs. 1, 2 and 6 would also be helpful. In summary, a simple electronic mechanism is proposed for explaining the various observations[1,2,6] of the behavior of the 4-aminonaphthalimides and some experimental consequences are suggested.

ACKNOWLEDGMENTS

We are pleased to acknowledge the support of this research by the Office of Naval Research and the National Science Foundation. It is a real pleasure to dedicate this article to Professor Norboru Mataga, whom one of us (RAM) has had the pleasure of knowing for many years and of appreciating his incisive research in photophysics and in electron transfer processes.

APPENDIX A: CALCULATIONS FOR THE COUPLING MATRIX ELEMENT

To obtain the coupling matrix element, a two-state picture is used for each of the two electron transfer reactions. In the two-state model, the Hamiltonian is written as[21]

$$H = \begin{pmatrix} H_{DD} & V \\ V & H_{AA} \end{pmatrix}, \tag{A1}$$

where H_{DD} and H_{AA} are the energies of the donor and acceptor diabatic states, respectively, and V is the coupling between the two states. When the donor and

acceptor states are chosen to be orthonormal to each other, as in the extended Hückel and Hartree-Fock calculations in this study, the energies of adiabatic states, denoted by E_1 and E_2, are obtained directly from the diagonalization of the Hamiltonian matrix as

$$E_1 = H_{DD} + V \tan \eta, \qquad E_2 = H_{DD} - V \tan \eta, \tag{A2}$$

where $\tan 2\eta = 2V/(H_{DD} - H_{AA})$. It then immediately follows that

$$V = (1/2)(E_1 - E_2) \sin 2\eta. \tag{A3}$$

As indicated by Eq. (A3) $E_1 - E_2$ has a minimum when $\sin 2\eta = 1$, and $E_1 - E_2 = 2V$. Equation (A3) then provides a way of calculating the coupling matrix element V, if the energies of two adiabatic states can be changed continuously in the neighborhood of $H_{DD} = H_{AA}$ to give the two adiabatic curves. The coupling matrix element is one half of the minimum splitting of the two adiabatic curves.

REFERENCES

[1] A. P. de Silva, H. Q. N. Gunaratne, J. Habib-Jiwan, C. P. McCoy, T. E. Rice, and J. Soumillion, Angew. Chem. Int. Ed. Engl. **34**, 1728 (1995).

[2] A. P. de Silva and T. E. Rice, Chem. Commun. 163 (1999).

[3] A. Pardo, J. M. L. Poyato, and E. Martin, J. Photochem. **36**, 323 (1986).

[4] M. S. Alexiou, V. Tychopoulos, S. Ghorbanian, J. H. P. Tyman, R. G. Brown, and P. I. Brittain, J. Chem. Soc. Perkin Trans. **2**, 837 (1990).

[5] A. P. de Silva, H. Q. N, Gunaratne, A. J. Huxley, C. P. McCoy, J. T. Rademacher, and T. E. Rice, Chem. Rev. **97**, 1515 (1997), and references cited therein.

[6] K. A. Mitchell, R. G. Brown, D. Yuan, S. Chang, R. E. Utecht, and D. E. Lewis, J. Photochem. Photobio. A **115**, 157 (1998).

[7] D. Yuan and R. G. Brown, J. Chem. Res. (S) 418 (1994); J. Chem. Res. (M) 2362 (1994).

[8] S. L. Dmitruk, S. I. Druzhinin, R. A. Minakova, A. I. Bedrik, and B. M. Uzhinov, Russ. Chem. Bull. **46**, 2027 (1997).

[9] H. Tian, T. Xu, Y. B. Zhao, and K. C. Chen, J. Chem. Soc. Perk. Trans. 2, 545 (1999).

[10] There is also a 10 nm blue shift for the fluorescence wavelength for the molecule **3**, but no blue shift was observed for the fluorescence of **4** and **5**.

[11] Experiments were performed for metal ions Cu^{2+}, Mn^{2+}, and Ni^{2+}.

[12] B. Ramachandram and A. Samanta, Chem. Commun. 1037 (1997).

[13] E. Galoppini and M. A. Fox, J. Am. Chem. Soc. **118**, 2299 (1996); J. K. Whitesell, H. K. Chang, M. A. Fox, E. Galoppini, D. M. Watkins, H. Fox, and B. Hong, Pure Appl. Chem. **68**, 1469 (1996).

[14] C. P. Hsu and R. A. Marcus, J. Chem. phys. **106**, 584 (1997).

[15] S. Creager, C. J. Yu, C. Bamdad, S. O'Connor, T. MacLean, E. Lam, Y. Chong, G. T. Olsen, J. Y. Luo, M. Gozin, and J. F. Kayyem, J. Am. Chem. Soc. *121* 1059 (1999).

[16] S. B. Sachs, S. P. Dudek, R. P. Hsung, L. R. Sita, J. F. Smalley, M. D. Newton, S. W. Feldberg, and C. E. D. Chidsey, J. Am. Chem. Soc. **119**, 10563 (1997).

[17] W. Rettig, Angew. Chem. Int. Ed. Engl. **25**, 971 (1986).

[18] C. J. Easton, J. M. Culbis, B. F. Hoskins, I. M. Scharfbillig, and E. R. T. Tiekink, Z. Kristallogr. **199**, 249 (1992).

[19] In Ref. 6, only data of **7** are presented. It was noted that the experimental results for **6** are similar.

[20] In fact, the fluorescence intensity is decreased by adding metal ions to the solution instead of being increased. It has been suggested that this effect is a result of the formation of a complex between the metal ions and the fluorophore.[6]

[21] M. D. Newton, Chem. Rev. **91**, 767 (1991) and references cited therein.

TABLES

TABLE I. Optical properties[a] for **1** to **5**.

	1	**2**	**3**	**4**	**5**
λ_{abs}^{max}(base[b])/nm	454	455	449	450	452
λ_{abs}^{max}(acid[b])/nm	454	455	431	432	433
λ_{shift}/nm	0	0	18	18	19
λ_{abs}^{max}(pH=7.0)/nm				432	452
λ_{flu}^{max}(acid[b])/nm	555	559	538	526[c]	524[c]
λ_{flu}^{max}(acid[b])/nm	555	557	549		
Φ_{flu}(acid[b])/nm	0.23	0.12	0.76	0.53	0.52
Φ_{flu}(pH=7.0)/nm	0.23	0.12	0.57	0.66	0.062
Φ_{flu}(base[b])/nm	0.23	0.15	0.030	0.030	0.070

[a] The properties for **1**, **2**, and **3** are taken from ref. 1, and those for **4** and **5** are taken from ref. 2.

[b] pH was only specified for **4** and **5**. Here, the pH was 3.0 in acidic solution and 10.8 in basic solution.

[c] Value changes very little with the pH.

Figure Captions

Fig. 1 The structures of the five molecules **1** through **5** studied by the pH-dependent fluorescence spectroscopy.[1,2]

Fig. 2 The structures of the fluorescent sensors **6**, **7**, and **8** studied by Mitchell *et al.*[6,7]

Fig. 3 Schematic diagram of the free energy *vs* nuclear coordinate for the ground and excited states for the fluorophore. $|g>$ is the ground state, $|\mathbf{e}\rangle$ is the fluorescence excited state, $|\mathbf{e}_{\mathrm{CT1}}\rangle$ is the charge-separated, non-fluorescent state due to the electron transfer from the distal nitrogen. When the distal nitrogen in the 4-substituent is protonated, the energy of the fluorescent state $|\mathbf{e}\rangle$, which is slightly charge-separated, is increased and there is a blue shift of the absorption. The $|\mathbf{e}_{\mathrm{CT1}}\rangle$ does not exist in **1** or **2**.

Fig. 4 The various diabatic states and the relevant orbitals. About 70% of the relevant orbital of $|\mathbf{e}\rangle$, which is the HOMO of the system, is localized at the 4-N (40%), 3-C, 4-C, and 10-C.

Fig. 5 The structure of the model system used in the calculations of electronic coupling matrix elements.

Fig. 6 The structures of **4** and **5** after the formation of the intra-molecular hydrogen bond.

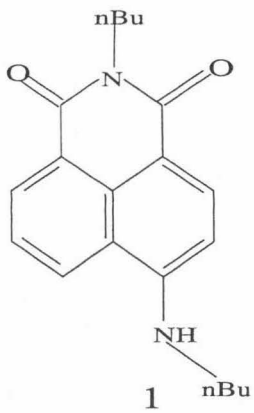

1

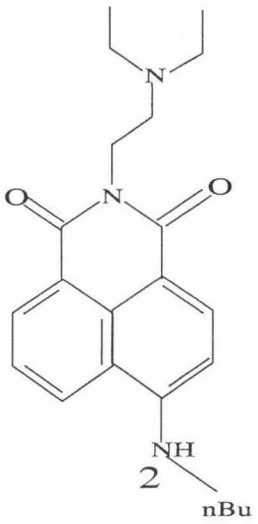

2

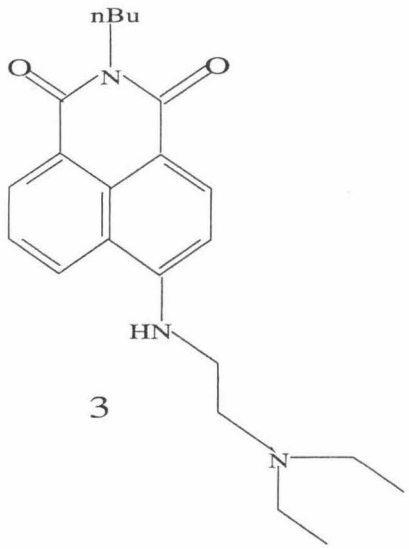

3

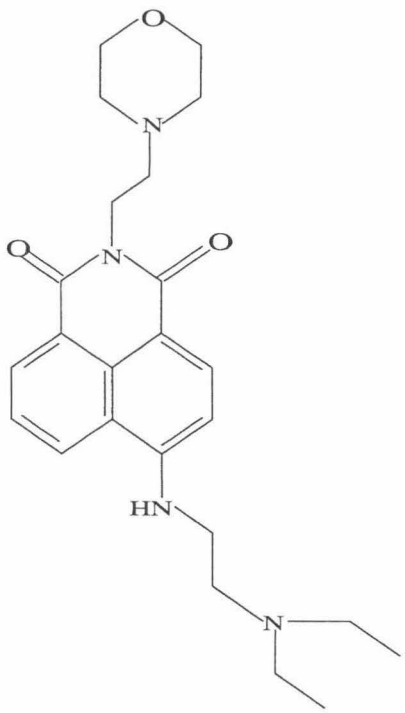

4

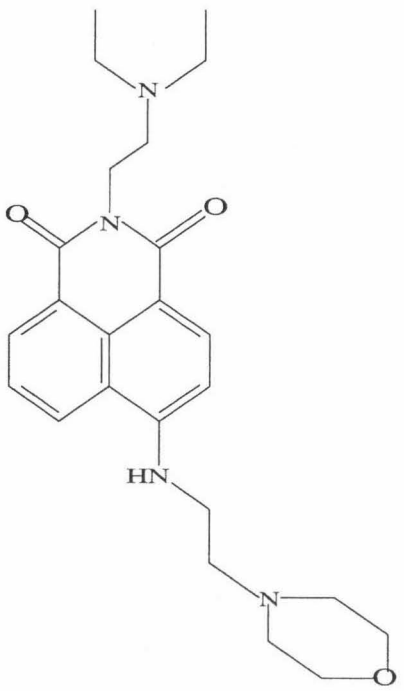

5

FIG. 1.

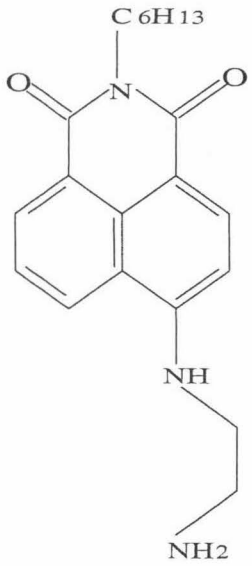

6

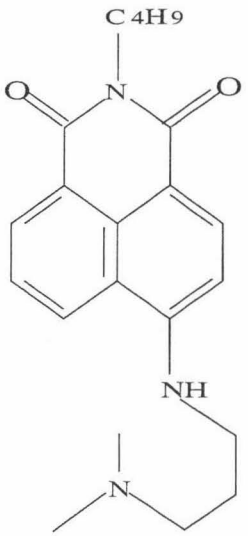

7

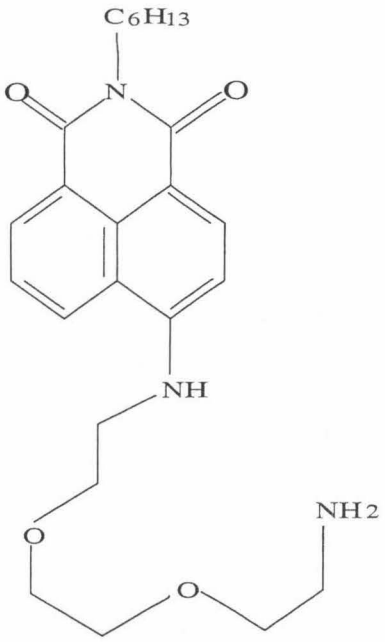

8

FIG. 2.

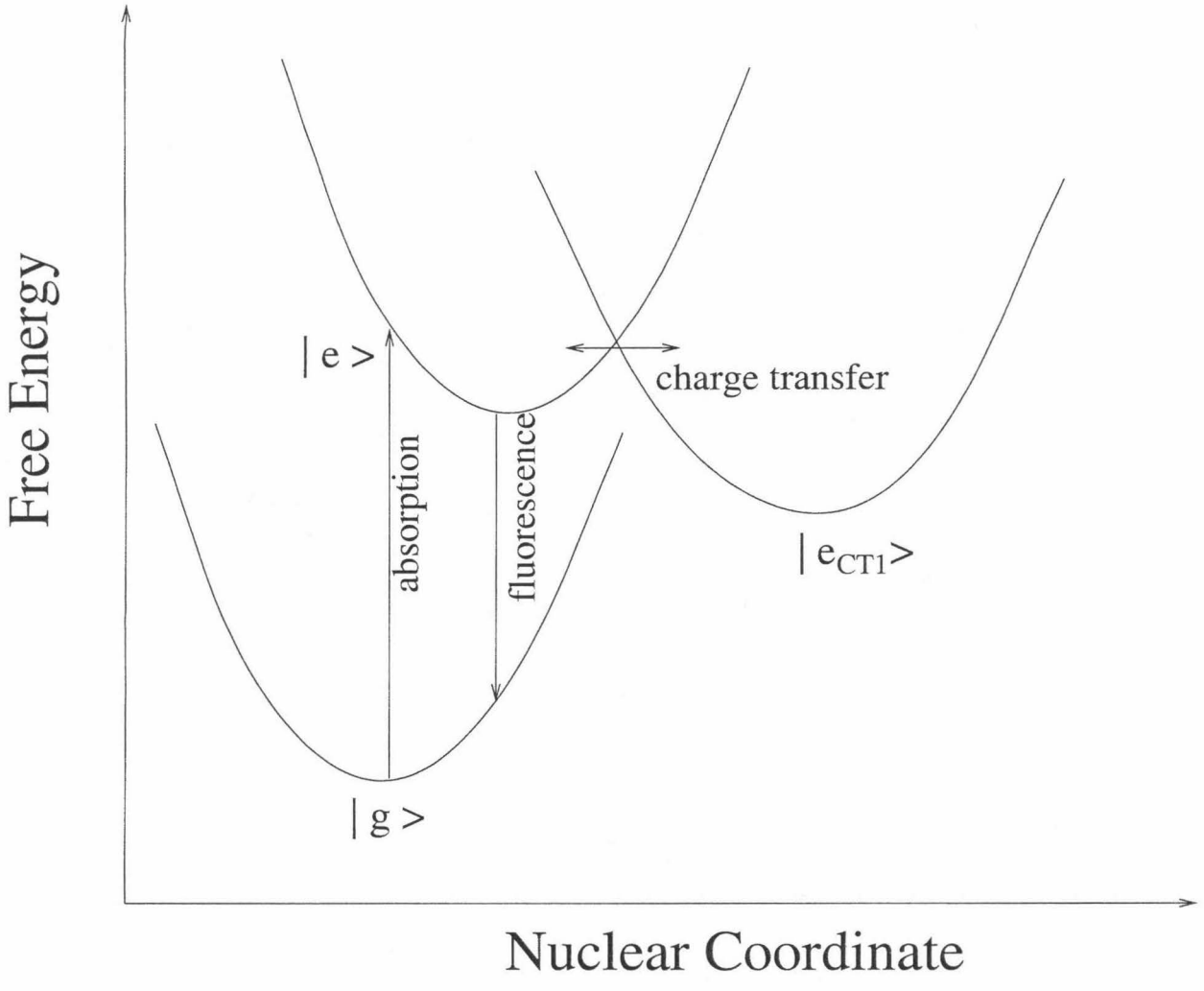
Free Energy
| e >
absorption
fluorescence
charge transfer
| e_CT1>
| g >
Nuclear Coordinate

FIG. 3.

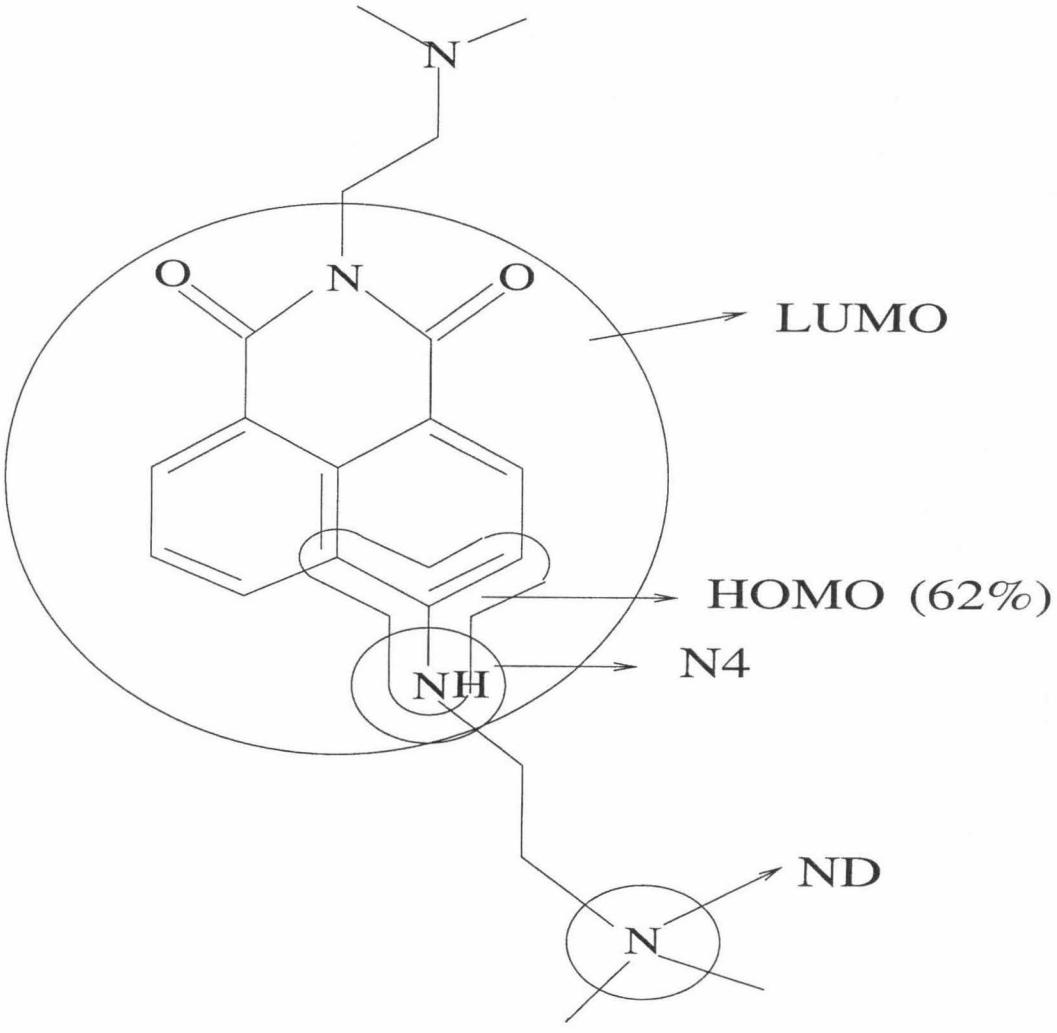

FIG. 4.

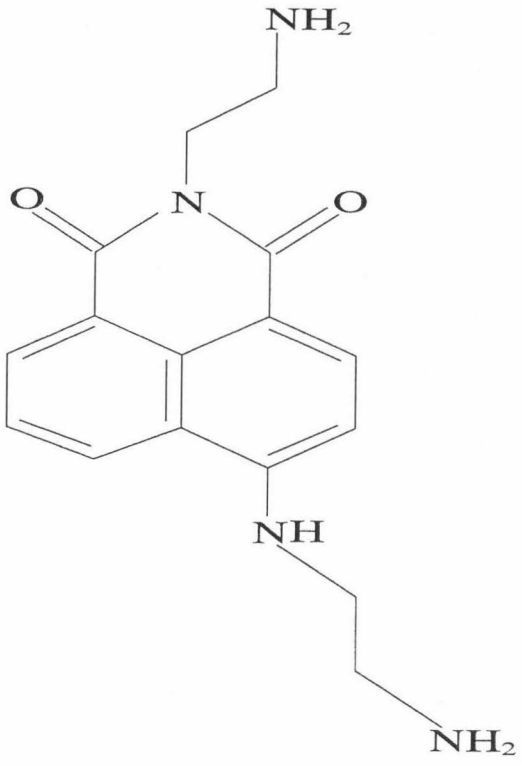

Compound 9

FIG. 5.

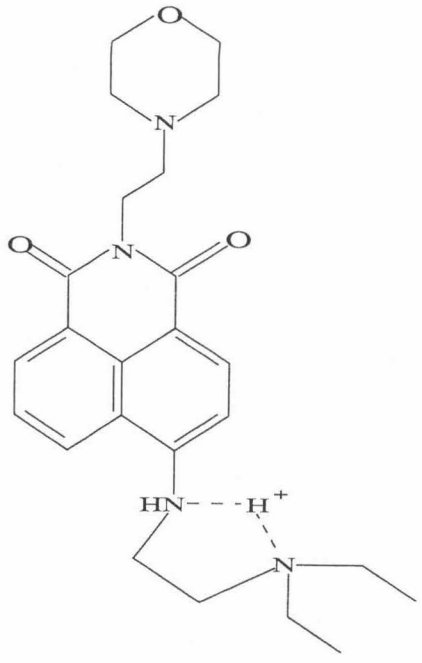

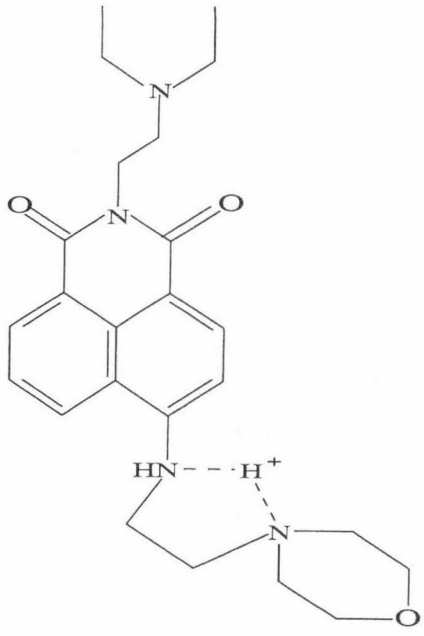

FIG. 6.

TABLE I. Supplement: Coordinates[a] for the atoms in compound **9**

atom	x	y	z
C	4.8230510044	-0.3202431448	-0.6322330717
C	5.3314123096	-0.8463867416	0.7170130084
N	6.5107271908	-1.6855480060	0.6318883857
H	4.6138234392	-1.1427535941	-1.3057447175
H	5.6064503504	0.2643353318	-1.1045595255
H	5.5606951848	-0.0027495506	1.3609009242
H	4.5491144263	-1.4070772611	1.2146705592
H	6.3362950750	-2.5151741063	0.0985787343
H	7.2773984780	-1.2046072295	0.2026040968
O	-1.9488737966	-2.4437315046	0.1652261903
O	-3.3598489565	1.8117499560	0.5132628936
N	-2.6570397602	-0.3207840034	0.3942461687
C	-0.2950912589	-0.7895881805	-0.0172085241
C	0.7249681017	-1.6785108577	-0.2103238109
C	2.0460594129	-1.2521944717	-0.3801761210
C	2.3705111016	0.0893216663	-0.3718209382
C	1.5197001319	2.4557073435	-0.2514894690
C	0.4931876216	3.3381757890	-0.0827623759
C	-0.8125820052	2.8660455104	0.1317642030
C	-1.0568719225	1.5227681644	0.1593240834
C	-0.0064679805	0.5936380213	-0.0177017292
C	1.3100764817	1.0560048559	-0.2094190026
C	-1.6698280683	-1.2769089962	0.1799013630
C	-2.4484710511	1.0462778508	0.3686119263
H	-1.6292561986	3.5488702926	0.2656579527
H	0.5023513057	-2.7286330004	-0.2159769515
H	2.8090459642	-1.9943427421	-0.5023698772
H	0.6786821099	4.3954831305	-0.1231013306

H	2.4985591246	2.8528974317	-0.4429622112
N	3.6549490042	0.5319047787	-0.5454213400
H	3.8443303750	1.4547608002	-0.2347824217
N	-6.1703655159	-1.4182275536	-0.5187698382
C	-4.8084709850	-0.9487928752	-0.6943895358
C	-4.0287500243	-0.7959085467	0.6132451245
H	-6.1890681707	-2.3165983394	-0.0755749081
H	-6.6998123881	-0.7879283107	0.0524242232
H	-4.8410956121	0.0062437193	-1.2054662598
H	-4.2886909644	-1.6462343143	-1.3405213356
H	-3.9633445889	-1.7447905237	1.1217432384
H	-4.5181895358	-0.0836981790	1.2589527244

[a] In units of Å.